Design and Synthesis of Molecular Tools for the Ubiquitin Proteasome System

Thesis submitted to the University of Strathclyde in fulfilment of the requirements for the degree of Doctor of Philosophy

by

Morag Elspeth Watson

April 2016

Declaration of Copyright

This thesis is the result of the author's original research. It has been composed by the author and has not been previously submitted for examination which has led to the award of a degree

The copyright of this thesis belongs to the author under the terms of the United Kingdom Copyright Acts as qualified by the University of Strathclyde Regulation 3.50. Due acknowledgement must always be made of the use of any materials contained in, or derived from, this thesis.

Signed:

Date:

Abstract

Alzheimer's disease (AD) has become one of the biggest global public health challenges, with 0.5% of the population living with dementia. The ubiquitin proteasome system (UPS), in particular the interaction between a mutant form of ubiquitin, Ubb+1, and the E2-conjugating enzyme E2-25K, has been identified as playing a possible pathophysiological role in the early and late stage progression of AD. The E2-25K/Ubb+1 protein-protein interaction (PPI) is regulated by the α-helix 9 of E2-25K. Creating a short helical peptide analogous to α-9 of E2-25K with the technique of peptide stapling could potentially block the action of Ubb+1 and provide a tool to investigate the role of the UPS in AD.

Following synthesis of the requisite alkenyl amino acids for peptide stapling, an initial palette of nine peptides, containing the wild-type E2-25K sequence, and eight stapled analogues, were successfully synthesized and ring-closed on the solid phase. Circular dichroism spectroscopy was used to analyse secondary structure, revealing the peptides exhibited a range of 16 – 91% helicity. Further NMR studies demonstrated the more precise helical nature of short helical peptides in solution. Preliminary biological assays indicated that the synthesised peptides are capable of inhibiting Ubb+1 incorporation into long polyubiquitin chains. Remarkably, these antagonists proved to be selective towards Ubb+1 over ubiquitin despite the high degree of similarity in the relative binding sites of the two proteins. Further *in silico* design led to the development of a second generation of six stapled peptides. Further biological evaluation revealed an additional sequence potentially capable of activating E2-25K mediated Ubb+1 capped PolyUb chain formation.

Overall, this preliminary study has shown that short helical analogues of E2-25K can be successfully synthesized and used to block or activate the E2-25K/Ubb+1 PPI. Further optimisation of these stapled peptides could provide valuable tool compounds into the investigation of Ubb+1 mediated inhibition of the UPS, and the downstream effects on the pathogenesis of AD.

Acknowledgements

Abbreviations

Aβ – Amyloid beta

Ac – Acetyl group

Ach – Acetylcholine

AD – Alzheimer's disease

ACM – Acylic closing metathesis

ADMET- Absorption, distribution, metabolism, excretion and toxicology

AIB – Aminoisobutyric acid

AM – Aminomethyl

ApoE – Apolipoprotein E

APP – Amyloid precursor protein

ATP – Adenosine triphosphate

BACE1 – Beta-secretase 1

BCL-2 – Apoptosis regulator protein

BID – BH3 interacting-domain death agonist member of the BCL-2 family

BH3 – Apoptosis promoting protein

Bn – Benzyl group

Boc – *t*-Butyl carbamate

BOP - (Benzotriazol-1-yloxy)tris(dimethylamino) phosphonium hexafluorophosphate

BP – Benzylproline

BPB – Benzylproline benzophenone

BuLi – Butyl lithium

CaMK – Calmodulin Kinase

Cbz – Benzyl carbamate protecting group

CD – Circular dichroism spectroscopy

CDI – Carbonyl diimidazole

CM – Cross metathesis

Con - Control

COMU – (1-Cyano-2-ethoxy-2-oxoethylidenaminooxy)dimethylamino-morpholino-carbenium hexafluorophosphate

Cy – Cyclohexyl group

DCC – N,N′-Dicyclohexylcarbodiimide

DCM – Dichloromethane

DIPEA – Diisopropylethylamine

DMF – Dimethylformamide

DMPA - 2,2-Dimethoxy-2-phenylacetophenone

DMSO - Dimethylsulfoxide

Dr – Diastereomeric ratio

DUB – De-ubiquitinating enzymes

EDTA – Ethylenediaminetetraacetic acid

Ee – Enantiomeric excess

E1 – Ubiquitin activating enzyme

E2 - Ubiquitin conjugating enzyme

E2 - Ubiquitin ligating enzyme

E2-25K – Specific ubiquitin conjugating enzyme

Fmoc – 9-Fluorenylmethoxy carbonyl

Fmoc-ONSU – *N*-(9-Fluorenylmethoxycarbonyloxy) succinimide

GI – Gastro-intestinal

GSK - GlaxoSmithKline

HATU – 1-[Bis(dimethylamino)methylene]-1*H*-1,2,3-triazolo[4,5-b]pyridinium 3-oxide hexafluorophosphate

HBS – Hydrogen bond surrogate

HCTU – O-(1*H*-6-Chlorobenzotriazole-1-yl)-1,1,3,3-tetramethyluronium hexafluorophosphate

hDM2 – Ubiquitin protein ligase

HeLa – Immortal cell line

HIV – Human immunodeficiency virus

HMDS - Hexamethyldisilylamine

HMP – 2-[4-(Hydroxymethyl)phenoxy]acetic acid

HMPA resin – 4-Hydroxymethylphenoxyacetic acid

HOAt – 1-Hydroxy-7-azabenzotriazole

HOBt – Hydroxybenzotriazole

HPLC – High performance liquid chromatography

IC_{50} – Half-maximal inhibitory concentration

IN – HIV-1 Integrase

INF – Intraneuronal fibre

IPA – Isopropanol

*i*Pr – Isopropyl group

IR – Infra-red spectroscopy

K_D – Ligand dissociation constant

K_i – Ligand binding affinity

KO – Knock-out

MALDI - Matrix assisted laser desorption/ionization

MBHA – Methylbenzhydrylamine linker

MeCN – Acetonitrile

MHPA – Methylhexahydrophthalic anhydride linker

mRNA – Messenger ribonucleic acid

MS – Mass spectrometry

MsCl – Mesyl chloride

Mtt – 4-Methyltrityl protecting group

MW – Molecular weight

NHC – *N*-heterocyclic carbene

Nle – Norleucine

NMDA - *N*-methyl-D-aspartate receptor

NMR – Nuclear magnetic resonance spectroscopy

N-MeIm – *N*-methyl imidazole

NMP - *N*-Methyl-2-pyrrolidone

NOE – Nuclear overhauser effect

Obs - Observed

p53 – Cellular tumour antigen p53

PDB – Protein data bank

PEG – Polyethylene glycol

PG – Protecting group

PL – Polystyrene resin

PolyUb – Polyubiquitin

PPI – Protein-protein interaction

PS – Polystyrene resin

PS1 – Presenilin 1

PS2 – Presenilin 2

PyBOP – (Benzotriazol-1-yloxy)tripyrrolidinophosphonium hexafluorophosphate

RCM – Ring-closing metathesis

ReBil - Recombinase enhanced biomolecular luciferase platform assay

ROMP – Ring-opening metathesis

RNA – Ribonucleic acid

SAHBs – Stapled alpha-helical mimics of BID

SCX – Strong cation exchange silica

SPPS – Solid phase peptide synthesis

Su – Succinimide

TBAI – Tetra-butylammonium iodide

*t*Bu – *Tert*-butyl group

TFA – Trifluoroacetic acid

TFE – Trifluoroethanol

THF – Tetrahydrofuran

TIS – Triisopropylsilane

Trt – Trityl protecting group

Ub – Ubiquitin

UBA – Ubiquitin domain A of E2-25K

Ubb+1 – Mutant form of Ubiquitin

UFD – Ubiquitinated fusion degradation product

UPS – Ubiquitin-proteasome system

UV – Ultraviolet spectrometry

Table of contents

List of Figures, Schemes and Tables

1. Introduction

1.1 - The pathogenesis of Alzheimer's disease

With an increasing elderly population, neurodegenerative disorders are becoming more prevalent in our society.[1] Dementia has become one of the biggest global public health challenges with approximately 0.5% of the population living with the condition,[1] with this number set to increase 4-fold to 131.5 million by 2050.[2] In the current climate, health and social care systems across the world are already struggling to provide adequate long-term care for sufferers whilst failing to invest in research and development,[2] with the UK annual spend on dementia research being twelve times lower than that spent on cancer research.[1] Alzheimer's disease (AD) is the most common form of dementia and is characterised by a loss in neuronal function, which results in memory loss and behavioural changes. The two primary causes of this dementia are abnormal levels of amyloid beta (Aβ) plaques, and intra-neuronal fibrillary (INF or Tau) tangles in the central nervous system. Build-up of these aggregates is thought to reduce the effectiveness of the neurons which carry messages around the brain, resulting in a loss of cognitive function and eventual neuronal cell death. Genetic mutations of amyloid precursor protein (APP), presenilin 1 (PS1), presenilin 2 (PS2) and apolipoprotein E (ApoE) have all been identified in patients with a family history of the disease, and are hypothesised as the root cause of imbalances in Aβ formation and clearance (Fig.1).[3] Amyloidosis is considered the most prominent early biomarker for the genetic autosomal form of AD, with Aβ deposition present years before the presence of cognitive decline or neurodegeneration.[4]
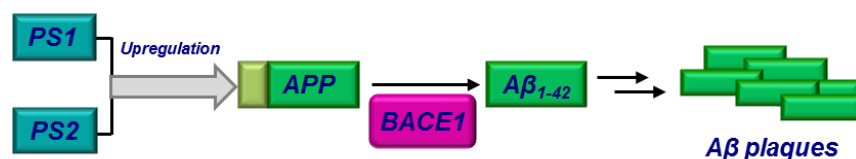
Figure 1 - Potential pathways to toxic Aβ plaques in AD

Subsequently, increases in Aβ can cause a cascade of events which can directly injure the synapses and neurites of brain neurons, as well as facilitating Tau tangles through the alteration of kinase activity by changing the pattern of Tau phosphorylation to epitopes prone to filament formation, and subsequent tangle development.[5,6] However, this hypothesis is not all encompassing and cannot

explain the majority of cases where the individual will have no genetic predisposition to dementia.[5]

1.1.1 - Current therapies towards AD

Another proposed factor towards the pathogenesis of AD is the cholinergic hypothesis in which a loss in cholinergic neurotransmission from neuronal degradation leads to deterioration in cognitive functions such as learning and memory.[7] Common neurotransmitters of the cholinergic system have been shown to be reduced in early stage AD for a majority of patients,[8] with reductions in the synthesis and uptake of acetylcholine (ACh).[9,10] Studies have also linked drops in this neuronal pathway to amyloid β production and Tau phosphorylation, providing support towards drug development for this target.[7] Consequently, choline esterase inhibitors, which reduce the hydrolysis of Ach, have been developed with the aim of improving the cognitive and behavioural problems associated with AD. Drugs such as donepezil (Aricept®) have been shown to be potent and selective towards choline esterase,[11] inducing dose-dependent improvements in cognition.[12] However, due to the non-competitive nature of their binding and action, they only produce slow and reversible cholinesterase inhibition. Therefore, such compounds are not effective in the long-term (>12 months) as the rate of inhibition will eventually be overtaken by the rate of choline esterase production.[13] Also, drugs of this kind are known to produce side effects such as GI discomfort, nausea and vomiting and have also been shown to be ineffective for some patients.[14,15]

In the last 15 years, efforts towards AD therapeutics has been primarily focused on BACE1 inhibitors. This target was linked to the amyloid β hypothesis in that the BACE1 enzyme is essential for processing APP, the precursor to amyloid β which aggregates to cause neuronal plaques (Fig. 1).[16] Initial studies using BACE1 knock-out (KO) mice showed that Aβ production was stopped when this biological pathway was deleted,[17–19] leading to the idea of BACE1 inhibitor drugs as a potential means of reducing Aβ plaques. Initial peptidic inhibitors, such as StatVal developed by Elan Pharmaceuticals,[20] were able to inhibit BACE1 with IC_{50} values in the nanomolar range. Once a crystal structure of the binding site became available,[21] structure based drug design allowed for more potent molecules with favourable pharmacokinetic properties to be identified. GlaxoSmithKline (GSK) developed the first small molecule drug to be approved for phase 1 clinical trials, demonstrating a dose-dependent reduction in plasma levels of Aβ levels.[22] This data was soon

mirrored in results from other major drug companies including Roche, Eli Lilly, AstraZeneca, Takeda, and Merck. However, recent evidence has suggested that BACE1 cleaves multiple substrates other than APP, which in BACE1 knock-out mice could lead to the phenotypic side effects of schizophrenia-like symptoms.[22,23] Further study into the neuronal substrates of the BACE1 protease revealed 34 major substrates, indicating the wider role of BACE1 in cell communication.[24]

Despite these side-effects being initially classed as relatively minor, further problems arose when different BACE1 KO mice demonstrated epileptic seizures and neurodegeneration arising from disruption of sodium gated ion channels.[22] Further mouse studies have also indicated the need for BACE1 activity in general synaptic physiology.[25] More serious toxicological issues arose when the Eli Lilly BACE1 inhibitor, LY2886721, was withdrawn from clinical trials due to liver toxicity in patients, however it was unclear whether these effects were due to the drug itself, or effective BACE1 inhibition.[26] Roche were the next company to halt phase 1 clinical trials on this target without official explanation, with Merck also subjecting its compound MK-8931 through extensive preliminary safety reviews before continuing trials into phase 2/3, with the phase 3 studies expected to conclude by 2018.[27] Therefore, despite the encouraging evidence that BACE1 inhibition leads to decreases in Aβ plaques, there are many toxicological issues to be overcome before these drugs can reach the market, with doubts still raised as to whether these drugs will mainly be effective as a preventative treatment, or only applicable to early stage AD patients.[16]

Despite advances in the understanding of AD progression through identification of genetic mutations, the role of altered redox potentials in the brain, the amyloid β hypothesis and the cholinergic hypothesis, there are still no effective treatments to alter the progression of the disease. Further advancement in the understanding of this form of dementia is needed so that a treatment to stall the progression of, or indeed, cure Alzheimer's disease can be found.

1.1.2 - The ubiquitin proteasome system and Alzheimer's disease

The ubiquitin-proteasome system (UPS) has been identified as playing a possible pathophysiological role in the early and late stage progression of AD.[28] The UPS is central to various cellular processes such as apoptosis, endocytosis, and the degradation of intracellular proteins. Excess or misfolded proteins are identified and tagged with polyubiquitin (PolyUb) chains through a complex series of conjugating

enzymes; E1 Ub-activating, E2 Ub-conjugating, and E3 Ub-ligating enzymes.[29] The E3 enzyme attaches a single Ub, or PolyUb chain onto its target *via* the *C*-terminal Gly[76] residue of Ub, which then acts as a signal to the 26S proteasome to identify and degrade the target protein (Fig. 2). The proteasome catalyses protein degradation and is composed of thirty one different subunits including: the barrel shaped 20S proteasomal core complex which consists of seven-homologous subunits, and the 19S regulatory complexes which form a ring at the proteasome entrance, exerting chaperone-like activity by recognising ubiquitinylated targets.[30] Deubiquitinating enzymes (DUBs) are capable of removing the PolyUb tags at various stages in the process; untagging target proteins in response to cellular feedback signals, or removing the PolyUb chain prior to target degradation to recycle ubiquitin monomers (Fig. 2). Through this system, levels of regulatory proteins are controlled to allow the cell to function normally.[31]
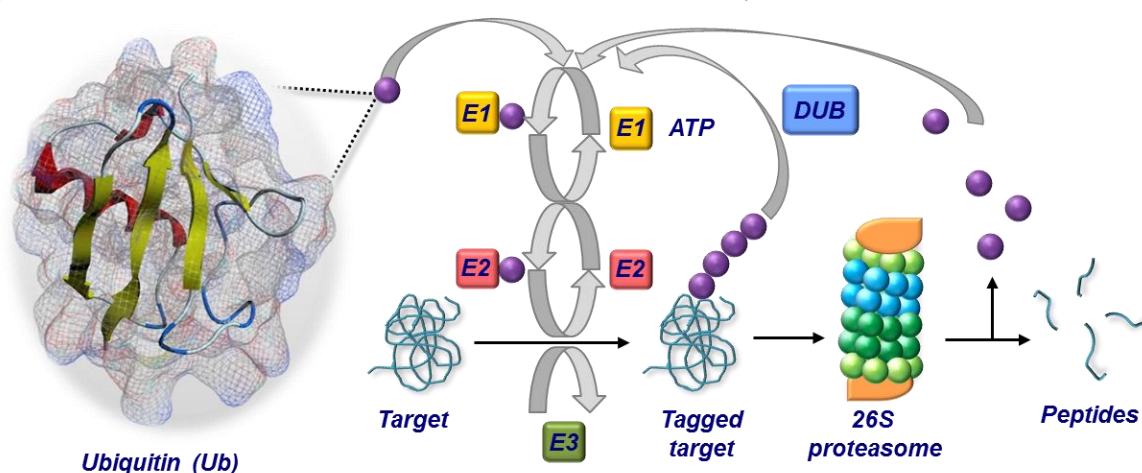
Figure 2 - The ubiquitin proteasome system

Purple spheres represent ubiquitin and how it becomes conjugated to the target protein via the E1, E2 and E3 enzymes. Tagged chains are recognised by the 26S proteasome. De-ubiquitinating enzymes (DUB) can remove polyubiquitin chains to give the free target.[32]

Impairment of the UPS has been considered as a factor in the formation of misfolded proteins which can lead to aggregation.[33] These aggregates can cause further proteasomal impairment as they are not recognised as natural substrates for the UPS. In AD, a significant decrease in proteasome activity has been observed,[34] however the exact mechanism by which this UPS dysfunction occurs is disputed. A recent genome wide association study also implicated protein ubiquitination as a potential AD therapy due to the presence of genetic markers of UPS malfunction in the brains of AD patients.[35]

Early evidence showed that ubiquitin was covalently conjugated with neurofibrillary tangles, yet these fibrillar structures showed resistance to proteasomal

degradation.[36,37] One proposed explanation as to why proteasomal function is impaired is that a mutant form of ubiquitin (Ubb+1) may contribute to the disruption of the UPS (Fig. 3).[38] Ubb+1 has been shown to accumulate in the neurones of patients with AD, with mouse models indicating high densities of Ubb+1 in INF tangles.[39,40] Mutations to ubiquitin such as this occur through mRNA editing, where genetic variability is produced from diverse modifications of RNA nucleotide sequences through an unknown mechanism.[41] Molecular misreading results in translation of the ubiquitin B precursor mRNA which has a +1 frameshift, resulting in the Ubb+1 protein which has a nineteen-amino acid extension but lacks the *C*-terminal glycine residue necessary for direct conjugation to proteins.[42]
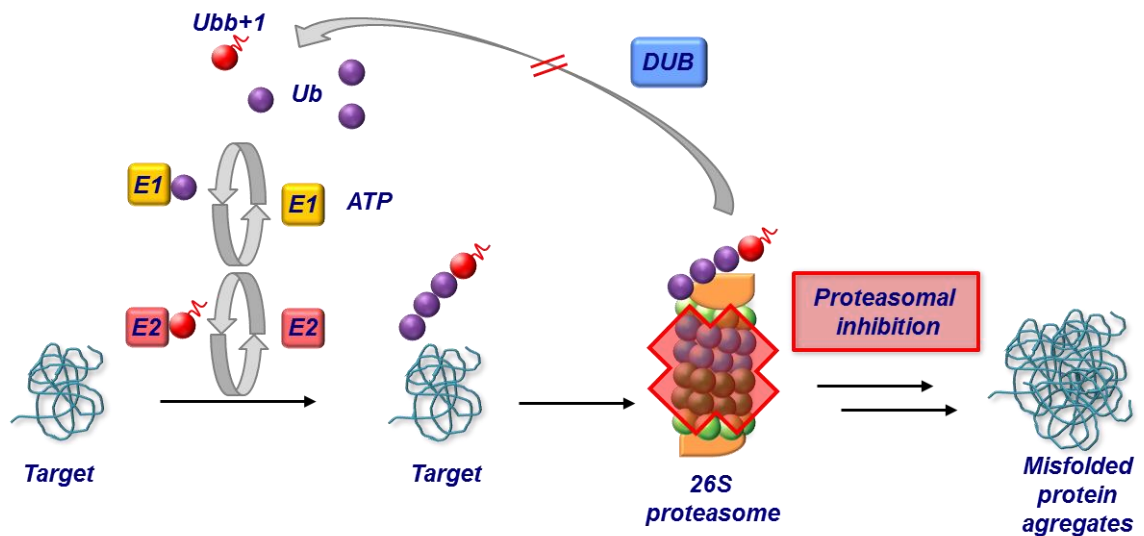
Figure 3 - Hypothesised mechanism of proteasomal inhibition by Ubb+1

This ubiquitin mutant is also not recognised and processed by deubiquitinating enzymes. It has been shown that Ubb+1 can itself be ubiquitinated *via* isopeptide bonds at Lys^{29} and Lys^{48}, yet in contrast to other ubiquitinated fusion degradation (UFD) products, the tagged mutant will not be degraded by the proteasome.[43] This is due to the nature of the *C*-terminal nineteen amino acid extension being too short to be recognised by the proteasome, which requires an unstructured polypeptide signal of twenty five amino acids minimum in order to process a UFD substrate.[44] Instead, the Ubb+1 mutant has been shown to be incorporated into unanchored polyubiquitin chains which are 100-fold more resistant to hydrolysis compared to normal unanchored polyubiquitin chains by DUBs such as isopeptidase T (Fig. 3).[45] It is these Ubb+1 capped polyubiquitin chains which have been demonstrated to inhibit the proteasome *in vivo.* [42] This inhibitory action was postulated as a complete block of the proteasome cavity, with the short *C*-terminal extension of Ubb+1 unable

to efficiently tether the UFD substrate into the active site.[42] Further accumulation of Ubb+1 was also shown to create a destructive feedback loop, where increased levels result in complete inhibition of the proteasome.[42,46] Regular unanchored PolyUb chains have also been shown to inhibit the proteasome through competition with target substrates, however normal levels are not considered toxic due to their degradation by isopeptidase T.[47] Despite the accumulation of Ubb+1 leading to proteasomal dysfunction, this inhibitory process has been shown to be reversible *in vivo*, with a concentration-dependent drift in action of Ubb+1 from inhibitor to substrate being possible.[46]

1.1.3 - Ubb+1 incorporation and neuronal degradation

If the action of the ubiquitin proteasome system is decreased or completely inhibited, then misfolded proteins and natural substrates will not be degraded, and cell function will be compromised. Such substrates include PS1 and PS2[45,48–50] which positively regulate amyloid precursor proteins, which can then be processed into Aβ in plaques.[51,52] This leads to the possibility that Ubb+1 capped PolyUb chains could be linked to the pathogenesis of AD, contributing to both Aβ and Tau pathologies (Fig. 4).

Figure 4 - The proposed role of the UPS in the pathogenesis of AD

Furthermore, the formation of aggregates could further initiate the Ubb+1 accumulation process which could ultimately lead to cell death.[42] Evidence has also shown the link between Ubb+1 associated proteasomal malfunction and mitochondrial damage, leading to the accumulation of cytotoxic basic amino acids.[53]

The mechanism by which the Ubb+1 mutant is incorporated into PolyUb chains could play a central role in Aβ neurotoxicity and restoring the UPS function in AD. In eukaryotic cells, the ubiquitin dependent proteolysis mechanism is initially activated by the ATP-dependent formation of a thiol ester between ubiquitin and the activating enzyme E1 (Fig. 2), followed by transfer of this activated ubiquitin to a cysteine residue at the active site of the ubiquitin conjugating enzyme E2. However, as Ubb+1 lacks the *C*-terminal glycine residue integral to this process, its incorporation into polyubiquitin chains must be mechanistically different. It has since been established that a widely expressed ubiquitin conjugating enzyme, known as E2-25K, can synthesise unanchored polyubiquitin chains *in vitro via* Lys[48] of ubiquitin and Ubb+1, independent of any E3 ligating action.[54]

Despite E2-25K having the highly conserved E2 core domain of one hundred and fifty amino acids, it has a unique forty seven-residue tail extension, or uniquitin associated domain (UBA), which was shown to contribute to the overall selectivity of the enzyme. It was shown that both the core residues and the tail were needed for optimum activity of E2-25K, with truncated derivatives only showing low rates of polyubiquitination. Another unique property of E2-25K is its ability to form cyclic unanchored polyubiquitin chains. Overall, the tail of E2-25K was initially thought to be the critical element in creating selectivity and catalytic activity, with the tail actually folding over the active site, forming a conformational recognition gate.[55] Direct links to Alzheimer's and Huntington's disease were also found as ubiquitination of E2-25K targets influenced aggregate formation, neurotoxicity and proteasome inhibition *in vitro*.[56–58]

Additionally, increased expression of E2-25K was also confirmed in the brain cells of AD patients.[56] Indeed, the presence of amyloid β peptide in cortical neurons was found to upregulate E2-25K, but not other E2 conjugating enzymes, in addition to an increased accumulation of ubiquitin conjugates (Fig. 4). Immunohistochemical analysis revealed that Ubb+1 was highly colocalised with E2-25K in the neuronal cells of AD patients, yet toxicity could be decreased if the Lys[48] of Ubb+1 was

mutated to Arg, implying that it is the E2-25K mediated incorporation of Ubb+1 into polyubiquitin chains that leads to proteasomal inhibition and eventual cell aptosis.[56]

1.1.4 - The E2-25K/Ubb+1 protein-protein interaction

Both X-ray crystal structural analysis and NMR studies of the E2-25K/Ubb+1 protein-protein interaction (PPI) showed that it was the E2-25K specific tail (or UBA) domain that interacts with Ubb+1, with no interaction between the mutant and the conserved E2 catalytic domain (Fig. 5).[59] This UBA domain consists of a three helical bundle from α7-α9, with α7 forming a hydrophobic core.
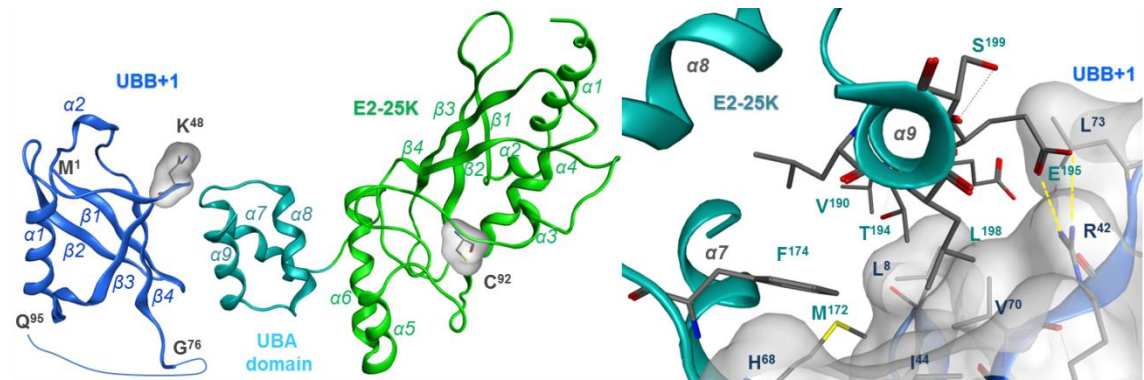
Figure 5 - X-ray crystal structure of the E2-25K/Ubb+1 PPI
Left diagram shows the interaction between Ubb+1 in blue and the tri-helical UBA domain of E2-25K in light green. Right diagram shows the residues involved in binding between the two proteins. PDB ID 3K9O.

The key interactions of this PPI were shown to be between the α9 helix and the α7-α8 loop of E2-25K with the hydrophobic surface of sheets β3 and β4 of Ubb+1 (Fig. 5) and Ub (not shown). In the case of the mutant, binding was similar to that of E2-25K/Ub PPI, except that the orientation of Ubb+1 was tilted by 15° due to a mutant specific interaction between Leu[73] and E2-25K. This binding mode differs greatly to most E2 enzymes where the active site is composed of the β4-α3 and α4-α5 loops in the conserved region of the protein, where Cys[92] is responsible for the conjugation of Ub. Mutations in the UBA domain (Met[172], Phe[174], Val[190], Thr[194] and Leu[198]) all disrupted the ability of E2-25K to bind with both Ub and Ubb+1 in NMR studies. These mutations also led to decreased neurotoxicity in cell death assays with Ubb+1, highlighting the correlation between disruption of the E2-25K/Ubb+1 PPI and reduced incidences of neuronal cell death.

In polyubiquitylation assays, complete deletion of the UBA domain of E2-25K resulted in the absence of long chain Ubb+1 unanchored polyubiquitin products, whilst wild-type E2-25K readily formed Ubb+1 unanchored chains.[59] These results indicate that the UBA domain is not essential for the action of E2-25K, as the UBA

deficient mutant could still form PolyUb chians of 2 or 3 units, but could potentially act as a directing group to facilitate formation of longer polyubiquitin chains. Proteasomal inhibition assays in mammalian cells showed that the E2-25K/Ubb+1 interaction impaired the UPS, most likely through the formation of Ubb+1 capped PolyUb chains. Overall, this work showed compelling evidence that there is a direct link between the E2-25K/Ubb+1 PPI and neuronal cell death, *via* impairment of the ubiquitin proteasome from Ubb+1 incorporated PolyUb chains.[59] With this structural and biological information in mind, it can be asserted that if the E2-25K/Ubb+1 PPI was disrupted by the action of an antagonist, then Ubb+1 incorporation into toxic long PolyUb chains would be decreased, potentially enabling the ubiquitin proteasome system to function normally. In the case of Alzheimer's disease, stopping proteasomal malfunction induced cell apoptosis and the downstream effects on Aβ induced neuronal cell death could create a positive feedback cycle in the treatment of the disease.

1.2 - Project overview

The aim of this project is to create a series of short helical peptides capable of antagonising the E2-25K/Ubb+1 PPI in order to further validate the hypothesis that incorporation of Ubb+1 into the ubiquitin proteasome system has a role in the pathogenesis of AD. This would demonstrate that antagonising this interaction has a beneficial effect in the progression of AD, and could lead to further interest in targeting this aspect of the UPS in a therapeutic sense.

The reasons for using a peptide as a potential tool molecule for this target, rather than a small molecule, will be explained in Section 1.3 below, as well as the synthetic methodology for creating such compounds (Section 1.4). The nature of the PPI surface and subsequent target recognition requires specific structural modifications of the peptide being synthesised in order to gain affinity for Ubb+1 (Section 1.5). More specifically, the peptide must be constrained in an α-helical shape, similar to that of the native substrate E2-25K (Section 1.14). Various techniques have been developed in order to gain this structural rigidification and have subsequently been reviewed in sections 1.4 – 1.7. The project utilises the all-hydrocarbon stapling approach (Section 5.7) to create stabilised helical peptides due to their precedented synthesis and emerging popularity as PPI inhibitors. This technique employs ring-closing metathesis (RCM) to create the macrocyclic tether which stabilises the peptide structure, therefore this catalytic technique has also

been reviewed in Section 1.6. Lastly, the various synthetic approaches available towards creating the requisite amino acid building blocks to create these bespoke peptides has also been reviewed in Sections 1.8.

1.3 - Ubb+1 as a drug target

In order to validate the concept that blocking Ubb+1 could slow down the progression of Alzheimer's disease, an effective antagonist of the E2-25K/Ubb+1 PPI is required. However protein-protein interactions are historically classed as undruggable targets due to lack of classical small-molecule binding sites on the protein surfaces.[60] The majority of approved small molecule drug targets are enzymes, ion channels, G-protein coupled receptors and nuclear hormone receptors. This is in part due to the relative abundance of ligand binding sites which can be characterised and screened in order to find efficient drug molecules. These active sites often lie in the interior of the protein, away from the solvent exposed exterior surface, and contain highly functionalised residues. The limitations of current small molecule therapies in targeting these pockets mean that only 20% of human targets are considered druggable.[61]

Traditional small molecule compound libraries tend to be inadequate in targeting PPIs due to the nature of the binding surface involved in the interaction, which is relatively flat and hydrophobic with an absence of pocket-like binding sites. Understanding into the nature of PPIs has shown that structural, kinetic and electrostatic interactions all contribute to surface binding.[62–66] PPI interfaces are mostly dominated by complementary hydrophobic interactions, in which these hydrophobic surfaces can slot together, leaving more hydrophilic residues accessible to solvent. Interfaces can range from surface areas of 750-3000 Å^2 and are structurally more similar to the protein core due to their hydrophobic nature and higher percentage of non-polar, or neutral polar residues.[67,65]

Binding at the E2-25K/Ubb+1 PPI is achieved through weak hydrophobic interactions between Leu^8, Ala^{46}, Gly^{47}, Ile^{44}, His^{68}, Val^{70}, of Ubb+1 with Met^{172}, Phe^{174}, Val^{190}, Glu^{191}, Thr^{192}, Thr^{194}, Leu^{198} of E2-25K, along with a salt bridge between Arg^{42} and Glu^{195} (Fig. 5). These interactions cover an area of roughly 400 Å^2, with six of the eight residues crucial for E2-25K binding present in α-9 of the UBA domain. (Fig. 6)[59]
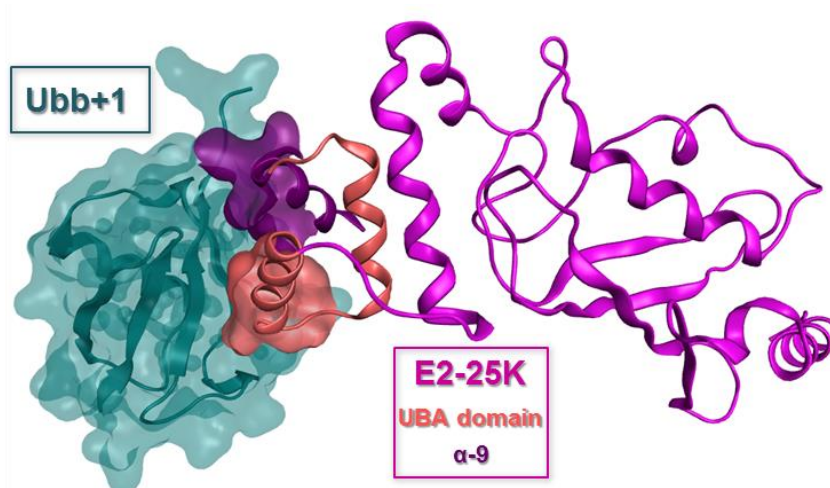
Figure 6 – Surface diagram of the E2-25K/Ubb+1 PPI
Ubb+1 shown in turquoise. Binding surface of the UBA domain of E2-25K highlighted. PDB ID 3K9O.

This is a relatively small surface area for a PPI but is consistent with the low binding affinity for Ubb+1 and E2/25K and many other ubiquitin system interactions.[68] For an antagonist of Ubb+1 to be successful, it would need to mimic these largely hydrophobic interactions over a large surface area as well as accounting for the topology of the binding site (Fig. 6).

1.3.1 - Small molecule inhibitors of PPIs

For small molecule inhibitors, the nature of a PPI surface becomes problematic as large hydrophobic molecules, which would bind well, are less likely to fit into drug-like guidelines due to their poor physicochemical and pharmacokinetic properties.[69] Extensive studies have been made towards the identification of hot spots at the protein-protein interface. Hot spots are defined as an area of less than 600 Å^2 around the centre of the PPI, which contains the residues which are deemed crucial for binding.[62,67] They tend to have a more favourable topology for small molecule binding, and can, through conformational flexibility, adopt a more conventional pocket-like site.[65] Small molecule inhibitors have been successfully developed in this way for various PPI targets. The Nutlin series of compounds were identified by Roche through screening and subsequently optimised against the p53/MDM2 interaction (Fig. 7).[70] In particular Nutlin-3 (**1**) has been used as a model compound in oncology research to investigate this interaction, as well as being patented as an MDM2 inhibitor for the treatment of ocular conditions.[71] HIV-1 integrase (IN) inhibitors have also been developed in a similar fashion from an initial hit compound for the PPI between HIV-1 IN and LEDGF/p57 through virtual screening of 200,000

commercially available compounds (**2**).[72] However, despite showing adequate potency, compounds which inhibit PPIs tend to be larger than most typical drug molecules due to the size of the interfaces being targeted.[64]
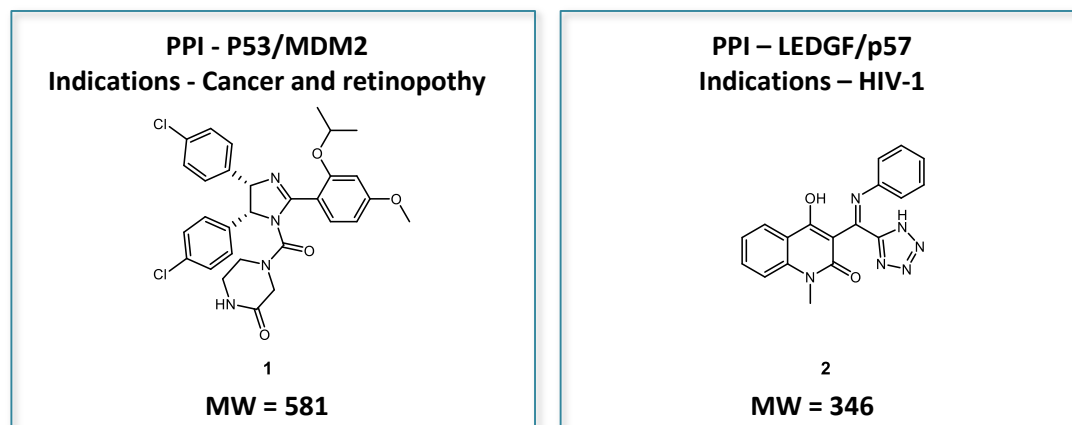
Figure 7 – Small molecule inhibitors of the HIV-1 LEDDGF/p57 PPI

This can cause difficulty when trying to achieve acceptable oral bioavailability and overall ADMET (absorption, distribution, metabolism, excretion, toxicology) profile of the molecule. Despite the few exceptions to the rule, most small molecule PPI inhibitors will require further optimisation for a balanced activity and pharmacokinetic profile.[67]

1.3.2 - Peptides as PPI inhibitors

Alternatively, small peptides have emerged as a successful method for targeting PPIs, using smaller analogues of the parent protein that can mimic the natural amino acid interactions to gain affinity and selectivity.[62,73] Peptides were historically viewed as poor drug candidates: rapid metabolic clearance by proteases mean that these molecules would have short biological half-lives. In addition, poor membrane permeability due to the polar nature of the amide backbone would decrease the likelihood of these therapeutics reaching their target *in vivo*, and low oral bioavailability allowing only intravenous dosage forms. However, recent developments in this area have led to a revival in their use as a result of new approaches to combat unfavourable physicochemical properties and improved drug delivery platforms (Sections 1.32, 1.6 and 1.7).[74] In 2012, six therapeutic peptides were approved in the USA[75] for diseases such as irritable bowel syndrome (Linzess®),[76] respiratory distress syndrome (Surfaxin®)[77] and Cushing's disease (Signifor®),[78] with their administration ranging from oral tablet, inhalation and subcutaneous injection, respectively. Drugs such as these have combined the

specificity and high potency of larger biologics with the metabolic stability and membrane permeability of small molecules.[79] The global peptide drug market is also expected to increase to \$25.4 billion in 2018 due to the increasing presence of peptide therapeutics, with one hundred and forty peptides in clinical development.[80]

1.4 - Solid phase peptide synthesis

Advancements in solid phase peptide synthesis (SPPS) have made synthetic peptides much more accessible for pharmaceutical research, with long and synthetically difficult sequences now commercially available, often on large scale.[81] The technique, which was pioneered by Merrifield in 1963, builds the polypeptide chain from the *C-* to the *N*-terminus stepwise on a solid supported resin (Fig. 8).[82]
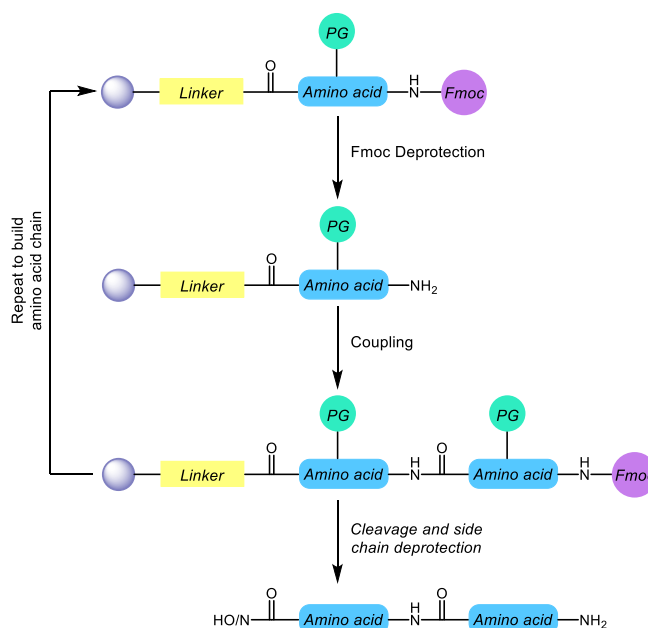
Figure 8 - Simple solid-phase peptide synthesis
Basic Fmoc deprotection and coupling steps are repeated until amino acid chain is complete. Simultaneous side chain deprotection and resin cleavage can then take place to give the free peptide.

This methodology was soon adapted and improved to become a fast and straightforward process compared to previous solution phase approaches. Full automation of the chain building process is possible using SPPS instruments in which the deprotection and coupling steps are carried out sequentially (Fig. 8).[83] By using 9-fluorenylmethoxy carbonyl (Fmoc) *N*-terminal protecting group chemistry,[84] the chain building process is carried out at a basic pH, with each subsequent Fmoc deprotection and coupling step using organic bases such as piperidine and DIPEA, respectively.[85] During this process, amino acid side chains, such as alcohols, acids and thiols, are protected using base stable groups such as O*t*Bu and Trt.[84] Following chain assembly, strong acidic conditions, commonly 95% TFA, are used to cleave

the peptide from the solid support. At this point in the synthesis, acid-labile side chain protecting groups are concomitantly removed to give the completed peptide. With careful consideration of resin type, protecting groups, coupling reagents, cleavage conditions and purification methods, sequences of up to seventy residues can be prepared on reasonable scale *via* this method.

1.4.1 – Resin development in SPPS

Numerous resins and linkers have been developed for use in SPPS, thus offering versatility in the process in terms of reaction scale and cleavage conditions (Fig. 9). For a majority of resins, a 1% divinylbenzene cross-linked polystyrene solid support is used (Fig. 9).
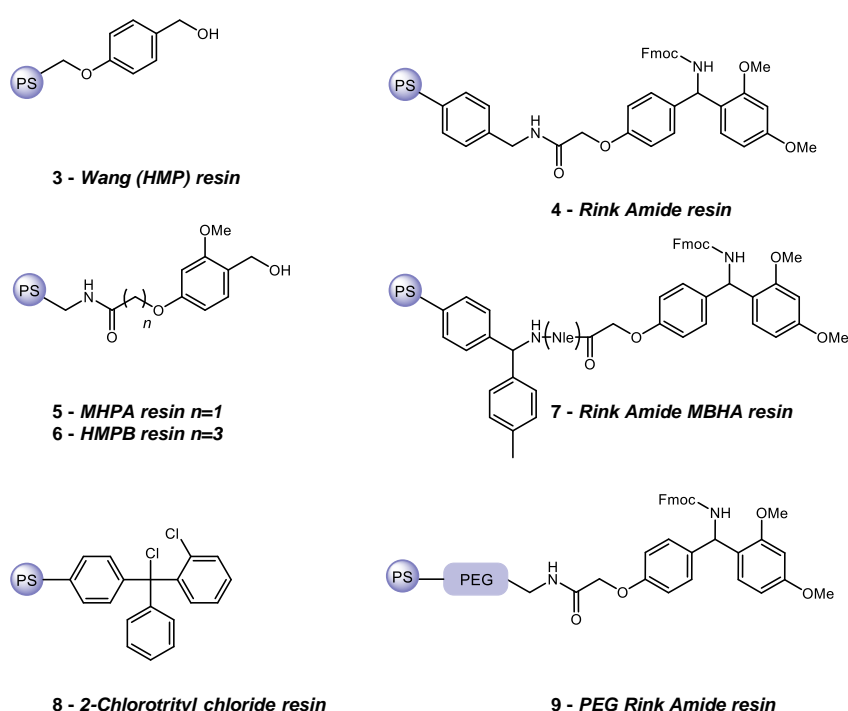
Figure 9 - Commonly used resins in Fmoc SPPS

This polymer is relatively inexpensive, can swell in solvents commonly used in the SPPS process (namely DCM and DMF)[86] and can be readily functionalised using Friedel-Crafts type chemistry to give polymers with bespoke linker moieties.[87] Derivitisation in this way has allowed for resins which cleave peptides with differing *C*-terminal functional groups, have a range of reactivity towards acidolysis, or allow for nucleophillic *C*-terminal modification.[87] Resin bound benzyl alcohol groups, such as those used in Wang (**3**) and MHPA (**5**) resins are derivatised with the first amino acid *via* esterification, and are post-synthetically cleaved to give peptides with *C*-

teminal acids. For peptides which undergo acidolysis to *C*-teminal amides, resins such as Rink amide (**4 & 7**) are employed. As with the Wang type resins, the precise nature of the linker and polymer support can vary the loading, and effectiveness of the cleavage reaction. For example, MBHA Rink amide resin furnishes amide products of greater purity than the standard AM Rink resin.[86] Depending on the nature and route of peptide synthesis chosen, milder cleavage conditions may be required to free the peptide from the solid support. Resins based on trityl linkers, such as the 2-chlorotrityl chloride resin shown (**8**) were developed for this purpose as they offer milder cleavage conditions of 1-5% TFA in DCM. These hyperlabile resins are valuable in the preparation of fully protected peptide fragments. For longer and more difficult sequences the distance between the resin and the point of chain assembly is an important factor to be considered. The longer this distance, the more solution-like the chemistry can become, allowing for better solvation of the peptide which in turn will prevent chain aggregation.[87] Too high a loading can also hinder the peptide chain growth for the same reason, with the resin surface becoming crowded, decreasing peptide solvation and increasing the probability of aggregation. Therefore, to overcome this problem, polyethylene glycol linked resins were developed in order to provide a solid support with a spacer unit between the resin and the linker (**9**), with swelling properties to allow for better solvent compatability.[87] These resins can be derivitised using the same linkers as polystyrene based resins, allowing for similar functionality such as the Wang and Rink amide (Fig. 9).

1.4.2 – Fmoc protection strategy

Once the first residue has been attached to the resin (the precise techniques used are sequence and resin dependent), the stepwise process of chain assembly can begin. Using the Fmoc strategy has not only enabled the deprotection step to be carried out under mild conditions, but also the use of UV monitoring to follow the progress of each coupling reaction.[85] Reactions carried out on a solid support are primarily monitored using IR and UV techniques as polymer resins preclude the routine use of spectroscopic techniques such as NMR and MS. Accordingly, the highly UV active adducts formed during *N*-terminal deprotection, such as the fulvene-piperidine (**10**) shown in Scheme 1, can be used for both qualitative and quantitative analysis of the deprotection step *via* UV monitoring through use of the Beer-Lambert law. As SPPS is carried out on a solid support, all soluble adducts can be washed off of the resin surface, leaving the clean peptide ready for the next

stage of synthesis. This enables the use of a large excess of reagents, driving the reactions to completion in shorter times.
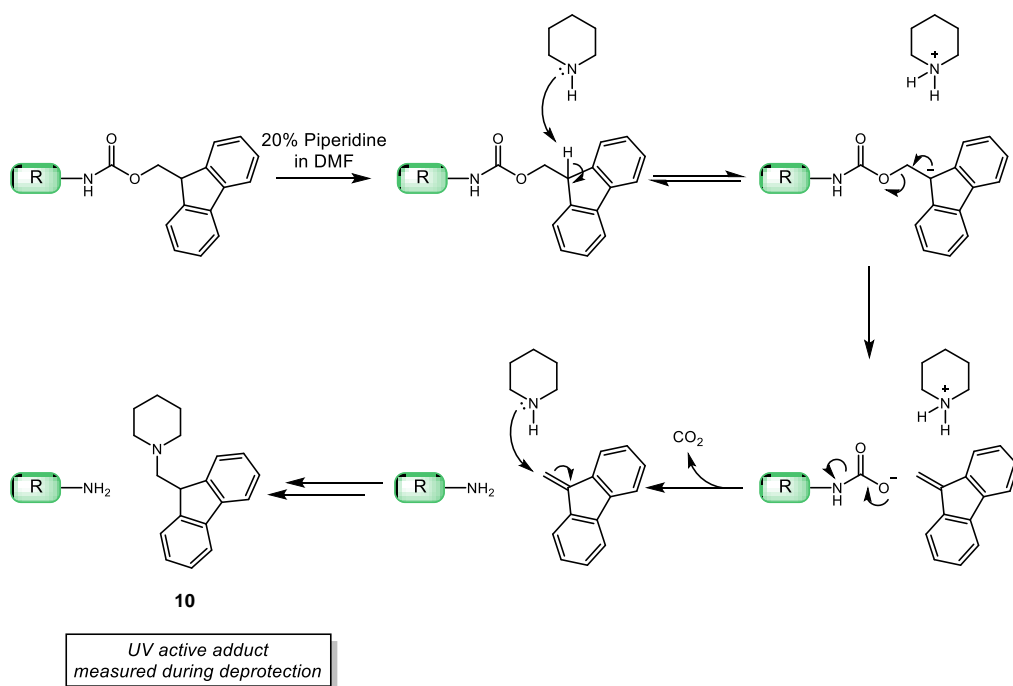
Scheme 1 - Fmoc deprotection mechanism

During Fmoc deprotection, the dibenzofulvene and piperidine-fulvene adducts shown can be difficult to remove when the reaction is carried out in the solution phase, often requiring multiple aqueous washes and coordinating amines.[88] However, these problems are overcome in the solid phase as these adducts can be simply washed away and the resin isolated by filtration, allowing for an efficient deprotection step.

1.4.3 – Amide coupling on the solid phase

The next stage in solid phase peptide synthesis is the amide bond coupling between the resin bound amine and the next carboxylic acid in the target sequence. The reagents and synthesis protocols for peptide couplings have significantly advanced since SPPS was first devised, with practitioners now having a plethora of coupling reagents available. The main obstacles which occur during amide bond formation are racemisation of the α-centre, and sufficient activation of the acid to allow attack from the incoming amine.[86,89] The proteinogenic amino acids commonly used in peptide chemistry are all stereospecific, with the natural form being the *L* enantiomer. The backbone configuration can be crucial to downstream biological activity; therefore, epimerisation of these chiral centres can be a major problem in peptide synthesis. The first mechanism by which racemisation can occur is removal

and reattachment of the α-hydrogen species which is more acidic once the carboxy group has been activated. A more problematic side reaction resulting in epimerisation is *via* formation, deprotonation and ring-opening of an oxazolone intermediate (**11**, Scheme 2).[86,89] By using carbamate *N*-protecting groups, such as Fmoc, the likelihood of oxazalone formation is reduced due to its electron donating properties.[89] Coupling techniques such as the use of acid chlorides are also avoided during peptide chemistry due to the increased probability of epimerisation *via* either of the routes discussed (Scheme 2).[86]
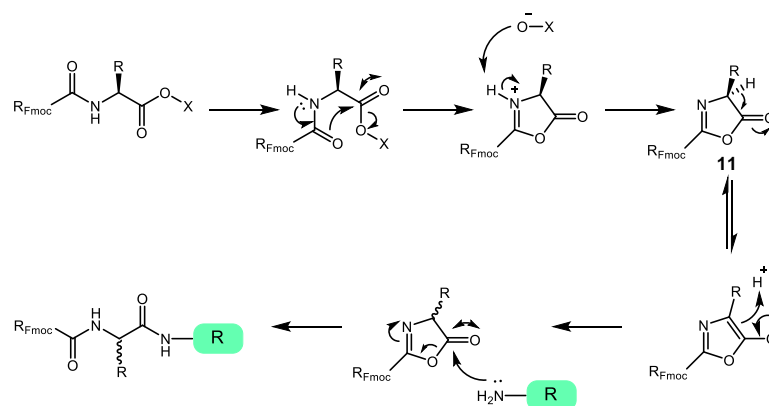
Scheme 2 - Oxazolone mediated epimerisation

Based on this, the use of bulkier coupling reagents has been popularised due to their high rates of amino acid activation at room temperature and corresponding low rates of epimerisation.[89] For automated SPPS, these coupling reagents are also required to work for a wide range of amino acids, be soluble in DMF, be stable in solution at high concentrations, have soluble by-products, and be produced in large quantities.[90] Carbodiimides, such as DCC (**12**, Scheme 3), which were traditionally used in amide bond formation were soon shown to be incompatible with Fmoc SPPS chemistry as the main by-product formed, *N,N'*-dicyclohexylurea, is only soluble in TFA and therefore difficult to separate from the resin without cleavage of the peptide.[89] Carbonyl diimidazole (CDI) (**18**) emerged as a useful reagent in SPPS as it does not require excess base to form the activated acid. Despite pre-activation times of up to an hour, this method can be used on large scale in peptide synthesis, with the main by-products being carbon dioxide and imidazole.[89] *N*-hydroxy based additives, such as HOBt (**16**)[91] and HOAt (**17**)[92] (Fig. 10) were soon used in conjunction with carbodiimide based couplings (Scheme 3). These compounds created active esters (**15**) through reaction with the *O*-acylisourea (**13**) intermediate formed, subsequently increasing rates of reactions, decreasing *N*-acylurea (**14**) by-products and minimising racemisation.
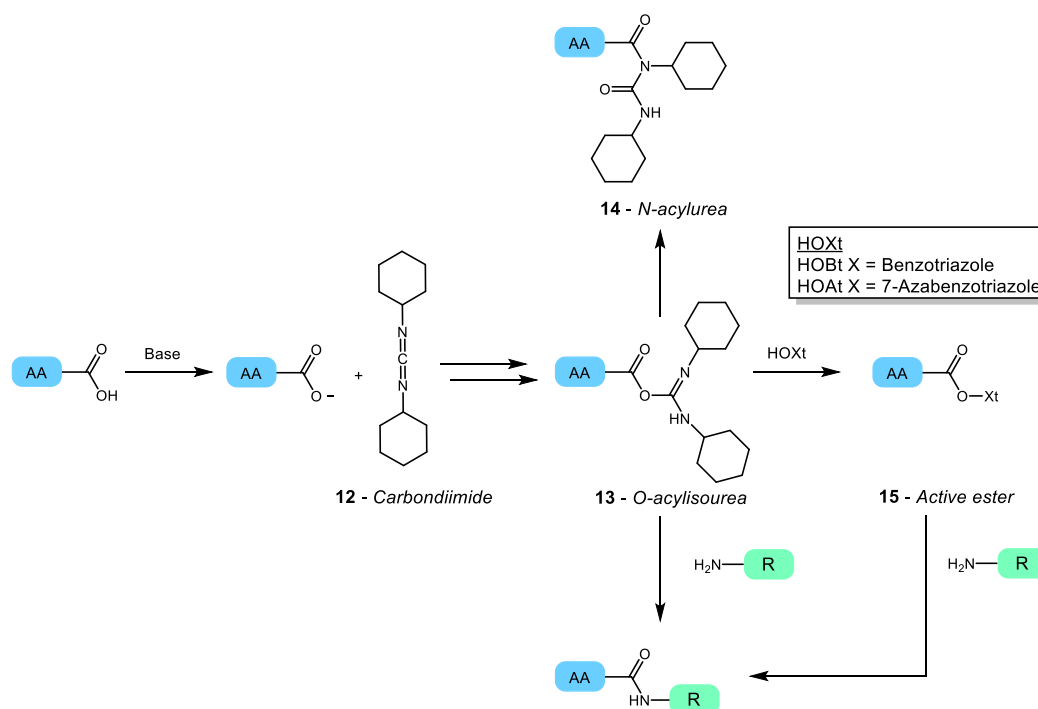
Scheme 3 - Carbodiimide mediated peptide coupling

HOAt (**17**) was shown to be superior to most additives, giving high yields in both solution and solid phase synthesis. This was due to the presence of the nitrogen at position 7 in the benzotriazole which has the additional effect of improving the ability of HOAt (**17**) as a leaving group through its electon-withdrawing properties, and increased reactivity by acting as an H-bond acceptor to the attacking amine.[89] However HOAt and HOBt could not be used on large scale due to their potentially explosive nature, being of low molecular weight and containing 3-4 consecutive nitrogen atoms.[93] The next generation of coupling reagents were designed by combining the desirable features of the *N*-hydroxybenzotriazoles with active phosphonium (BOP (**19**)[94] and PyBOP (**20**)[95]) and uronium (HATU (**22**),[92] HCTU (**21**))[96] salts to give highly active but more stable compounds (Fig. 10). BOP (**19**) was one of the earliest of the HOBt salt derivatives to be developed, however, despite its excellent coupling ability, it became unpopular due to the toxic HMPA generated as a by-product.[97] Oxyma based uronium salts such as COMU (**23**) have also become popular due to their non-explosive, efficient couplings.[98] However, of the plethora of coupling reagents available, HCTU (**21**) and HATU (**22**) have become extremely commonplace in SPPS due to their fast, efficient coupling of both simple and sterically hindered amino acids.[99]
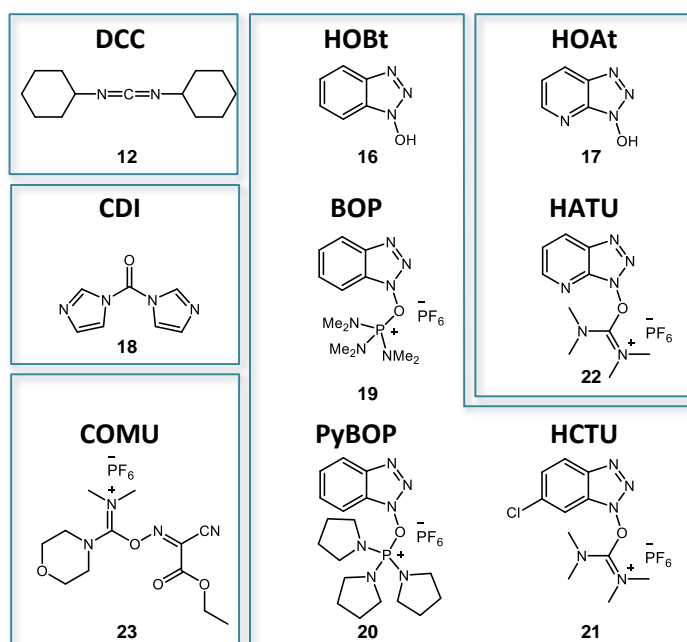
Figure 10 - Commonly used coupling reagents in SPPS

Extensive studies into the efficiency of various coupling reagents for fast reaction times or difficult sequences have consistently shown that HATU (**22**) and HCTU (**21**) are the best activators for SPPS.[100,101] In 2002, a study into the synthesis of traditionally difficult sequences by SPPS showed that HCTU (**21**), the far cheaper of the two uronium based reagents, to be comparable to HATU (**22**) in producing high yields in automated peptide synthesis.[102] However, phosphonium salts such as PyBOP (**20**) consistently coupled less efficiency by comparison. These results were reinforced by similar studies in 2008 and 2011 in which HATU (**22**) and HCTU (**21**) gave comparable peptide purities, even when using fast coupling times of 5 minutes on a range of sequences.[100,101]

The mechanism by which reagents such as PyBOP (**20**), HATU (**22**) and HCTU (**21**) activate amide bond formation is very similar (Scheme 4). In the case of HATU (**22**), an equivalent of base is needed to first deprotonate the acid, allowing for attack onto the most electron deficient centre at the uronium. The HOAt anion released (**24**) can then attack the reactive *O*-acyl(tetramethyl)isouronium group to give the HOAt active ester (**25**). As discussed previously, a neighbouring group effect arises from the pyridine nitrogen atom, stabilising the conformation of the incoming amine, forming a 7-membered cyclic transition state (**26**). This effect, coupled with the strong leaving group of HOAt, allows for efficient attack of the amine into the carbonyl centre, giving the required amide bond.[89]
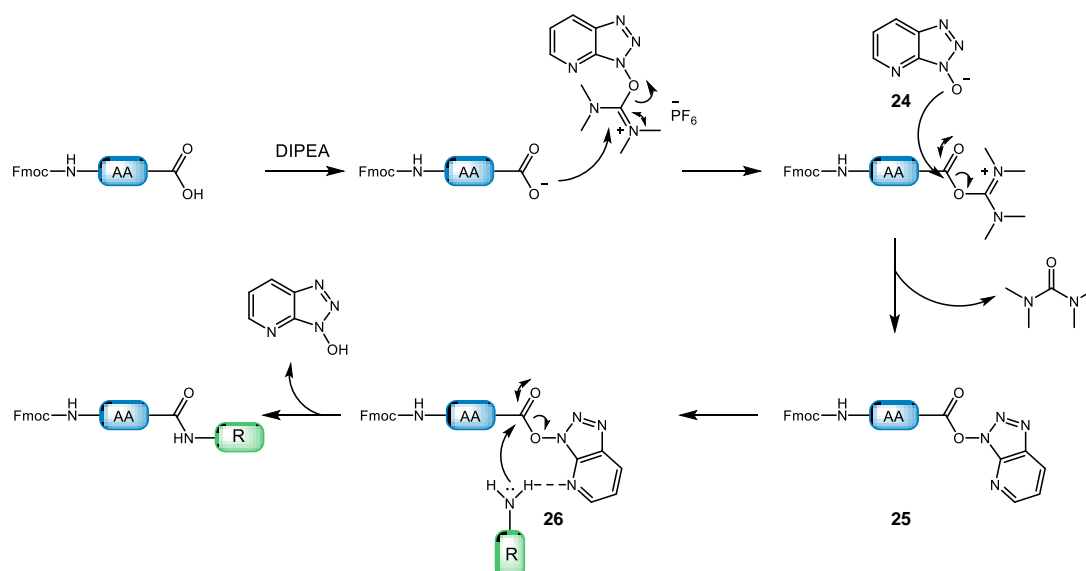
Scheme 4 - HATU mediated SPPS amide bond formation

Once the peptide chain has been assembled the *N*-terminus can be deprotected to give the free amine, or capped with acetic anhydride to give the acetamide (Scheme 5).
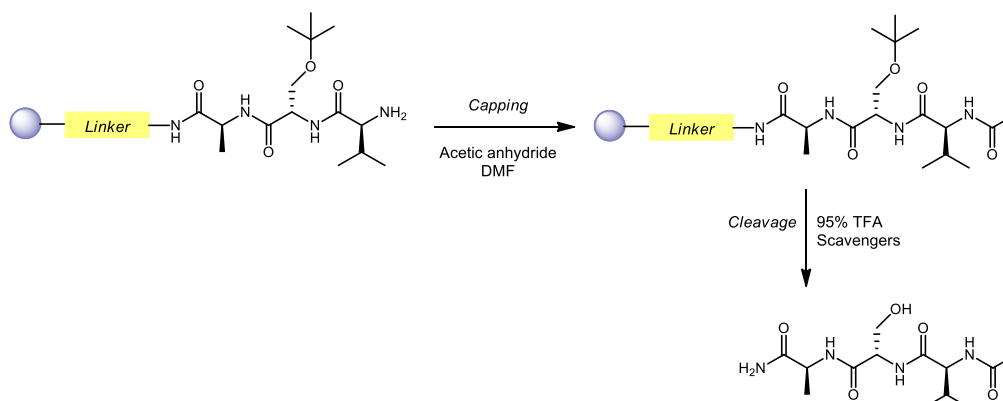
Scheme 5 - Example of resin cleavage

Rink amine resin bound tripeptide NH$_2$-Ala-Ser-Val-Ac shown

The final cleavage from the resin requires strongly acidic conditions, most commonly 95% TFA unless a trityl or other acid labile resin is being used. Scavenger reagents such as triisopropyl silane, ethane dithiol and ammonium iodide are also added to the reaction mixture at this stage in order to prevent by-products of cleaved protecting groups, such as the *t*Bu cation, from reacting with the free peptide. Once the reaction is complete, the reaction mixture can be filtered into cold diethyl ether to separate the resin beads and precipitate the peptide as a white solid. Centrifugation, ether washing and preparative HPLC can then yield the target peptide, which is

analysed by mass spectrometry and analytical HPLC for purity along with other techniques depending upon the sequence of interest.

Advancements in resin and linker design, efficiency of coupling reagents and choice in protecting group chemistry has positioned SPPS as a fast and efficient process for the synthesis of short peptides. Using chemical synthesis to create short peptides offers advantages over recombinant technologies: unnatural amino acids may be simply incorporated into peptide chains using SPPS, giving the final peptide greater side chain functionality or backbone stability compared to a natural analogue, as well as the use of pseudo-peptide bonds and cyclisation techniques to create greater chemical diversity.[103]

Techniques such as these have been shown to increase the metabolic stability of pharmaceutically active peptides, overcoming the short half-lives expected due to proteasomal degradation.[74] The stepwise process of SPPS also allows for a therapeutic peptide to be diversified reasonably quickly enabling optimisation of, for example, potency and bioavailability, through altering the sequence by inversion of stereochemistry or replacement of amino acid residues.[74] As a result of this, interest in synthetic therapeutic peptides has increased in the pharmaceutical industry as tools for structurally diverse biological systems.[79] Of particular interest, and as previously mentioned in Section 1.3.2, is the application of peptides as inhibitors of PPIs due to their ability to complement the large hydrophobic surface of a PPI interface, whilst maintaining binding affinity by mimicking the natural non-covalent bonding interactions.[79] Unfortunately, designing a peptide PPI inhibitor is not as simple as creating a linear peptide of matching sequence to the natural protein and this is expanded upon in subsequent sections.

1.5 - Helical peptides as PPI antagonists

Designing a peptide antagonist for a particular PPI requires a level of understanding of the non-covalent forces present at the protein-protein interface when using the natural protein as a model system. To gain the surface recognition needed to bind with the target, the shortened peptide must have the same sequence and structural topology as the parent enzyme. However, in cases such as the E2-25K/Ubb+1 interaction, the section of E2-25K at the interface has a well-defined α–helical secondary structure (Section 1.1.4). It has been shown that helical interfaces are involved in 13% of the protein structures present in the protein data bank (PDB).[104] This correlates with the fact that α-helices account for the largest class of secondary

structure present in protein-protein interactions, with helix length increasing with the size of the interface.[105] The average helix length for a PPI was also found to be fourteen residues long, with the mean being ten residues.[104] The interface helix of interest to the current study, α-9, of E2-25K is eleven residues long and spans from Val[190] to Asn[200] (Fig. 11). Hydrophobic residues make up 34% of interface interactions,[106] which is reflected in the composition of α-9 of E2-25K however, somewhat unusually, it contains no aromatic residues which in general account for a further 27% of residues at PPI interfaces.[106] It is also interesting to note that only five residues are making close interactions with Ubb+1, whilst two have weak interactions (Shown by light blue and dark blue highlights in Fig. 11, respectively).
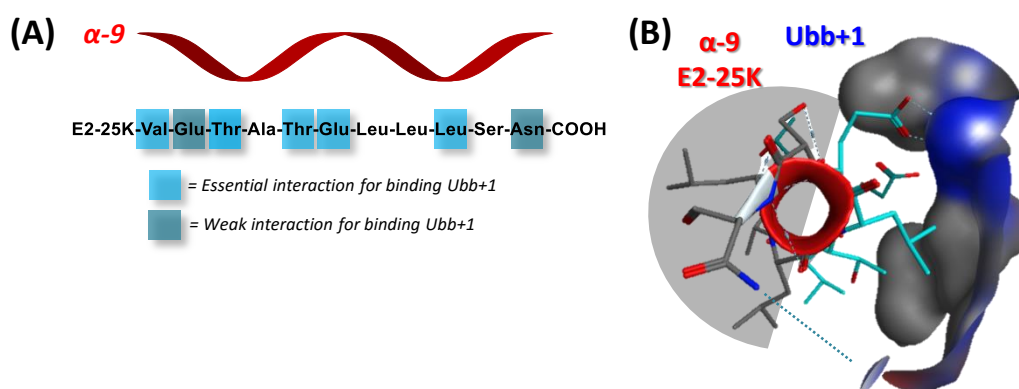
Figure 11 – Binding of helice 9 of E2-25K with Ubb+1
A) Amino acid sequence of α-9 of E2-25K with residues essential for binding with Ubb+1 highlighted. B) Close up image of α-9 binding with Ubb+1 with essential binding residues highlighted in blue. Grey area shows 2 faces of the helix which are not involved in substrate binding.

On average seven residues per PPI are deemed essential for binding,[105] further accounting for the fact that E2-25K and Ubb+1 have a low binding affinity for each other.[68] Therefore, for a small peptide analogue of α-9 to have reasonable affinity for the target, it will need to mimic this helical shape so that the binding residues can interact with Ubb+1 in the correct way.

1.5.1 - Properties of helical peptides

If a small peptide corresponding to the α-9 helical binding domain of E2-25K (e.g. **27**, Fig. 12) was synthesised, it is unlikely that it would exhibit the same secondary structure as the parent protein in solution. Indeed, peptides with sequences derived from α–helical motifs energetically favour random coil formations despite any side chain stabilisation, Van der Waals interactions and back-bone hydrogen bonding properties that should help stabilise the helix.[107,108]

Ac-Val–Glu-Thr-Ala-Thr-Glu-Leu–Leu–Leu-Ser-Asn–CONH₂
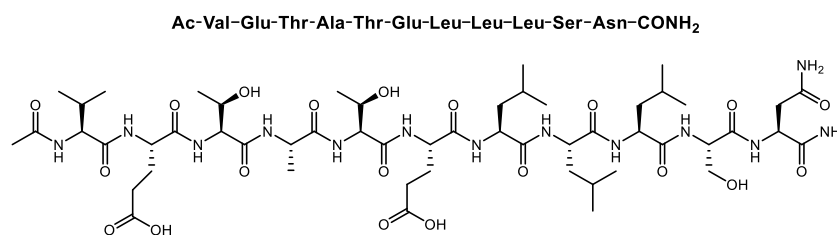
27

Figure 12 – Small peptide analogue of the parent sequence of α-9 E2-25K

For the Wild type peptide (Fig. 12), a simple technique to create a more helical assembly is to cap the *N*-terminus with an acetyl group (Ac), and to cleave the *C*-terminus as an acetamide rather than the free carboxylic acid. This gives the sequence two terminal amide bonds in addition to the ten bonds linking the amino acids, effectively constraining the terminal backbone angles. For short peptides, having unconstrained end groups can make formation of a short helix difficult, with stability instead being dependent on the number of residues present.[108] Structurally, the spiral shape of an α–helix is formed due to hydrogen bonding in the backbone every three to four residues, giving backbone dihedral angles of φ = -60° and Ψ = -45° (Fig. 13).
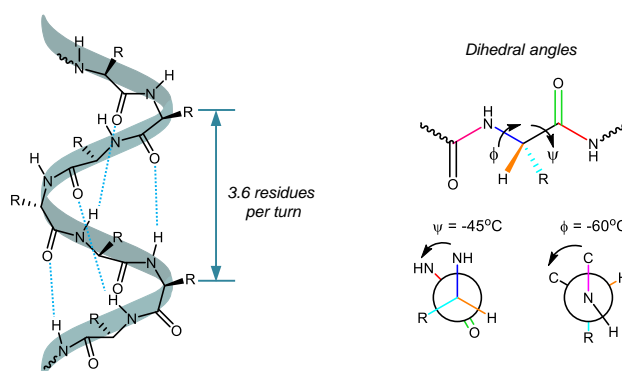
Figure 13 – Properties of the α-helical backbone
Hydrogen bonds shown by the blue dotted lines

For peptides, there is an energetic cost to helix formation as four residues must be constrained to form the first hydrogen bond (Fig. 13), termed helix nucleation. In helix-random coil transition models, once nucleation has occurred, formation of an additional hydrogen bond only requires the conformation of one additional residue.[109] Each turn of the spiral consists of 3.6 residues, meaning every three to four residues sit on top of each other, giving the helix essentially four-faces. With α-9 of E2-25K, the residues which are crucial for binding to Ubb+1 all lie on one half (2 faces) of the helix (Fig. 11) which is common for side chains crucial to any PPI

interface. Side chains in the helix point towards the *N*-terminus and can play an important structural role in encouraging helix formation. Certain amino acids, such as Met, Ala, Leu, Glu and Lys have a preference for helical conformations whilst others, such as Pro and Gly, do not,[109] which correlates with the helix in the present study where 45% of the residues contained in α-9 are helix inducing.

1.5.2 - Stabilisation of helical peptides

PPIs with helical interfaces have been considered the most tractable PPI targets due to their ordered structure,[104] therefore in the past two decades many advances have been made in creating stabilised short helical peptides, with various techniques developed to drive small peptides into helical conformations rather than random coils. Some of these approaches are summarised in the following sections.

1.5.3 - Hydrogen bond surrogates

Advances in the field of helical stabilisation led to the development of hydrogen bond surrogates (HBS). By using a covalent linker between the *i*, *i*+4 positions to mimic the backbone hydrogen bonding of an α-helix (Fig. 13), it was thought that helix nucleation in water would be established to give a stable conformation.

Initial work into this approach in 1999 proposed a hydrazone linker to replace the hydrogen bond (**28**, Fig. 14).[110] As these intermolecular bonds are relatively flexible, this hydrazone linker was required to adapt to different angles and conformations depending on the protein sequence.
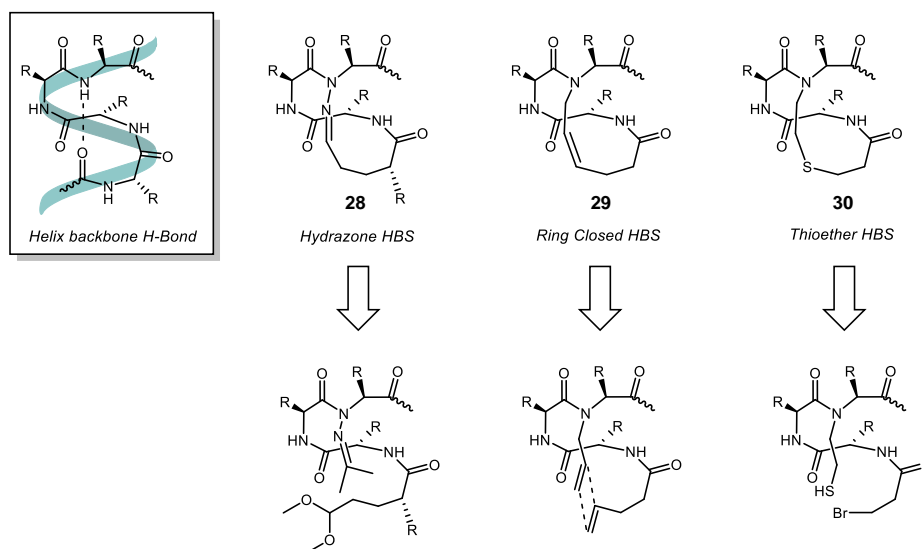
Figure 14 – Hydrogen bond surrogate linkers[110–112]

The thirteen-membered ring formed was designed to give one stable helical turn to potentiate further helical formation along the peptide chain. The requisite building blocks, 5,5-dimethoxy-1-oxopentanoic acid and (1-methyethylidene-2-Fmoc)hydrazinoacetic acid, were incorporated by solid phase synthesis into the peptide chain and further cyclised on the solid support using 20% TFE in DCM (Fig. 14). NMR analysis of the cleaved peptide showed increased helical stabilisation in water at ambient temperatures compared to the linear analogue. The group were able to successfully initiate helix formation using a quick and convenient synthesis showing that the hydrazine link was a sufficient hydrogen bond mimic.[110]

The hydrogen bond mimic approach was extended in 2004 when the cross link was created using ring-closing metathesis (**29**, Scheme 14).[111] The utility of RCM in creating peptide macrocycles had already been explored by Grubbs in 1997 (Section 1.6.3) and was shown to have the exceptional functional group tolerance needed when applied in the context of solid phase peptide chemistry (Section 1.6.3, Scheme 15). Incorporation of olefinic side chains at the *i, i*+4 positions, similar to the previous hydrazine HBS,[110] using solid phase peptide synthesis allowed for a resin bound ring closing metathesis to create a single helical loop (**29**, Fig. 14).[111] Initial eight-mer constrained peptides were shown to have up to 100% helical conformations by circular dichroism (CD) and NMR spectroscopy compared to the linear peptides which showed no helical structure. NOE studies indicated that the most helical peptide had no frayed edges and was completely constrained due to the hydrogen bond surrogate, despite nucleation probability of peptides less than 10 residues long being extremely unlikely based on helix-coil transition theory.[108] Overall, SPPS of these thirteen-membered macrocycles overcame the nucleation barrier for helix formation, however, the RCM step was low yielding (~55%) and required elevated temperatures (50 ^{o}C) for the reaction to proceed. Further work by the same group employed this HBS cross linking method to stabilise biologically significant peptides into helical conformations, including sequences with no helix forming indicators. These stabilised helices were shown to have increased thermal stability, retaining 60-70% helicity at 85 ^{o}C.[113]

Due to the problems encountered with the RCM of the olefin chains discussed above, a thioether linked HBS (**30**) was designed in 2012 to overcome the high catalyst loadings and elevated reaction temperatures required to generate the macrocyclic system (Fig. 14).[112] By utilising a nucleophillic substitution reaction, the

resulting thioether was designed to nucleate helical formation as before, but also to be stable in biological systems. It was interesting to note that after optimisation of the key cyclisation step, the resulting peptide was of a higher purity than previously synthesised HBS peptides. CD and NMR studies again showed the thioether link nucleated helix formation, with helicity up to 54%. This work also discussed the importance of these HBS helices to be able to interact with biological targets, in this case MDM2, to mimic a PPI. Fluorescence polarisation assays showed that the artificial HBS helix interacted with the target with a similar affinity as the natural peptide sequence. This work provided compelling evidence that synthetic HBS helices were capable of participating in natural PPIs in systems similar to those discussed above, as well as demonstrating the robust helical nucleation propensity of hydrogen bond mimics.[112]

1.5.4 - Side chain bridged helices

Despite the apparent utility of HBS stabilisation, the most robust and effective techniques developed to stabilise synthetic α-helical peptides has been the use of side chain bridges. Incorporation of natural or synthetic amino acids into the peptide chain *via* SPPS can allow for various covalent linkers to be formed across one or two turns of the helix, giving locked conformations which have been shown to be highly stable and biologically active in various contexts.

1.5.5 - Metal chelation

Natural proteins commonly use transition metals to stabilise their secondary and tertiary structures, creating tetrahedral coordination spheres from polar residues such as histidine and cysteine. This has been adapted to the stabilisation of helical peptides *via* coordination to residues on a single face of the helix. An early study used an exchange-inert metal complex to attempt stable helix formation of random coil peptides (Scheme 6). By creating a seventeen-mer residue peptide with histidine residues positioned three residues apart in the *i* and *i*+4 positions, they intended to form a macrocyclic $[Ru(NH_3)_4His_2]^{3+}$ complex (**32**) to encourage helix nucleation and stability.[114] The study demonstrated successful coordination of Ru^{3+} to the histidine imidazole units to form the desired complexes. Overall, the metallopeptides had more locked conformations, exhibiting up to 80% helicity as determined by CD spectroscopy.[114]
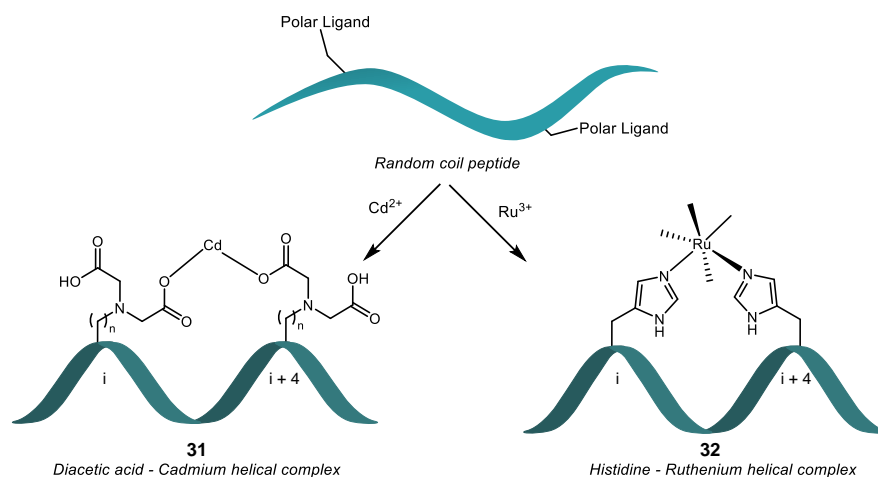
Scheme 6 - Helical stabilisation using metal chelation[114,115]

A related study screened various transition metals as cross-linking agents to establish if they improved the coil-helix equilibrium through coordination to diacetic acid side chains (**31**).[115] The results showed that the helical content of the peptides were strongly dependent on spacing between the chelating residues, tether length and the metal ion present. In one particular case, helical content of a short eleven-mer peptide was increased to 80% when the tethered residues lay in the *i* and *i*+4 positions, and complexed with Cd^{2+} to form a twenty four bond macrocycle. It was demonstrated that peptides which should have had negligible helical content from their primary sequence could be forced into predominantly helical conformations *via* this form of metal chelation.[115] These early investigations into helical peptide stabilisation provided the proof that side chain modification and cross linking could yield stable secondary structures. However, these systems were only valuable for structural investigation, as metal chelation would not be amenable to biological systems due to their potential toxicity.

1.5.6 - Lactam bridges

Taking inspiration from the natural non-covalent interactions that hold protein conformations in place, the use of salt bridges at the *i*, *i*+4 positions evolved into an effective bridging technique to stabilise helical structures (Fig. 15). Initial work tested the helix stabilisation on Glu^- / Lys^+ salt bridges at the *i*, *i*+3 and *i*, *i*+4 positions in aqueous conditions (**33**).[116] The interaction between these oppositely charged side chains was shown to lock the conformation of the peptide, with the *i*, *i*+4 substituted peptides showing the greatest helical content of 80%. However, the helical structure was shown to be strongly temperature dependent, with the salt bridge interaction not

being strong enough to prevent unfolding of the helix with increasing temperatures.[116]
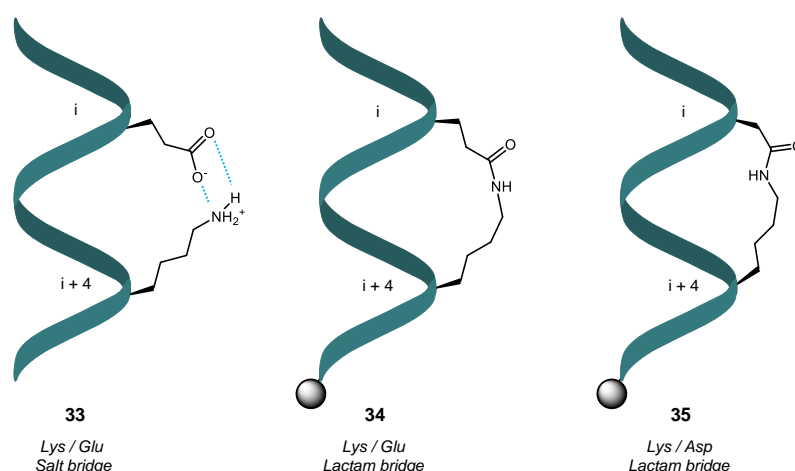
Figure 15 – Salt and lactam bridged peptides using natural amino acids [116–119]

To overcome this thermal instability, the next step was to covalently link these side chains to form a lactam bridge (**34**, **35**). Subsequently, it was demonstrated that a Lys / Asp lactam bridged peptide was 5-10 fold more potent towards the PTH receptor than the linear analogue (**35**).[117] Despite no data indicating the extent of the helicity, the implied conformational lock enforced by the lactamisation constrained the peptide into a bioactive conformation. Another interesting observation was that when the *i*, *i*+4 Asp / Lys residues were switched from *L-* to *D-* configurations, there was a significant drop off in biological activity, showing that either the receptor would only recognise the natural stereoisomer, or that the lactam link was under greater steric strain in this conformation due to clashing with neighbouring amino acids, decreasing helical stability.[117] Based on the above, a related study examined the effect of multiple Lys / Glu and Lys / Asp lactam bridges in a twenty one-mer peptide.[118] The peptide with three Lys / Glu bridges was shown to be 21% helical whilst the corresponding peptide with three Lys / Asp bridges was 69% helical compared to the model linear peptide at 13%. This was attributed to the shorter bridge length of the Lys / Asp peptide giving a more closely packed and stable structure (Fig. 15). This stability was further demonstrated in thermal denaturation studies which showed that even at 90 °C, the multiple Lys / Asp peptide was not completely unfolded and retained some degree of helical structure compared to the Lys / Glu analogue. Similar results were obtained in chemical denaturation studies which showed the Lys / Asp peptide retained most of its helical structure in up to 4M guanidinium hydrochloride solution. However, it was also noted that depending on

the biological target, a synthetic peptide with a longer, more flexible bridge such as the Lys / Glu link may be more appropriate for target binding than a tightly wound Lys / Asp helix, as excessive rigidity may diminish affinity for the site.[118] Lactam bridging (Lys / Asp, *i*, *i*+4) has also been used to stabilise a single turn of short pentapeptides to give water soluble, proteolytically stable, helical substrates.[120]

Another interesting approach to lactam peptide stapling uses a stepwise Glu deprotection strategy to give variable peptide staples (Scheme 7).
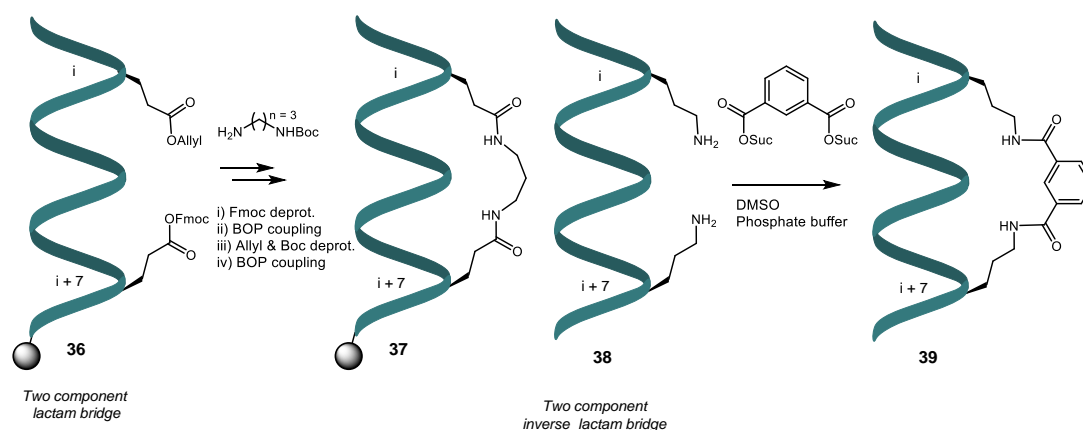
Scheme 7 - Two component lactam bridged peptides

By installing a Glu(OFmoc) and Glu(OAllyl) at the *i*, *i*+7 positions using standard SPPS (**36**), stepwise deprotection and amide coupling with alkyl di-amines gave bis-lactam bridged peptides on the solid phase (**37**, Scheme 7). Dependent on bridge length (n = 3, 4, or 5) these constrained helices were up to 100% helical in aqueous solution once cleaved from the resin.[119] A similar lactam system was developed, with installation of ornithine residues at the *i*, *i*+7 positions (**38**).[121] A simple bridging reaction with various disuccinimydyl carbonates could give bridged helices with variable functionality. Overall, the salt and lactam bridged peptides have shown improved utility compared to model linear sequences with greater stability, and subsequent affinity for biological targets due to their ability to mimic the natural α-helical conformation of specific binding sites. However, despite their synthetic simplicity, they have not been utilised extensively for biological studies. This is likely due to the relative lability of the amide bond *in vivo*, compared to other bridging techniques

1.5.7 - Thioether bridged helices
Another method used in nature to stabilise protein conformations is the disulfide bridge in which a covalent bond is formed between two cysteine residues *via* the

side chain thiol groups. This technique has been utilised in peptide science to stabilise short helical sequences through disulfide bridged side chains (Scheme 8). Direct disulfide bridge formation between cysteine residues at the *i*, *i*+3 (**40**) positions has been shown to induce pseudohelical structures in small peptides when bound to a cognate molecular target, for example estrogen receptor-α.[122] This study showed that disulfide bridged peptide derivatives of a coactivator fragment had the highest affinity for the target versus linear and lactam bridged analogues. These results were supported by computational studies showing that the *i*, *i*+3 disulfide bridge gave the best helical fit, however CD spectroscopy showed no evidence of helical character in water, and only 7% in helix inducing solvents such as trifluoroethanol (TFE). Therefore, in this case the helicity of the peptide was induced by target binding but strengthened once bound by the thioether bridge.[122]
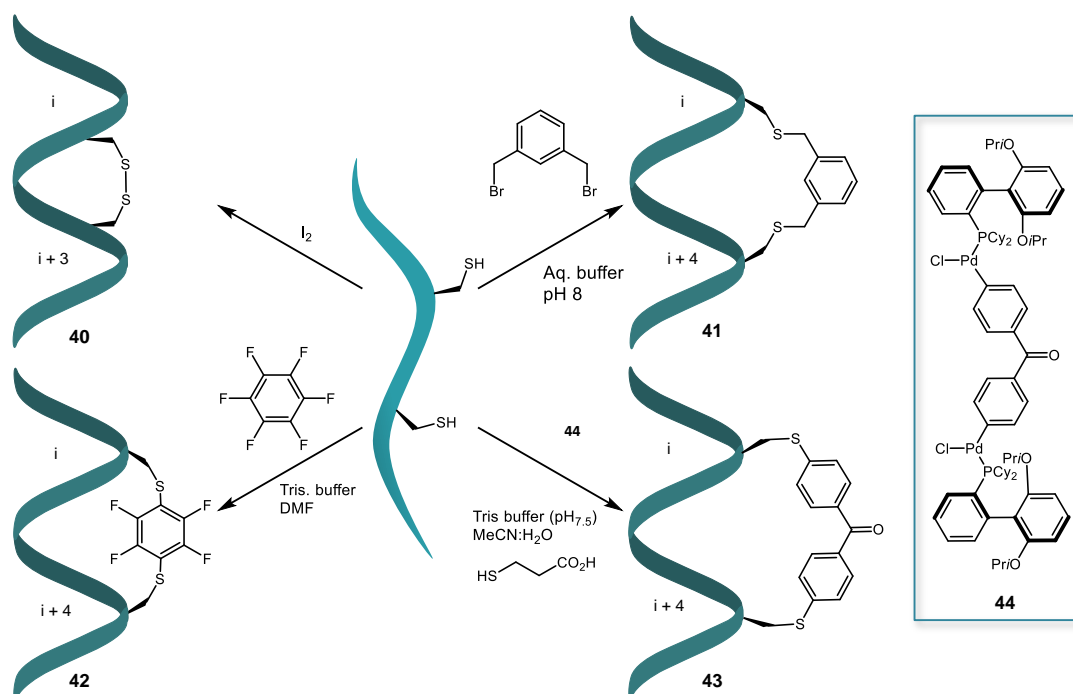
Scheme 8 - Cysteine bridged helical peptides

Another development in the use of thiol bridged helical peptides was the use of structurally rigid cross linkers *via* cysteine alkylation (**41**, Scheme 8).[123] By incorporating cysteine residues at the *i*, *i* +4 positions, bis-alkylating agents could be used to react with the two thiols and form a covalent link between them in a one-pot process, thus stabilising a helical conformation (Scheme 8). Through screening of a palette of cross linkers, the group showed that meta-xylyl groups gave the most stable, low-energy conformations, with these peptides exhibiting the highest degree

of helical content compared to the model linear peptide by CD spectroscopy in 40% TFE. The *m*-xylyl cross linked peptide also demonstrated increased inhibition of their associated biological target, calpain, subsequently blocking the binding site from natural substrate binding. These results indicated that it was the increased helical character of the peptide which gave the uniquely selective and potent binding to calpain over other similar cysteine proteases.[123]

Further exemplification of the effective bridging of thioether-aryl linked peptides was also reported *via* an S_NAr approach.[124] Unprotected peptides with Cys at the *i*, *i*+4 positions could be reacted under mild buffer conditions to give perfluorinated bridged peptides (**42**, Scheme 8). CD analysis of a model peptide showed 53% helicity, however the authors note abnormalities in the CD spectrum due to the absorptivity of the perfluoroaryl group.[124] The synthetic routes to **41** and **42** are advantageous due to the stability of the thioether link over a disulfide bridge, the relatively mild reaction conditions and the ease of linker variation.

Recent work by Buchwald into thiol compatible palladium catalysts for Suzuki couplings was utilised to create the first Pd catalysed Cys bridged system.[125] Catalyst systems, such as **44** (Scheme 8), were deemed amenable to bioconjugation type reactions due to their selectivity for thiols over alcohols in line with their less-electrophillic nature over standard Suzuki catalysts. Coupling between **44** and a model *i*, *i*+4 peptide was reported as quantitative in 10 minutes. This reaction was synthetically interesting, however is unlikely to be adopted in the field of helical peptide stapling. The synthesised peptide **43** was never isolated, and therefore lacks information regarding ease of isolation and helicity data by CD, both which are standard in the field. Synthesis of catalysts systems such as **44** also require glovebox conditions for the pre-catalyst, therefore are unlikely to be adopted in the biological chemistry community. Finally, the use of Pd which is highly toxic in biological systems, is problematic for development of therapeutic peptides to be used *in vivo* without information on Pd content after work-up.[125]

Alternative forms of thioether bridges peptides have been developed using unnatural thiol amino acids (Scheme 9). In an early example, a two turn α-helix was successfully stabilised using a disulfide bridge between the *i*, *i*+7 positions of 8 to 16-residue peptides (**45**).[126]
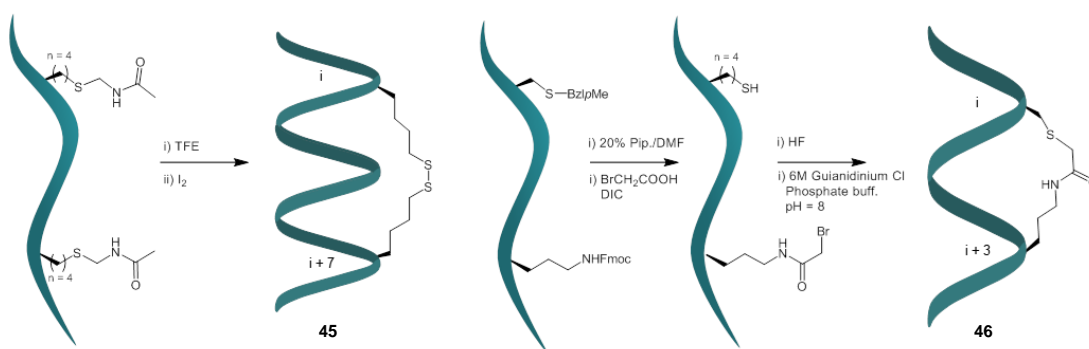
Scheme 9 - Alternative thioether bridged helical turns

A solid phase synthesis approach was used to incorporate two long chain protected thio-amino acids (Scheme 9). Trifluoroethanol was used as a helix initiator before oxidation using I_2 to give the conformationally locked peptide **45**. Multiple examples of high helical content at 0 ^{o}C were shown, suggesting that these oxidised peptides had two turns of the helix completely locked as well as efficiently propagating further helicity of neighbouring residues. The thioether bridging was shown to be a powerful means of helix nucleation as when using this technique a short eight residue peptide demonstrated 59% helicity at elevated temperatures of 60 ^{o}C, compared to only 13% for the protected unbridged analogue. Stereochemistry of the bridging amino acids was also shown to be important, with the *L,L* bridged peptides having higher levels of helicity than the *L,D* analogues, showing similar results to the previously mentioned lactam bridged systems where *L,L* analogues showed optimum stability.[117,126] A hybrid thioether/lactam bridged system has been demonstrated to show utility in short 10 amino acid mimics of gp41, a glycoprotein involved in HIV. SPPS incorporation of protected Cys and orthithine (Orn) residues allowed for deprotection and chemoselective ligation (**46**), giving products which were cleaner than the single lactam bridged analogues (Scheme 9). CD analysis also showed increased helicity to the lactam bridged controls, however the 20% TFE solution used for the spectra to aid solubilisation would also contribute to any helicity measurement. Again, these different forms of thiol bridged helical peptides have shown to be useful probes for investigating various helix mediated PPIs, demonstrating the benefit of peptides in this locked conformation compared to their linear analogues at PPI antagonism. The reversibility of dithio bridged peptides would make them prone to reduction in cellular systems, and hence would potentially not be useful in an *in vivo* setting. However the relative ease of installation of Cys with variable linker options such as shown in compounds **41** and **42** gives a simple approach to stabilising α-helical sequences into biologically active

peptides. The main drawbacks to these systems are risk of thio-oxidation and the bulky aromatic linkers used. These large, hydrophobic moieties may not be amenable to certain PPI targets, as well as their lack of demonstrated utility *in vivo*, with no data on cell permeability or proteolytic stability currently available.

1.5.8 - Light activated helical peptide stabilisation

Bioconjugation chemistry has been adapted for peptide synthesis, providing inspiration for various novel peptide stabilisation techniques. One such technique is the photoinduced cycloaddition of tetrazoles with alkenes due to its high selectivity.[127] The highly functionalised building blocks required for this form of peptide stapling were formed through branching of Fmoc protected lysine (Scheme 10, A). Amide bond formation with the alkene-containing acid chloride **48**, or acid chloride tetrazole **47** gives the two Fmoc protected amino acids which are amenable to SPPS.
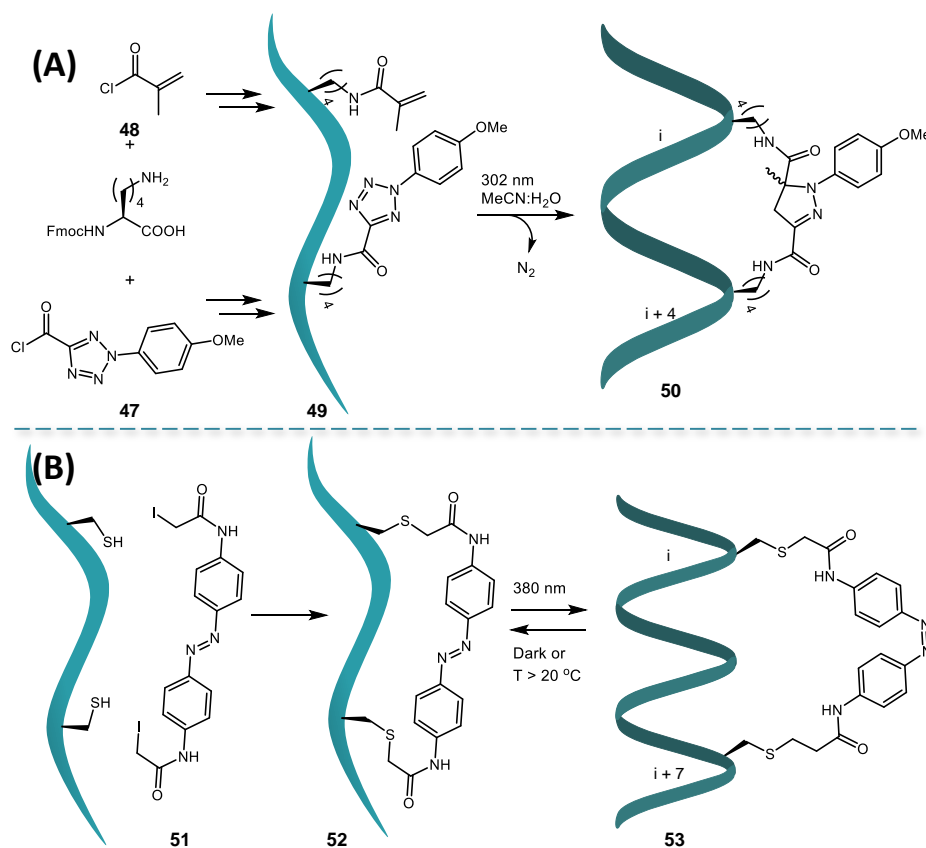
Scheme 10 - Photo-controlled helix formation approaches
A) – Photo-induced 1, 3-dipolar cycloaddition. Tetrazole and alkene derived from lysine are installed via SPPS.
B) – Photoisomerisable stapled peptides. *Trans* form is inactive whilst light activated *cis* form is α-helical.

Once peptide synthesis, cleavage and purification are complete, the sequence is set up for the photoinduced 1,3-dipolar cycloaddition (**49**). Irradiation of the peptide at

302 nm gave the stable pyrazoline cross-linked peptide **50** in up to 90% yields with the only by-product being nitrogen gas. Despite the absence of helicity data, inhibitors of the model p53/MDM2 PPI were identified using this novel bridging technique.[127] As with other helical stabilisation techniques (Sections 1.5.6 – 1.5.7), the target affinity and cell permeability was dependent on bridging site and overall peptide charge (net positive charge resulted in increased cell permeability). Overall, this was the first example of photo-induced helical peptides which were active *in vivo*. UV irradiation has also been shown to be effective in the activation of radical intiators, such as DMPA, to facilitate thiol-ene couplings between cysteine-containing peptides and various dienes.[128] This technique was selective for the free thiol of cysteine over other acidic and basic unprotected side chains allowing for effective synthesis of helical p53 mimetics (not shown).

A similar light activated approach to helical peptide stabilisation used reversible photoregulation through an azobenzene crosslinker.[129] Linker **51** was chosen due to the relative ease in which the azobenzene chromophore can be isomerised whilst being rigid enough to stabilise the α-helix. Cross linking of Cys residues using photoactive compound **51** gave the *trans* thioether linked peptide (**52,** Scheme 10, B). UV-Vis spectroscopy showed that upon irradiation of the peptide with UV light of varying wavelengths, varying populations of *cis* and *trans* conformation can be established. Analysis by CD spectroscopy demonstrated that helical content of *trans* (**52**) to *cis* (**53**) peptide increased from 12 to 48%, respectively at 11 ^{o}C. This process was reversible with exposure to heat (>20 ^{o}C) or placing the peptide in the dark, causing the structure to return to *trans*.[129] These photo-controlled peptide staples have been utilised in the design of inhibitors of the anti-apoptotic protein BCL-X$_L$.[130] Effectiveness of inhibition was dependent on cysteine spacing in conjunction with activation or deactivation by light. These studies are interesting examples demonstrating that helicity can be switched on and off depending on environment.

1.5.9 - Triazole bridged helical peptides

The emergence of click chemistry in small molecule library applications, introduced by Sharpless, led to the development of various catalytic processes which required readily available starting materials and benign solvents to achieve high yielding products with simple product isolation.[131] One of the most widely used reactions in this field is the 1,3-dipolar cycloaddition of azides with alkynes to give 1,4-

disubstituted triazoles using copper(I) catalysis. Pioneering work in 2002 used this under utilised reaction to form various triazole linked peptides and triazole branched amino acids on the solid phase (Scheme 11).[132] Relatively simple reaction conditions using CuI in THF, and easily accessible azide and alkyne building blocks, furnished triazoles with high purity (>95%) in a majority of cases.[132] This click chemistry was later adapted to the stabilisation of helical peptides due to the success at which the chemistry could be accomplished on the solid phase, and the utility of the triazole as a bioisostere of the carboxylic acids often utilised in lactam bridged helices (Section 1.5.6).
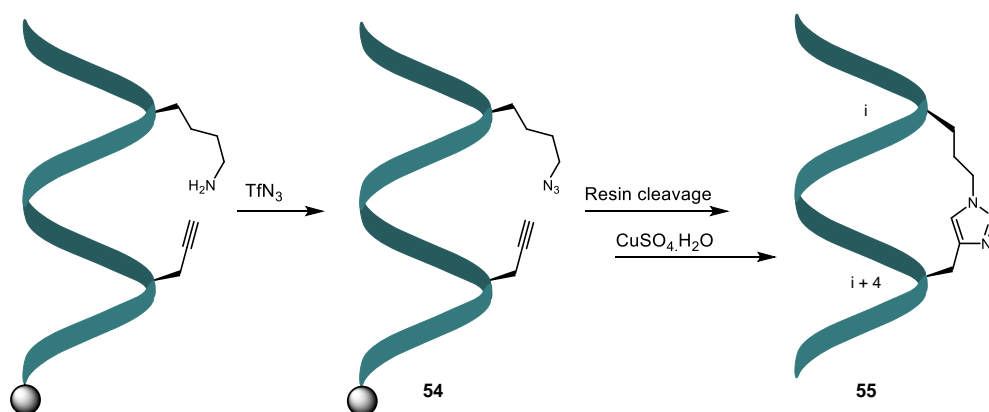
Scheme 11 - First triazole stabilised helical peptide[133]

Incorporation of propargylglycine and Mtt protected lysine into the peptide chain at the *i, i*+4 positions using standard Fmoc solid phase techniques allowed for selected deprotection and ε-azido leucine formation to give the click enabled helical peptide precursor **54** (Scheme 11).[133] In this case, no solid phase triazole formation could be accomplished, however resin cleavage and a solution phase click reaction using copper sulfate gave the first triazole stabilised helical peptide **55**. Structural analysis by CD spectroscopy showed helical content of over 50% for two model triazole linked systems.[133]

Further development of solid phase click chemistry for helical formation allowed for functionalised triazole linked peptides similar to those seen in thioether bridged helical systems (**41**, Scheme 8). A scalable route to Fmoc protected azido-ornithine,[134] developed by the Spring group, has allowed for SPPS of azido containing peptides, such as **56**, which can be functionalised with variable linkers. Aromatic dialkynes, such as compound **57**, are capable of forming stabilised helical peptides *via* double triazole formation on the solid phase (Scheme 12). This form of two-component click reaction gave increased helicity in a model system from 16 to

51%.[135] This technique has been utilised in a well-studied model PPI, the p53/MDM2 interaction, to a give bridged peptide with the structure and functionality tailored to strong *in vitro* binding with MDM2. An aromatic bridged peptide, such as **58** modified with a fluorescent tag, was shown to have low levels of cellular uptake by confocal microscopy.[135]
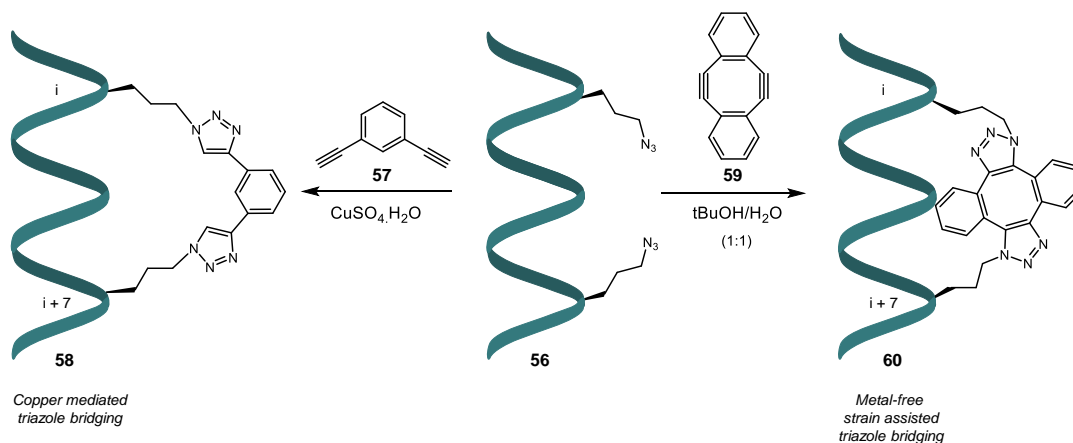
Scheme 12 - Functionalised triazole linkers for peptide stabilisation[135,136]

From this two-component strategy, a range of dialkynyl linkers can be utilised in the solution phase to give a palette of stapled peptides with varying physicochemical properties from one single peptide sequence with azido-ornithine at the *i*, *i*+7 positions (**56**).[137] However, due to the use of cytotoxic copper, these double-click peptides must be extensively purified before being used in cellular systems. In principle, if a metal free approach to this form of peptide stabilisation could be developed, then sequences could be bridged *in situ* for fast *in vivo* evaluation. This led to a proof of concept study using strain assisted azide alkyne triazole formation between peptides such as **56**, with di-alkynyl compounds such as **59**.[138] Peptides such as **60** could be synthesised in 60% yield without the need for copper, with the majority of the peptide being the *anti*-isomer (Scheme 12). Peptides were screened against the model p53/MDM2 PPI, with X-ray crystallography confirming helical structure and target affinity. This work provided a leap forward in biocompatible stabilisation of alpha helical peptides due to the utility of the fast strain assisted triazole reaction.[138] However, the Sondheimer diyne (**59**) used to facilitate this reaction is extremely hydrophobic and rigid, meaning this technique is unlikely to provide linkers compatible with a majority of PPI targets due to clashing with the surface and occluding the peptide from the ideal binding site.

Triazole linked helical peptides, despite showing increased helical content to linear model sequences and their relatively simple synthesis have not gained similar popularity in the last 5 years compared to the all-hydrocarbon stapled peptide system discussed in Section 1.7. This is potentially due to the explosive nature of the azide precursor compounds required for the initial peptide formation, leading researchers to focus on more chemically benign methods for helical peptide stabilisation.

1.6 - The utility of ring-closing metathesis in peptide stabilisation

As discussed above in Section 1.5.3, ring-closing metathesis has become a powerful tool in the formation of conformationally stable peptides.The evolution of RCM catalysts has facilitated a wide functional group tolerance which is necessary when dealing with peptides, as well as an extensive size range of macrocyclic structures that can be formed. Without such extensive research into RCM mechanism and catalyst development, the powerful technique of peptide stapling (Section 1.7.1) would not have developed into such a successful means of constraining bioactive peptides. The key reaction is a form of alkene metathesis in which olefinic bonds are rearranged *via* a series of [2+2] and retro-[2+2] cycloadditions, catalysed by a metal carbene. The metathesis reaction itself requires no additional reagents apart from the catalyst and the olefins being reacted, with the by-product (in most cases) being ethene gas.

1.6.1 - Alkene metathesis

The main subtypes of alkene metathesis reactions are; ring-opening metathesis (ROMP), ring-closing metathesis, acyclic closing metathesis (ACM) and cross metathesis (CM) (Fig. 16), with each form having a variety of applications in several fields of chemistry.[139,140] Alkene metathesis was formally recognised in the 1960s as the redistribution of olefinic moieties *via* a metal catalysed process.[141] Despite the low costs of the reagents, metathesis reactions were unreliable due to the poor functional group tolerance and low activity due to the low concentrations of active species being formed. Over time, it became apparent that the choice of metal played an essential role in tuning the reactivity and functional group tolerance of the catalysts (Fig. 16). Through careful optimisation, a structure-activity relationship between the metal and the efficiency of the reaction could be defined, with ruthenium proving to be the transition metal with the highest reactivity with olefins and selectivity over acids, alcohols, carbonyls and esters.[140,142]

Figure 16 – Development of the RCM Reaction[140]

A breakthrough came in the addition of diphenylcyclopropene to $RuCl_2(PPh_3)_3$ by Grubbs to give the first metathesis active single species ruthenium catalyst (**62**).[143] These Ru-Diphenyl species were more stable to water and alcohols in the reaction mixture, yet despite this, were limited to ROMP of highly strained monomers.[143] To extend the scope of these more stable catalysts, further optimisation of the steric and electronic properties of the co-ordinated ligand had to be carried out to allow for broader metathesis activity. Therefore, by using the most sterically encumbered and basic phosphine available (PCy_3), the Grubbs group created their first generation catalyst (**63**), the first metathesis active benzylidene of this type which was air stable.[144,145] By this point in time, *N*-heterocyclic carbenes (NHCs) had been popularised in the literature as valuable alternatives to phosphine ligands in various metal catalysed transformations. This was exploited by Grubbs and co-workers in the development of a second generation ruthenium catalyst system (**64**).[146] Despite phosphine dissociation being relatively slower compared with the first generation catalyst, the second generation species could perform multiple metathesis reactions before phosphine association would bring it back to its resting state.[146] Direct electron donation by the phosphine ligand in these complexes is thought to stabilise the metallocyclobutane intermediate which is a fourteen electron complex (Scheme 13). In this respect, every catalyst created could actually be considered a pre-catalyst as metathesis relied on phosphine dissociation before an active catalytic process would be carried out.[147]

Overall, these new ruthenium catalysts have comparable activity to the earlier Schrock Mo species (**61**), with the advantage of broad functional group tolerance not

observed with other transition metals. In addition, these systems are reactive towards a large range of substrates whilst being stable towards the presence of water, minor impurities in solvents and being stored under air without decomposition for several weeks.

1.6.2 - RCM in organic chemistry

As a result of the significant efforts made into the optimisation of these catalysts, olefin metathesis has now become a standard, reliable process in organic chemistry for carbon-carbon bond formation. However, the most significant advance facilitated by the Grubbs ruthenium catalysts was in the RCM reaction (Scheme 13).
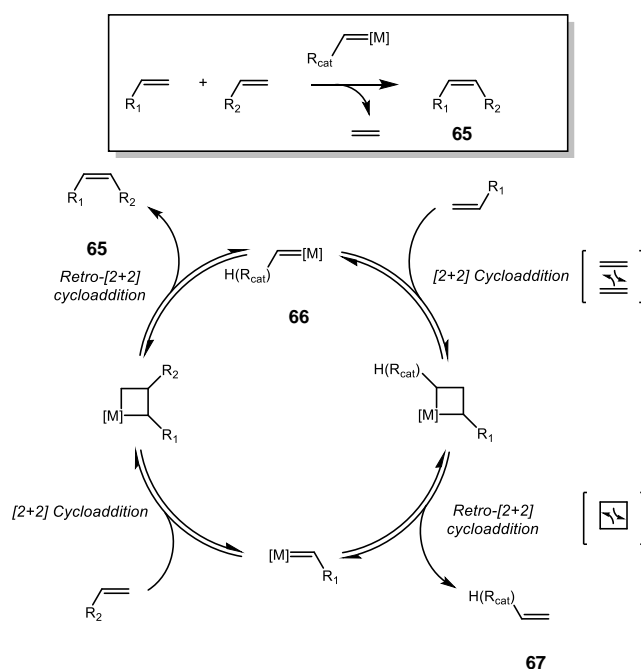
Scheme 13 - RCM mechanism
During the first cycle, ethylene R_{cat} is formed but for every subsequent cycle only ethene is released

The improved functional group tolerance and increased activity allowed for cyclisation of diverse substrates, from total synthesis of natural products to large macrocyclic systems which previously were impossible to construct. The reaction mechanism proceeds *via* a series of [2+2] cycloadditions and retro-[2+2] cycloadditions (Scheme 13). The metal carbene species acts as an initiator rather than a catalyst in that it does not return to its original form. During the first catalytic cycle, the metal is bound to the catalyst alkylidene (**66**), whilst for every subsequent cycle the metal is bound to a methyl alkylidene. It is also noteworthy that the main by-product of this reaction is ethene gas (**67**), making these reactions relatively easy to work-up provided conversion to the product (**65**) is high.

1.6.3 - RCM in peptide stabilisation

Examples of RCM in the literature cover various ring sizes and complex functionalities due to the tolerance of Grubbs catalysts towards functional groups and reaction conditions. The observed efficiency of RCM in creating highly functionalised macrocyclic compounds meant it was soon adapted for peptide chemistry as a means of structural stabilisation. Initial work focused on the cyclisation of various tetrapeptides using synthetic amino acids with olefinic side chains (**68**, Scheme 14). The reactions were carried out in solution at 40 $^{\circ}$C, giving 60% yields of the fourteen-membered cyclic analogues (**69**). It was also noteworthy that peptides with unstructured sequences (containing no Pro or Aib residues) were also successfully bridged to give a more stable conformation.[148] Due to the low solubility of peptides in solution, it was unlikely that longer sequences would be able to be ring closed using this approach.
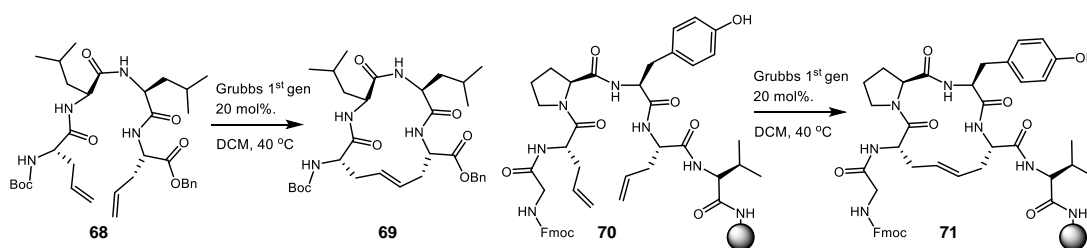
Scheme 14 - Solution phase peptide cyclisation[148]

Based on this, it was next determined if the reaction could be carried out on the solid phase, effectively ring closing a solid supported peptide. To this end, a tetrapeptide sequence which had already been successfully cyclised in solution was tested in a resin bound form (Scheme 14).[148] The solid phase synthesis of the peptide was carried out using standard methods, with the only change being the incorporation of the propyl olefinic amino acids to be cyclised (**70**). Analogous RCM conditions were used for the solid phase as with the solution phase reactions, with cleavage from the resin showing a 65% conversion of the starting material to the cyclic peptide **71**. These results opened up new possibilities for installing synthetic secondary structural motifs in short peptides *via* efficient resin bound ring-closing cyclisations.

1.7 - RCM in helical stabilsation

Grubbs and co-workers next turned their attention to the utility of RCM in forming synthetic α-helical peptides *via* the bridging of two olefinic side chains at the *i*, and *i*+4 positions.[149] As noted with other bridging techniques (Sections 1.5.5 – 1.5.9), introducing a tether between these positions would give an aliphatic link on one side

of the helix, effectively locking a single turn of this secondary structure. By forcing this conformation, the peptides were reasoned to have increased thermal and biological stability, potentially leading to higher affinity for biological targets. A hydrophobic model system was chosen (Scheme 15) as this apolar sequence would allow for conformational analysis and characterisation in organic solvents, where intramolecular H-bonding, hydrophobic interactions and electrostatic interactions alone control peptide folding, negating polar solvent effects. Using apolar organic solvents would also increase the likelihood of helical formation due to the solubility of the ruthenium RCM catalyst, which is poorly solvated in common aqueous peptide conditions, and the documented ease of helical folding in organic solvents.[108,109] The model system alone had already demonstrated an α–helical conformation in the solid state by X-ray crystallography. Therefore, by further constraining of this system, these ring closed peptides had the potential to probe the importance of the helical conformation on ion channel forming activity. By replacing the *i*, *i*+4 alanine residues with *L*-serine or *L*-homoserine *O*-allyl ethers, the linear peptides **72** and **73** were created using standard solution phase peptide chemistry (Scheme 15).[149]

Linear sequence   Boc–Val–**Ala**-Leu–Aib–Val–**Ala**-Leu–OMe
Stabilised sequence   Boc–Val–**X**—Leu–Aib–Val–**X**—Leu–OMe

Grubbs 1st gen 20 mol%.
DCM, 25 °C

10% Pd/C H$_2$ (1 atm)
EtOH, 25 °C

72 X = Ser (*n*=1)
73 X = Hse (*n*=2)

74 (*n*=1) **85%**
75 (*n*=2) **90%**

76 (*n*=1) **98%**
77 (*n*=2) **98%**
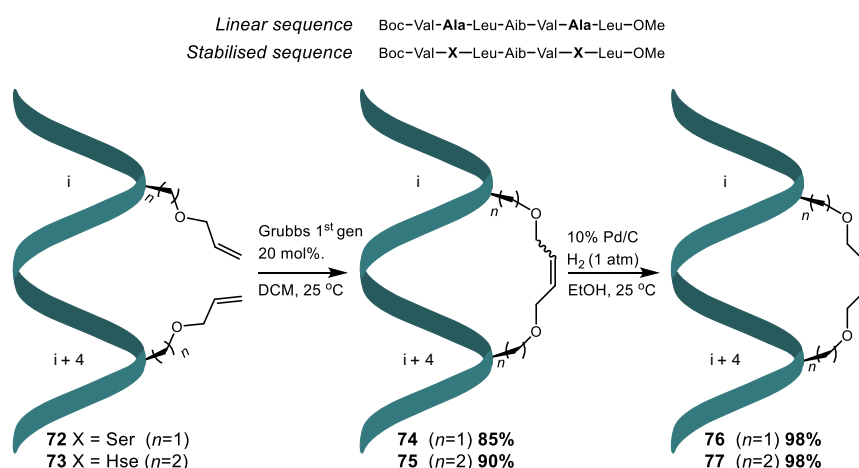
Scheme 15 - *O*-allyl ether helical peptides[149]

Molecular modelling predicted the diene side chains would be in close enough proximity for effective RCM, which was proven through the successful ring-closure of both peptides in 85% and 90% yield, respectively, giving compounds **74** and **75**. The olefinic peptides, in an isomeric mix of 5:1 *E:Z*, were then hydrogenated to peptides **76** and **77** to negate any isomeric effects on the conformational studies. Analysis by CD spectroscopy showed that the precursor peptides **72** and **73** were pre-organised in helical conformations, which had been previously been inferred

through the fast reactions and yields of the cyclisations. It was also encouraging to note that the stabilised peptides **76** and **77** had similar ellipticities to the precursors, implying that the helical conformation was retained upon cyclisation. A final X-ray crystal structure of **77** confirmed that the peptide backbone adopted a helical conformation for the first five residues with consistent 4-1 hydrogen bonding, with fraying occurring towards the *C*-terminus.

However, an interesting observation was that the precise shape of the helix changed from a standard α–helix with the precursor peptides, to a 3_{10}-helix upon cyclisation. As with a standard α-helix, the 3_{10}-helix is right handed, but hydrogen bonding occurs every 3 amino acids at the *i* and *i*+3 positions, rather than *i* and *i*+4 in a standard helix, giving a structure in which each amino acid represents a 120° turn in the helix.[150] In the cyclised system, the conformational lock was thought to change the backbone torsion angles towards this less standard helical form. The ease in which this backbone stabilisation was achieved *via* solution phase RCM showed how this methodology allowed for efficient synthesis of macrocyclic peptides in hydrophobic solvents, offering the possibility of increased biological activity through greater helical stabilisation, as observed with alternative stapling techniques discussed previously.[149]

1.7.1 - All-hydrocarbon peptide staples

The next major development in RCM mediated stabilisation of helical peptides was the creation of an all-hydrocarbon cross-linking bridge by the Verdine group (Scheme 16).[151]
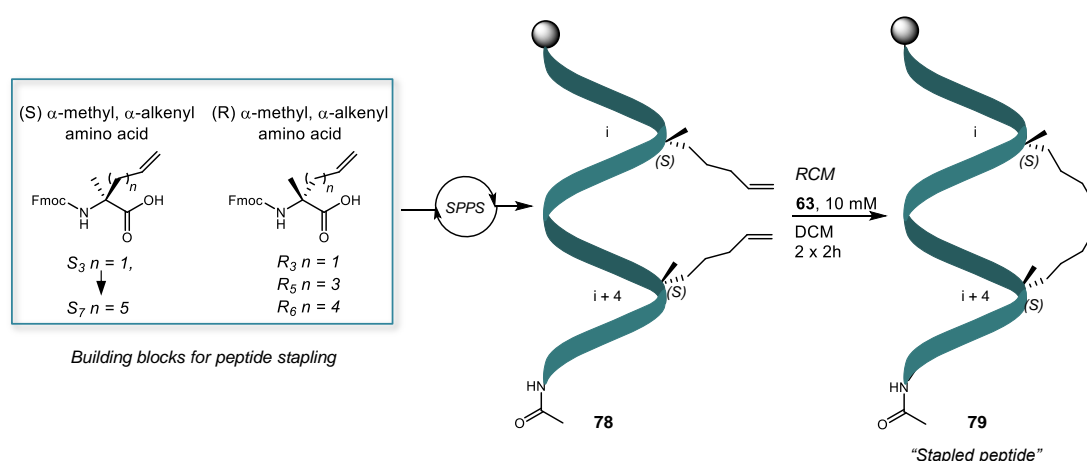
Scheme 16 - Solid phase ring closing metathesis to form a peptide staple[151]
Boxed structures show amino acid building blocks. On resin metathesis of the single stapled S_i, S_{i+4} peptide shown.

This work aimed to stabilise α-helical conformations with a linker that was not pharmacologically labile, such as previous disulfide or lactam bridges, in order to increase the resistance of the target peptides to proteolysis. An all hydrocarbon linker would reduce the exposure of the polar H-bonded backbone to hydrophobic systems, such as biological membranes, which would improve peptide permeability. To achieve this goal, screening of multiple configurations of this new all-hydrocarbon linker had to be carried out in order to elucidate optimum tether length, stereochemistry and position of the link in the peptide. Novel synthetic amino acids were designed (Scheme 16) to incorporate terminal alkenes to allow for an RCM based approach, with the added helix stabilising effect of α,α-disubstituted amino acids, such as AIB. Whilst α-methylated amino acids are known to stabilise the peptide backbone by reducing flexibility, the olefinic side chain itself should also be helix promoting due to its linearity, as both natural and unnatural amino acids with linear side chains have been shown to be strongly helix stabilising.[152] These building blocks could be made with either R or S stereochemistry and incorporated into the peptide at the i and $i+4$, or $i+7$ positions using standard solid phase chemistry (**78**), allowing for tethers of multiple lengths and configurations to be tested over one or two turns of the helix (Scheme 16). Metathesis was tested on the solid phase using Grubbs 1st generation catalyst (**63**) to give alkenyl linked hydrocarbon tethers to stabilise the helix (**79**). With the single turn peptides, the length and stereochemistry of the tether had a major effect on the extent of metathesis depending on the proximity of the olefinic side chains. Only hydrocarbon bridges of matching stereochemistry, S_i, S_{i+4} (**80**) or R_i, R_{i+4}, (**82**) with a chain length of eight-carbons underwent metathesis to complete conversion (>98%), with shorter or enantiomerically mismatched sequences (R_i, S_{i+4}, **81**) failing to ring close (Fig. 17). For the double turn helices, only the R_i,S_{i+7} (**84**) system was tested as the steric strain of forming an S_i,R_{i+7} (**85**) link would be too great, whilst the S_i,S_{i+7} or R_i,R_{i+7} (**83**) systems would likely clash with the side chain of the i, $i+4$ residue (Fig. 17).

The efficiency of the RCM increased with the chain length, with optimum conversions achieved (>98%) for tethers of eleven carbons or more. This was believed to be due to the side chain olefins being able to span the gap along the face of the helix, with macrocycles of thirty one-members or less being too sterically hindered to ring close.
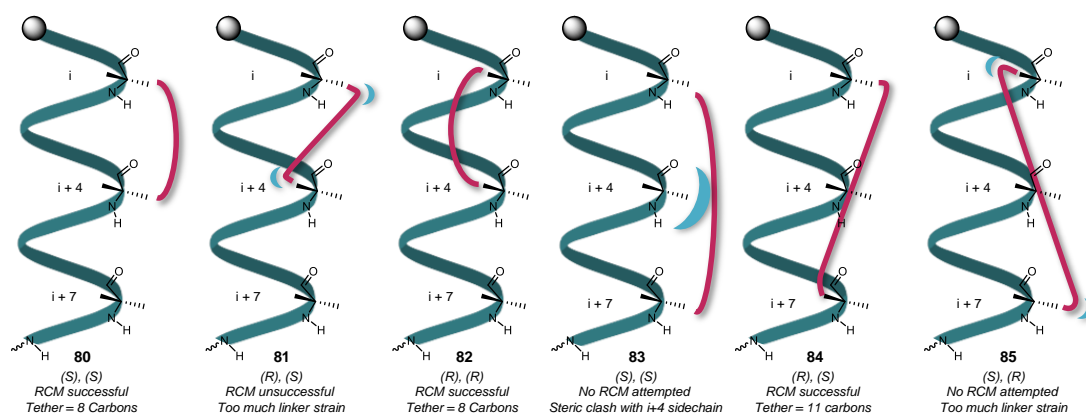
Figure 17 – Position and relative stereochemistry of all-hydrocarbon bridges[151]
Pink bands show relative positions of various single and double turn staples of different stereochemical combinations

It is also important to note that due to the key ruthenium catalysed step occurring whilst the peptide is still on the solid phase, the metal content of the final peptides is considered negligible due to the extensive washing, cleavage and purification protocols. Once the metathesis optimisation was complete, CD structural analysis was carried out to test the helical content of the tethered, or stapled, peptides. The non-cyclised peptides were all shown to have increased helical content compared to the natural sequence due to the incorporation of the two α,α-disubstituted amino acids which induce backbone rigidity and helix stabilisation. With the 8-carbon single turn staples, both peptides saw a very slight increase in helicity compared to the unstapled closed analogues, with the S_i, S_{i+4} peptide showing greater overall stabilisation than the R_i, R_{i+4}. With the double turn peptide staples, the length of the bridge had a major effect of the stabilisation of the helix, with the shorter tethers of 9 and 10-carbons actually destabilising the helix by 21% and 12%, respectively. Fortunately, the eleven and twelve-carbon length tethers increased helicity by up to 26%, with the eleven-carbon tether being the optimal length with an overall helicity of 44%. It was also interesting to note that subsequent hydrogenation of the tether double bond had no effect on the overall helicity of the peptide.[151]

The metabolic stability of these conformationally locked structures was then examined. The resistance to hydrolysis by the protease trypsin for each of the systems correlated with the data for overall helicity. The most helical peptide, the eleven-carbon tether R_i,S_{i+7}, had the lowest rate of proteolytic cleavage of 0.058 M^{-1} s^{-1} compared to the linear control at 2.38 M^{-1} s^{-1}, indicating that by inducing this helical effect, a synthetic peptide can be considerably more resistant to tryptic digestion.[151] Considering the previous reluctance of the pharmaceutical industry to

use peptides as drug molecules due to their metabolic instability, this study provided a significant advance in methodology to creating drug-like peptides with desirable pharmacokinetic properties.

More in depth studies were carried out on the precise nature of the single turn i, $i+4$ tethers to investigate what effect the stereochemistry of the staple had on the conformation and cellular uptake of these compounds (Fig. 18).[153] It was interesting to note that whilst the model S_i, S_{i+4} unstapled peptide had an 8% increase in helicity compared to the linear sequence, the R_i, R_{i+4} unstapled peptide actually had a 5% decrease in helicity compared to the natural sequence.
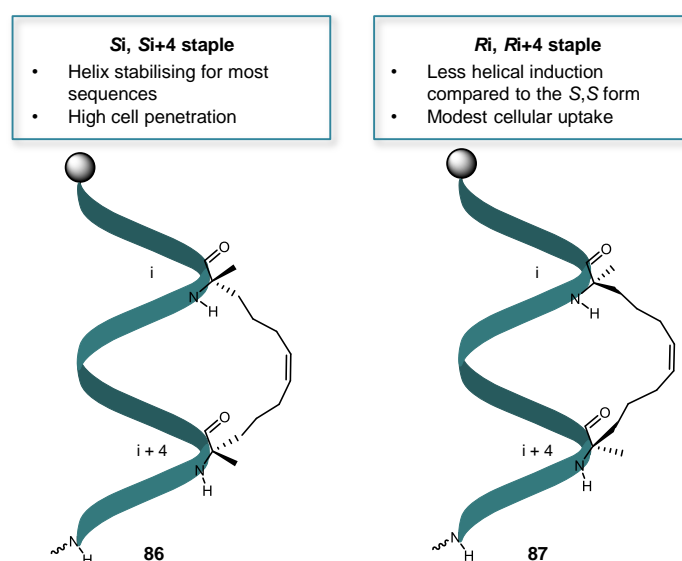
Figure 18 - Effect of stereochemistry of single turn staples on cell permeability[153]

Both S_i, S_{i+4} (**86**) and R_i, R_{i+4} (**87**) staples underwent RCM to ~90% in 2 hours, therefore the complementary stereochemistry had no effect on staple formation. Stapling of these peptides increased helicity from 36% to 72% for the S_i, S_{i+4} peptides and 24% to 40% for the R_i, R_{i+4}, with a net increase in helicity of 44% and 11% from the linear sequence, respectively. A trend was observed where sequences which were stabilised by the S_i, S_{i+4} staple often had a substantial loss in helical induction when the R_i, R_{i+4} enantiomeric pair was employed. To probe this observation further, both the S,S and R,R stapled peptides were tested for cellular uptake, empirically showing whether the differences in helicity induced by stereochemical inversion played a significant role in cell permeability. The linear sequence was shown to be non cell-penetrant by fluorescent flow-cytometry using HeLa cells, as expected. A modest uptake was seen with the R,R stapled peptide,

however the *S,S* stapled peptide was shown to be highly cell permeable by comparison. This trend was repeated when alternative sequences were tested, in which the *S,S* stapled peptides were consistently more helical and cell permeable than the *R,R*. Therefore, the overall trend in the data, from this and previous studies, confirmed that the overall helix stabilisation of the single and double turn staples can vary from sequence to sequence and position along the chain, yet by using the S_i, S_{i+4} or the R_i,S_{i+7} staple, the probability of enhanced helicity and cell permeability is greatly increased.

1.7.2 - Stapled peptides as anti-cancer agents

Due to the encouraging results of improved helicity and measured proteasomal stability exhibited by stapled peptides, this methodology rapidly was applied to create biologically active species. In 2004, the BCL-2 family of proteins was targeted using a small peptide α–helical mimic of the BH3 essential death domain.[154] This family of proteins is a control point for cell apoptosis, regulating this process through a series of protein-protein interactions between BCL-2 members, and is an interesting target in oncology. Given the requirement for a drug-like helical mimetic, this PPI system was an ideal model to test stapled helical peptides as potential therapeutic agents (Fig. 19).

Peptide	Sequence
BID BH3	Ac-E-D-I-I-R-N-I-A-R-H-L-A-Q-V-G-D-S-N_L-D-R-S-I-W-CONH$_2$
SAHB$_A$	Ac-E-D-I-I-R-N-I-A-R-H-L-A-S_5-V-G-D-S_5-N_L-D-R-S-I-W-CONH$_2$
SAHBA$_{(G-E)}$	Ac-E-D-I-I-R-N-I-A-R-H-L-A-S_5-V-E-D-S_5-N_L-D-R-S-I-W-CONH$_2$
SAHB$_B$	Ac-E-D-I-I-R-N-I-S_5-R-H-L-S_5-Q-V-G-D-S-N_L-D-R-S-I-W-CONH$_2$
SAHB$_C$	Ac-E-D-I-I-R-N-I-A-S_5-H-L-A-S_5-V-G-D-S-N_L-D-R-S-I-W-CONH$_2$
SAHB$_D$	Ac-E-D-I-I-R-N-I-A-R-R_5-L-A-Q-V-G-D-S_8-N_L-D-R-S-I-W-CONH$_2$

N_L = Norleucine
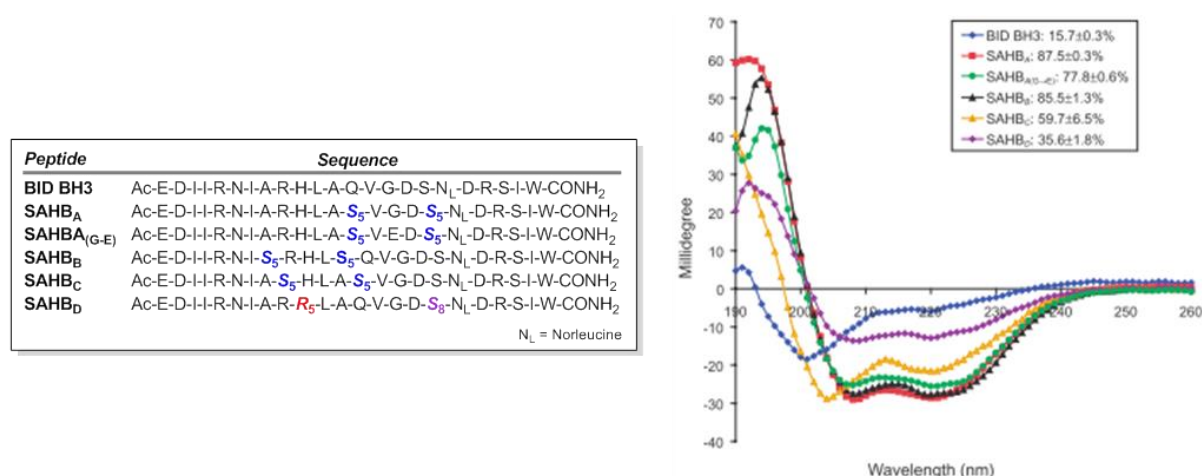
Figure 19 - Panel of BID BH3 stapled analogues and their CD helicity values[154]

To achieve this, the previous methodology was used to incorporate two α-alkenyl amino acids (Scheme 16) at the *i* and *i*+4, or *i*+7 positions at various points along the BH3 sequence to create a panel of stapled peptides to mimic this PPI. The helicity of the synthesised peptides was determined by CD spectroscopy, with the linear twenty three-mer BH3 peptide only showing 16% helicity as a baseline, indicating essentially a random coil conformation. The stapled α-helical mimics of

BID (SAHBs) peptides showed increased helical content from 35 to 87%, demonstrating the robust nature of the stapling methodology to induce helical secondary structure on novel peptide sequences (Fig. 19). SAHB$_A$, the most helical of the peptides tested, was chosen for further activity and stability assays. This decision was based on the premise that the most ordered structure would have both the greatest proteasomal stability and, optimal affinity for the target due to maintaining the most similar structure to the natural PPI. A BCL-2 fluorescence polarization binding assay indicated that SAHB$_A$ had a six-fold enhancement in binding compared to the linear sequence, BID BH3. This correlated with further *in vitro* data on mouse liver mitochondria, in which the action of SAHB$_A$ induced apoptosis of cells whilst the BID BH$_3$ did not.

Another interesting result was in relation to the cellular permeability of these stapled peptides. As discussed previously (Section 1.3.2), peptides were historically viewed as being undesirable drug molecules due to their inability to cross biological membranes as a result of the polarity of the peptide backbone. However, data from a fluorescence labelling study demonstrated that treatment with SAHB$_A$ showed discrete cytoplasmic localisation, with a time dependent uptake into cells. More encouraging than this was that SAHB$_A$ was capable of penetrating leukaemia cells through an energy-dependant, pinocytotic route, inducing the apoptotic pathway hypothesised.

Overall, the optimal stapled peptide from this study showed inhibition of the proliferation of a wide panel of leukaemia cells as well as immunodeficient mice infected with human leukaemia xenografts. These *in vivo* results showed that SAHB$_A$ supressed leukaemia growth, with tumor expansion suppressed after three days, and tumor regression after five. The serum half-life of SAHB$_A$ in mice was also found to be up to 1.5 hours, which is significantly longer than most peptide therapeutics. Further histological examination showed that the peptide appeared to have no obvious toxicity in normal tissue, indicating the apoptopic affect was specific to the cancerous cells. SAHB$_A$ successfully demonstrated the utility of stapled peptides as mimics of native protein sequences present at a PPI, and how this could be used to induce a biological effect. The introduction for the all-hydrocarbon staple was essential in stabilising the helical structure of this class of peptide, and subsequently improved the *in vitro* and *in vivo* activity against leukaemia cells. Locking the conformation was also vital in providing metabolic stability and cell

permeability of SAHB$_A$, two properties which are notoriously low in linear peptide sequences.[154]

Not content with creating a synthetic biologic capable of antagonising the BCL-2 apoptic pathway, the Verdine group next utilised the stapled peptide methodology to probe another biological pathway common to most human cancers, the p53/MDM2 PPI. By blocking MDM2 with a synthetic stapled analogue of p53, it was reasoned that p53 activity could be restored to normal levels, which could resensitise cancer cells to apoptosis through retranscription of p53 responsive genes. A panel of *i*, *i*+7 stapled alpha helices were designed around the residues considered essential for binding, Phe[19], Trp[23] and Leu[26] (Table 1).

Table 1 – Development of p53 stapled peptides[155]

Synthetic α-,α-disubstituted amino acids in green and blue at the i, and i+7 positions. Sequence mutations in orange

Compound	Sequence	Charge at pH 7.4	α-helicity	K_d (nM)	Cell Permiable	Cell Death
WT	Ac-L-S-Q-E-T-F-S-D-L-W-K-L-L-P-E-N-NH2	-2	11%	410 ± 19	-	-
SAH-p53-1	Ac-L-S-Q-E-T-F-S-D-*R$_8$*-W-K-L-L-P-E-*S$_5$*-NH2	-2	25%	100 ± 8	-	-
SAH-p53-2	Ac-L-S-Q-E-*R$_8$*-F-S-D-L-W-K-*S$_5$*-L-P-E-N-NH2	-2	10%	400 ± 50	-	-
SAH-p53-3	Ac-L-S-Q-*R$_8$*-T-F-S-D-L-W-*S$_5$*-L-L-P-E-N-NH2	-2	12%	1200 ± 89	-	-
SAH-p53-4	Ac-L-S-Q-E-T-F-*R$_8$*-D-L-W-K-L-L-*S$_5$*-E-N-NH2	-2	59%	0.92 ± 0.11	-	-
↓ SAH-p53-8	Ac-*Q*-S-Q-*Q*-T-F-*R$_8$*-*N*-L-W-*R*-L-L-*S$_5$*-*Q*-N-NH2	+1	85%	55 ± 11	Yes	Yes

As before, synthetic α-,α-disubstituted amino acids, S_5 and R_8, were incorporated into the peptide chain *via* solid phase synthesis, then ring closed to give the corresponding stapled peptide. The first four compounds created, SAH-p53 1-4, which contained the *i*, *i*+7 staple at different positions along the sequence, were shown to have helicity varying from 10-59%. As SAH-p53-4 had the highest helical content out of this subset, and subsequently the highest binding affinity for the MDM2 (K_D = 0.92±0.11), this model was chosen to test the effect of sequence mutation on activity and cell permeability (Table 1). With respect to the cell permeability, it is known that positively charged peptide sequences (at physiological pH) have a greater chance of penetrating cell membranes.[156] Therefore, the first cycle of mutations performed was replacing the glutamic acid and aspartic acid residues with their amide analogues, glutamine and asparagine, to balance the overall charge of the sequence. Subsequent mutated sequences were also created with deleted ubiquitylation sites (Leu[14] to Gln, and Lys[24] to Arg) and a deletion of the active Phe[19] residue. Out of these compounds, SAH-p53-8 had the best helicity, balance of charge and binding to give a highly active, cell penetrable stapled

peptide. SAH-p53-8 treatment was shown to reactivate the stunted p53 tumor suppressor cascade as previously hypothesised, giving the first example of a stapled peptide which targeted a transcriptional pathway to successfully kill cancer cell lines.[155] Overall, this work provided further evidence to the validity of the all-hydrocarbon stapling of peptides to give active pharmaceutical molecules capable of interacting with targets previously inaccessible to traditional drug design.

1.7.3 - Advancements in peptide stapling

The apparent utility of stapled α-helical peptides for enhanced target affinity with PPIs has led to multiple research groups using the methodology to investigate various biological systems. However, there has been some controversy over the reproducibility of assay results, and in particular the reliability of cell penetration data. Early results from Verdine, discussed in Section 1.7.2, showed the ability of stapled peptides of varying sequence to enter cells, with the overall consensus that a net positive charge combined with an S_i, S_{i+4} or R_i, S_{i+7} staple for short peptides would give the highest probability of cell penetration (Fig. 18). Uptake was demonstrated using fluorophore labelled peptides by high-resolution microscopy, or quantitatively measured using flow cytometry to measure intracellular fluorescence. The development of an assay technique named ReBiL, a highly sensitive recombinase enhanced biomolecular luciferase platform, has further enhanced the understanding of the mechanism of cell penetrating peptides.[157] In cellular systems with 0% serum, the activity of a MDM2 binding helical peptide was significantly higher than the serum based assays. It was noted that stapled peptide substrates had a dose-dependent cytotoxicity, but this was p53 dependent and could be prevented by the addition of 10% serum. These results could potentially account for the difficulty in reproducibility of certain stapled peptide MDM2 inhibitors. Dependent on assay conditions, cytotoxicity of some stapled peptides is dependent on their ability in compromising the integrity of biological membranes.[157]

In response to these results, the Verdine group published a further investigation into the mechanism of cell permeability of stapled peptides.[158] Through development of a high-throughput assay, they quantitatively measured the cellular uptake of up to two hundred stapled peptide sequences. These peptides varied in primary sequence, staple position and physichochemical properties in order to investigate any trends. In general, stapled peptides were more effective for penetrating cells compared to unmodified sequences, with a formal positive charge also correlating with

membrane permeability. As previously reported, stapled peptides accumulated in cells in a dose dependent manner over a few hours to reach steady intracellular levels. Mechanistic investigations also demonstrated an energy-dependent endocytosis pathway for the cell penetration of stapled peptides.[158] However, it is important to note that these cellular assays were run without serum, so there is still no general trends for full *in vivo* cell penetration of stapled peptides.

Nevertheless, stapled peptides continue to provide evidence that they exhibit pharmacologically useful levels of cell permeability.[159] Despite this debate, the first Phase I clinical trial of a stapled peptide was successfully completed in 2013. Aileron therapeutics stapled peptide drug, ALRN-5281, was evaluated as a long-acting growth-hormone-releasing hormone agonist for treating endocrine disorders such as HIV lipodystrophy and adult growth hormone deficiencies.[160] The once-weekly subcutaneous dosing campaign is hoped to be safe and more effective than current growth hormone therapies. Aileron initiated a second stapled peptide Phase I clinical trial in 2015, in this case an MDM2 and MDMX suppressor to re-activate tumour supressing protein p53.[161] In light of the apparent clinical success of the stapled peptide methodology, this technique has been adopted by multiple research groups for investigating systems of biological interest. Example therapeutic areas for stapled peptides outwith the oncology targets such as MDM2, BCL-2 and BCL-9[162] include antiviral targets against HIV-1,[163,164] and hepatitis C,[165] as well as the estrogen[166] and NMDA[167] receptors. Similar research has also accomplished helical peptide stapling using the glycine derivatives of the alkenyl building blocks described previously (Scheme 16 and Fig. 20). Various groups have shown that the added helix propogation of α,α-disubstituted amino acids is not necessary in certain cases, with the all hydrocarbon tether being sufficient in stabilising the α-helix upon ring-closing.[168,169]

The raft of data and expertise acquired for stapled peptides compared to alternative helical stapling techniques was instrumental in the decision to use this technique for creating a small peptide to inhibit the E2-25K/Ubb+1 interaction in this project. Adoption of the stepwise staple scanning approach, creating peptides of varying staple position, length and overall physicochemical properties was likely to give the greatest chance of success in mimicking the α-9 segment of E2-25K to antagonise Ubb+1 in relation to the ubiquitin proteasome system.

1.8 - Building blocks towards stapled peptides

As peptide stapling using alkenyl amino acids was identified as the technique of choice in creating helical mimics of the α-9 system of E2025K, the α,α-disubstituted building blocks required for the solid phase synthesis of these compounds were therefore required on a large scale with high enantio-purity. All four building blocks required for this project (Fig. 20) are reported as being commercially available; however, despite their utility the requisite amino acids are very expensive costing up to £290 per gram with varying degrees of enantiopurity (*vide infra*).
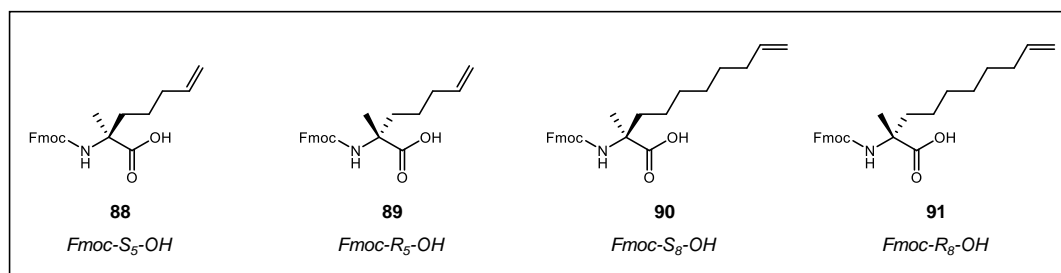
Figure 20 – Fmoc protected amino acids required for peptide stapling

Therefore, a robust synthesis towards these building blocks (**88** – **91**) was required for the current project which would preferably be amenable to scale-up without the need for excessive temperatures or large quantities of expensive reagents. The use of chiral auxiliaries is well established as a route towards various novel α,α-disubstituted amino acids due to their applicability on large scale, and in most cases, versatility towards side chain functionality. Based on this strong precedence and high probability of success, auxiliary based approaches to amino acid synthesis is discussed further in subsequent sections.

1.8.1 - The Schöllkopf method

One of the most widely used methods towards chiral amino acid derivatives is the Schöllkopf auxiliary. First disclosed in 1983,[170] a 2,5-diketopiperazine auxiliary was used as a novel method of creating pro-chiral non-proteinogenic amino acids (Scheme 17). To create the auxiliary, *L*-Valine (**92**) is Boc-protected then coupled with another amino acid methyl ester.[171] If an α-monosubstituted product is required then glycine is used (**93**), however if the α,α-disubstituted, or cyclic amino acid products are required then substrates such as alanine can be used. Cyclisation then affords the diketopiperazine (**95**) which is then methylated to give the auxiliary **96**.[171]
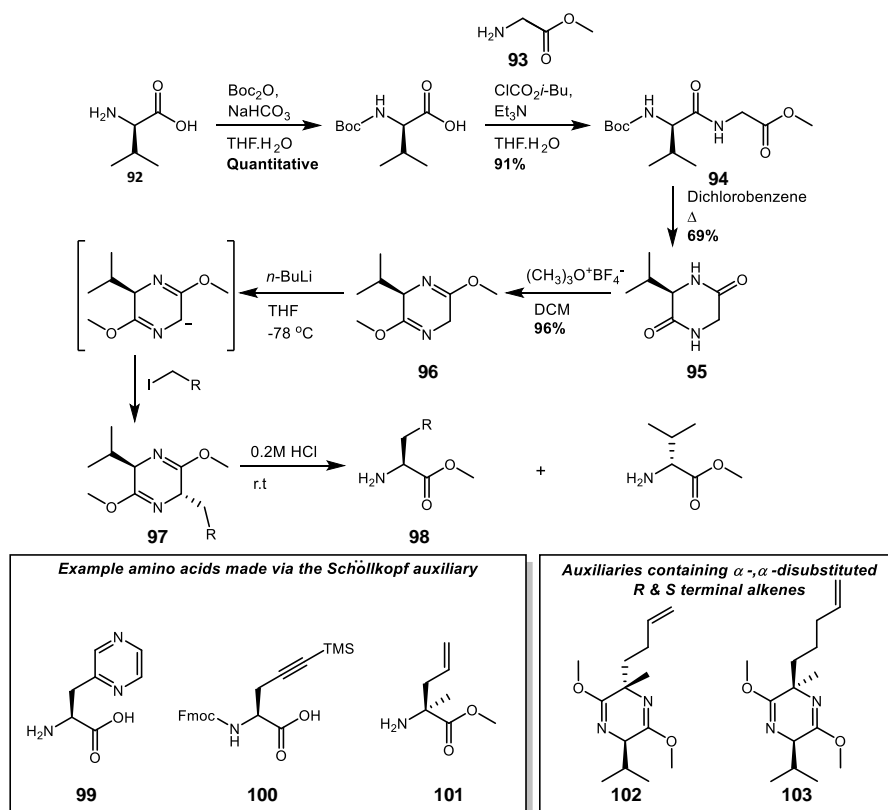
Scheme 17 - Large scale synthetic route using the Schöllkopf auxiliary

Once the auxiliary has been deprotonated, in most cases with BuLi, the nucleophillic attack on to the target alkyl halide will preferentially proceed on the opposite face of the auxiliary to the valine side-chain due its steric bulk (**97**). The final step is acid hydrolysis of the auxiliary, yielding the target amino acid (**98**) and an equivalent of valine (Scheme 17). Enantiomeric excesses (ee) of >95% are often reported using this technique on a wide range of alkyl halide substrates, demonstrating the utility of this method. Novel heterocyclic amino acid derivatives, such as the pyrazine **99**,[172] and novel alkyne amino acids (**100**),[173] which can be utilised for further click chemistry, have been created using this method. Of relevance to the current study is the preparation of the enantiospecific α,α-disubstituted compound **101**,[174] isolated in 63% yield *via* this method, which represents a truncated analogue of the building blocks used in peptide stapling. No direct synthesis of S_5 and R_5 have been attempted using this method, however the intermediate **103**,[175] which could be hydrolysed to the required R_5 stereoisomer, has been reported in 78% yield with a diastereomeric excess (de) of 90%. Compound **102**,[176] with a chain length of only four carbons, has also been synthesised in 80% yield with a diastereomeric excess of greater than 95%, implying that S_5 could also be synthesised *via* this route. A

large scale procedure is also available for creating the auxiliary **96** which would be required for the current study.[171] However, the main drawback of this route is the use of BuLi in the alkylation step which may be difficult to accomplish on scale.

1.8.2 - The Williams auxiliary

Alternatively, the original methodology used to create S_5 and R_5 by the Verdine group[151] utilised the Williams oxazinone auxiliary (Scheme 18)[177] with high enantioselectivity.
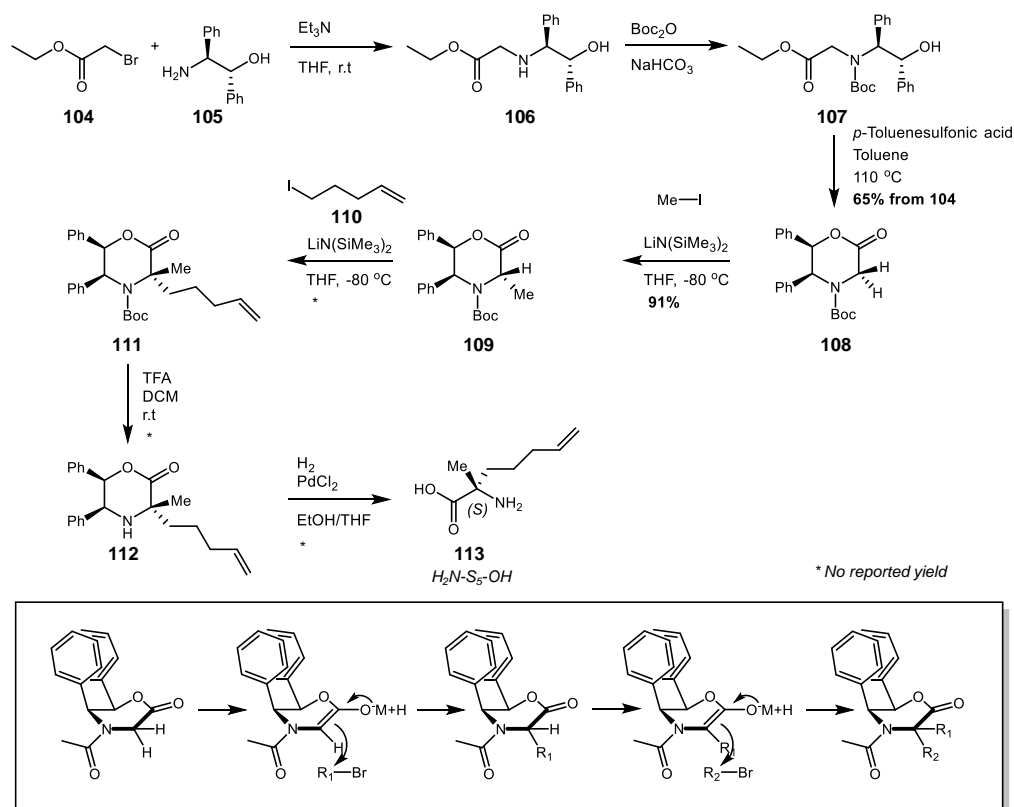
Scheme 18 - Williams oxazinone auxiliary
Synthesis of S_5 and boxed mechanism of chiral induction

Starting from commercially available ethyl bromoacetate (**104**) and (1*R*,2*S*)-2-amino-1,2-diphenyl ethanol (**105**), intermediate **106** is Boc deprotected (**107**) and cyclised using strong acid to the oxazinone auxiliary **108**.[178] To create the (*S*) form α-methyl, α-alkenyl amino acids, the methyl group is added to the auxiliary first[179] using a strong base, in this case lithium hexamethyldisilylamide (**109**). The second addition of the alkene (**110**) can then occur using the same conditions (**111**), with the stereochemistry of the methyl group being inverted from the previous compound.[179] This is attributed to the steric bulk of the two phenyl groups only allowing nucleophillic attack on one face of the auxiliary, therefore at the second

addition (Scheme 18, boxed region), R_1 is forced onto the opposite face from before. Controlling which alkyl group is added to the auxiliary first means that this method can allow for quick access to both R and S α,α-disubstituted amino acids. This route towards S_5 and R_5 has been proven to work in reasonable yields, however with no quoted enantiomeric excess.[151] As noted with the Schöllkopf auxiliary, the Williams method has some synthetically undesirable features for large scale applications. The cyclisation step requires high temperatures as well as a strong acid, and the nucleophillic additions of the side chains require strong bases at very low temperatures.

1.8.3 - Seebach derived oxazolidinone auxiliary

Another auxiliary based route towards building blocks **88** and **89** has been exploited in order to utilise the stapled peptide methodology towards HIV-1 integrase inhibitors.[164] This particular approach optimised Seebach's oxazolidinone conditions towards the target α–methyl, α-alkenyl substrates.[180] Seebach's innovative method towards creating enantiospecific α–methyl prolines employed a condensation/cyclisation reaction between L-proline (**119**) and pivaldehyde (**120**) to create the oxazolidinone intermediate **121** (Scheme 19, boxed region).[181,182] This intermediate could then be selectively deprotonated at the α-proline position, then alkylated with MeI to give the single diastereomer **122**. The oxazolindinone is then hydrolysed with aqueous acid to give the single enantiomer of (S)-methyl proline **123**.[182]

In order to create Fmoc-S_5-OH **88**, a modification on this route has been successfully implemented starting from (R)-Cbz-Alanine (**114**).[164] Formation of the Ala acid chloride and subsequent cyclisation with benzaldehyde dimethyl acetal gives the *cis*-auxiliary **116**. As with previous alkenyl additions, iodopentene **110** can selectively react with the auxiliary after deprotonation of the α–centre with a lithium base. As observed with the Seebach and Williams routes, the steric bulk residing on one face of the cyclic auxiliary directs the alkene into the correct stereochemistry (**117**). However, in this case, the diastereomeric ratio was reported as 5:2, therefore this particular system may not be best suited for this alkenyl addition, despite using optimised conditions.[164] Aqueous basic conditions then free the Cbz protected amino acid (**118**) which, if solid phase amide coupling is required, can then be Fmoc protected (**88**).
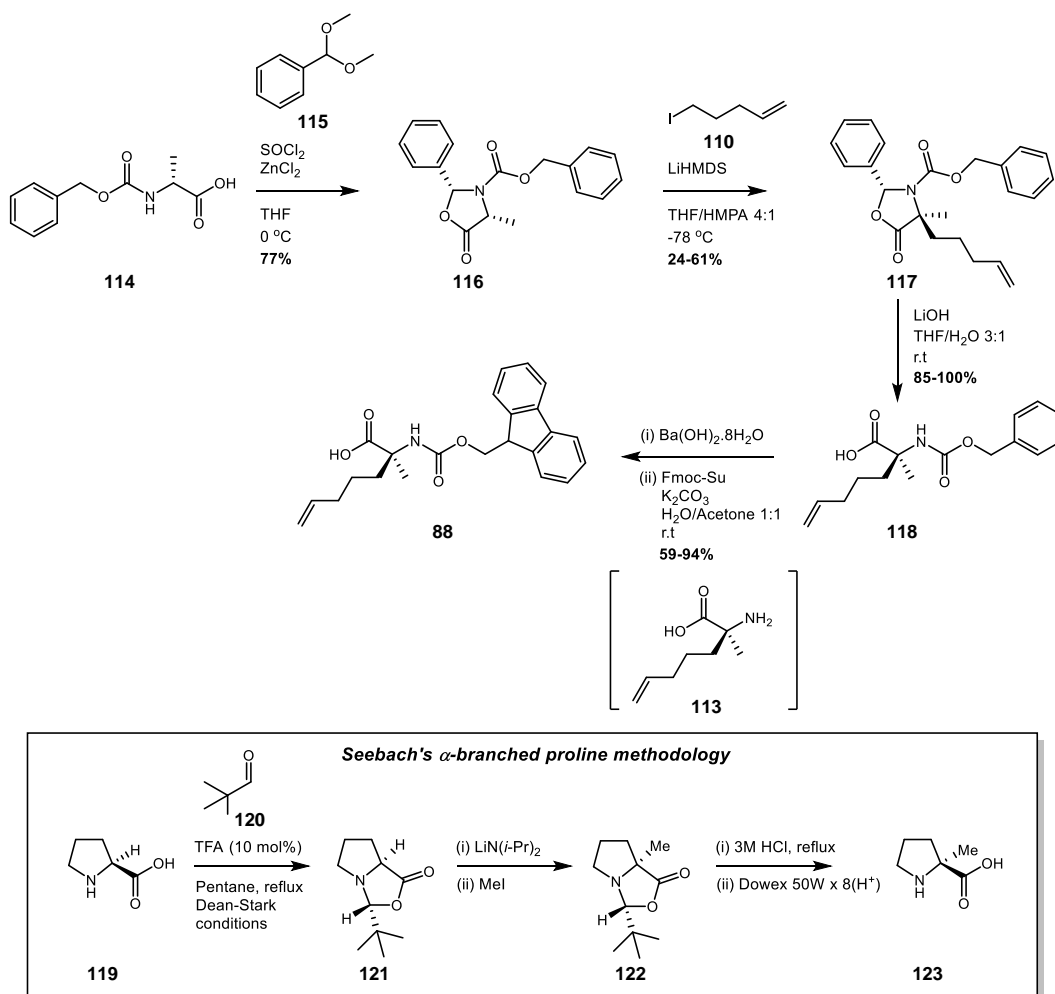
Scheme 19 - Modified Seebach oxazolidinone auxiliary

No final enantiomeric excess was reported for the Fmoc amino acid **88** however, as evidenced by the diastereomeric ratio discussed previously, the sample cannot be guaranteed as enantiopure *via* this route.

1.8.4 – BPB-Ni(II)-Ala Schiff base auxiliarys

Another frequently encountered route towards chiral unnatural amino acids is the use of metal coordinated auxiliary systems. The benzylproline-nickel(II)-alanine (BPB-Ni(II)-Ala) complex **127** (Scheme 20) has been shown to be applicable towards the creation of a range of α,α-disubstituted unnatural amino acids. First disclosed in 1985 as a method towards the enantioselective synthesis of β-hydroxy-α-amino acids,[183] the complex has been shown to be amenable to various enantiospecific chemical reactions at the α-centre such as aldol type additions,[183–185] Michael additions,[186–188] Mannich reactions,[189] oxidative cross-dehydrogenative cross couplings[190] and basic alkylations.[191–193] Synthesis of the auxiliary has also

been reported on a large scale (>1 kg) using relatively cheap materials (Scheme 20).[194]
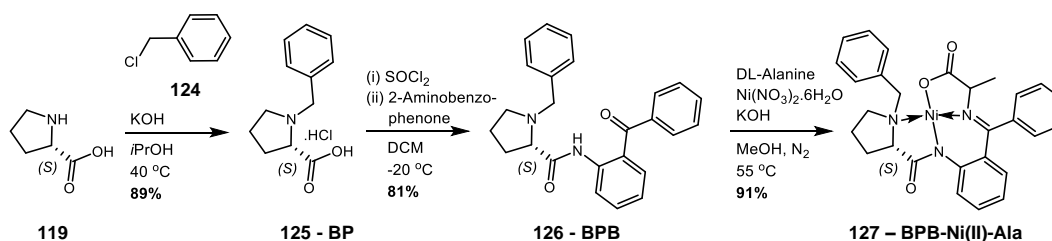
Scheme 20 - Scalable procedure towards BPB-Ni(II)-Ala complex

Starting from a single enantiomer of proline (**119**), benzyl proline **125** (BP) is formed from the base mediated reaction with benzyl chloride (**124**). Benzyl proline benzophenone **126** (BPB) is then created *via* a simple amide coupling of the acid chloride of **125** and 2-aminobenzophenone at -20 °C in order to prevent racemisation. Imine formation between BPB (**126**) and alanine, followed by a final complexation step with nickel (II) gives the chiral BPB-Ni(II)-Ala auxiliary (**127**).[194]

If the α-side chain being installed is required to be in the *S* configuration, then *S* (or *L*) proline (**119**) is used as the starting material to give **127**, conversely with *R* (or *D*) proline being used if the *R* configuration is required to give **128**. The conformation of the benzyl proline unit of the auxiliary directs the enantiospecific side chain addition (Fig. 21) due to the benzyl moiety blocking formation on one face of the complex to specifically give the (*S*)-BPB-Ni(II)-α-methyl-α*R*-(**127b**) from (*S*)-BPB-Ala-Ni(II) (**127a**), and (*R*)-BPB-Ni(II)-α-methyl-α*R* (**128b**) from (*R*)-BPB-Ni(II)-Ala (**128a**).
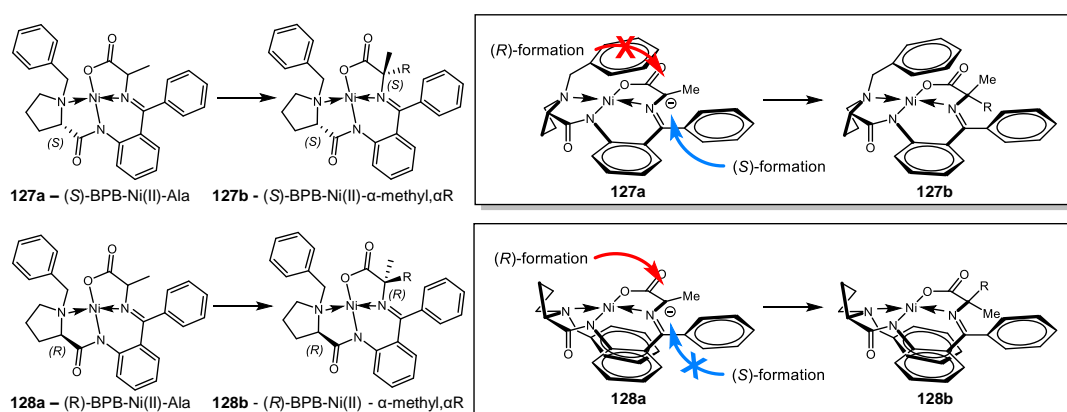
Figure 21 – Auxiliary mediated chiral induction for both R and S stereoisomers

Stereospecific alkylation has been accomplished using this auxiliary, specifically to attach pentenyl moieties which would give the R_5 and S_5 amino acids upon de-complexation. Two separate patents were published in 2009 claiming that this

method produced **88** (S_5) and **89** (R_5) in scalable quantities with reportedly high enantiomeric excess. In one such disclosure, the inventors have patented this complete route alone,[195] claiming high yields and efficient couplings to the α-methyl, α-alkenyl intermediate **130** in 55-80% yield using NaH under N_2 to give full deprotonation at the α-centre (Fig. 21) and nucleophillic addition of bromo (**129**) or iodo (**110**) pentene. Decomplexation using HCl in methanol is achieved in 65-70% yield, however the authors claim to purify the zwitterionic product **113** *via* normal phase column chromatography. Finally Fmoc protection using Fmoc succinimide in sodium carbonate solution gives the final product **88** in 40-70% yields. However, this Chinese language document appears to lack full characterisation,[195] simply supplying the ^{1}H NMR data, so no accurate value for enantiomeric excess can be drawn from this.

The second patent report published the same year by Aileron Therapeutics also contained the BPB-Ni(II)-Ala auxiliary as the synthesis route towards S_5 and R_5 (Scheme 21).[196] In this particular method, bromopentene (**129**) and potassium *tert*-butoxide are used to form the intermediate complex **130** in 67% yield.
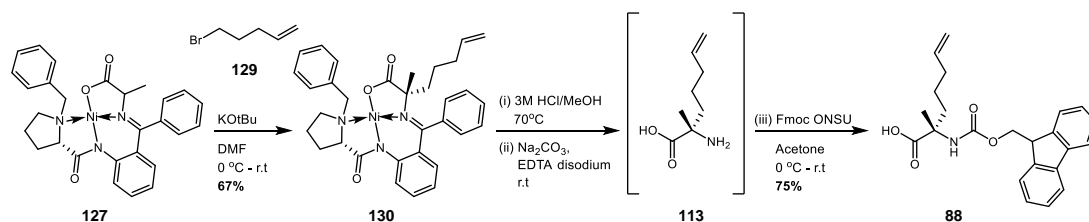
Scheme 21 - Ailereon route towards Fmoc S_5/R_5 using the BPB-Ni(II)-Ala auxiliary

A three step reaction process of decomplexation, nickel removal and Fmoc protection gives the final product **88** in 75% yield. As before, no enantiomeric excess data was supplied, however these building blocks were used in the synthesis of all-hydrocarbon stapled peptides which were tested in biological systems.[196]

Due to the apparent success of this method in creating Fmoc S_5 (**88**) and Fmoc R_5 (**89**) (as well as similar building blocks of varying alkenyl chain length), the BPB-Ni(II)-Ala auxiliary was deemed a promising synthetic route to be utilised in the current study. The relatively mild and scalable conditions required in the methodology are advantageous, however, further optimisation is likely to still be required as a subsequent report in 2013 failed in using this route towards creating the BPB-Ni(II)-α-methyl-α-pentyl complex **130** due to the synthesis being capricious in their hands.[168] Instead, the group opted for creating the BPB-Ni(II)-Gly complexes

and using only mono substituted pentenyl amino acid building blocks in their solid phase synthesis (Scheme 22).[168] A related study found that the alkylation step to **130** was not as diastereoselective or high yielding as claimed for the alanine based auxiliary **127**.[169] Replacement of the benzyl group with a 2-fluorobenzyl moiety was investigated for both the glycine (**131**) and alanine (**135**) based auxiliaries to improve diastereoselectivity (Scheme 22).
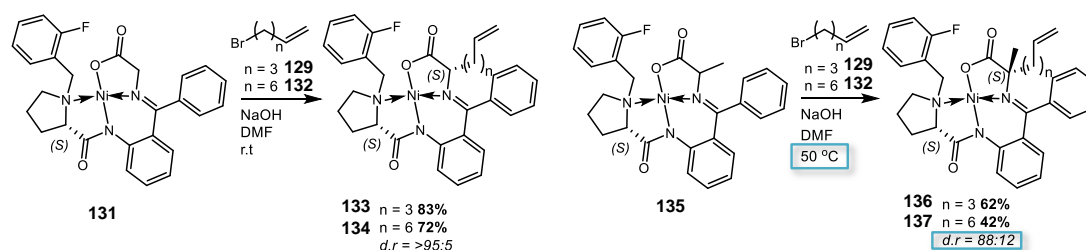
Scheme 22 - Alterations in Ni(II) based auxiliaries for amino acid synthesis

Encouragingly, high yields and diastereoselectivities were obtained using the glycine based complex **131** to gain both the pentyl (**133**) and octenyl (**134**) substituted complexes. However these results could not be matched when using the alanine based complex **135**. An increase in reaction temperature is required from room temperature to 50 °C, implying the reaction was low yielding at room temperature due to the slow reactivity at the substituted α-centre. The subsequent yield of complex **136** was marginally lower than claimed in the Aileron patented route for the pentenyl addition, however whether the limiting factor was the choice of base or the increased steric bulk around the auxiliary was not commented upon. Increasing the reaction temperature would appear to have an effect on the selectivity of the addition, with the complex diastereomeric ratio only 88:12.[169] Despite subsequent data observed for these glycine derived stapled peptides being comparable to the α-methyl disubstituted system pioneered by Verdine; claiming similar proteolytic stability, helix propensity and biological efficiency, the use of a α-monosubstituted building blocks in helical peptides could reduce the probability of helix nucleation and propensity. This is attributed to the fact that α-methylated amino acids rigidify the peptide backbone, enhancing the stability of an α-helical construct.[152] Therefore, through adaptation of the published methodology towards Fmoc S_5 (**88**) and R_5 (**89**) through the BPB-Ni(II)-Ala auxiliary, a scalable and efficient route towards the building blocks required for the solid phase synthesis of all-hydrocarbon stapled peptides could be produced, allowing for different tether lengths and variation in stereochemistry to be explored through simple alkenyl substitution or auxiliary modifications, respectively.

2. Project aims

As discussed in Chapter 1, inhibiting the E2-25K/Ubb+1 PPI could provide valuable information regarding the role Ubb+1 has to play in the pathogenesis of Alzheimer's disease. Accordingly, the aim of this project was to create tool compounds capable of selectively binding with Ubb+1 to antagonise this biologically relevant PPI. By doing this, there exists the possibility of elucidating whether incorporation of Ubb+1 into polyubiquitin chains is a factor in Ubb+1 mediated inhibition of the 26S proteasome. To accomplish this, the Verdine peptide stapling methodology was chosen to create α-helical peptides capable of mimicking the α-9 segment of E2-25K in order to selectively bind with Ubb+1 (Fig. 22, A). This macromolecular approach was chosen over small molecule screening due to the higher probability of success in creating compounds quickly which will target the large hydrophobic binding site associated with a PPI.
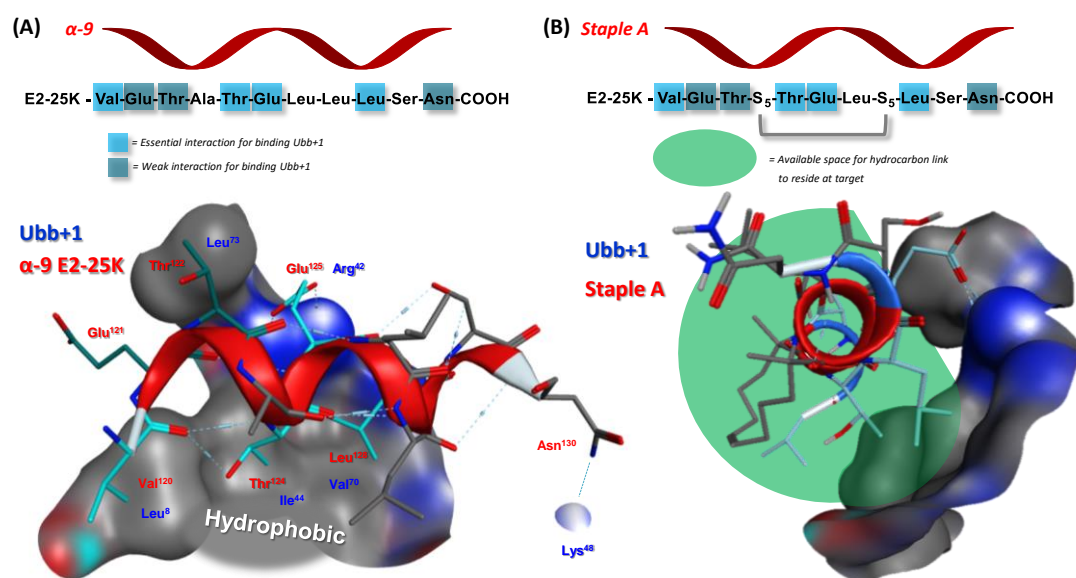
Figure 22 – Design of stapled peptides based on E2-25K/Ubb+1 crystal structure
A) – Key interactions between Ubb+1 and α-9 of E2-25K. B) – Available chemical space for staples to maintain key interactions.

The initial challenge of this project will be in generating a scalable route to the four target Fmoc protected α-methyl, α-alkenyl amino acids. Development of this route considered the scalability of the procedure in conjunction with high enantioselectivity as SPPS requires a large excess of building blocks in order to drive coupling reactions to completion. The BPB-Ni(II)-Ala auxiliary route was chosen due to the established precedent in synthesising the required substrates, and its relative ease of synthesis using inexpensive materials. Optimisation of the key alkylation step was

anticipated to be required in order to maintain yields above 65% without compromising enantioselectivity due to the capricious nature of this stage in the literature.

Once the target amino acids have been synthesised, they will be used to create a palette of stapled peptidic analogues of the α-9 segment of E2-25K (Table 2). The published crystal structure of the E2-25K/Ubb+1 PPI will be used to rationally design stapled peptides which are capable of maintaining the key interactions required for binding to Ubb+1.

Table 2 - Example staple scan across the sequence of α-9 of E2-25K

Peptide	Staple	Sequence
Wild type	-	Ac-V-E-T-A-T-E-L-L-L-S-N-NH$_2$
Staple A	i, i+4	Ac-V-E-T-**S$_5$**-T-E-L-**S$_5$**-L-S-N-NH$_2$
Staple B	i, i+4	Ac-V-E-T-A-**S$_5$**-E-L-L-**S$_5$**-S-N-NH$_2$
Staple C	i, i+4	Ac-V-E-**S$_5$**-A-T-E-**S$_5$**-L-L-S-N-NH$_2$
Staple D	i, i+7	Ac-**R$_8$**-E-T-A-T-E-L-**S$_5$**-L-S-N-NH$_2$
Staple E	i, i+4	Ac-V-E-T-**R$_5$**-T-E-L-**R$_5$**-L-S-N-NH$_2$
Staple F	i, i+4	Ac-V-E-T-A-T-E-**S$_5$**-L-L-S-**S$_5$**-NH$_2$
Staple G	i, i+4	Ac-**S$_5$**-E-T-A-**S$_5$**-E-L-L-L-S-N-NH$_2$
Staple H	i, i+7	Ac-V-E-T-**R$_8$**-T-E-L-L-L-S-**S$_5$**-NH$_2$

A staple scan will be completed, creating peptides with varied hydrocarbon staple position, stereochemistry and length to investigate the effect on helicity and target affinity. As the Ubb+1 binding site is mainly hydrophobic, there is a significant amount of chemical space available to place the all-hydrocarbon staple and still gain affinity for the target (Fig. 22, B). Once synthesised, these stapled peptides will be analysed by CD spectroscopy to evaluate helical content compared to the wild type peptide (Table 2). Upon completion of structural analysis, the peptides will be evaluated in polyubiquitination assays. The aim of these assays will be to determine whether these peptides are capable of inhibiting Ubb+1 incorporation into polyubiquitin chains, whilst maintaining regular polyubiquitination processes. If successful candidates are found, computational modelling can then be used to establish a structure-activity relationship for stapled peptides against Ubb+1. This information will then be used to develop a second generation of stapled peptides with increased affinity and selectivity for Ubb+1. Overall, during the course of this project, the first generation compounds capable of inhibiting the incorporation of

Ubb+1 into PolyUb chains will be developed. It is anticipated that these tool compounds will further assist in delineating the role Ubb+1 has to play in the pathogenesis of AD, as well as determining if this PPI is chemically tractable using peptide antagonists.

3. Results and discussion

3.1 - Chiral amino acid synthesis

Synthesis of the four target α–methyl, α-alkenyl amino acids required for this project was anticipated to be challenging. This is due to the need for high enantiomeric excess (≥ 90%) and the requirement to produce each of the building blocks on an appropriate scale to support SPPS. Despite advances in the synthesis of mono-substituted chiral amino acids, the available routes to α-, α-disubstituted chiral amino acids are not as well exemplified compared to mono-substituted systems, and are often laborious. As discussed in Section 1.8.4, the BPB-Ni(II)-Ala auxiliary approach was chosen for this work due to previous precedent which suggests it could be used on scale. The lack of pyrophoric reagents or low temperatures implies the route will be robust in nature once optimised, starting from relatively inexpensive reagents.

3.1.1 – Test of scale up procedures to BPB-Ni(II)-Ala chiral auxiliary

Various published approaches to auxiliary **127** have been reported in the literature, and in particular a scale up procedure to 100 grams (Scheme 20).[194] The first step is benzylation of (*S*)- or (*R*)-proline (**119** & **139**), depending on whether the (*S*) or (*R*) final amino acid is required (Scheme 23). This simple reaction using KOH in IPA was accomplished in comparable yields to the literature to give both enantiomers of benzyl proline (**125** & **140**) as hydrochloride salts.
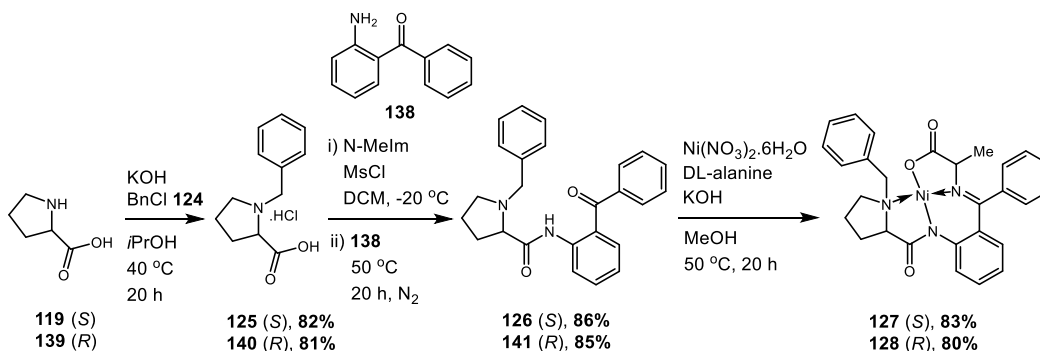
Scheme 23 – Modified procedures for BPB-Ni(II)-Ala complex formation

During scale up procedures (40 g, 350 mmol), the yield was most affected by the HCl salt formation due to larger volumes of solvent slowing the rate of precipitation. Formation of BPB (**126** & **141**) was accomplished using conditions adapted from a more recent procedure.[197] Replacing thionyl chloride mediated acid chloride formation with a mixed anhydride approach was deemed more favourable due to the

milder conditions and decreased likelihood of racemisation at the α-proline centre. These modified conditions also recommended maintaining a nitrogen atmosphere and using dry DCM. The reaction temperature was maintained in a -20 °C salt bath during the reaction of **124** & **140** with *N*-methyl imidazole and methane sulfonyl chloride due its exothermic nature. This was particularly important on scale up (35 g, 150 mmol), maintaining the internal temperature at a maximum of -5 °C to prevent side reactions. Upon addition of 2-aminobenzophenone (**138**) the reaction was heated to reflux overnight to give both enantiomers of BPB (**126** & **141**) in high yields.

The final complexation step (Scheme 23), requires a large excess of base (7 equiv.) and elevated temperatures (50 °C) in order to form both the Schiff base with alanine and benzophenone, as well as the square planar nickel(II) complex. Therefore, in order to decrease any potential racemisation of the α-proline centre, the reaction time was minimised to two hours. Initial attempts at forming **127** and **128** were relatively low yielding (≤ 70%) in the first instance when following the reported procedure. Increasing the equivalents of base, whilst leaving the reaction to stir overnight, had a profound effect on the yields of **127** and **128**, increasing them in excess of 80%. However, these results could not be replicated on larger scales (130 mmol) with yields decreasing drastically to 39% compared to the smaller scale procedures (Scheme 1) which were conducted on a tenth of the scale. The resulting (*S*) complex **127** was assayed using optical rotation in order to ascertain whether any epimerisation had taken place at the α-proline centre using the alternative conditions (Scheme 23). Encouragingly, this analysis indicated that the complex had a comparable optical rotation to the literature. The diastereomeric ratios of the isolated compounds were on average 70:30 as determined by ^{1}H NMR. Whether complexation of one enantiomer of alanine was more favourable with the auxiliary, or if base mediated epimerisation was taking place at the α-alanine centre was not clear at this time. It was interesting to note that crystallisation of the nickel complexes were relatively simple, giving vivid blood red crystals. Accordingly, an X-ray crystal structure of the (*R*) enantiomer, **128** was obtained elsewhere in our laboratories,[198] to afford a more complete characterisation of the auxiliary, as well as investigating the stereochemistry of the major diastereomer (Fig. 23). The auxiliary **128** is a Ni(II) 16-electron complex and adopts a square planar geometry with the benzyl moiety above the metal centre (Fig. 23). The diastereomer of **128** crystallised was (*R*)/(*R*), with the proline maintaining its chiral integrity, and the alanine methyl

group adopting the least sterically hindered conformation, potentially after epimerisation during synthesis.
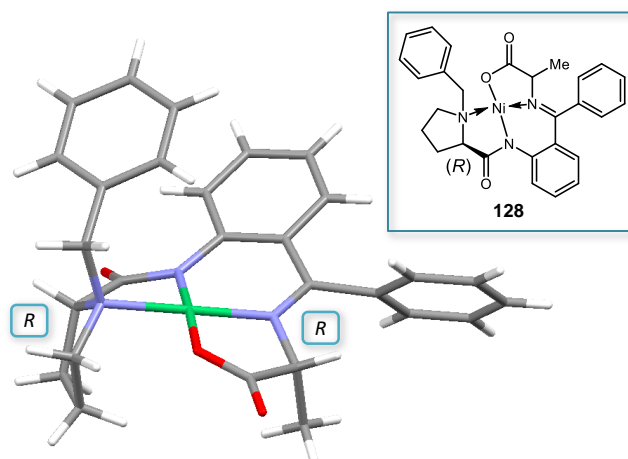
Figure 23 – X-ray crystal structure of auxiliary 128

This crystal structure implied that the main diastereomer formed during complex formation was the (R)/(R) structure of **128**, despite the longer reaction times being employed. The optical rotation data for the complex was also concordant with the literature for the *(R)/(R)* diastereomer. At this point, the proportion of other potential diastereomers formed could not be ascertained, excluding the *(R)/(S)* complex which could be calculated from the ^{1}H NMR of **128**. Therefore, both complexes **127** and **128** were taken forward to the next step in the synthesis.

3.1.2 – Optimisation of BPB-Ni(II)-Ala alkylation step

Alkylation of the BPB-Ni(II)-Ala complex is consistently the lowest yielding step across the reported literature for the synthesis of α–methyl, α-alkenyl amino acids due to the relatively hindered nature of the alanine centre in the auxiliary. Various combinations of reagents have been published for haloalkenes of chain lengths ranging from three to nine carbons with the complex **127**. However, as previously stated in Section 1.8.4, the patented conditions for the desired substrate **130** can be capricious. Therefore, a small screen was conducted to test these conditions in our hands, and to determine if any improvement in yield and diastereomeric ratio could be achieved through simple optimisation (Table 3). From consideration of the primary literature, some of the highest yields for enantioselective alkylation with haloalkenes had been achieved using sodium hydroxide.[169,191] Despite these reactions being used on the glycine derived complex, it was deemed appropriate to start with the highest yielding reported procedures for similar substrates. The

published conditions employing sodium hydroxide as a base used dry acetonitrile and DMF as solvents, therefore acetonitrile was chosen for an initial reaction as the resulting work-up and isolation was reasoned to be less problematic. The bromo-alkene **129** was chosen as the substrate due to its commercial availability and apparent success claimed in the patented conditions.[196] Finally, the reaction temperature would be maintained at ambient temperature as increasing the temperature was anticipated to lower the diastereomeric ratio.

Table 3 – Optimisation of alkylation conditions
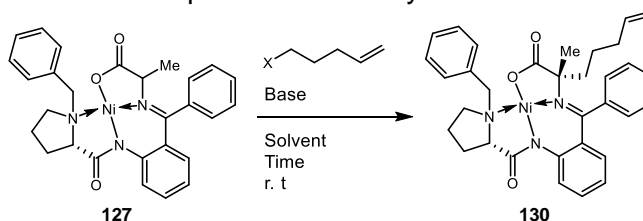
	X - pentene		Base	Solvent	Additive	Reaction time	Yield
1	Br	**129**	NaOH	MeCN	-	2 h	No reaction
2	Br	**129**	tBuOK	MeCN	-	2 h	No reaction
3	Br	**129**	tBuOK	THF	-	2 h	Trace
4	Br	**129**	*t*BuOK (sub.)	THF (dry)	TBAI (0.1 equiv)	5h	35%
5	I	**110**	*t*BuOK (sub.)	THF (dry)	-	5 h	43%
6	I	**110**	*t*BuOK (sub.)	THF (dry)	TBAI (0.1 equiv)	5 h	70%
7	I	**110**	*t*BuOK (sub.)	DMF	TBAI (0.1 equiv)	16 h	Not isolated

Unfortunately, the first test reaction (Table 3, row 1) was unsuccessful, with no product formation observed after two hours. When the base was changed from NaOH to *t*BuOK, which was used in the Aileron patent[196] (Scheme 21), there was still no reaction after two hours (Table 3, row 2). This was potentially due to the base being insoluble, or the reaction solvent not being dry enough, as anhydrous conditions appeared to be beneficial according to earlier literature reports.[169,191] Therefore the solvent was changed from acetonitrile to THF to aid solubility. Encouragingly, a trace amount of product was detected by TLC after two hours, however, the reaction was not worked up at this point (Table 3, row 3). Instead, a further test reaction was carried out using vigorously dry conditions, employing sublimed *t*BuOK and dry THF. Tetrabutylammonium iodide was also added to determine if introducing alternative counterions (Bu$_4$N$^+$ vs K$^+$) around the enolate centre of the complex (Fig. 21) would have an effect on reactivity. Pleasingly, an isolated yield of 35% was obtained after five hours, confirming the formation of complex **130** (Table 3, row 4). As this was still significantly lower than the reported

yield of 67%,[196] further optimisation was required before moving on to amino acid isolation. For the next test reaction, the iodoalkene **110** was chosen as it had shown some success in the Williams (Scheme 18) and Seebach (Scheme 19) auxiliary based routes to the target amino acid **88**. Compound **110** was successfully synthesised from the bromo alkene **129** *via* the Finkelstein reaction (Scheme 24).
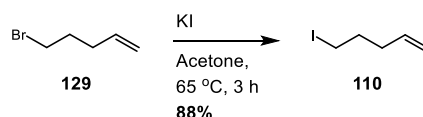
Scheme 24 – Finkelstein conditions to 5-Iodopent-1-ene

Reflux of bromopentene **129** in acetone with two equivalents of KI gave the product in three hours. A simple hexane work-up with a slow Kugelrohr distillation gave the product in an excellent yield of 88%. The product was then used for the complex alkylation (Table 3, row 5) to give the complex **130** in 43% isolated yield. Upon addition of TBAI, the yield increased further to 70% (Table 3, row 6), confirming that the change in counterion could result in an increase in yield. When the solvent was changed to DMF to reflect the Aileron patented conditions (Scheme 21), analysis of the reaction mixture showed increased formation of multiple by-products compared to the THF conditions, which upon work-up made chromatographic purification very difficult. No clean product could be isolated, with ^{1}H NMR confirming that multiple impurities were still present. Therefore, the conditions shown in Table 3, row 6 were chosen as the optimum due to their simplicity and comparative ease of isolation.

3.1.3 – α-Methyl, α-pentyl amino acid isolation

Following optimisation, the isolated yields of the alkylated complex were comparable to the reported literature,[169,196] and the diastereomeric ratio of complex **130** was in excess of 95% by ^{1}H NMR (*(S)/(S)* to *(S)/(R)*) which was extremely encouraging (Scheme 25).
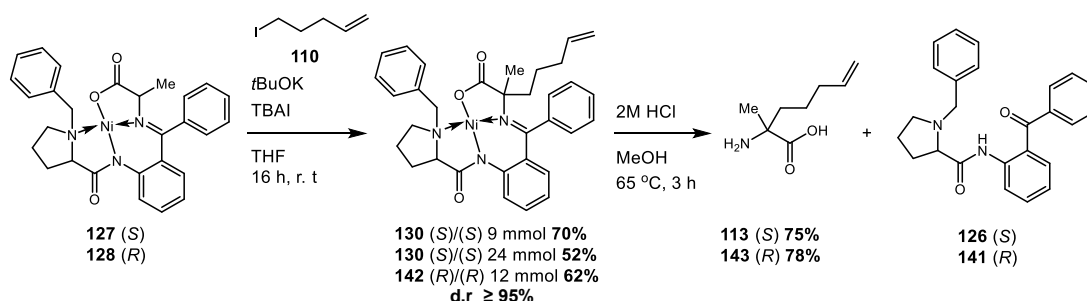
Scheme 25 – Optimised alkylation conditions with amino acid isolation

However it was noted that when the synthesis of **130** was scaled up to 24 mmol the yields decreased slightly to 52%. The procedure was also reproducible, with the analogous synthesis of (*R*) – **142** being achieved in 62% yield with a similarly high diastereomeric ratio (Scheme 25).

The next stage in the synthesis was the acid hydrolysis of auxiliaries **130** and **142** to give the free amino acids (**113** & **143**), along with recovered BPB. Reflux of the auxiliaries in 2M HCl in methanol for 3 hours afforded the products in high yields, with the reaction being easily monitored by a colour change of deep red to light yellow. As compounds **113** and **143** are water soluble, work-up with organic solvent allowed for facile separation of the product from the auxiliary precursors **126** and **141**. The next issue was separation of the water soluble nickel adducts from the free amino acids which were both isolated in the aqueous phase. Initial attempts using catch and release chromatography were unsuccessful as the amino acid appeared to be retained on the stationary phase of cartridges, such as SCX (strong cation exchange) sorbents, and could not be isolated. This was most likely due to the acid-base interaction of the functionalised silica and **113** being too strong to disrupt.[199] In a subsequent attempt at this reaction, purification was carried out by recrystallization of the aqueous residue using 1M HCl. The recovered material, however, was not clean by ^{1}H NMR with a range of unknown impurities observed.

At this point, we examined the use of ion-exchange resins in the purification of the target amino acids. These polymer beads, commonly formed from styrene and divinyl benzene, can be functionalised in order to give them specific properties, such as anionic and cationic capacities. Industrially, such resins are used most often in water purification, however their applications on laboratory scale allow for specific catch and release separations through the exploitation of specific resin functionality, cross linkage and particle size. For the purpose of this experiment, a strong cation exchange (sulfonic acid functionalised) resin was used (Dowex 50WX8 H-form).[200] After elution from the column using aqueous ammonia and drying, the white solid obtained from the resin was confirmed as product in high yields for both enantiomers (Scheme 25).

For the final Fmoc protection step, mixed solvent systems were required with a dioxane:water (1:1) system giving higher yields in our hands compared to the acetone:water mix claimed by Aileron (Scheme 21).[196] Use of the Fmoc-succinimide (**144**) also gave a cleaner reaction than Fmoc-chloride, with sodium carbonate as

the base being the optimum conditions (Scheme 26). During small scale synthesis it became apparent that a major Fmoc based by-product was formed during the protection process, which co-eluted with the product during column chromatography. A short optimisation of the procedure demonstrated that adding the Fmoc-ONSU (**144**) in batches to the reaction mixture over an hour at 0 °C decreased the by-product formation, however despite this, no product of appropriate purity could be obtained due to contamination with this impurity.

113 (*S*)
143 (*R*)

88 (*S*) 84%
89 (*R*) 55%
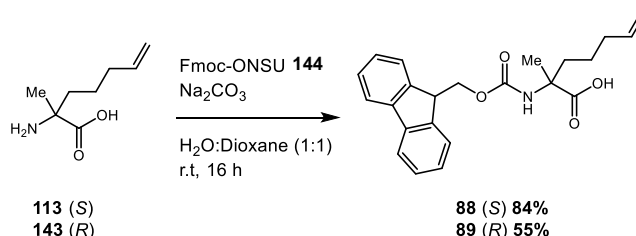
Scheme 26 – Fmoc protection of free amino acid

Isolation of a pure sample of the by-product revealed the structure of this impurity to be Fmoc-carbamate **145** (Scheme 27). It was proposed that excess ammonia present from the DOWEX purification step of the free amino acids (**113** & **143**), which had not been detected by NMR, was condensing with Fmoc-succinimide (**144**) to give the carbamate **145**.

144

145
9-Fluoroenylmethyl carbamate
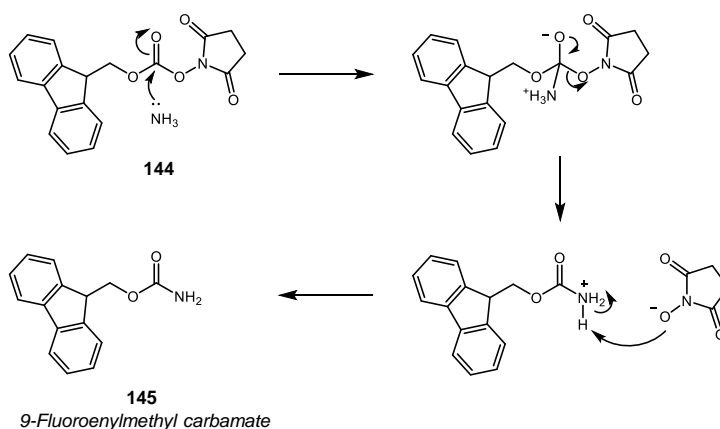
Scheme 27 – Proposed mechanism of by-product formation

In order to decrease ammonia content in the purified amino acids (**113** & **143**), the amino acid isolated by ion exchange chromatography was isolated by freeze drying rather than by concentration on a rotary evaporator. An extensive washing protocol was also introduced to extract the majority of the by-product before column chromatography. A test reaction with (*S*)-**113** gave a reasonable yield of 49% for the Fmoc protected amino acid **88**, however the chromatographic purification remained

arduous. Therefore, when isolating (R)-**89**, preparative HPLC was used to purify the final product with relative ease (Scheme 26). The subsequent yield was also increased to 55% for the Fmoc protected amino acid **89**.

3.1.4 – Analysis of optical purity of Fmoc protected building blocks

Having enabled a route towards the target Fmoc R_5 (**89**) and Fmoc S_5 (**88**) compounds it was then necessary to determine an accurate enantiomeric purity for these systems. Accordingly, a chiral HPLC method was developed to enable quantification of enantiomeric excess. Using a CHIRALPAK IA column (Amylose tris(3,5-dimethylphenylcarbamate)) a suitable method was developed to separate the enantiomers (Fig. 24).
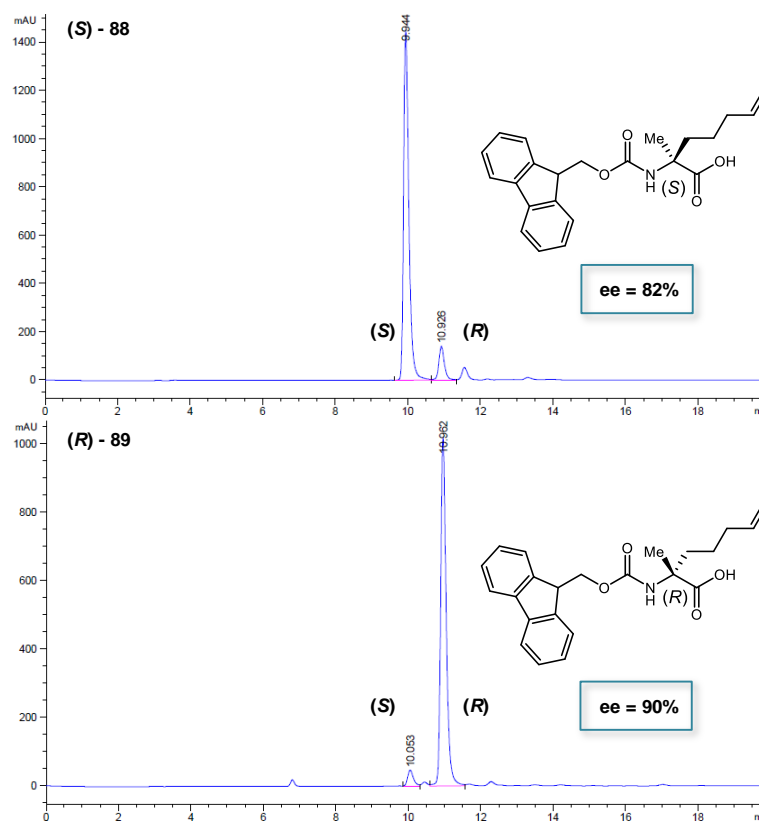
Figure 24 – Chiral HPLC analysis of Fmoc amino acids 88 & 89

The chromatograms obtained for both (S)-**88** (Fig. 24, top) and (R)-**89** (Fig. 24, bottom) showed in each case that a small percentage of the opposite enantiomer was present. When the enantiomeric excess was calculated, the (S)-amino acid had a disappointing value of 82%, whilst the (R)- had a more acceptable enantiomeric excess of 90%. At this point it became apparent that the BPB-Ni(II)-Ala auxiliary process was effective in producing α-methyl, α-alkenyl amino acids with relatively

high enantiomeric excesses. However, the optical purities of the final compounds could be variable with an 8% difference in the optical purity of the two samples (*S*)-**88** and (*R*)-**89.** These results implied that an inconsistency was present in the current BPB-Ni(II)-Ala auxiliary procedure, resulting in final products of diminished optical purity.

It was deemed that despite the high purity of compound (*S*)-**88**, the enantiomeric excess was not sufficient for use in solid phase peptide synthesis, as the risk of forming diastereomeric peptides which could not be separated from each other would be too great. Based on this, it was necessary to re-evaluate the synthesis of (*S*)-**88** and establish how this erosion in enantiomeric excess could have occured, given that the ^{1}H NMR of the precursor **130** appeared to have no (*S*,*R*) diastereomer present (Section 3.1.3).

In order to investigate this process further, a crystal structure of the (*S*)-**130** complex was obtained elsewhere in our laboratories (Fig. 25).[198] This structure proved to be particularly informative as it revealed that compound **130** contained both the (*S*,*S*) and (*R*,*R*) enantiomeric forms, rather than the single component suggested by ^{1}H NMR.
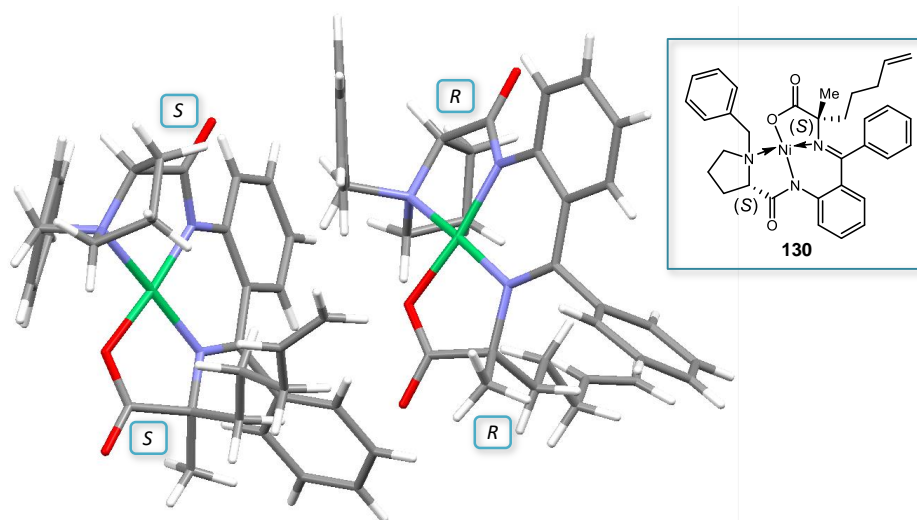
Figure 25 – Crystal structure showing both (*S*,*S*) and (*R*,*R*) diastereomers of 130

The presence of the opposite enantiomer of our required (*S*,*S*) complex implied that at some point in the synthesis racemisation was occurring at the α–proline centre. Consequently, the unwanted (*R*)-complex formed (**128**) was then selectively alkylated to give the (*R*,*R*) complex (**142**) which could not be differentiated from the

(*S*,*S*) complex by ^{1}H NMR as they represent enantiomers of each other as opposed to diastereomers.

Analysis of complex **130** by chiral HPLC provided additional insight into the relationship between the ratio of (*S*,*S*)- to (*R*,*R*)-complex (Fig. 26), and its effects on the optical purity of the final Fmoc amino acid, **88**. The (*S*,*S*)-complex had an enantiomeric excess of 84% which corresponded well to the final product (*S*)-**88** with an enantiomeric excess of 82% (Fig. 24). Similar results were noted for the (*R*,*R*)-complex **142** (Fig. 26) where an enantiomeric excess of 90% corresponded exactly with the final Fmoc product **89**, which also had an enantiomeric excess of 90%.
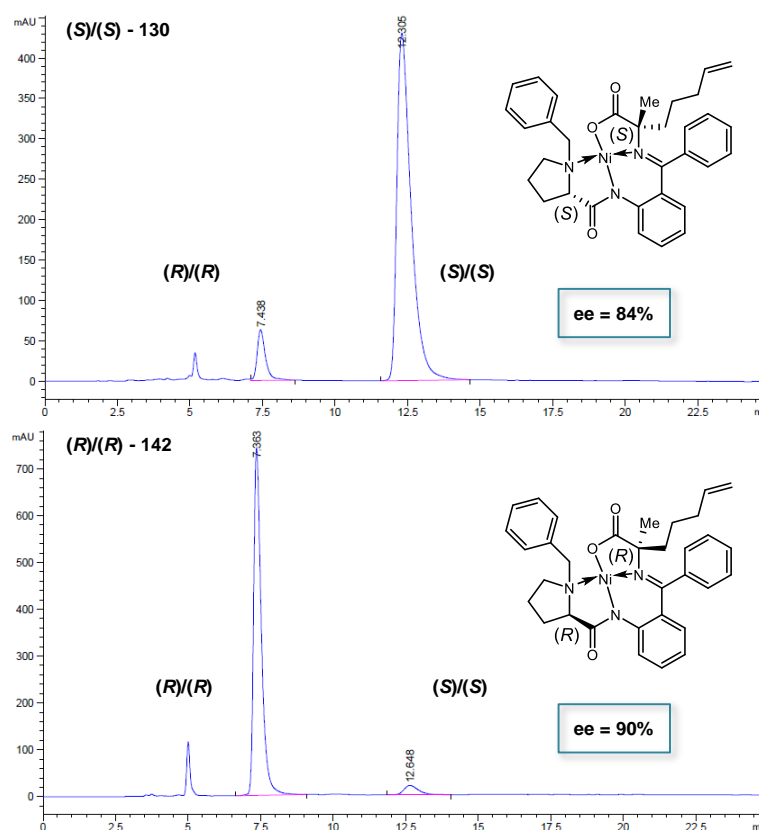
Figure 26 - Chiral HPLC analysis of α-methyl, α-alkenyl complexes 130 & 142

This analysis proved that the extent of racemisation at the α-proline centre would directly affect the optical purity of the final compounds and that care would have to be taken to maintain the integrity of all the chiral centres present.

3.1.5 – Re-assessment of complex formation

Despite positive analysis by optical rotation, the chiral integrity of the α-proline centre was likely being eroded during the first 3 steps of the synthesis (Scheme 23).

71

This degradation was likely due to the large excess of base being used during the complex formation step from **126** to **127**. Accordingly, a chiral HPLC assay was developed for the precursor compounds (S)-**126** and (R)-**141** to confirm whether the BPB auxilliary formation took place with retention of stereochemistry. Despite the presence of some 2-aminobenzophenone (**138**), it could be demonstrated that both enantiomers were optically pure with enantiomeric excesses of over 98% (Fig. 27). Therefore, it was evident that the α-proline degradation was occuring during the base mediated complexation step, and not during benzyl protection or subsequent amide bond formation with 2-aminobenzophenone (**138**).
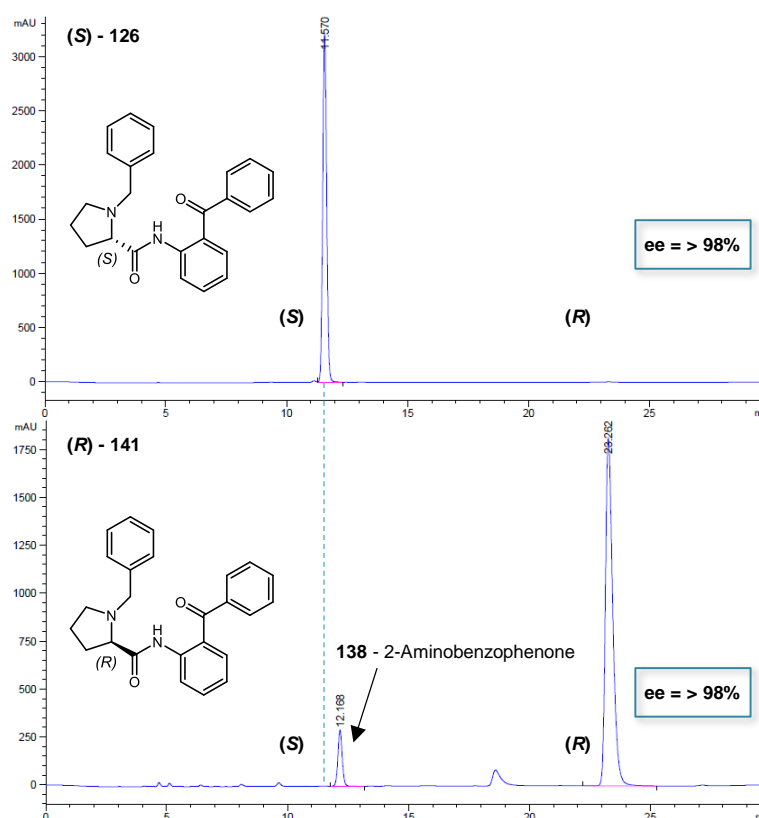
Figure 27 – Chiral HPLC analysis of BPB precursors

Unfortunately, a chiral HPLC method for the BPB-Ni(II)-Ala complexes **127** and **128** to examine enantiomeric excess could not be developed at this point. This was possibly attributed to the complex mix of 4 diastereomers present: (S)-Pro/(S)-Ala, (S)-Pro/(R)-Ala, (R)-Pro/(S)-Ala and (R)-Pro/(R)-Ala, making complete separation by HPLC extremely difficult. Consequently, the chiral HPLC assay developed for the alkylated complexes, **130** and **142** (Fig. 26), represented the earliest opportunity for analysing the extent of proline racemisation as the optical rotation values obtained previously were not reliable. Due to the direct correlation between proline

racemisation and enantiomeric excess of the final amino acid product, it was proposed that the two major diastereomers of complex **130** were the (*S*)/(*S*) (**130**) and (*R*)/(*R*) (**142**).

3.1.6 – Correlation between proline epimerisation and optical purity of product

At this point, it was clear that the current conditions used to form complexes **127** and **128** (Scheme 23) were not consistent as they were giving final amino acid products with enantiomeric excesses ranging from 84 to 90%. During complexation the majority of the complex remains in the (*S*) configuration at the proline centre, with a minor amount (in this case ~16%) epimerising to the (*R*) form **128** (Fig. 28), with the stereochemistry at the alanine centre remaining variable. Upon alkylation of the alanine unit, 4 diastereomers can be formed. However, formation of the *trans* diastereomers **146** and **147** are negligible as the reaction is extremely *cis* selective, with this selectivity determined by the diastereomeric ratio determined by [^1]H NMR.
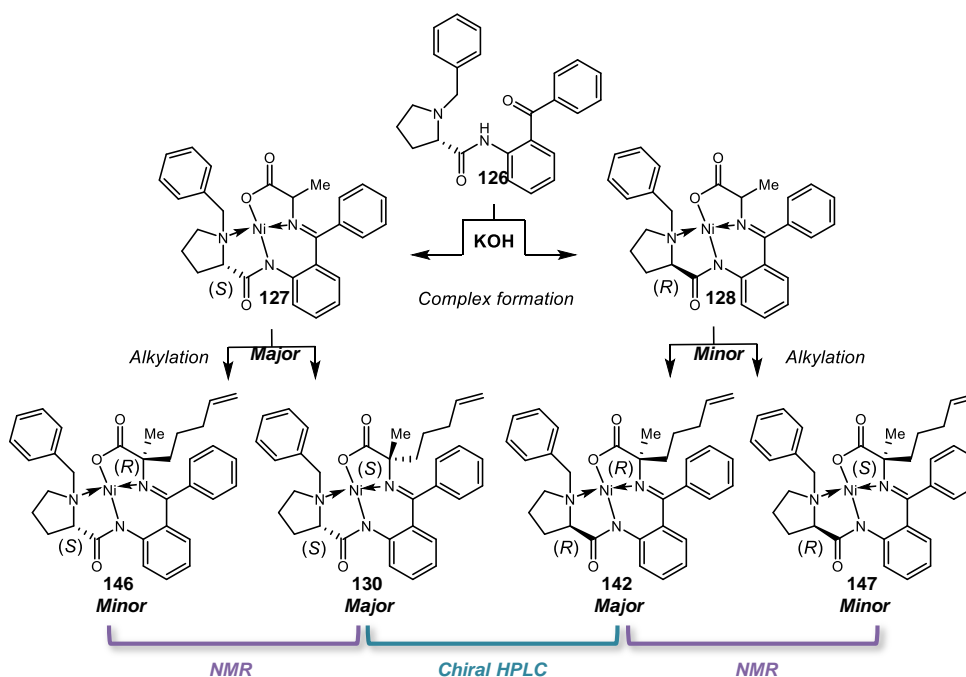
Figure 28 – Mix of four diastereomers when forming α-methyl, α-alkenyl complexes

Therefore, the ratio between the two *cis* diastereomers **130** & **142**, should be an effective means to determine the enantiomeric excess of the final Fmoc-protected product, as demonstrated in Fig. 24 *vs* Fig. 26. Further evaulation of the previously reported literature[194] implied that the reason for the low yields when initially using the scale up procedure to **126** (Scheme 20) may have been due to the addition of powdered KOH, rather than as a solution in MeOH. With the short reaction time of two hours, the time taken for the KOH to fully dissolve would likely affect the yield,

especially on a larger scale. It was hypothesised that by returning to seven equivalents of KOH and a reaction time of two hours the yields may be improved. These conditions should also alleviate the extent of proline epimerisation, giving a product of greater optical purity on a more consistent basis.

An initial trial reaction using (*S*)-**126** on a 5 mmol scale gave an acceptable yield of 77% for **127a** (Scheme 28).
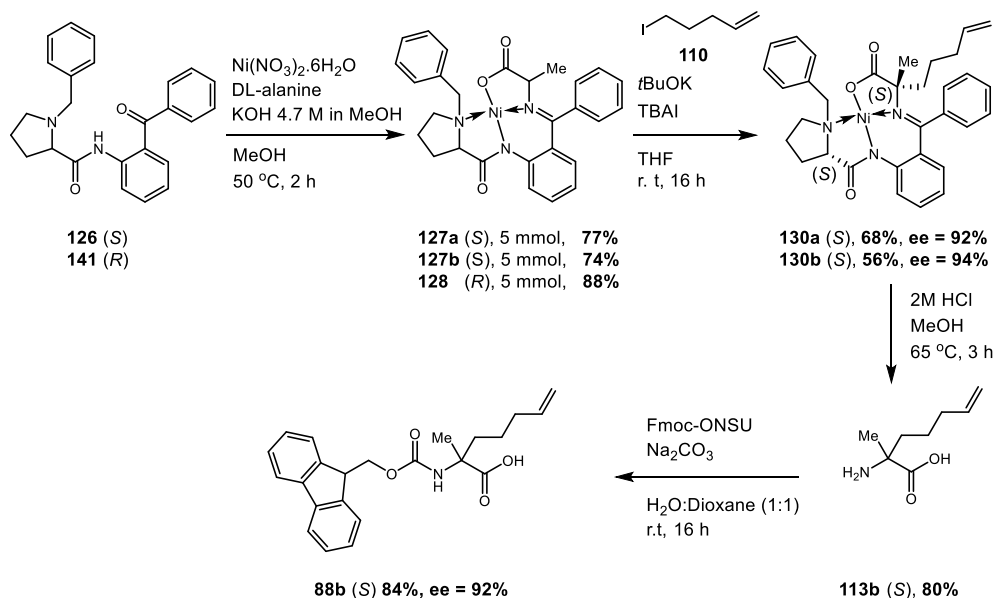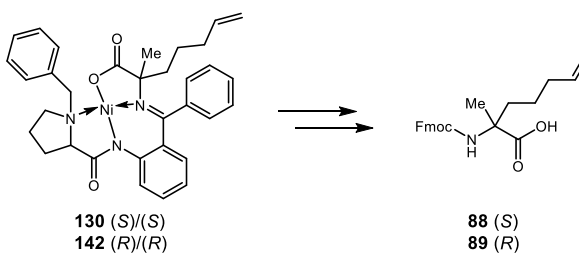
Scheme 28 – Re-evaulation of complex formation

Adding the KOH as a solution resulted in a vast improvement in yield in a two hour reaction time compared to the solid addition. However, the important consideration at this point was whether these conditions maintained the integrity of the α-proline centre. Therefore, an alkylation was carried out using iodopentene (**110**) as before (Scheme 25) to give the α-methyl, α-alkenyl complex **130a** which could be analysed by chiral HPLC. Encouragingly, the chiral HPLC of complex **130a** showed an enantiomeric excess of 92%. This increase of 6% from the previous synthesis meant the final amino acid would likely have an enantiomeric excess of ≥ 90% which was within the threshold deemed to be acceptable for building blocks for SPPS. A repeat reaction with complex formation to **127b** and subsequent alkylation to **130b** gave comparable yields, and a final enantiomeric excess of 94% for **130b**. A similar reaction using (*R*)-BPB (**141**) gave a suprisingly high yield of 88% to compound **128**. At this point it was apparent that these conditions gave consistently lower levels of proline epimerisation, despite the fact the yield associated with initial alanine complex formation could be variable.

In order to confirm the hypothesis that the enantiomeric excess of complex **130** was directly proportional to that of the final amino acid **88**, complex **130b** was elaborated to the final Fmoc-amino acid **88b** (Scheme 28). High yields for both the amino acid isolation and Fmoc protection steps were obtained due to the familiarity with the procedures. The completed Fmoc amino acid **88** had a high enantiomeric excess of 92%, which was comparable to that of parent complex **130** (Table 4).

Table 4 – Correlation between pentenyl complex and amino acid optical purity

	130 (*S*)/(*S*)		**88** (*S*)
	142 (*R*)/(*R*)		**89** (*R*)

Complex	ee	Amino acid	ee
130 (*S*)/(*S*)	94 %	**88** (*S*)	92 %
142 (*R*)/(*R*)	92 %	**89** (*R*)	90 %

These results were deemed consistent and within experimental error, confirming our hypothesis that through adequate control of reaction conditions, the BPB-Ni(II)-Ala auxiliary could furnish α-methyl, α-alkenyl amino acids with high enantioselectivity, with any loss in optical purity derived from proline epimerisation during the complexation step.

3.1.7 - Synthesis of octenyl amino acids

Stapled peptides which span two turns of an α-helix (*i*, *i*+7), such as **Staples D** and **E** (Table 2), require the α-methyl, α-octenyl amino acids **90** and **91**. In order to utilise the BPB-Ni(II)-Ala auxiliary route to these substrates, the iodo-octene compound **149** would be required for the key alkylation step. The Finkelstein conditions employed for the pentenyl substrate **110** (Scheme 24) provided the eight-carbon analogue **148** in equally high yields (Scheme 29). Due to the higher molecular weight of **149** in comparison to **110**, the Kugelrohr distillation was more successful as the product was less volatile, and therefore easier to separate from hexane.
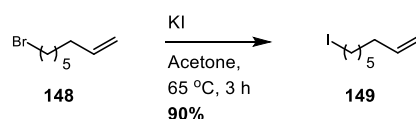
Scheme 29 – Finkelstein reaction of 5-bromo-oct-1-ene

With alkene **149** in hand, the key alkylation step of complexes (*S*)-**127** and (*R*)-**128** could be attempted (Scheme 30). The starting complexes were freshly synthesised using the procedures described previously (Scheme 28) in order to maintain low levels of proline epimerisation. Encouragingly, comparable yields were obtained for the octenyl alkylation to **150** and **152** (Scheme 30) compared to the pentenyl substrates (Scheme 25). The optimised conditions enabled more consistent alkylation reactions, independent of alkene chain length than previously reported conditions (Scheme 22).[169] Hydrolysis of the complexes (**150** & **152**) proceeded well in three hours with 2M HCl, however significant variations in yield of free amino acids was noted between (*S*)-**151** and (*R*)-**153** (Scheme 30).

127 (*S*)
128 (*R*)

150 (*S*)/(*S*), **68%**
152 (*R*)/(*R*), **55%**

151 (*S*), **36%**
153 (*R*), **89%**

90 (*S*), **47%**
91 (*R*), **30%**
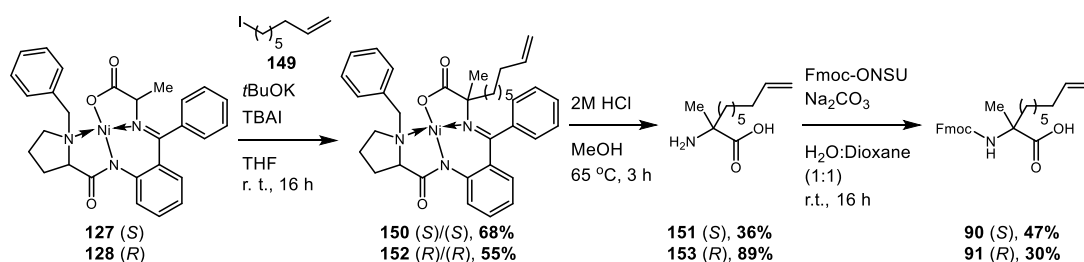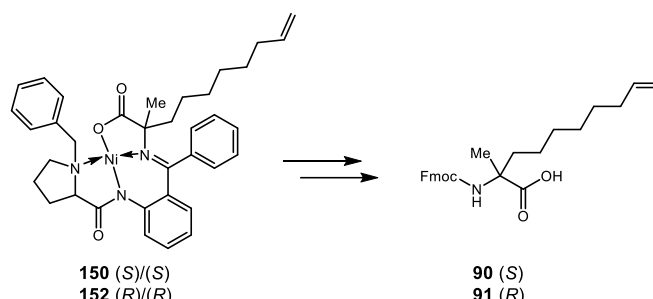
Scheme 30 – Synthesis of octenyl amino acids

This could potentially be attributed to compound **151** being purified with aged DOWEX resin, whilst compound **153** utilised a freshly prepared batch of resin. Disappointingly low yields were obtained after the subsequent Fmoc protection step and HPLC purification to furnish compounds **90** and **91**, however a sufficient quantity of material was isolated to support the planned SPPS efforts.

Compared to the pentenyl substrates, the octenyl yields were consistently lower throughout the synthesis, however this was likely due to the difficulties associated with purification discussed previously (Section 3.1.3). Despite these drawbacks, the enantiomeric excess of the final amino acids **90** and **91** were shown to be 94% by chiral HPLC which was the highest achieved throughout this work (Table 5). Chiral HPLC of the precursor complexes **150** and **152** during the early stages of the synthesis had shown high enantiomeric excesses of 96%. Therefore, it was reasoned that the final compounds **90** and **91** would be of equally high optical purity.

As demonstrated previously, there was a direct correlation between the extent of proline epimerisation and the optical purity of the final compound (Table 5). This was further evidence that our optimised route was highly reliable in providing the chiral α-methyl, α-alkenyl amino acids in high optical purity.

Table 5 – Correlation between octenyl complex and amino acid optical purity

150 (*S*)/(*S*)   **90** (*S*)
152 (*R*)/(*R*)   **91** (*R*)

Complex	ee	Amino acid	ee
150 (*S*)/(*S*)	96 %	**90** (*S*)	94 %
152 (*R*)/(*R*)	96 %	**91** (*R*)	94 %

Through extensive optimisation and rigorous analysis, we have demonstrated that the BPB-Ni(II)-Ala auxiliary can be used to give final compounds of consistently high optical purity.

3.1.8 – Discussion of BPB-Ni(II)-Ala diastereoselectivity

This study has provided new information in relation to potential issues associated with the BPB-Ni(II)-Ala Schiff based auxiliary. None of the previously reported syntheses had reported racemisation at the α-proline centre as a potential cause of low enantiopurity of the final α-methyl, α-disubstituted substrate.[195,196] This could be attributed to the use of optical rotation as the main form of measurement of optical purity for these compounds, and that only through the development of a chiral HPLC assay could this issue have been highlighted. Interestingly, various earlier reports have commented on the ineffectiveness of the addition step being the main cause of optically impure final compounds,[197,201,202] highlighting the need for further work in modifying the BPB-Ni(II)-Ala and related BPB-Cu(II)-Gly auxiliaries around the benzyl systems to improve stereoselectivity (Fig. 29)[197,201,202]

127   **154**   **155**   **156**
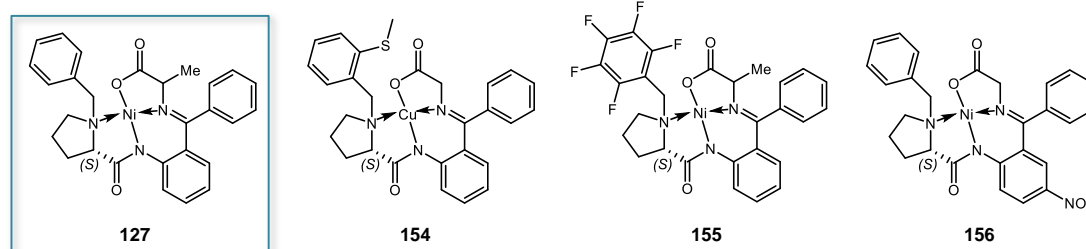
Figure 29 – Modified BPB-Ni(II)-Ala auxiliaries to improve diastereoselectivity

Therefore, it would be interesting to determine if other researchers who report the use of this auxiliary and assess optical purity of the final compound by the diastereomeric analysis of the alkylated complex are unable to discern erosion in enantiopurity from α-proline racemisation of **127,** as this enantiomer of this complex would not be detected by ^{1}H NMR. It is reasonable to assume that if the literature procedure to the BPB-Ni(II)-Ala auxiliary **127** (Scheme 20) is followed precisely, then the complex would be enantiopure, yet any deviations in procedure or scale, as discussed in Section 3.1.6, could have a detrimental effect on the quality of any final compounds synthesised *via* this route.

3.1.9. Comparison of α,α-disubstituted amino acids against commercially available substrates

During the time that this work was being carried out, all four target Fmoc amino acid building blocks became commercially available, on average for £250 per gram. The commercial Fmoc protected α-methyl, α-pentenyl amino acids (*S*)-**88** and (*R*)-**89** had very high enantiomeric excesses of 98% and 94%, respectively by chiral HPLC assay. However the Fmoc protected α-methyl, α-octenyl amino acids (*S*)-**90** and (*R*)-**91** appeared to be not only optically impure by HPLC assay (Fig. 30), but also chemically impure by ^{1}H NMR. Despite the compounds being marketed as single enantiomers, it was apparent from the chiral HPLC assay that neither enantiomer was optically pure. The enantiomeric excess of (*S*)-**90** was only 54%, while (*R*)-**91** was even lower at 34%. These results were somewhat disturbing considering the expense of the reagents and the reputation of the supplier, but also serve to highlight the technical difficulty associated in preparing these substrates.
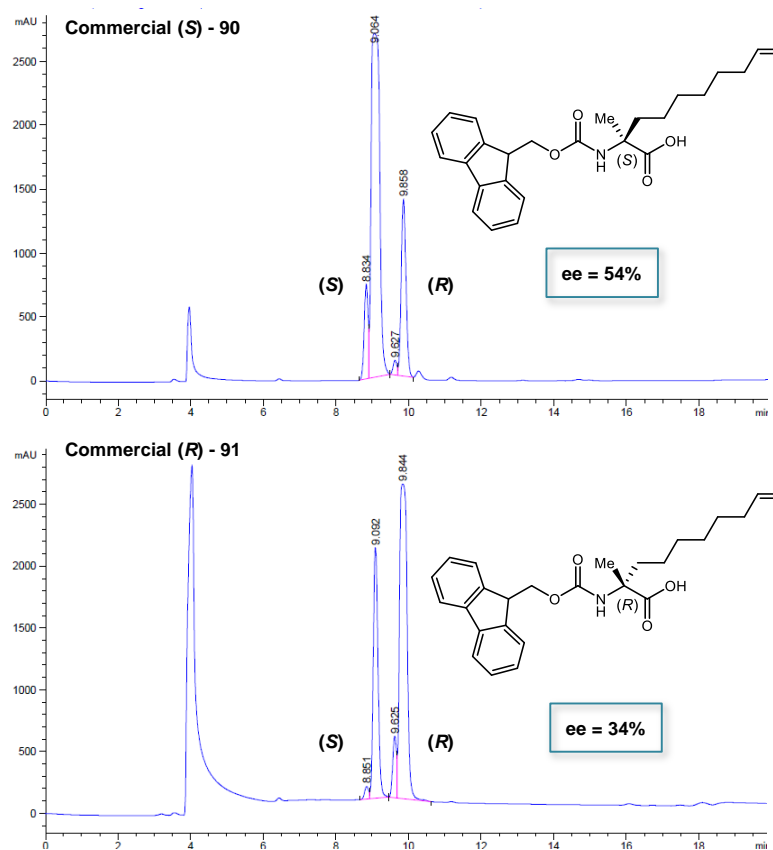
Figure 30 – Chiral HPLC of commercial Fmoc S_8 and Fmoc R_8 amino acids

3.2 - Stapled peptide synthesis and evaluation

With sufficient quantities of the requisite Fmoc α-methyl, α-alkenyl amino acids in hand, attention then turned to the solid phase synthesis of target peptides. An initial palette of the wild type and 8 stapled peptides was designed around the sequence of the α-9 segment of E2-25K, as discussed in Section 2 (Table 2). These peptides would ultimately allow assessment of the tractability of the E2-25K/Ubb+1 interaction as a potential drug target. However, as peptide synthesis is frequently not a straightforward process, with factors such as solubility and sterics affecting the synthesis, an initial optimisation of the wild type sequence would be carried out. This would allow for any difficult residues to be identified and the synthesis optimised at an early stage, prior to using the bespoke α-methyl, α-alkenyl amino acids. In particular, the two threonine residues towards the *N*-terminus of the sequence were assumed to be potentially problematic (Table 6) as they are more sterically hindered than the other amino acids present in the peptide.

Table 6 – Initial peptide sequences to be synthesised

Grey residues are more sterically hindered than their counterparts, and are anticipated to be more difficult to couple

Peptide	Staple	N												C
Wild type	-	Ac	V	E	T	A	T	E	L	L	L	S	N	NH_2
Staple A	i, i+4	Ac	V	E	T	S_5	T	E	L	S_5	L	S	N	NH_2

Once chain assembly was enabled, **Staple A** would be synthesised as a model stapled peptide (Table 6). The α-methyl, α-alkenyl amino acids, in this case S_5 (**88**), were again considered to be potentially problematic as they are more sterically hindered, being disubstituted compared to the mono-subtituted native amino acids. In particular, the *N*-terminal region of **Staple A** in which S_5 has a Thr residue on either side may require relatively forcing conditions. Evaluation of the published ring closing procedures for creating stapled peptides on the solid phase would also be carried out on **Staple A**.

3.2.1 – Trial synthesis of the Wild type peptide

To create the **Wild type** sequence the initial resin of choice was a high loading (1.12 mmol/g) PL-rink amide resin. Upon cleavage this would furnish a *C*-terminal carboxamide peptide (Scheme 31). Deprotection of the resin and coupling of the first amino acid was completed manually in a Merrifield bubbler. A HATU-mediated coupling was used to load the first asparagine residue (Scheme 31). Subsequently,

an Fmoc-loading test[86] was carried out to determine the extent of Asn coupling, as not all of the resin will have coupled effectively with the first residue. The test, based on the UV absorbance of the Fmoc/piperidine adduct (Scheme 1), indicated a resin loading of 0.41 mmol/g.
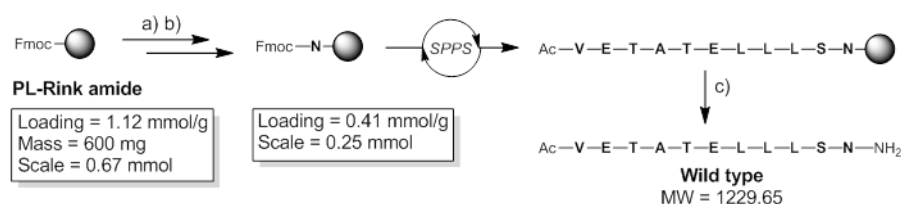
a) 20% piperidine in DMF, 3 x 5 min b) Fmoc-Asn(Trt)-OH, HATU, DIPEA, DMF, 4 h c) TFA:TIS:H$_2$O (95:2.5:2.5), 4 h

Scheme 31 – Initial conditions for the Wild type peptide

The resulting mass of reagents required for the SPPS was calculated based on the loading value established after coupling of the Asn residue. At this point in the synthesis, the coupling reagent was changed from HATU to the substantially cheaper related compound, HCTU. However, as discussed in Section 1.4.3, HCTU is equally as effective in SPPS. The remainder of the peptide was synthesised on an automated peptide synthesiser using standard methods: twenty minute coupling times, concentrated reaction conditions (0.3 M) and *N*-methyl morpholine as the base. One of the main advantages of using an automated peptide synthesiser is the opportunity to monitor the progress of the synthesis and ascertain how well the peptide is assembling. This is achieved by measuring the UV absorbance of the filtrate after an Fmoc-deprotection step; under the assumption that the higher the UV absorbance, the greater the proportion of Fmoc protected amino acid present on the resin and the more effective the previous coupling has been. When the UV signal drops below that of the previous residues, it suggests that the amide coupling has been less effective. This can lead to truncated analogues of the target sequence, which can prove difficult to separate during the purification process, or ultimately a failure in the overall synthesis.

During this first synthesis of the linear peptide, a drop in UV absorbance was noted after installation of the Ala residue, implying the Thr, Glu and Val residues had failed to couple to the resin effectively (Fig. 31, A). This was potentially due to the steric bulk of Thr(O*t*Bu) which has a disubstituted β carbon containing a large *t*Bu protecting group, potentially inhibiting the coupling with the resin bound alanine. At this point in the synthesis, a full cleavage of the peptide from the resin was undertaken to allow mass spectrometry and HPLC analysis of the crude material to

determine if the complete sequence had assembled, or if it had failed after attempting to couple the Ala residue as the UV trace indicated. As the sequence contained no Arg(Mtr), Cys(Trt), Met or Trp protected residues, a simple cleavage cocktail of 95% TFA: 2.5% H_2O: 2.5% TIS (Scheme 31) could be used to effectively deprotect and scavenge cations produced from cleavage of *t*Bu, O*t*Bu and Trt protected side chains.
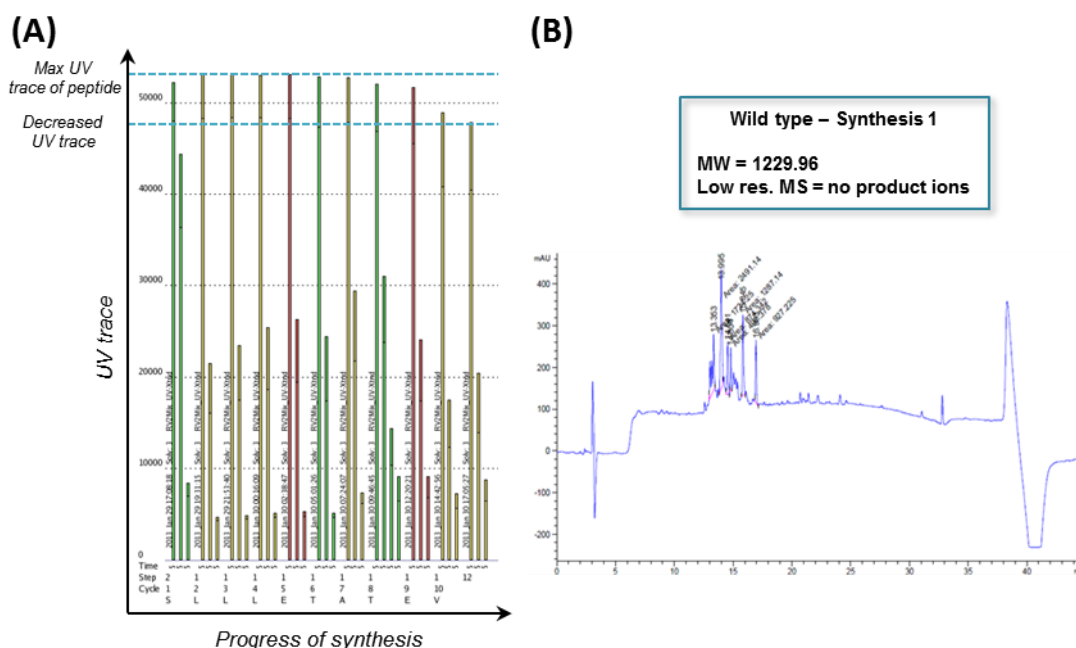
Figure 31 – Analysis of first Wild type peptide synthesis
A) - UV monitoring. Blue lines indicate the drop in UV signal for the final three residues which suggests issues with the synthesis. B) - HPLC and MS analysis of crude peptide

Unfortunately, the HPLC analysis suggested that the synthesis had failed due to the multiple peaks observed in the chromatogram (Fig. 31, B). Purification of this mixture was deemed too problematic, in particular when considering the low yield that would result. Analysis by mass spectrometry also gave no clear indication of the target sequence or truncated by-products being present in the crude mixture. Therefore, this initial attempt at creating the wild type peptide was not successful, confirming the data from the SPPS UV analysis during the course of the synthesis.

3.2.2 – Change in procedure towards the Wild type peptide

Due to the apparent failure in coupling of the last three residues of the sequence, there was a need for optimisation of the SPPS coupling procedures for this target sequence. The first variation made was to alter the resin from PL-rink amide to a MBHA linked rink amide resin (Scheme 32). As discussed in Section 1.4.1, the incorporation of an additional spacer to the resin enables the peptide assembly to

take place further away from the resin surface, aiding solvation and decreasing the likelihood of aggregation. This would potentially aid the difficult Thr coupling and improve the overall synthesis. Another factor which was altered was the bed volume used during the automated SPPS. Observations made during the previous synthesis (Scheme 31) had shown that 2 mL was not a sufficient volume of solvent to allow the resin to mix well in the reaction vessel. Therefore, the bed volume was increased to 5 mL to allow free movement of the resin in solution without being too dilute, decreasing the concentration of the reactions from 0.3 M to 0.06 M at resin loading.

a) 20% piperidine in DMF, 3 x 5 min b) Fmoc-Asn(Trt)-OH, HATU, DIPEA, DMF, 4h c) TFA:TIS:H$_2$O (95:2.5:2.5), 4 h
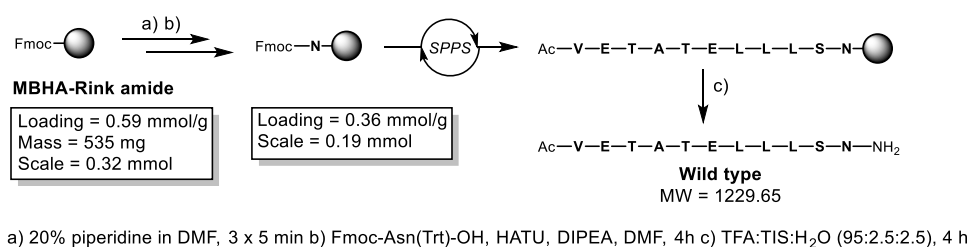
Scheme 32 – Synthesis of the Wild type peptide using MBHA linked resin

The measured loading after Asn coupling was lower for the MBHA linked resin than the PL, which was to be expected, resulting in the synthesis being executed on a 0.19 mmol scale (Scheme 32). Automated synthesis was carried out as before using the same reagents and reaction times, however, as stated above, the bed volume was changed to 5 mL to allow for better resin solvation and mixing.

Unfortunately, the UV monitoring during synthesis indicated that the peptide assembly appeared to fail again for the last three residues; Thr, Glu and Val (Fig. 32, A). It was clear at this point that more extensive optimisation would be required to couple the *N*-terminal threonine, however automated synthesis up to the preceding alanine residue would be possible. A full cleavage of the peptide was performed as described previously (Scheme 32), and HPLC and MS analysis was carried out to assess the composition of the cleaved material. Interestingly, the HPLC trace of the crude peptide (Fig. 32, B) was significantly cleaner than the previous synthesis (Fig. 31, B), with three main components present. Mass spectrometry analysis showed that the crude peptide contained the target native sequence as well as two truncated analogues; the native sequence up to the 8th residue, Ala, and the native sequence up to the 9th residue, Thr.

Figure 32 – Analysis of second Wild type peptide synthesis
A) - UV monitoring. Blue lines indicate the drop in UV signal for the final three residues equate to failing synthesis.
B) - HPLC and MS analysis of crude peptide

These results, along with the UV trace (Fig. 32, A), confirmed that the *N*-terminal Thr couplings were not successful. This concurred with the previous hypothesis discussed in Section 3.2 that the *N*-terminal threonines could be problematic (Table 6). No further purification was attempted due to the presence of two major by-products which were anticipated to compromise isolated yield. Accordingly, a new approach towards synthesis of the target sequences was required in order to overcome the coupling issues observed with the current chemistry.

3.2.3 – Screening of conditions to couple the *N*-terminal threonine

As previous attempts at preparing the native sequence on a 0.2 mmol scale had been unsuccessful, it was decided that an array of small scale test procedures would be carried out on both the **Wild type** and **Staple A** sequences (Table 7) as both would be needed for initial structural testing. A screen was created to compare a range of known coupling procedures for use in this particular sequence. A stapled sequence was chosen over the **Wild type** peptide in order to determine if the quaternary amino acids needed for stapling could be incorporated into this problematic sequence. As the stapled peptide was reasoned to be more difficult to synthesise due to the α-,α-disubstituted amino acids (Table 6), it was decided to optimise this sequence over the **Wild type** peptide in order to overcome any issues early on in the project.

The peptide sequence of **Staple A** (Table 7) was chosen to be synthesised using different solid phase coupling techniques, represented by different colours. These colours correspond to coupling methods (Table 8) which vary in reagent excess and coupling time. The first experiment, **Staple A** (Table 7, Row 1), would use forcing conditions, where a standard amino acid is double coupled for twenty minutes (Method i) and a sterically hindered residue is double coupled for two hours (Method ii). For **Staple A**, the sterically hindered amino acids included: both S_5 units, the residues directly after S_5, and the final three *N*-terminal residues which had been failing in previous syntheses.

Table 7 – Peptides chosen for small scale screen

No.	Peptide	Staple	Scale	N				Sequence								C
1	Staple A	i, i+4	0.1 mmol	Ac	V	E	T	S_5	T	E	L	S_5	L	S	N	NH$_2$
2	Staple A	i, i+4	0.2 mmol	H				S_5	T	E	L	S_5	L	S	N	NH$_2$
3	Staple A	i, i+4	0.1 mmol	Ac	V	E	T	S_5	T	E	L	S_5	L	S	N	NH$_2$
4	Wild type	i, i+4	0.1 mmol	Ac	V	E	T	A	T	E	L	L	L	S	N	NH$_2$

■ = *Method (i)*   ■ = *Method (ii)*   □ = *Method (iii)*   ■ = *Method (iv)*

These extended coupling times are not usual in SPPS, however were deemed necessary in order to prepare the peptide in reasonable yields in an expedient fashion without any need for further optimisation. In addition, this approach had not been utilised previously as twice the amount of reagents are used per coupling which raises issues regarding atom economy.

Table 8 – Coupling methodology used in screen

Method	Manual / Automated	Amino acid equiv.	Coupling Agent (Equiv.)	Base (Equiv.)	Solvent	Coupling time
i)	Automated	5	HCTU (5)	DIPEA (10)	NMP	2 x 20 min
ii)	Automated	5	HCTU (5)	DIPEA (10)	NMP	2 x 2 h
iii)	Automated	5	HCTU (5)	DIPEA (10)	NMP	20 min
iv)	Automated	5	HCTU (5)	DIPEA (10)	NMP	1 h

As a precaution against the *N*-terminal Thr coupling failing again, **Staple A** (Table 7, Row 2) would also be synthesised up to the second S_5 residue in the event that more residue specific coupling methods had to be tested. In addition, **Staple A** (Table 7, Row 3) would be synthesised using more economical methods. For this sequence, residues which were already known to couple well using the previously established procedures were only single coupled (Table 8, Method iii). The S_5

residues were also only single coupled to conserve supplies, however extended reaction times of one hour were employed (Table 8, Method iv). The Leu and Thr residues which follow the α-,α-disubstituted amino acids would be treated with the same forcing conditions as before, whilst the two *N*-terminal amino acids, Glu and Val, would be double coupled to ensure successful synthesis. The **Wild type** peptide (Table 7, row 4) would use similar forcing methods to **Staple A1** to create the native peptide sequence, with the expectation that the Thr reaction will yield more complete conversion when double coupled for two hours.

Once automated synthesis of the four peptides (Table 7) was complete, trial cleavage reactions were carried out in order to obtain LCMS data. Disappointingly, **Staple A 1 & 3** both had the threonine deletion peptide present as a major by-product in the crude mixture, despite the modified conditions used (Fig. 33). It was interesting to note that for both peptides the *N*-terminal Glu coupled to S_5 as it is not as sterically encumbered as Thr(O*t*Bu).

Ac—V—E—T—S_5—T—E—L—S_5—L—S—N—NH$_2$
Staple A
MW = 1323.73

Ac—V—E—T—A—T—E—L—L—L—S—N—NH$_2$
Wild type
MW = 1229.65

Ac—V—E—S_5—T—E—L—S_5—L—S—N—NH$_2$
Thr deletion product
MW = 1222.68

H—A—T—E—L—L—L—S—N—NH$_2$
Thr truncation product
MW = 923.36
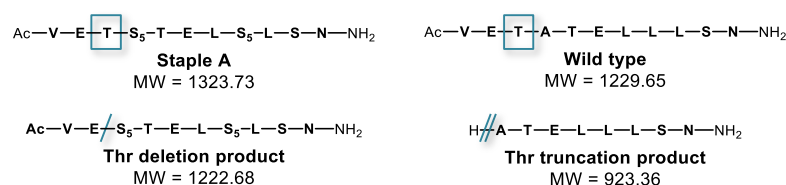
Figure 33 – Major by-product formation from methodology screen

Similar results were obtained for the **Wild type** peptide in which the peptide assembly halted at the 8th Ala residue as previously noted (Fig. 32). From these results it was clear that a screen of coupling reagents would be needed to fine tune the threonine reaction as the approach of increasing stoichiometry alone was unsuccessful.

LCMS analysis indicated that the more economical conditions of **Staple A3** worked as equally well as the extreme conditions of **Staple A1** to assemble the target sequence (Fig. 34). Despite the presence of the major by-product, these results were encouraging as less wasteful methodology could be used for similar stapled peptides (Table 7) once the issue of successfully coupling the *N*-terminal Thr could be resolved. Assembly of the shortened peptide **Staple A2** was successful, with the crude mixture showing no major by-products.
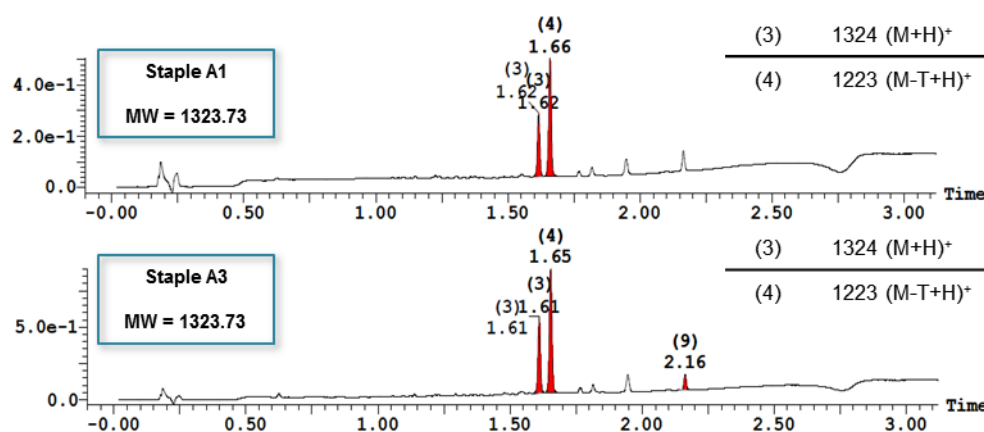
Figure 34 – LCMS comparison of Staple A methodology 1 & 3

This resin from **Staple A2** could then be split into smaller batches to test various Thr coupling conditions. Combining HATU and its corresponding active agent HOAt was used in an attempt to force the reaction with threonine to completion (Scheme 33) through promoting the formation of the HOAt active ester (Scheme 4). This combination of reagents is not common in coupling chemistry due to the relative ease in which HATU reacts with most amino acids, however, due to the steric bulk at the β-carbon of Thr it was reasoned that saturation of the reaction vessel with HOAt could increase the rate of amide formation through ensuring active ester formation.
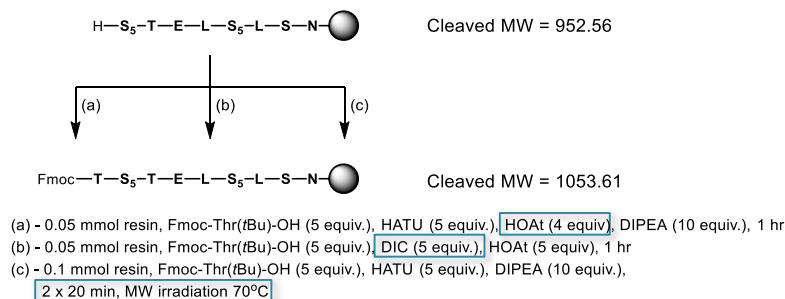
Scheme 33 – Thr coupling test procedures

Carbodiimide mediated amide coupling was also attempted using the conditions (b) to establish if this alternative mechanism of acid activation (Scheme 3) was more successful than HATU based couplings. Lastly, a microwave assisted solid phase amide coupling was attempted using standard HATU conditions at 70 ^{o}C to investigate whether microwave irradiation would accelerate the rate of reaction, as shown with conditions (c) (Scheme 33).

Small scale Fmoc-deprotections and trial cleavages were carried out on the three sets of conditions to facilitate LCMS analysis of the threonine coupling conditions. The first set of conditions examined (a) gave almost complete conversion to the threonine coupled product, as indicated by the LCMS analysis (Fig. 35). The increased concentration of the HOAt additive in the reaction vessel appeared to allow more efficient attack of the *O*-acyl(tetramethyl)isouronium intermediate to give the active ester, which could subsequently efficiently couple with the resin bound amine.
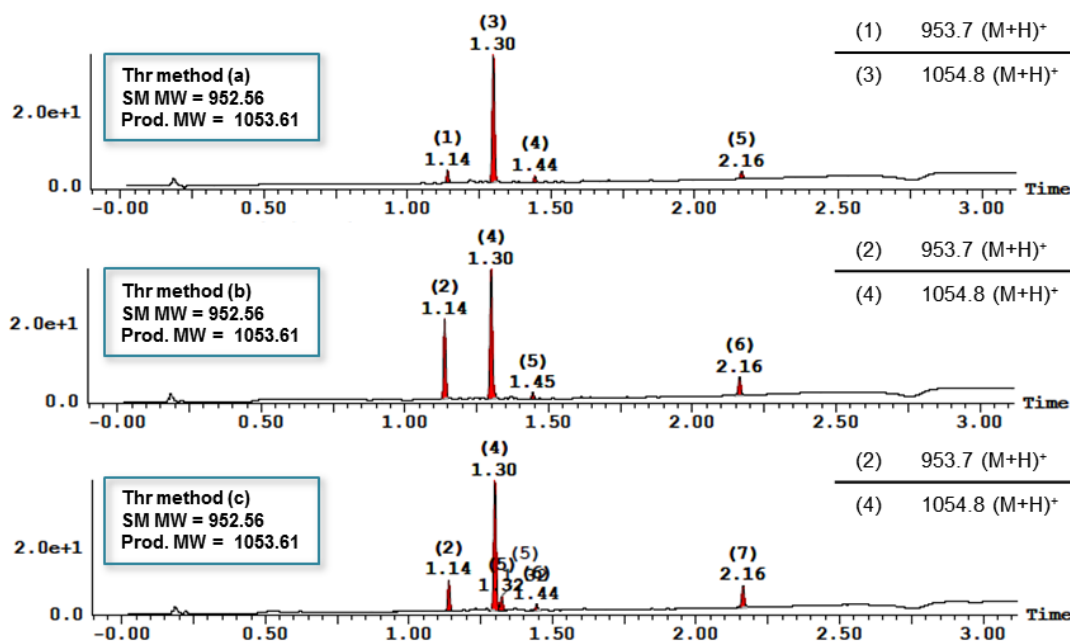
Figure 35 – LCMS analysis of Thr optimisation

The DIC initiated coupling conditions of (b) appeared to give about 60% conversion to product, estimated by UV, however, a large amount of starting material was observed, implying that either *O*-acylisourea formation was not as efficient for threonine, or that five equivalents of HOAt was not sufficient to force active ester formation. Lastly, it was interesting to note that the microwave assisted process (c) gave conversion to the product using standard HATU conditions, but still had a greater proportion of starting material unreacted after double coupling at 70 °C. Overall, the HATU/HOAt combination (a) gave the required product with high conversion under relatively mild conditions compared to the next best conditions using a microwave.

3.2.4 – Ring-closing metathesis of Staple A

Having identified a solution to coupling the problematic Thr residue, the next stage in the synthesis of **Staple A** was to complete the peptide sequence and undergo ring-closing metathesis to give the stapled resin bound peptide. Due to the relatively small scale of the Thr coupling trial reactions (Scheme 33), the peptides from method (a) and (c) were combined to give 0.15 mmol of **Staple A**, as method (c) only contained a small amount of starting material compared to Thr coupled product. Using the *N*-terminal coupling methods described previously (Table 8, i), the sequence was completed with a trial cleavage from the resin showing the required peptide with a small amount of the threonine deletion analogue, which was detected by LCMS.

Ring-closing metathesis on the solid phase (Sections 1.6 and 1.7) of the two alkenyl side chains was the next challenge in the synthesis of **Staple A**. The reaction was carried out using Grubbs 1st generation catalyst using 3 consecutive treatments of a 10 mM solution in DCM (Scheme 34).

Unstapled peptide A
MW = 1323.73

Staple A
MW = 1295.70

(a) - 0.15 mmol resin, Grubbs 1st gen. cat. (40 mol%), 6 mL DCM, 2 h, sonication
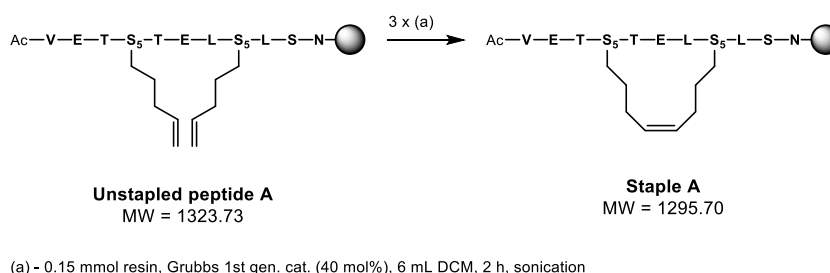
Scheme 34 – RCM of Staple A

A trial cleavage of the peptide showed complete conversion to the ring-closed product by HPLC and MS (Fig. 36). The shift in retention time of the main product peak by 2.5 minutes was a clear indication that RCM had been successful, with the MS analysis confirming the result. A full cleavage of the ring-closed product from the resin was performed using the same conditions described previously (Scheme 32), and the crude product purified by preparative HPLC to give 32 mg of the product **Staple A**. Purity analysis by reverse phase HPLC and high resolution mass spectrometry confirmed the peptide was in excess of 90% purity which would be required for further biological testing.
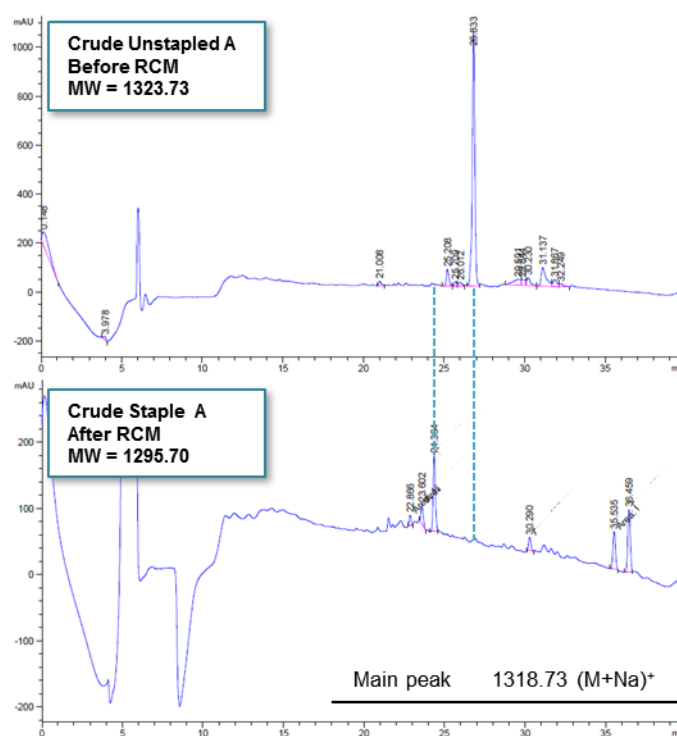
Figure 36 - Analysis of Staple A RCM product

3.2.5 – Synthesis of Wild type peptide and Staples B - H

Given the success of optimised Thr coupling conditions, the remaining peptide sequences could be synthesised using this methodology on Rink-amide MBHA resin. Each sequence required a different approach to the peptide synthesis (Table 9), with multiple coupling methods required per peptide (Table 10).

Table 9 – Synthesis towards Wild type and stapled peptides

Peptide	Staple	N	Sequence											C
Wild type	-	Ac	V	E	T	A	T	E	L	L	L	S	N	NH₂
Staple B	i, i+4	Ac	V	E	T	A	S₅	E	L	L	S₅	S	N	NH₂
Staple C	i, i+4	Ac	V	E	S₅	A	T	E	S₅	L	L	S	N	NH₂
Staple D	i, i+7	Ac	R₈	E	T	A	T	E	L	S₅	L	S	N	NH₂
Staple E	i, i+4	Ac	V	E	T	R₅	T	E	L	R₅	L	S	N	NH₂
Staple F	i, i+4	Ac	V	E	T	A	T	E	L	S₅	L	S	S₅	NH₂
Staple G	i, i+4	Ac	S₅	E	T	A	S₅	E	L	L	L	S	N	NH₂
Staple H	i, i+7	Ac	V	E	T	R₈	T	E	L	L	L	S	S₅	NH₂

■ = *Method (i)*   □ = *Method (ii)*   ■ = *Method (iii)*   ■ = *Method (iv)*   ■ = *Method (v)*   ■ = *Method (vi)*

As the α-9 sequence of E2-25K has been shown to be problematic, even the simple **Wild type** peptide required four separate coupling methods in order to minimise

deletion or truncation analogues. Furthermore, stapled analogues required up to six methods in order to assemble the target sequence successfully.

Table 10 – General coupling methods towards stapled peptides

Method	Manual / Automated	Amino acid equiv.	Coupling Agent (Equiv.)	Base (Equiv.)	Coupling time
i)	Manual	5	HATU (5)	DIPEA (10)	4 h
ii)	Automated	5	HATU (5)	DIPEA (10)	20 min
iii)	Manual	2.5	HATU (2.5)	DIPEA (5)	2 h
iv)	Automated	5	HATU (5)	DIPEA (10)	2 x 2 h
v)	Automated	5	HATU (5), HOAt (4)	DIPEA (10)	2 x 2h
vi)	Automated	5	HATU (5)	DIPEA (10)	2 x 30 min

For each peptide, excluding **Staples F** and **H**, the first Asn residue was coupled manually (Table 10, i), with the Fmoc loading value calculated to allow for a more accurate calculation of reagents. Alkenyl amino acids were also coupled manually to conserve supplies. Only 2.5 equivalents of the Fmoc-α-methyl, α-alkenyl amino acids were used per step, however in conjunction with a two hour reaction time, the coupling went to completion in all cases (Table 10, iii). Subsequent residues were coupled on an automated synthesiser using HATU / DIPEA conditions, with standard single couplings only taking twenty minutes (Table 10, ii). Due to the sterically hindered nature of the α-methyl, α-alkenyl amino acids, the residues directly following in the sequence also required extended coupling times (Table 10, iv). The optimised threonine coupling conditions developed in Section 3.2.3 could also be completed in an automated fashion, with the excess HOAt being delivered with the HATU and amino acid (Table 10, v). Finally the *N*-terminal amino acids were also exposed to longer coupling times of 2 x 30 minutes (Table 10, vi), as Glu and Val truncation had been observed in earlier syntheses when shorted coupling times had been used (Fig. 32).

With the exception of **Staples F** and **H**, all peptides were successfully synthesised using the methods described (Table 9). In relation to the two remaining analogues, it became apparent that the presence of an S_5 residue at the *C*-teminus was not compatible with the remainder of the peptide synthesis. Initial coupling of Fmoc-S_5-OH (**88**) to the resin was successful, with trial cleavage reactions proving the presence of Fmoc-S_5-NH$_2$ (Scheme 35). Further peptide synthesis was carried out utilising the previous methods (Tables 9 and 10), however a trial cleavage from the

resin after coupling of the Ala residue showed no product ions present by MS, despite the HPLC only showing a single peak.
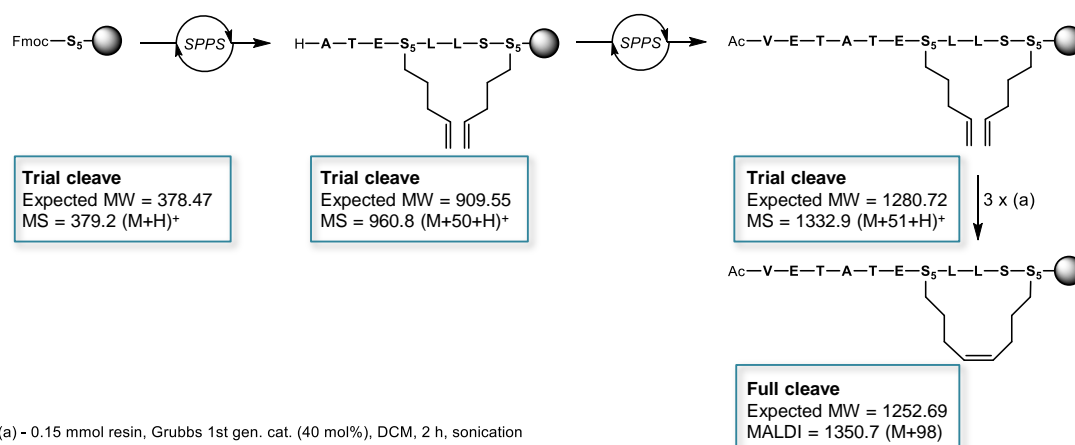
Scheme 35 – Attempted synthesis of Staple F

Due to the apparent purity of the synthesised peptide, the remainder of the sequence was synthesised (TEV-Ac) in the event that the MS analysis had been an anomaly. Unfortunately, a trial cleave of the completed sequence also showed a single peak by HPLC, but with no product mass ions present. Instead, a similar result of plus 50 mass units was observed, however this could not be attributed to any salt or potential structure of **Staple F**. Based on this, it was decided to ring-close the synthesised peptide at this point in the event that additional insight into the identity of the product could be obtained. A standard ring-closing metathesis, full resin cleavage and preparative HPLC was carried out on **Staple F** to give a pure sample for mass spectometry analysis. Unfortunately, as before, no product ions were found by MALDI spectrometry. Instead a mass peak 1350.7 was observed, which was +98 units from the expected sequence. This result was peculiar as, in a majority of cases, the peptide by-products being synthesised were deletion or truncation analogues which have a lower mass than expected. A mass increase of 98 could not be ascribed to any double addition of any amino acids present in the sequence of **Staple F**. As this is the only sequence with an α-methyl, α-alkenyl amino acid directly attached to the resin, there is a possibility that during the highly acidic resin cleavage conditions a side reaction takes place between the amino acid and the functionalised resin (See Fig. 9, Section 1.4.1 for resin structure). Despite this proposal, no logical structures could be elucidated for the +98 product of **Staple F**. A test synthesis of the first seven residues of **Staple H** also showed no product during a trial cleave, with a similar MS pattern to that observed for **Staple F**

(Scheme 35). Based on these results, the synthesis of both **Staples F** and **H** was not progressed further.

Returning to the synthesis of the remaining peptides; **Staples B**, **C**, **D**, **E** and **G**, were progressed to the ring closing metathesis step. Each peptide was subject to metathesis using the conditions described previously (Scheme 34), with a trial cleavage reaction confirming full conversion to the ring-closed product. The peptides, including the **Wild type** sequence, were then cleaved fully from the resin using standard conditions (Scheme 32), and subsequently purified using preparative HPLC. Six stapled peptides were successfully isolated overall, as well as the unstapled **Wild type** peptide (Table 11).

Table 11 – Sequences of first generation peptides successfully synthesised

Peptide	Staple	Sequence	Yield
Wild type	-	Ac-V-E-T-A-T-E-L-L-L-S-N-NH$_2$	3%
Staple A	i, i+4	Ac-V-E-T-**S$_5$**-T-E-L-**S$_5$**-L-S-N-NH$_2$	16%
Staple B	i, i+4	Ac-V-E-T-A-**S$_5$**-E-L-L-**S$_5$**-S-N-NH$_2$	5%
Staple C	i, i+4	Ac-V-E-**S$_5$**-A-T-E-**S$_5$**-L-L-S-N-NH$_2$	13%
Staple D	i, i+7	Ac-**R$_8$**-E-T-A-T-E-L-**S$_5$**-L-S-N-NH$_2$	4% *trans* : 1% *cis*
Staple E	i, i+4	Ac-V-E-T-**R$_5$**-T-E-L-**R$_5$**-L-S-N-NH$_2$	17%
Staple G	i, i+4	Ac-**S$_5$**-E-T-A-**S$_5$**-E-L-L-L-S-N-NH$_2$	7%

Despite the optimised threonine coupling conditions discussed in Section 3.2.3, half of the peptides synthesised still had small amounts of Thr truncation or deletion analogues present when the crude cleavage mixture was analysed. This is likely due to the variation in the *N*-terminal region on the precise position of the α-methyl, α-alkenyl amino acid residues. These changes in environment, as well as the different aggregation potential around the *N*-terminal Thr of each sequence, may have decreased the coupling efficiency, and subsequent process yield.

All *i, i*+4 sequences isolated were assumed to be *cis* alkenes based on the established literature precedent,[203] and the presence of only one clear ring-closed product observed by HPLC in all cases. It was interesting to note that both the *trans* and *cis* isomer were isolated as pure compounds from the ring-closing of **Staple D**. The major product was assumed to be the *trans* isomer due to the preference of Grubbs 1st generation catalyst for forming *trans* double bonds for larger

macrocycles,[139] as well as the literature precedent showing that *i*, *i*+7 staples form predominantly *trans* products.[203]

3.2.6 - Analysis of helicity of synthesised peptides

With the initial subset of peptides in hand, attention was then focused on the generation of structural data to ascertain the helical content of each substrate. Circular dichroism spectroscopy is an established method of analysis for determination of secondary structure content of proteins and peptides.[204] When circularly polarised light is passed through a chiral molecule, such as a peptide, two effects can occur; optical rotation (α), and circular dichroism (θ). When a molecule has both these effects, the transmitted circularly polarised light is said to be elliptically polarised. Measurement of ellipticity and optical rotation over a range of wavelengths gives rise to the CD spectra. For proteins and peptides, the amide bond is the key chromophore which, when analysed in the far UV range (190 – 260 nm), gives detailed information on the secondary structure. The CD spectra of an α-helical peptide has a distinctive shape, with a maxima at 195 nm and two minima at 208 nm and 222 nm. The measured ellipticity value at 222 nm can then be used to calculate mean residue ellipticity which factors in peptide length, n (in residues), concentration, C (M), and path length, l (mm) (Fig. 37).

$$\% \, Helicity = \frac{[\theta]_{222}}{[\theta]_{max}}$$

$$[\theta]_{222} = \theta_{obs} \div (Cln)$$

$$[\theta]_{max} = (-44000 + 250T)\left(1 - \frac{k}{n}\right)$$

Figure 37 – Helicity calculations for stapled peptides

Percentage helicity can then be calculated from mean residue ellipticity against the maximum ellipticity for a particular sequence which is derived from temperature of the sample (20 $^{\circ}$C), the number of amino acids in the peptide sequence (n), and a correction factor (k) which ranges from 2 – 4, but is kept constant at 3 for carboxyamidated peptides (Fig. 37).[204]

The **Wild type** peptide derived from the α-9 sequence of E2-25K exhibited an unstructured character in solution, with a single minima at 200 nm, as shown by the dark blue line in the spectra (Fig. 38). This was to be expected as this control peptide contains no chemical constraint to induce a helical shape in solution. It was pleasing to note that all the stapled peptides synthesised (Table 11) demonstrated an α-helical character in phosphate buffer (Fig. 38), with a maxima at 195 nm and

two minima at 208 nm and 222 nm. Before any helicity values were calculated, it was clear from inspection of the CD spectra obtained that there was a wide range of helicity present, with the stapled peptides ranging from being unstructured in nature to tightly coiled.

Peptide	Staple	Sequence	% Helicity
Wild type	-	Ac-V-E-T-A-T-E-L-L-L-S-N-NH$_2$	— 16 —
Staple A	i, i+4	Ac-V-E-T-**S$_5$**-T-E-L-**S$_5$**-L-S-N-NH$_2$	— 91 —
Staple B	i, i+4	Ac-V-E-T-A-**S$_5$**-E-L-L-**S$_5$**-S-N-NH$_2$	— 41 —
Staple C	i, i+4	Ac-V-E-**S$_5$**-A-T-E-**S$_5$**-L-L-S-N-NH$_2$	— 42 —
Staple D *trans*	i, i+7	Ac-**R$_8$**-E-T-A-T-E-L-**S$_5$**-L-S-N-NH$_2$	— 80 —
Staple D *cis*	i, i+7	Ac-**R$_8$**-E-T-A-T-E-L-**S$_5$**-L-S-N-NH$_2$	— 21 —
Staple E	i, i+4	Ac-V-E-T-**R$_5$**-T-E-L-**R$_5$**-L-S-N-NH$_2$	— 16 —
Staple G	i, i+4	Ac-**S$_5$**-E-T-A-**S$_5$**-E-L-L-L-S-N-NH$_2$	— 42 —
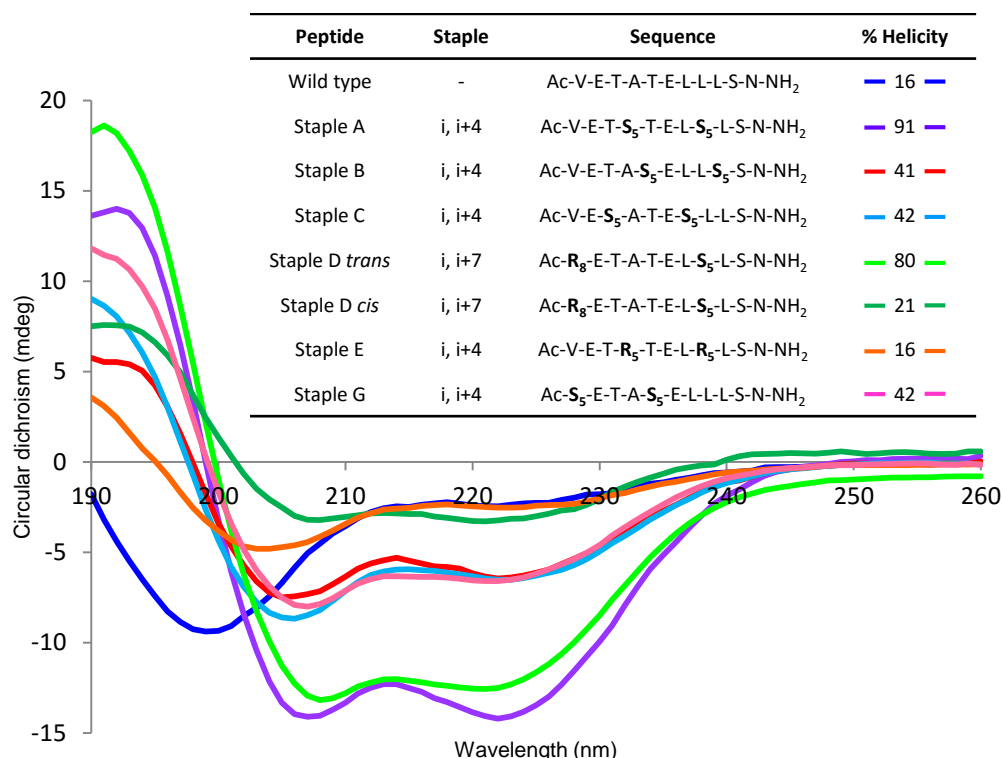
Figure 38 – Circular dichroism analysis and helicity values of stapled peptides
Percent α-helicity calculated from the observed circular dichroism value at 222 nm

It was surprising to note that the first stapled peptide synthesised, **Staple A**, had a 91% helical character in solution. This extremely tight α-helical structure may be attributed to the all-hydrocarbon tether lying in the centre of the peptide, with three residues on each side of the staple, preventing the peptide from uncoiling at the *C*- and *N*-termini. The remainder of the S_i, S_{i+4} peptides, **Staples B**, **C** and **G**, were shown to be around 40% helical. This was encouraging as the incorporation of the S_i, S_{i+4} staples were giving a net increase in helicity of 25% compared to the **Wild type** peptide when placed at either termini of the α-9 sequence. It was equally encouraging to note that the *trans* alkene linked *i*, *i*+7 peptide, **Staple D**, had a high degree of helicity, measured as being of 80%. This is likely attributed to two thirds of the peptide being contained within the stabilised double turn, allowing for strong backbone hydrogen bonding to occur. Interestingly, when the *cis* linked alkene (**Staple D** *cis*) is formed, the observed helicity drops to 21%. This result demonstrates the importance of the conformation of these staples when forming α-

helices, as the *cis* conformation would appear to twist the peptide backbone away from the ideal dihedral angles for helical hydrogen bonding (Fig. 13). **Staple E** was another noteworthy result, as it contains the same primary sequence and staple position as **Staple A**, but has the opposite (R_i, R_{i+4}) stereochemistry. The low helicity of 16% was no improvement from the **Wild type** peptide, and was significantly lower than the 91% helicity of the S_i, S_{i+4} analogue. However, this result is not suprising due to the previous results from the Verdine group discussed in Section 1.7.1, in which the (*R*, *R*) form gives less helical induction on average than the corresponding (*S*, *S*) diastereomer (Fig. 18).[151]

Overall, this initial palette of peptides had a range of helicities from 16 to 91% depending on staple length, position, stereochemistry, and regiochemistry. These results were an interesting example of how a simple staple scan can have a major effect on the secondary structure of a short eleven-residue peptide. In particular, it would be interesting to find any correlation between helicity and target affinity, or whether more residue specific interactions are key to binding with Ubb+1 over gross secondary structure in this case.

In general, examination of the literature relating to peptide staples suggests that there is no general trend between extent of helicity and target affinity. A lead stapled peptide targeting a particular PPI will tend to incorporate a staple at a position in the primary sequence which will not disrupt key interactions with the target, whilst inducing an efficient degree of secondary structure to fill the binding site appropriately.[205] Alternatively, it could be argued that an extremely rigid peptide may not be the best substrate for a PPI inhibitor. Native proteins may require a degree of flexibility when forming a PPI, therefore the conformation at the binding interface may not be a perfect α-helix in order to gain key interactions with the protein binding partner. Therefore, the large range of helicities present across the α-9 E2-25K peptide mimics may give a higher probability of one sequence being active against the target Ubb+1.

3.2.7 – Synthesis of an isomeric analogue of Staple A

Following on from the successful synthesis of the initial stapled peptides, it was planned to create further helical analogues of the α-9 sequence of E2-25K which could gain more additional interactions with Ubb+1 beyond those of the native sequence. As the nature of the E2-25K/Ubb+1 PPI is predominantly mediated by hydrophobic interactions, along with a key salt bridge, it was interesting to establish

what extent of modification of these interactions could be tolerated to maintain binding with Ubb+1. Of particular interest was whether the key glutamic acid residue could be replaced with a neutral (at physiological pH) polar species such as threonine, thereby replacing the salt bridge with a hydrogen bond. This key change would investigate whether the weaker hydrogen bond (6-8 kcal/mol) would provide a similar key interaction as the salt bridge (120 kcal/mol) with Arg[42] of Ubb+1. This could also be important if the net charge of the peptide has to be modified, as the **Wild type** peptide has an overall charge of -2. In general, for a peptide to be cell permeable, it requires an overall positive charge to effectively cross the cell membrane. Therefore, if the key Glu/Thr replacement is effective in binding with Ubb+1, this strategy could be utilised at a later stage to modify the overall peptide charge without affecting target affinity. To this end, **Staple I** was designed to have the same physicochemical properties as **Staple A**, but with slight variations in the binding residues to investigate their effect on Ubb+1 affinity (Table 12).

Table 12 – Design of mixed Staple A analogue

Peptide	Staple	Charge	N												C
Staple A	i, i+4	-2	Ac	V	E	T	S_5	T	E	L	S_5	L	S	N	NH$_2$
Staple I	i, i+4	-2	Ac	L	T	E	S_5	N	T	L	S_5	S	V	E	NH$_2$

| = Hydrophobic | = Polar, uncharged | = Acidic |

For this sequence, both Glu residues were replaced with a polar uncharged equivalent, in this case Thr (Table 12). The Glu residues were then placed in more solvent accessible positions away from the Ubb+1 surface (Fig. 39). In order to investigate how these changes may affect the structure of **Staple I** in relation to **Staple A**, both peptides were analysed by the author using MOE software,[206] using the α-9 sequence of E2-25K as a template to build each peptide (Fig. 39).

N-   *Solvent accessible face*   -C   C-   *Ubb+1 binding face*   -N
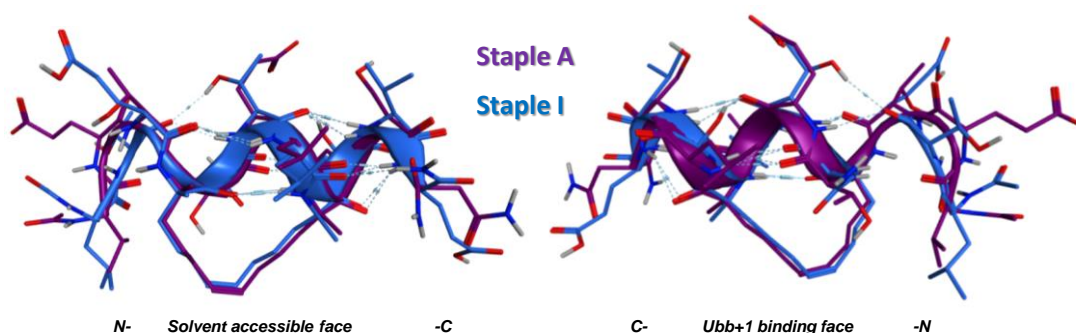
Figure 39 – Overlay of Staple A and Staple I

The peptide models built from α-9 of E2-25K were energy minimised and the structures overlayed to compare peptide conformation. Both peptides appeared to adopt similar conformations within the stabilised region, with **Staple I** unravelling towards the *N*-terminus (Fig. 39). This would suggest that both peptides could potentially make similar interactions with Ubb+1.

It was also of interest to determine whether the *C*-terminal Glu of **Staple I** would enhance the weak H-bond between the corresponding Asn[130] of E2-25K with Lys[48] of Ubb+1 present in the X-ray crystal structure (Fig. 22). The remaining hydrophobic residues were not altered significantly, with the exception of the *C*-terminal Leu/Ser switch. This Leu residue is within close proximity to a large hydrophobic section of Ubb+1, therefore a change to a small polar Ser residue may affect target affinity. Overall, **Staple I** had the potential to provide valuable information as to the variability of residues within the α-9 sequence of E2-25K.

Synthesis of **Staple I** required the same six solid phase methods developed for **Staple A** (Table 9). The resin loading and the first five couplings proceeded as expected from previous syntheses (Table 13).

Table 13 – Methodology towards the synthesis of Staple I

Peptide	Staple	*N*	Sequence											*C*
Staple I	i, i+4	Ac	L	T	E	S_5	N	T	L	S_5	S	V	E	NH_2

= Method (i)   = Method (ii)   = Method (iii)   = Method (iv)   = Method (v)   = Method (vi)

Isomerisation of the sequence proved to be problematic in terms of synthesis as both Thr residues now required the HATU/HOAt mixed forcing conditions previously developed for the *N*-terminal Thr of **Staple A** (Table 10, v). Despite this unexpected modification in procedure, the primary sequence of **Staple I** was successfully synthesised on the solid phase without the need for additional optimisation. As with previous peptides (Scheme 34), **Staple I** was ring-closed on resin using Grubbs 1st generation catalyst to give a single product shown. Subsequent preparative HPLC purification afforded the final stapled peptide in a 3% overall yield. Associated structural analysis of **Staple I** will be discussed in Section 3.2.9.

3.2.8 – Design and synthesis of the Staple A extended series

In addition to the preparation of the isomeric sequence of **Staple A**, further interrogation of the X-ray crystal structure of the E2-25K/Ubb+1 PPI led to the

development of an extended **Staple A** series discussed below. It was noted that there was a large hydrophobic cleft in proximity to the *N*-terminal Glu of the α-9 segment of E2-25K. This potential binding site is also present in natural ubiquitin as when the two crystal structures of Ub and Ubb+1 were superimposed there was only a slight variation in pocket shape (Fig. 40, A). Due to the flexibility of the tail domain of Ubb+1, it is unclear whether this hydrophobic cleft is actually accessible or whether it is blocked by the extended tail. The lowest energy NMR solution structure of Ubb+1 implies that the the position of the tail could potentially render this pocket inaccessible. A comparison of the NMR structure with the X-ray crystal structure of Ubb+1 (Fig. 40, B) shows, Leu[8] of Ubb+1 is shifted up to 6 Å away from the E2-25K interface, essentially blocking the hydrophobic cleft.
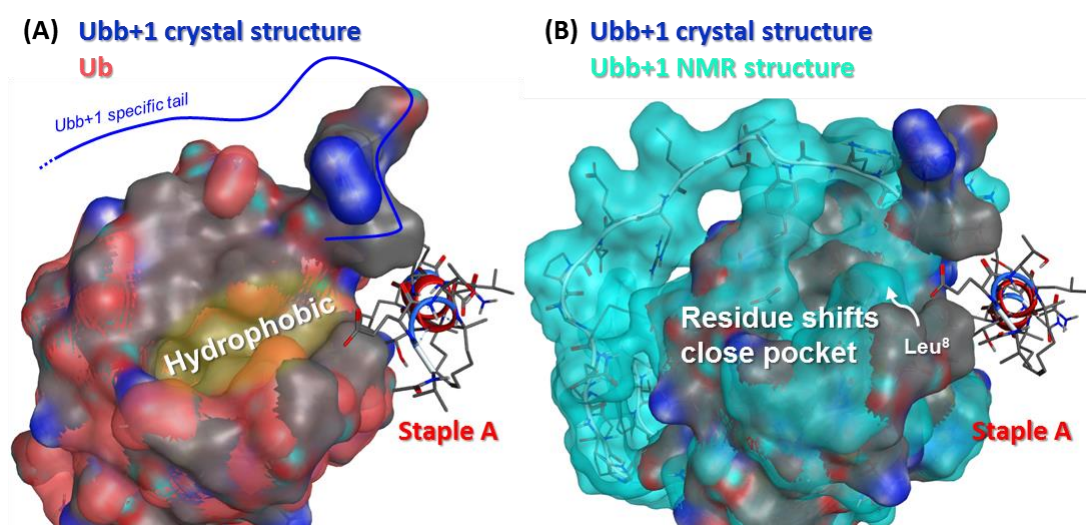
Figure 40 – Comparison of hydrophobic cleft targetability

As the NMR solution structure is a simulated energy minimised model, it was reasoned that pursuing this site could still be feasible. Considering the E2-25K/Ubb+1 PPI is a relatively weak, any potential for increasing binding affinity between our peptides with Ubb+1 without disrupting the primary sequence is favourable. However, there is a possibility that targeting the hydrophobic cleft may render the modified peptides more selective to Ub over Ubb+1 depending on the conformation of Leu[8]. Therefore, these extended compounds could offer additional insight on the conformational preference of Ubb+1 in solution

As the *N*-terminal Glu of the α-9 sequence does not form any key binding interactions with the surface of Ubb+1, it was proposed that by simply extending off from the glutamic acid side chain using simple hydrophobic amines, it may be

possible to form novel interactions with Ubb+1. In order to prioritise which hydrophobic groups would be well tolerated in this position, a simple computational model was designed by the author using MOE software.[206] The X-ray crystal structure of the E2-25K/Ubb+1 PPI was used to create a model peptide through paring back the E2-25K enzyme to the α-9 eleven amino acid segment. **Staple A** was chosen as the model peptide due to its high helicity in solution as discussed in Section 3.2.6. The software was then used to modify the structure of α-9 into that of **Staple A** through acetate capping at the *N*-terminus, carboxamide formation at the *C*-terminus, and modification of the native amino acids into the S_i, S_i+4 *cis* linked hydrocarbon bridge. This structure was then energy minimised so that the overall conformation would be more similar to the peptide in solution (Fig. 41). Once minimised, the **Staple A** model was then minimised against Ubb+1 in order to gain an understanding of how the peptide may bind to Ubb+1.
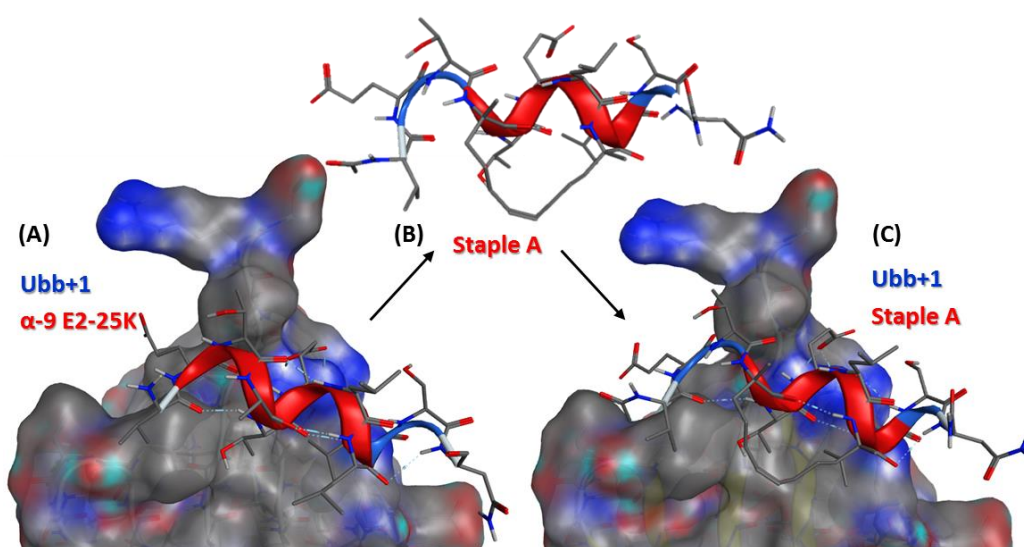
Figure 41 – Energy minimised model building

This initial study implied that **Staple A** maintained the same key interactions as the α-9 segment of E2-25K, however, due to a slight shift in binding mode compared to the native sequence, the *N*-terminus appears to lie further into the solvent rather than towards Lys[48]. This model was interesting as it implied that **Staple A** could have a slight conformational shift to α-9 of E2-25K against Ubb+1, in particular orientating away from Lys[48] which is key in PolyUb chain formation.

The next step was to construct *in silico* hydrophobic extensions from the *N*-terminal glutamic acid *via* an amide bond. Based on the size of the lipophilic cleft of Ubb+1, aliphatic tethers of two or three carbons were thought to be optimal in order to gain

access to this putative pocket. A total of twenty extended peptides of **Staple A** (Fig. 42, A) were screened *in silico* in order to determine what potential interactions could be gained. Variations in the extensions tested included aromatic ring size, heterocycle inclusion, saturated ring structures and tether length. The most favourable extensions modelled (Fig. 42) contained heterocyclic motifs hypothesised to have the closest fit in the hydrophobic cleft of Ubb+1. This was thought to be due to the lack of planar hydrogens on one face of the extension allowing the side chains to bury into the putative pocket of Ubb+1.
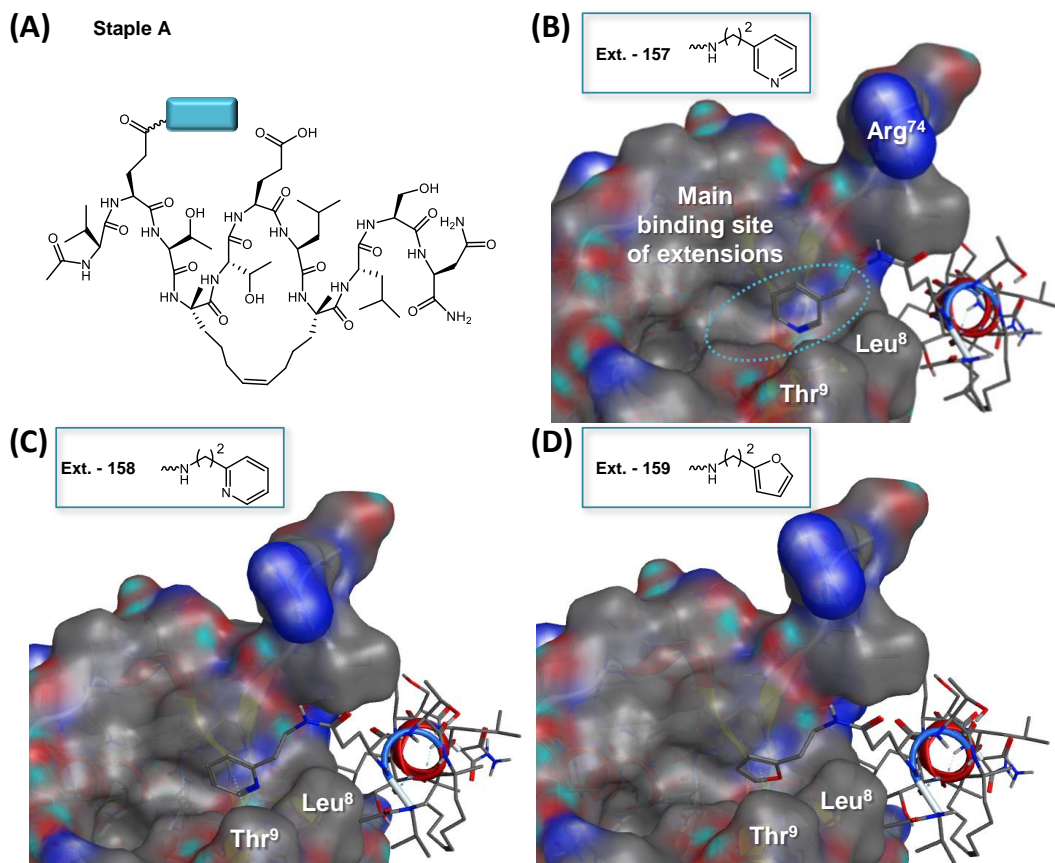
Figure 42 – Compound screen against hydrophobic cleft of Ubb+1

Overall, this small *in silico* screen gave potential candidates to gain novel interactions with the hydrophobic cleft of Ubb+1 when combined with **Staple A**. Due to the cost of the amine building blocks required, only a small number of heterocycles were prioritised initially to evaluate this extended peptide series. The *meta*- and *ortho*-pyridine compounds **157** (**Staple J**) and **158** (**Staple K**), as well as the simple furan **159** (**Staple L**) were chosen due to their potentially favourable interactions with Ubb+1 inferred from the *in silico* modelling (Fig. 43).
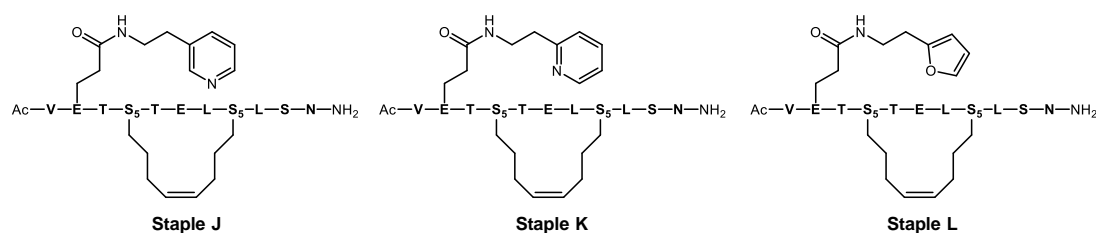
Figure 43 – Stapled peptides designed from *in silico* screening

The proposed synthetic route to these extended peptides would rely on a selective deprotection strategy, utilising Fmoc-Glu(OAllyl)-OH which can be deprotected on the solid phase using palladium chemistry. The solid phase synthesis towards **Staples J**, **K** and **L** was analogous to that of **Staple A**, but with an additional method developed for the Glu(OAllyl) (Table 14).

Table 14 – Methodology towards allyl protected precursor

Peptide	Staple	N	Sequence											C
Extended precursor	i, i+4	Ac	V	E*	T	S₅	T	E	L	S₅	L	S	N	NH₂

Method	Manual / Automated	Amino acid equiv.	Coupling Agent (Equiv.)	Base (Equiv.)	Coupling time
Vii)	Automated	5	HATU (5)	DIPEA (10)	2 h

■ = *Method (i)* □ = *Method (ii)* ■ = *Method (iii)* ■ = *Method (iv)* ■ = *Method (v)* ■ = *Method (vi)*

A 2 hour coupling to install the allyl protected glutamic acid was successful at the sterically hindered *N*-termini without the need for excessive amounts of reagent. Once the amino acid chain was assembled, attention then turned to the selective deprotection of the Glu(OAllyl) residue using tetrakis(triphenylphospine)palladium (0) on the solid phase. For this particular sequence, it was established that four consecutive treatments of palladium with phenylsilane as a reducing agent were required to effectively deprotect the *N*-terminal glutamic acid. The unprotected Glu could then be coupled on the solid phase with the extended amines of choice (Scheme 36). Pre-activation of the resin bound peptide with HATU and DIPEA was carried out for five minutes to form the active ester on the solid phase before addition of the *meta*-pyridyl amine **160** to the reaction mixture. A trial cleavage reaction at this point indicated the presence of a major by-product with a similar mass to **Staple A**, but with a different retention time by HPLC. However, as a sufficient amount of the desired acyclic precursor to **Staple J** was present in the sample, the synthesis was continued through to ring-closing metathesis and full

resin cleavage under the conditions previously developed for this series (Scheme 36).

(a) - Pd(PPh$_3$)$_4$ (10 mol%), PhSiH$_3$ (10 equiv.), DCM, 4 x 15 min (b) **160** (5 equiv.), HATU (5 equiv.), DIPEA (10 equiv), DMF, 2 h
(c) - Grubbs 1st gen. cat. (40 mol%), 10 mM DCM, 3 x 2 h d) TFA:TIS:H$_2$O (95:2.5:2.5) 4 h
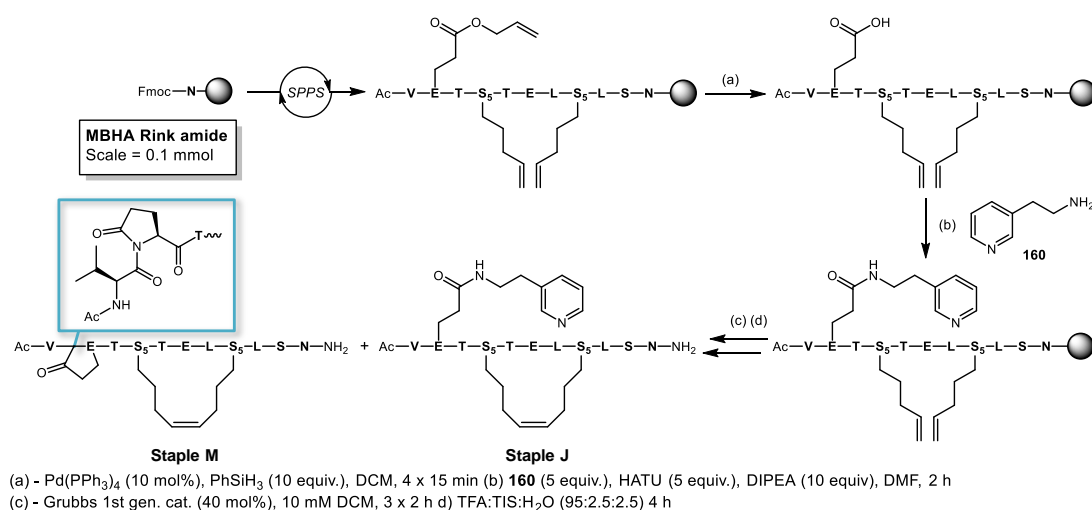
Scheme 36 – Formation of Staple J with major by-product Staple M

Two peptide stapled peptide products were isolated after purification: **Staple J** as expected, and the unexpected by-product **Staple M** (Scheme 36). It became apparent that the side chain coupling was relatively slow allowing for condensation between the side chain of Glu and the backbone NH. This pyroglutamic acid formation was interesting as the peptide was still able to undergo ring-closing metathesis on the solid phase, giving the major product from this synthesis. As the *N*-terminal Glu is not essential for binding to Ubb+1, **Staple M** was retained as a new serendipitous analogue of **Staple A**.

In order to decrease the extent of pyroglutamic acid formation during the amide coupling step during the formation of **Staple K** and **Staple L**, a modified synthetic route was developed. This alternative synthesis carried out the RCM step first prior to allyl deprotection and subsequent coupling steps (Scheme 37). It was hypothesised that by stapling the peptide first, the five-membered ring formation may then be less favourable than the side chain coupling due to the peptide backbone being in a locked formation and having decreased rotational freedom. However, it was noted that this route could be problematic due to the presence of the allyl group during the ring-closing step. This could potentially form an unwanted *i*, *i*+2 link between S$_5$ and the Glu(OAllyl) giving a seventeen-membered lactone rather than the required twenty one-membered all-hydrocarbon macrocycle. A trial cleavage reaction performed after the RCM step (a) (Scheme 37) showed one major product, with multiple smaller by-products observed by HPLC. However, it was

pleasing to note that after allyl deprotection, the major product appeared to be the required *i*, *i*+4 ring-closed intermediate, peptide **161**. The resin was divided into two portions at this point to enable synthesis of both **Staple K** and **Staple L** from the common precursor **161**.
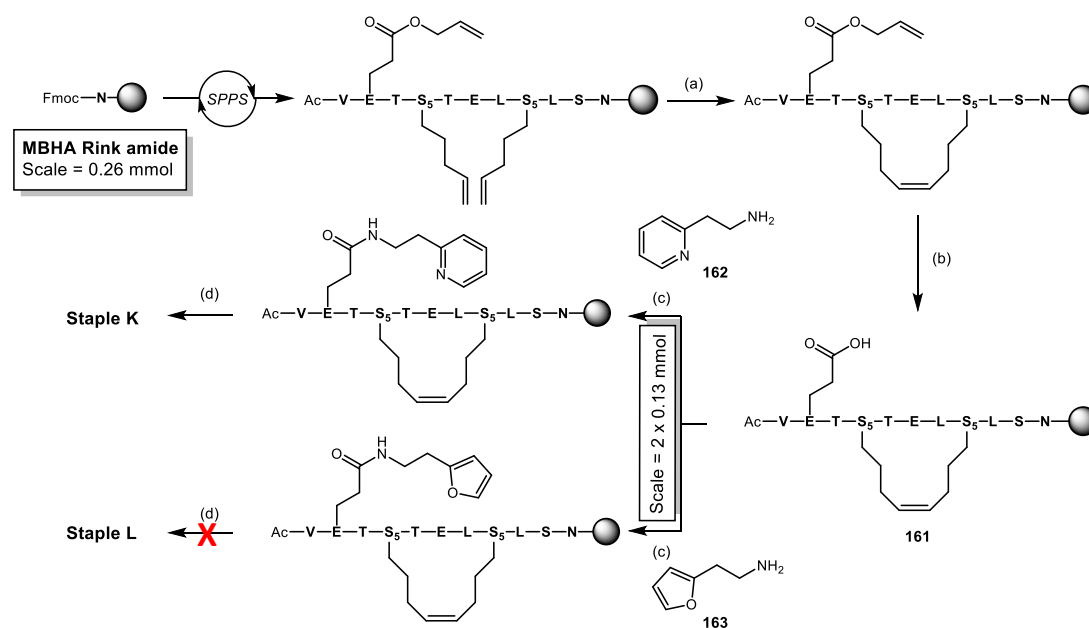
(a) - Grubbs 1st gen. cat. (40 mol%), 10 mM DCM, 3 x 2 h (b) - Pd(PPh$_3$)$_4$ (10 mol%), PhSiH$_3$ (10 equiv.), DCM, 4 x 15 min
(c) **162 / 163** (5 equiv.), HATU (5 equiv.), DIPEA (10 equiv), DMF, 2 h d) TFA:TIS:H$_2$O (95:2.5:2.5), 4 h

Scheme 37 – Change in route towards extended series
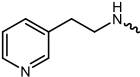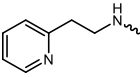
Coupling of amine **162** was carried out using analogous HATU conditions as those in the synthesis of **Staple J**. Upon cleavage from the resin it was pleasing to note that only a small amount of cyclised product **Staple M** was present, with the majority of product being the extended amide **Staple K**. The change in synthetic route had successfully decreased the amount of pyroglutamic acid formation, however the ring-closing step was not as clean a reaction as previous peptides due to the presence of the allyl group, possibly due to the competing metathesis reactions.

Unfortunately, **Staple L** could not be isolated despite the success of the coupling between peptide **161** and furan **163**. Trial resin cleavage conditions had shown traces of the product **Staple L**, however upon full scale cleavage conditions, it was found that no product could be isolated. This was likely due to the furan being unstable to TFA in the cleavage mixture for prolonged periods of time. Despite multiple attempts at isolation using decreased reaction times and expedient work-up, **Staple L** was eventually abandoned due to the potential instability of the furan side chain.

3.2.9 – Analysis of Staple A analogue peptides

Through sequence isomerisation and side-chain extension, four additional analogues of **Staple A** were successfully synthesised and ring closed (Table 15). As discussed previously, the yield of **Staple I** was lower than expected due to difficulties in coupling both threonine residues giving rise to deletion and truncation analogues. The yields of the peptides in the extended series were also low. In the case of **Staple J** this was due to the formation of the major pyroglutamic acid by-product **Staple M** in a 10% yield.

Table 15 – Completed Staple A analogues

Peptide	Staple	Sequence	Yield	Extension
Staple I	i, i+4	Ac-L-T-E-**S₅**-N-T-L-**S₅**-S-V-E-NH₂	3%	-
Staple J	i, i+4	Ac-V-**E***-T-**S₅**-T-E-L-**S₅**-L-S-N-NH₂	2 %	
Staple K	i, i+4	Ac-V-**E***-T-**S₅**-T-E-L-**S₅**-L-S-N-NH₂	2%	
Staple M	i, i+4	Ac-V-**E***-T-**S₅**-T-E-L-**S₅**-L-S-N-NH₂	10%	

Despite no pyroglutamic by-product being isolated in the synthesis of **Staple K**, the isolated yield was not improved due to the ring-closing metathesis step having a less clean reaction profile than the previously synthesised peptides. Having stated this, sufficient material was isolated in each case to support structural work and biological evaluation.

As with the previously synthesised peptides, secondary structure content was then determined *via* circular dichroism spectroscopy. All of the analogue peptides analysed (Fig. 44) had lower helicity than the progenitor peptide **Staple A** (Purple line). **Staple I**, in which the primary sequence was isomerised to give a peptide with analogous physiscochemical properties to **Staple A**, had a decreased helicity of 24%. This was an interesting result as, despite the staple position being the same as that of **Staple A**, the helicity was vastly decreased, demonstrating the importance of primary sequence on the secondary structure. This was further evidence that simply installing an all-hydrocarbon staple in any sequence will not guarantee a helical structure.

Peptide	Staple	Sequence	% Helicity
Staple A	i, i+4	Ac-V-E-T-S_5-T-E-L-S_5-L-S-N-NH$_2$	91
Staple I	i, i+4	Ac-L-T-E-S_5-N-T-L-S_5-S-V-E-NH$_2$	24
Staple J	i, i+4	Ac-V-**E***-T-S_5-T-E-L-S_5-L-S-N-NH$_2$	10
Staple K	i, i+4	Ac-V-**E***-T-S_5-T-E-L-S_5-L-S-N-NH$_2$	14
Staple M	i, i+4	Ac-V-**E***-T-S_5-T-E-L-S_5-L-S-N-NH$_2$	39
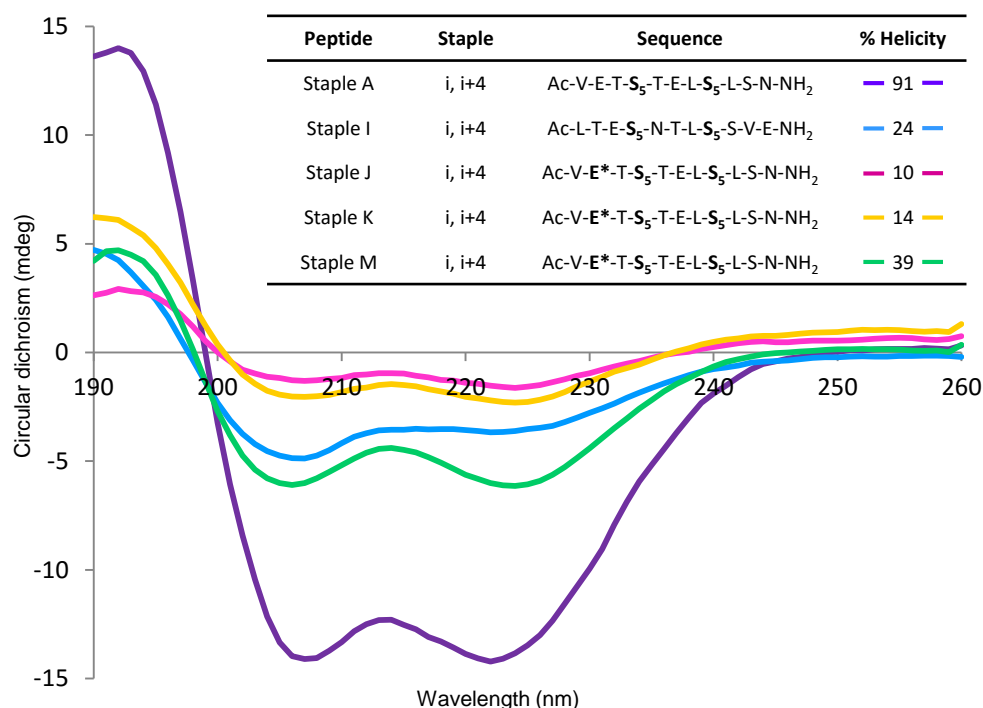
Figure 44 – Circular dichroism analysis and helicity values of Staple A analogues

The extended peptides, **Staple J** and **Staple K**, only exhibited 10% and 14% helicity in phosphate buffer, respectively. Despite this value being comparatively low, the CD spectra of both peptides still maintained a maxima at 198 and two minima at 208 nm and 222 nm, implying the peptides were still helical and not completely unstructured. These low helicity values are likely due to the large flexible aromatic side chains causing the peptide to fold over on itself towards the *N*-terminus, disrupting the helix. Finally, **Staple M** had a reasonable helicity of 39%. This was interesting as the cyclisation to form the pyroglutamate system appeared to be disrupting the tight α-helix compared to **Staple A**.

3.3 – Structural analysis of selected stapled peptides

Based on the range of helicities noted in the first generation of peptides synthesised, an NMR study was carried out by the author to confirm the data observed by CD. Through application of various biological NMR techniques, the objective of this study was to confirm the highly ordered α-helical structure of **Staple A** (91%) compared to the less helical analogues **Staple G** (42%) and **Staple I** (24%). To accomplish this goal, a series of NMR spectra were obtained for each stapled peptide. Peptide samples (**Staples A**, **G** and **I**) were diluted to 2-3 mM in phosphate buffer (50 mM, pH 7) made from 10% D$_2$O and 90% H$_2$O in order to obtain ^{1}H, NOESY and TOCSY data with clear NH shifts. Initial investigation into pulse gradients resulted in an ideal

water suppression which gave rise to a well resolved ^{1}H spectra. A further COSY spectra of **Staple A** was obtained with 100% D_2O to allow for clarity of the assignment of the all-hydrocarbon staple. In order to obtain a full assignment of **Staple A**, and investigate further structural information of **Staples G** and **I**, SPARKY NMR visualisation software was used to interpret, assign and integrate all 2D spectra.[207] Once completed, the data was then interrogated for evidence of secondary structure as discussed below.

3.3.1 – Chemical shift indexing

The first technique used to analyse the structure of the stapled peptides was chemical shift indexing. As the chemical environment surrounding a proton influences the magnetic environment, certain protein secondary structures have a direct correlation to chemical shift. These upfield and downfield shifts are proportional to the average folding of a peptide or protein in a given solution. Through comparison of a measured chemical shift value with a reference random coil chemical shift, information relating to a protein chemical structure can be derived.[208] This allows for rapid elucidation of basic secondary structure using ^{1}H NMR data. When the measured NH chemical shift values of **Staple A** were compared to the literature standard random coil resonance shifts for each amino acid in the sequence, there are clear differences between the two sets of data (Table 16). If this difference was greater than 0.2 ppm then a "+1" index was applied and, similarly if the difference was less than -0.2 then a "-1" index was applied. Finally any differences between -0.2 and +0.2 were assigned as "0". To convert this information into secondary structure, the index along the sequence was analysed for distinctive patterns. If the sequence contained four "-1" indexes uninterrupted by a "+1" then that section of sequence was considered α-helical.[209] Alternatively, if three "+1" indexes were uninterrupted by a "-1" then the sequence was considered a β-sheet. The α-helix or β-sheet was considered terminated when an opposite sign index or two consecutive zero values were present in the chain.[209] This analysis can give valuable information regarding the average population of secondary structures in both peptides and proteins.

For **Staple A**, the NH chemical shift index showed that two thirds of the sequence had -1 values, with six consecutive negative residues (Table 16). Although there is no reference for the S_5 residue, this data implies that the middle to *C*-termini of **Staple A** maintained an α-helical structure in solution. A similar result was obtained

for the αH chemical shift data, which is considered to be more consistent than the NH chemical shift data due to the potential for solvent effects.

Table 16 – Chemical shift indexing for Staple A

NH chemical shift	Staple A	V	E	T	S₅	T	E	L	S₅	L	S	N
	Measured shift	8.12	8.75	8.04		7.88	7.60	7.46		7.80	7.79	7.96
	Random coil shift	7.88	8.29	8.22		8.22	8.29	8.12		8.12	8.26	8.33
	Difference	0.24	0.46	-0.18		-0.34	-0.69	-0.66		-0.32	-0.47	-0.37
	Index	+1	+1	0		-1	-1	-1		-1	-1	-1
αH chemical shift	Staple A	V	E	T	S₅	T	E	L	S₅	L	S	N
	Measured shift	3.99	4.22	4.21		3.78	3.91	4.04		4.11	4.27	4.66
	Random coil shift	4.14	4.28	4.33		4.33	4.28	4.35		4.35	4.48	4.60
	Difference	-0.15	-0.06	-0.12		-0.55	-0.37	-0.31		-0.24	-0.21	0.06
	Index	0	0	0		-1	-1	-1		-1	-1	0

The five consecutive -1 values between the stapled region towards the *C*-termini was further evidence that **Staple A** adopts an α-helical structure in solution. It can also be inferred that the helix could potentially begin to unravel towards the *N*-termini due to the presence of two +1 values in the NH region.

Chemical shift analysis of **Staple G** contained a majority of -1 index values (Table 17). The NH chemical shifts appeared to contain eight consecutive -1 values, implying a majority helical structure. By comparison, the αH region contained only six consecutive -1 values towards the *N*-terminus.

Table 17 – Chemical shift indexing of Staple G

NH chemical shift	Staple G	S₅	E	T	A	S₅	E	L	L	L	S	N
	Measured shift	8.48	9.46	7.62	7.26	8.16	7.63	7.66	7.67	7.85	7.91	7.91
	Random coil shift		8.29	8.22	8.11		8.29	8.12	8.12	8.12	8.26	8.33
	Difference		1.35	-0.60	-0.85		-0.66	-0.46	-0.45	-0.27	-0.35	-0.42
	Index		+1	-1	-1		-1	-1	-1	-1	-1	-1
αH chemical shift	Staple G	S₅	E	T	A	S₅	E	L	L	L	S	N
	Measured shift		3.84	3.93	3.96		3.83	4.03	4.09	4.15	4.29	4.61
	Random coil shift		4.28	4.33	4.25		4.28	4.35	4.35	4.35	4.48	4.60
	Difference		-0.44	-0.40	-0.29		-0.45	-0.32	-0.26	-0.20	-0.19	0.01
	Index		-1	-1	-1		-1	-1	-1	0	0	0

When comparing the two indexes there is the potential that **Staple G** is less structured towards the *C*-terminus (Table 17). However, overall this study would suggest an α-helical structure.

The analysis of the chemical shift index of **Staple I** was interesting when compared to that of **Staples A** and **G**, as there appeared to be far less helical character (Table 18).

Table 18 – Chemical shift indexing of Staple I

	Staple I	L	T	E	S₅	N	T	L	S₅	S	V	E
NH chemical shift	Measured shift	8.24	8.09	8.40	8.29	8.46	7.98	7.34	8.13	7.56	7.54	7.88
	Random coil shift	8.12	8.22	8.29		8.33	8.22	8.12		8.26	7.88	8.29
	Difference	0.12	-0.13	0.11		0.13	-0.24	-0.78		-0.70	-0.34	-0.41
	Index	0	0	0		0	-1	-1		-1	-1	-1
αH chemical shift	Staple I	L	T	E	S₅	N	T	L	S₅	S	V	E
	Measured shift	4.25	4.17	4.08		4.38	4.25	4.12		4.18	3.97	4.13
	Random coil shift	4.35	4.33	4.28		4.60	4.33	4.35		4.48	4.14	4.28
	Difference	-0.10	-0.16	-0.20		-0.22	-0.08	-0.23		-0.30	-0.17	-0.15
	Index	0	0	0		-1	0	-1		-1	0	0

The index of NH chemical shifts for **Staple I** only contained five -1 values, implying a helical structure is only maintained towards the *C*-terminus. By comparison, the αH values demonstrated no α-helical character. These results appeared to be concordant with the CD analysis of **Staple I** in which the peptide was shown to only contain 24% helicity (Fig. 44).

3.3.2 – Investigation into the stapled peptide backbone

The next aspect of the ¹H NMR spectrum analysed was the coupling constants observed within the NH region of the spectra. This information can be related to the backbone dihedral angle as the ^3J value between the NH and αH of a spin system relates to the torsion angle between the two protons. As previously discussed in Section 1.5.1, protein secondary structure is defined by backbone dihedral angles, with an α-helix maintaining the angles Φ = -60° and Ψ = -40°. The correlation between ^3J coupling constant and backbone dihedral angle depends on the Karplus expression: $^3J_{ij}(θ) = A\cos^2θ + B\cosθ + C$. For the dihedral angle of interest, Φ, this expression becomes $^3J_{NH-αH}(Φ) = 6.4\cos^2(Φ - 60°) – 1.4\cos(Φ - 60°)) + 1.9$ (Fig. 45).[210] For an α-helical peptide (hydrogen bonds every *i*, *i*+4 residues), Φ = 60° corresponds to a $^3J_{NH-αH}$ coupling constant of 4.2 Hz. Alternative helical structures

such as a 3^{10} helix (hydrogen bonds every i, $i+3$ residues), π-helix (hydrogen bonds every i, $i+5$ residues) and left handed α-helices have higher or lower coupling constants depending on their specific backbone conformation (Fig. 69).[210]
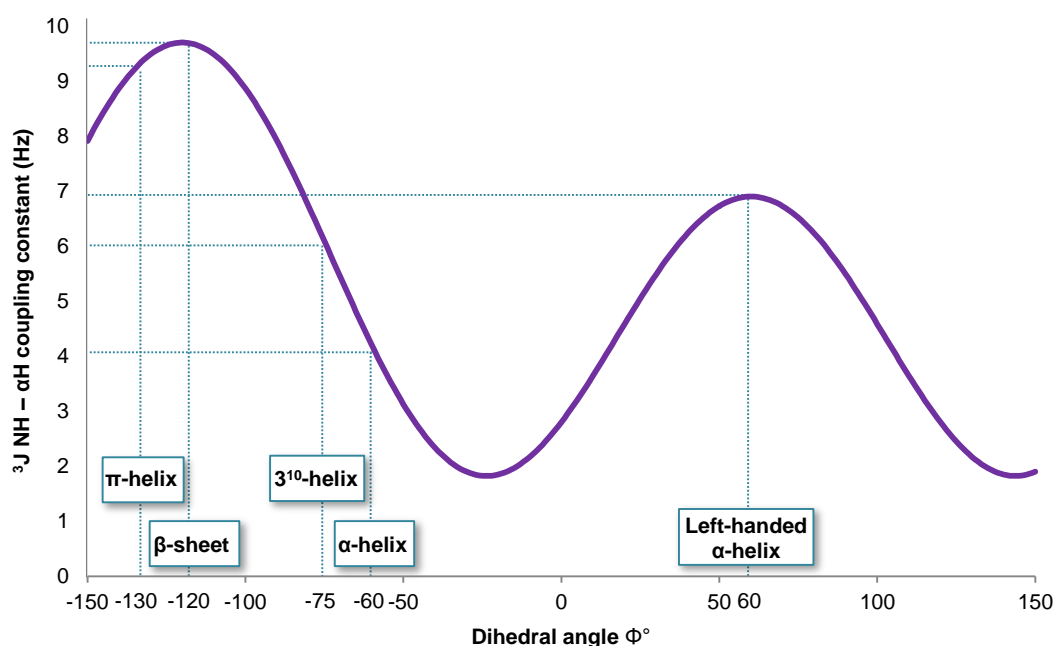
Figure 45 – Karplus correlation between dihedral angle Φ and ^3J coupling constant

The ^{1}H spectra obtained for **Staple A** showed clear coupling constants for 5 of the 9 expected residues. The $^3J_{\text{NH-αH}}$ coupling constants ranged from 5.1 to 7.1 Hz which are higher than the 4 Hz expected for a standard α-helix (Table 19). These higher coupling constants implied that the backbone angle of **Staple A** is larger than a standard α-helix, with the structure being more similar to that of a 3^{10}-helix on average.[211] This was an interesting observation as a 3^{10}-helical structure had not been apparent from analysis of the CD spectra of **Staple A** (Fig. 38) in Section 3.2.6.

Table 19 - $^3J_{\text{NH-αH}}$ coupling constants of Staples A, G and I

Staple A	V^1	E^2	T^3	S_5^4	T^5	E^6	L^7	S_5^8	L^9	S^{10}	N^{11}
^3J NH – αH (Hz)	7.1	5.1	6.3	-	-	-	6.5		-	-	6.8

Staple G	S_5^1	E^2	T^3	A^4	S_5^5	E^6	L^7	L^8	L^9	S^{10}	N^{11}
^3J NH – αH (Hz)	-	-	-	5.7	-	3.2	-	-	6.2	-	-

Staple I	L^1	T^2	E^3	S_5^4	N^5	T^6	L^7	S_5^8	S^9	V^{10}	E^{11}
^3J NH – αH (Hz)	6.2	6.6	-	-	3.1	6.2	6.6	-	5.3	7.0	7.0

The results from the chemical shift indexing of **Staple A**, which suggested that the peptide potentially was less structured towards the *N*-terminus were mirrored in the coupling data in that the coupling constants of Val[1] and Glu[2] differed by 2 Hz, implying flexibility in this region of the sequence. Unfortunately, the peaks for both Thr[5] and Glu[6] were too broad to gain accurate coupling constants as this could potentially have provided valuable information concerning backbone conformation within the stapled region. The *C*-terminal residues Leu[9] and Ser[10] had NH peaks which overlapped giving an apparent triplet with *J* values of 6.1 and 6.5 Hz, respectively, which were similar to the ^3J values for the remaining sequence of **Staple A** (Table 19), implying that the *N*-termini also retained a 3^{10}-like helical structure.

The ^{1}H spectra obtained for **Staple G** only contained three residues in the NH region which contained clear coupling constants. Glu[6] contained a very small ^3J value of 3.2 Hz (Table 19). This was potentially due to a slight twist in the peptide backbone before the S_5 residue due to its steric bulk. The other two ^3J values obtained ranged from 5.7 – 6.2 Hz, which was similar to those seen in **Staple A**, implying a similar 3^{10}-like helical structure.

Further analysis indicated that **Staple I** exhibited the greatest number of $^3J_{NH-\alpha H}$ coupling constants. As with **Staple G**, a single residue adjacent to a S_5 residue contained a very low ^3J value of 3.1 Hz, however, the majority of the coupling constants ranged from 5.3 to 7.0 Hz (Table 19). Overall these results would suggest that all of the peptides analysed again adopted a more 3^{10}-like helical population. This was interesting as helix-coil transition theory suggests that there can be free interconversion between an α-helix and a 3^{10}-helix structure in solution,[212] with short sequences (3-7 residues) having a greater propensity for 3^{10}-helix formation.[210] This is due to the lower entropic penalty in forming *i*, *i*+3 hydrogen bonds over the *i*, *i*+4 distance of a standard α-helix in α-9 of E2-25K.[212] The formation of a more 3^{10}-like helical structure could also be due to the incorporation of the α-, α-disubstituted amino acids key to the hydrocarbon staple. It is well documented that the α-methyl, α-methyl residue, AIB, favours 3^{10}-helices due to the steric interactions forcing a more energetically favourable conformation.[213] The only reported examples of stapled peptides forming a definitive 3^{10}-helical structure was the original cross-linked systems synthesised by Grubbs *et al* (Section 1.7), in which the conformation of the short nine residue sequence was confirmed by X-ray crystallography.[149] The

presence of 3^{10}-helices in all-hydrocarbon stapled peptides has not been reported, however this may be due to the preference for structural conformation using X-ray crystallography in which an active stapled peptide is bound to the target protein. Conformation of a peptide in solution compared to when bound to a protein target could be variable due to the formation of key binding interactions and the absence of solvent interactions. There is also the possibility that when bound to Ubb+1, the synthesised stapled peptide mimics of E2-25K could conform in a more standard α-helical conformation to gain closer interactions with the protein binding site, compared to a putative 3^{10}-like helical structure when characterised in isolation.

3.3.3 – NOE analysis of helical structure

The next step to investigate the helical character of **Staple A** was to analyse the NOESY data to assess conformational preferences. As an NOE contact is a through-space correlation, this can give information whether individual protons are proximal despite not being present in the same residue (spin system). Due to the spiral configuration of an α-helix, the NH and αH backbone protons all point parallel to one another which allows for characteristic NOE patterns. The amide NH protons all orientate towards the *N*-termini along with all *S*-amino acid side chains, while all the αH protons point towards the *C*-termini. Due to this conformation, an NOE walk along the backbone can be achieved for each sequential NH-NH and NH-αH interaction at the *i*, and *i*+1 positions. In the case of **Staple A**, a majority of the NH protons in the 11 amino acid sequence experienced an NOE from the preceding residue (light blue arrows in Fig. 46). Similarly, all α-protons also experienced an NOE from the preceding backbone NH proton, with the exception being the S_5 residues which lack an αH. This is strong evidence of an α-helical secondary structure as these NOEs would not be observed in an unstructured peptide.
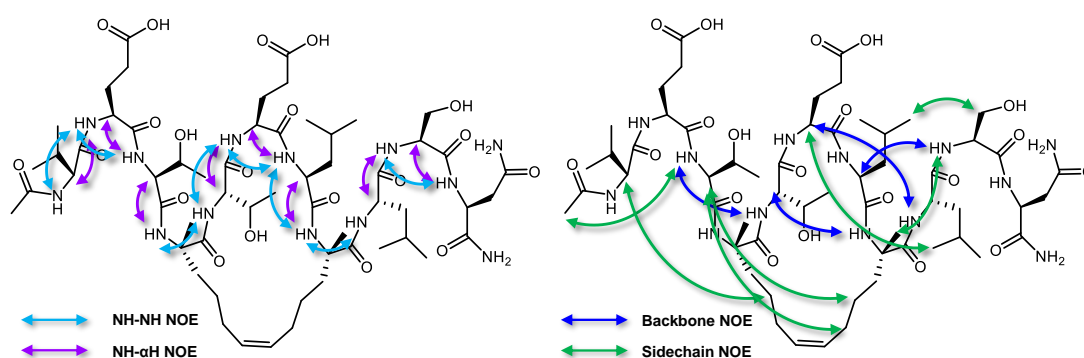
Figure 46 – NOEs present in Staple A

The next aspect of the NOE spectra to be investigated were the presence of long range NOEs, in particular those between i, $i+2$, $i+3$ and $i+4$ residues of the peptide backbone. These interactions would only be present due to the characteristic turns of the α-helix, bringing residues which are distant in the primary sequence into close proximity to one another. However, when comparing α-helical peptides to 3^{10}-helices, these long range interactions can be diagnostic of the precise type of helical conformation present. Peptides which contain NH-NH and NH-αH interactions between predominantly i, $i+2$, $i+3$ residues are considered 3^{10}-helices, while peptides which contain these backbone interactions between predominantly i, $i+3$, $i+4$ residues are considered α-helical.[210] It was interesting to note that **Staple A** contained a number of long range NOEs across the sequence (dark blue arrows in Fig. 46), with a range of characteristic α-helical i, $i+2$ and $i+3$ backbone NOEs were present (Table 20).

Table 20 – Backbone NOE patterns of Staple A

Staple A	i+1	i+2	i+3	i+4
NH-NH	10	1	-	-
NH-αH	8	-	3	-

It was interesting to note that a majority of these additional backbone NOEs were between i, $i+3$ residues, with a single i, $i+2$ interaction. Similar long range interactions were present between the amino acid side chains which would only be possible if the peptide was constrained in a helical structure. This data in conjunction with the chemical shift indexing (Table 16) and backbone analysis (Table 20) implied that **Staple A** adopts a well ordered helical structure, with the likelihood of the overall conformation being closer to a 3^{10}-helix rather than an α-helix, which had not been apparent by CD spectroscopy.

Analysis of the backbone NOE interactions was more problematic for **Staple G** compared to **Staple A** as the spectra were not as well resolved. In particular, the NH peaks of Leu[7] and Leu[8] overlapped as well as the NH peaks of Ser[10] and Asn[11], leaving definition of the *C*-terminus difficult. The NH-NH and NH-α analysis of the **Staple G** backbone was only definitive towards the *N*-termini of the peptide (Fig. 47). As some backbone NOEs are present towards the *N*-termini it is uncertain whether the peptide unravels from an α-helical structure or whether it is an anomaly due to the limited resolution of the spectra.
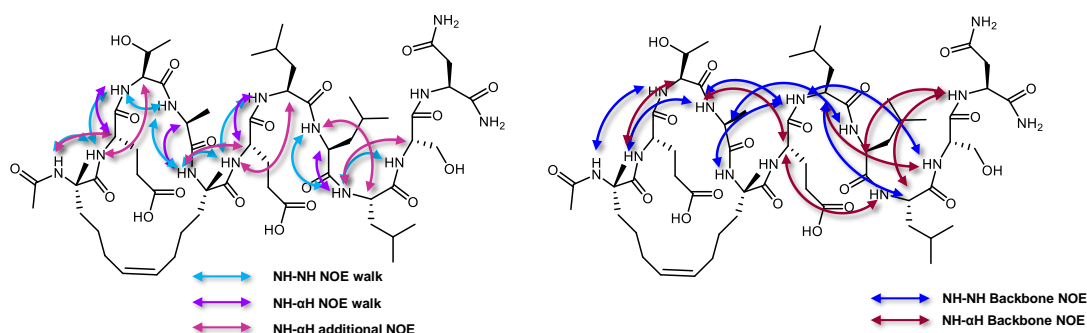
Figure 47 – Backbone NOEs present in Staple G

It was noteworthy that the spectra of **Staple G** exhibited many long range NOEs across the whole sequence from *i*, *i*+2 to *i*, *i*+6. Upon extensive analysis of the NOE data, it became apparent that **Staple G** appeared to fold over on itself, with the *C*-terminus interacting towards the stapled *N*-terminus. Of particular interest was the NOE between the *N*-terminal S_5 residue and the side chain of Leu[7] or Leu[9] (Fig. 48).
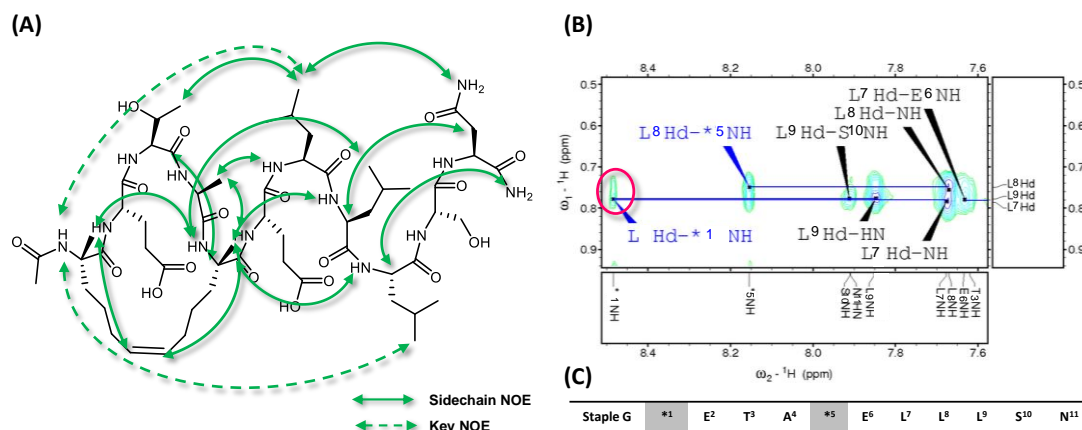
Figure 48 – NOE data indicates an additional folding of Staple G
A) – Long range NOEs present in the [^{1}H, ^{1}H] NOESY spectra of Staple G. Dotted line indicates an NOE which could exist between either Lee side chain. B) – Zoomed in area of the NH-aliphatic region of the [^{1}H, ^{1}H] NOESY spectra. Circled peak could be from eith L[7] or L[9] resonance. C) – Residue labelling if Staple G.

A direct assignment of the leucine residue producing the NOE with S_5^1 was not possible due to a resonance overlap (Fig. 48, B). Despite this uncertainty, the highlighted peak represented a long range NOE of *i*, *i*+6 or *i*+9, which would be unlikely without an additional folding of the peptide outside the expected helical conformation. This result for **Staple G** was very interesting as this part-helical folded conformation was very different to the highly ordered structure of **Staple A** in which the all-hydrocarbon staple lies in the centre of the sequence, therefore folding is not possible. There was also a higher proportion of backbone NOEs between *i*, *i*+2

residues when compared to **Staple A**, implying a higher likelihood of the peptide adopting a 3^{10}-helical structure in solution (Table 21).

Table 21 - Backbone NOE patterns of Staple G

Staple G	i+1	i+2	i+3	i+4
NH-NH	8	3	3	-
NH-αH	4 + 6	2	2	-

This data provided compelling evidence that the overall structure of **Staple G** is more complicated than the previous CD analysis had implied, with the peptide adopting a folded helical structure when in aqueous solution.

Upon analysis of the NOE spectra of the final peptide, **Staple I**, it became apparent that the 24% helicity value calculated from the CD spectra (Fig. 44) was likely to be accurate. The NOE analysis of backbone *i*, *i*+1 residues which is characteristic of an α-helical structure, was only accomplished for two thirds of the peptide sequence (Fig. 49). These interactions were mainly present in the stapled region and towards the *C*-terminus of the peptide.
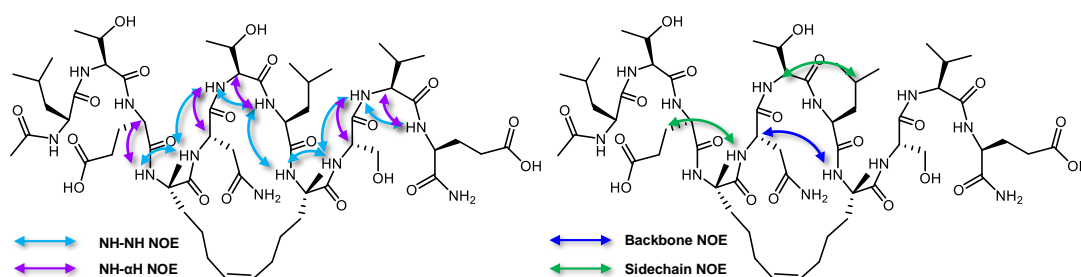
Figure 49 – NOEs present in Staple I

It was very interesting to note that **Staple I** only contained three long range NOE interactions between *i*, *i*+2 and *i*+3 residues (Table 22). In particular these interactions were only present in the central stapled region of the peptide.

Table 22 - Backbone NOE patterns of Staple I

Staple I	i+1	i+2	i+3	i+4
NH-NH	7	-	-	-
NH-αH	5	-	1	-

This data implied that **Staple I** only has a small proportion of helical character which correlates well with the chemical shift data (Table 18) and the calculated helicity of

24%. As discussed in Section 3.2.7, this is likely due to the isomeric sequence not containing residues presented in an order which is pre-organised for a helical conformation.

Overall, the results obtained from the NMR studies of **Staples A**, **G** and **I** gave valuable insight into the conformations of these peptides as a whole, in addition to the helicity data obtained by CD. Combination of the data generated using a range of techniques implied a potential for each of these peptides to adopt mixed-helical character. The ^3J NH-αH coupling constants were consistently higher than those of an α-helix and were closer to the range of a 3^{10}-helix in most cases. In addition, the presence of multiple *i*, *i*+2 backbone NOEs in **Staples A** and **G** further confirm the hypothesis that these helices have significant 3^{10}-character. These results were interesting as this had not been identified from the CD spectra of these peptides. Despite some evidence to the contrary,[214] it has been proposed that the CD spectrum of a 3^{10}-helix can be differentiated from that of a standard α-helix.[213] In particular the 3^{10}-helix will have differing ellipticity values (θ) between the characteristic 208 nm and 222 nm minima. In a standard right handed α-helix the absorbance between the parallel component of the π-π* (208 nm) transition and n-π* (222 nm) transition of the amide backbone is of similar energy, however in a 3^{10}-helix the n-π* transition is reduced in intensity. Therefore the ratio of $\theta_{222} / \theta_{208}$ is a useful diagnostic of 3^{10}-helical structure, with values between 0.15 – 0.4 considered to confirm this type of secondary structure being present.[213] It was interesting to note that none of the synthesised peptides displayed a $\theta_{222} / \theta_{208}$ ratio within this range (Table 23).

Table 23 – CD spectra ratios to define helical conformation

Peptide	Staple A	Staple B	Staple C	Staple D *trans*	Staple D *cis*	Staple E	Staple G	Staple I	Staple J	Staple K	Staple M
$\theta_{222} / \theta_{208}$	1.01	0.90	0.80	0.95	1.01	0.61	0.83	0.77	1.18	1.10	1.04

Staple A appeared to have a perfect ratio of 1, which indicates an ideal α-helix, in contrast to what can be inferred from the NMR data. Despite the ratios of **Staples G** and **I** being lower than **Staple A**, they were not considered low enough to suggest a completely 3^{10}-helical structure.

In conclusion, the NMR studies of these selected stapled peptides enabled further understanding of the more discreet nature of helix formation in these constrained

species. The absence of definitive data to confirm α-helical or 3^{10}-helical conformation is not problematic as it is likely that these short sequences can exchange between the two conformations. The proportion of α-helical content compared to 3^{10}-conformation is also potentially variable depending on sample concentration and spectral timescale as the CD spectra were completed in under 10 minutes in 200 µM solutions, whilst the NMR experiments took several hours and were more concentrated at 2 mM. Overall the NMR data obtained was in concordance with the helicity data obtained from the CD spectra which was the overall goal of these experiments.

3.3.4 – Thermal stability investigation

In addition to the NMR studies of **Staple A**, it was also of interest to study the thermal stability of the constrained α-helix. This was accomplished using CD spectroscopy due to the relative ease of temperature ramping peptides in solution as well as the clear indication of helical content. In these studies it was shown that **Staple A** had significant tolerance for temperature, with helicity being maintained up to 80 ^{o}C in phosphate buffer (Fig. 50).

Peptide	Staple	Sequence	Temp. (°C)	Helicity	$\theta_{222}/\theta_{208}$
Staple A	i, i+4	Ac-V-E-T-S_5-T-E-L-S_5-L-S-N-NH$_2$	20	89%	0.94
			25	88%	0.92
			30	86%	0.91
			35	84%	0.90
			40	81%	0.89
			45	79%	0.87
			50	77%	0.86
			55	75%	0.85
			60	73%	0.85
			65	72%	0.84
			70	70%	0.82
			75	69%	0.80
			80	68%	0.80
			20	89%	0.92
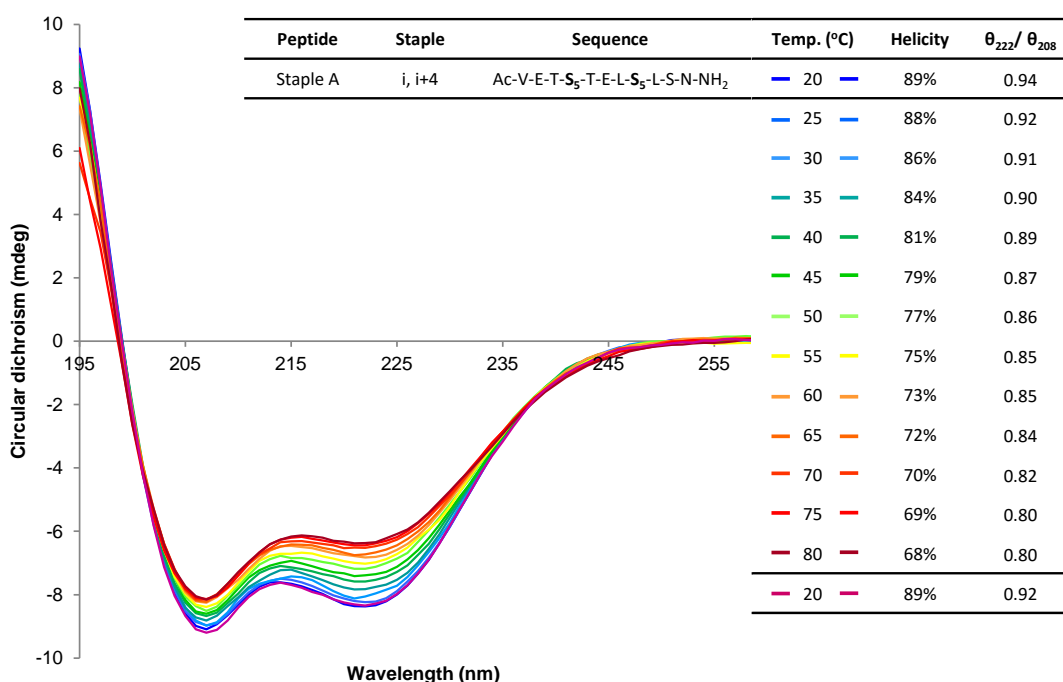
Figure 50 – Temperature ramped CD spectra of Staple A
Sample run at 15 µM in a 2 mm cell

It was interesting to note that the percent helicity of **Staple A** decreased on average by 2% per 5 ^{o}C increase in temperature. At the maximum temperature tested,

Staple A maintained a 68% helical structure. It was also noteworthy that upon cooling back to 20 $^{\circ}$C, the peptide regained its highly ordered structure with the helicity returning to the original value of 89% (within this particular experiment). In addition to this, a further intriguing result was the effect of temperature on the ratio of $\theta_{222}/ \theta_{208}$ in relation to the extent of α-helical *vs* 3^{10}-helical structure. It was apparent that upon temperature increase, **Staple A** began to adopt a more 3^{10}-like structure. Despite never forming a well defined 3^{10}-helix with a $\theta_{222}/ \theta_{208}$ ratio between the ideal values of 0.15 and 0.4, **Staple A** began to adopt a preference for this alternative conformation at higher temperatures. This was interesting as an α-helix formation should be more favourable at higher temperatures according to first-principle free-energy analysis.[215] However, as with the overall helicity value, this ratio returns to almost one upon cooling of the sample.

Comparative thermal stability studies were carried out on **Staples B** and **M** to investigate how sequences with lower helicity (41% and 39%, respectively) behaved at higher temperatures compared to tight helical peptides such as **Staple A**. The first comparative analysis showed that the rate of helix unfolding for **Staple B** was less pronounced compared to that of **Staple A** (Fig. 51).

Peptide	Staple	Sequence	Temp. (°C)	Helicity	$\theta_{222}/ \theta_{208}$
Staple B	i, i+4	Ac-V-E-T-A-**S$_5$**-E-L-L-**S$_5$**-S-N-NH$_2$	20	38%	0.83
			25	37%	0.82
			30	36%	0.80
			35	35%	0.79
			40	34%	0.77
			45	33%	0.76
			50	32%	0.76
			55	32%	0.75
			60	31%	0.74
			65	30%	0.73
			70	30%	0.72
			75	30%	0.73
			80	29%	0.71
			20	37%	0.81
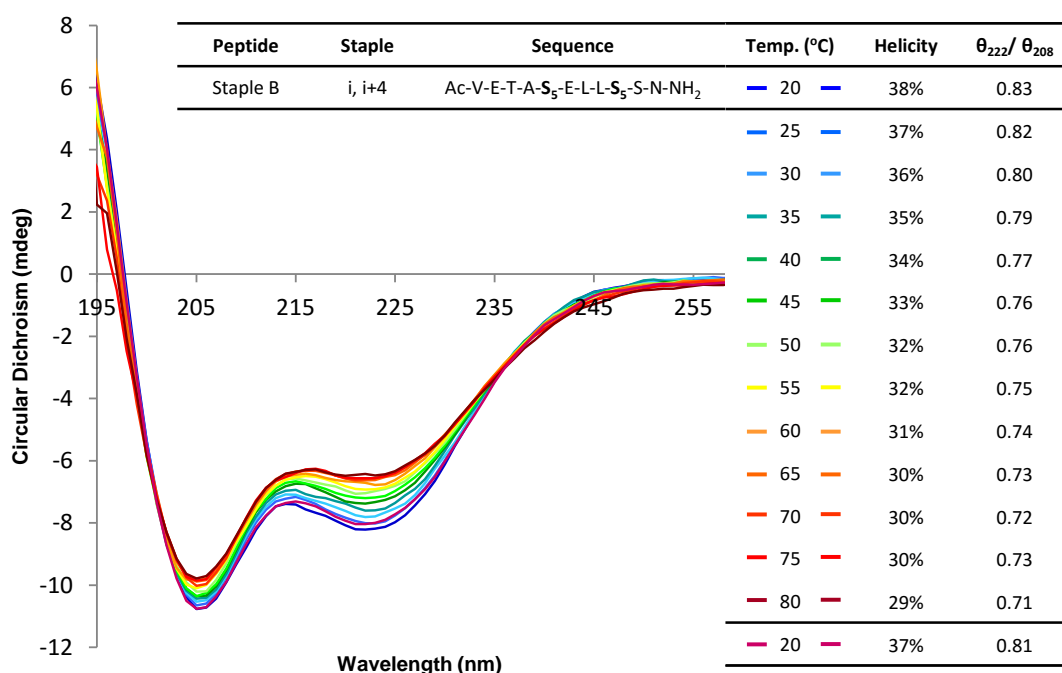
Figure 51 - Temperature ramped CD spectra of Staple B
Sample run at 35 µM in a 2 mm cell

The overall helicity of **Staple B** only decreased by 9% compared to **Staple A** which was 21% less helical at 80 °C compared to 20 °C. It was also pleasing to note that **Staple B** returned to its original secondary structure upon cooling to 20 °C. This implied that despite the lower helicity of **Staple B** in general, the overall conformation of the peptide was more consistent when subjected to temperature variation. It was also noteworthy that **Staple B** exhibited a higher proportion of 3^{10}-helicity compared to **Staple A**, as shown by the $\theta_{222}/\theta_{208}$ ratio. **Staple B** also acquired a greater degree of 3^{10}-helical character upon heating, similar to that of **Staple A**.

A final thermal stability experiment was carried out on **Staple M**, in which the *N*-terminal cyclisation of **Staple A** significantly changes the overall peptide helicity from 91% to 39% by CD. The overall helicity of **Staple M** only decreases by 10% from 20 °C to 80 °C, again returning to its original conformation upon cooling during the temperature ramp experiment (Fig. 52).

Peptide	Staple	Sequence	Temp. (°C)	Helicity	$\theta_{222}/\theta_{208}$
Staple M	i, i+4	Ac-V-E*-T-**S₅**-T-E-L-**S₅**-L-S-N-NH₂	20	40%	0.97
			25	40%	0.98
			30	39%	0.95
			35	38%	0.94
			40	37%	0.92
			45	36%	0.90
			50	35%	0.90
			55	34%	0.88
			60	33%	0.85
			65	32%	0.84
			70	31%	0.82
			75	30%	0.80
			80	30%	0.78
			20	40%	0.94
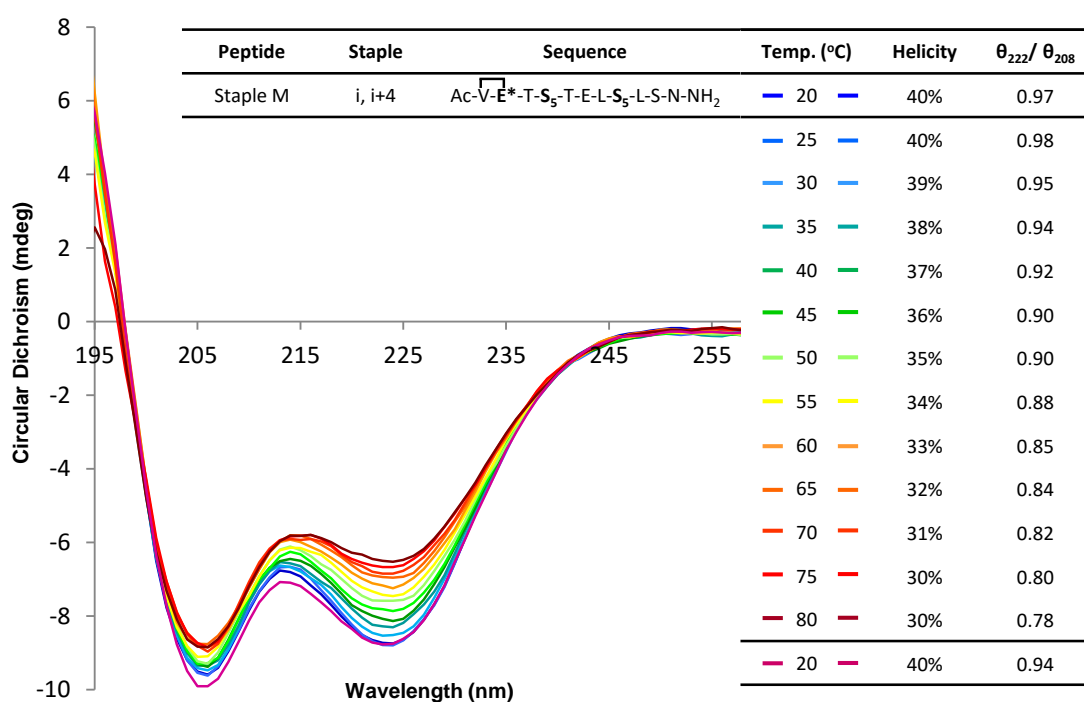
Figure 52 - Temperature ramped CD spectra of Staple M
Sample run at 35 µM in a 2 mm cell

As with **Staple A**, **Staple M** also gained more 3^{10}-helical character upon heating. These results would imply that the *N*-terminal cyclised peptide is equally stable to high temperatures as the uncyclised peptide, **Staple A**.

In conclusion, the CD temperature ramp experiments of **Staples A**, **B** and **M** implied that these stapled peptides were highly stable up to 80 $^{\circ}$C, with no apparent denaturation upon cooling. The overall conformations of the less helical peptides, **Staples B** and **M**, were less affected by temperature than **Staple A**, which unfolded to a greater extent upon heating. Of particular interest during these experiments was the implication that for this short eleven-residue sequence, *i*, *i+*4 stapled peptides can have varying proportions of α-helical and 3^{10}-helical character depending on staple position and solution temperature, allowing for mixed helix/coil intermediates. Overall, these experiments were further evidence that the all-hydrocarbon stapling technique is a robust method for creating thermally stable helical peptides, which can exhibit extremely ordered and highly stable secondary structures in solution.

3.4 – Summary of stapled peptide synthesis

In total, the **Wild type** peptide, eight stapled analogues and two extended peptides were synthesised based on the primary sequence of α-9 of E2-25K. Despite the initial difficulties in synthesising the primary sequence, optimisation of the coupling methodology for these peptides allowed for expedient synthesis of all target peptides. The only exceptions to this rule were **Staple F** and **Staple H** in which the S_5 residue was directly attached to the resin. Unfortunately, these peptides were not amenable to SPPS, with an investigation into the literature only showing a single example of α-methyl, α-octynyl residues residing at the *C*-termini, which would suggest a low probability of success in synthesising these systems.[203] Circular dichroism analysis of the initial seven stapled peptide sequences showed a range of helicities from 16 – 91% depending on staple position, stereochemistry and length. Due to the surprisingly high helicity of **Staple A**, it was chosen as the model sequence on which to make various analogues to investigate various aspects of the Ubb+1 binding site. **Staple I** was successfully synthesised in which the primary sequence of **Staple A** was isomerised whilst maintaining the staple position. This peptide could potentially offer insight into the tolerance of the α-9 sequence to substitution which may be necessary in subsequent optimisation of peptide antagonists of the PPI of interest. In particular, this sequence would establish whether key interactions could be maintained despite changing charged residues such as Glu to polar uncharged moieties such as Thr. As the chosen sequence has a net -2 charge, this may be problematic for creating a compound which is cell penetrant as a majority of cell penetrating peptides have an overall net positive charge.[156]

Additionally, an extended series of peptides was synthesised in which the *N*-terminal glutamic acid was modified with selected aryl amines which had been prioritised by using *in silico* modelling. These peptides could potentially accomplish two things: increase binding with Ubb+1 or reverse selectivity from Ubb+1 to Ub depending on whether the conformation of Ubb+1 is analogous to that of the X-ray crystal structure or that of the NMR solution structure. This is due to the flexibility and unstructured nature of the nineteen amino acid tail of Ubb+1, which can potentially shift the key binding residue Leu^8 targeted in this work, depending on environment.

Finally, NMR analysis of **Staples A**, **G** and **I** was carried out to support the circular dichroism data. In general, the synthesised peptides appeared to adopt levels of helical structure in solution which corresponded well with the helicity determined by circular dichroism. Having stated this, NMR data suggests that these structures can vary between α-helical and 3^{10}-helical characteristics in solution. Temperature ramping experiments using circular dichroism also confirmed that peptides **Staples A**, **B** and **M** are stable in solution up to 80 $^{\circ}$C, with little variation in overall peptide conformation.

In conclusion, this initial palette of peptides was designed to cover a broad variety of molecular space around the parent sequence of E2-25K to increase the probability of identifying a potent inhibitor of the PPI with Ubb+1. The potential for finding an active compound is increased by the range of helicities present and the variations in staple position along the surface of Ubb+1.

3.5 - Biological investigation and development of a structure activity relationship

As outlined in Section 1, the ubiquitin proteasome system is hypothesised as being inhibited by the incorporation of mutant ubiquitin (Ubb+1) into toxic Ubb+1 capped polyubiquitin chains (Section 1.1.2). This inhibition is believed to be mediated by the action of the ubiquitin conjugating enzyme E2-25K, which enables the formation of unanchored polyubiquitin chains. Despite the raft of literature implicating Ubb+1 mediated proteasomal malfunction in Alzheimer's disease, little is known about the precise mechanism and rate by which this inhibition takes place. This research programme aimed to investigate whether blocking the incorporation of Ubb+1 into polyubiquitin chains could provide a novel disease modifying approach to Alzheimer's by preventing proteasomal inhibition.

As discussed previously (Section 2), an initial palette of tool peptides were designed around the α-9 sequence of E2-25K due to their potential to gain both target affinity and selectivity for Ubb+1. Through utilising the peptide stapling technique, eight stapled peptide analogues of the E2-25K α-9 sequence were successfully synthesised along with the unstapled **Wild type** control peptide (Table 24).

Table 24 – Initial screen of peptides to be tested in polyubiquitination assay

Peptide	Staple	Sequence	% Helicity	Charge
Wild type	-	Ac-V-E-T-A-T-E-L-L-S-N-NH$_2$	16	-2
Staple A	i, i+4	Ac-V-E-T-**S$_5$**-T-E-L-**S$_5$**-L-S-N-NH$_2$	91	-2
Staple B	i, i+4	Ac-V-E-T-A-**S$_5$**-E-L-L-**S$_5$**-S-N-NH$_2$	41	-2
Staple C	i, i+4	Ac-V-E-**S$_5$**-A-T-E-**S$_5$**-L-L-S-N-NH$_2$	42	-2
Staple D *trans*	i, i+7	Ac-**R$_8$**-E-T-A-T-E-L-**S$_5$**-L-S-N-NH$_2$	80	-2
Staple E	i, i+4	Ac-V-E-T-**R$_5$**-T-E-L-**R$_5$**-L-S-N-NH$_2$	16	-2
Staple G	i, i+4	Ac-**S$_5$**-E-T-A-**S$_5$**-E-L-L-L-S-N-NH$_2$	42	-2
Staple I	i, i+4	Ac-L-T-E-**S$_5$**-N-T-L-**S$_5$**-S-V-E-NH$_2$	24	-2
Staple M	i, i+4	Ac-V-**E***-T-**S$_5$**-T-E-L-**S$_5$**-L-S-N-NH$_2$	39	-1

A staple scanning technique, in which staples are installed at varying points in the peptide sequence with differing length and stereochemistry, was used in conjunction with isomeric and cyclised analogues of **Staple A** to create the intial test series. This was thought to increase the probability of finding peptides capable of binding with Ubb+1 through maintaining the key residues in combination with optimal helical conformation. It would be interesting to note any difference in activity between **Staple A** and its analogues: **Staple E** with inversion of staple stereochemistry and decreased helicity, **Staple I** with the mixed sequence to test the importance of key binding residues, and lastly **Staple M** with the pyroglutamate cyclisation and a decrease in net charge. The extended peptides **Staples J** and **K** were not evaluated in the biological assay at this point but were tested in a subsequent round of screening (*vide infra*).

3.5.1 – E2-25K mediated unanochored polyubiquitin chain formation

Polyubiquitination assays were chosen to determine the effectiveness of the test peptides (Table 24) in blocking the formation of Ubb+1 capped polyubiquitin chains. During typical E2-25K mediated polyubiquitination, it is understood that monoUb or PolyUb is conjugated on to Cys^{92} of the E2-domain of E2-25K *via* a standard E1-activation pathway (Fig. 53).
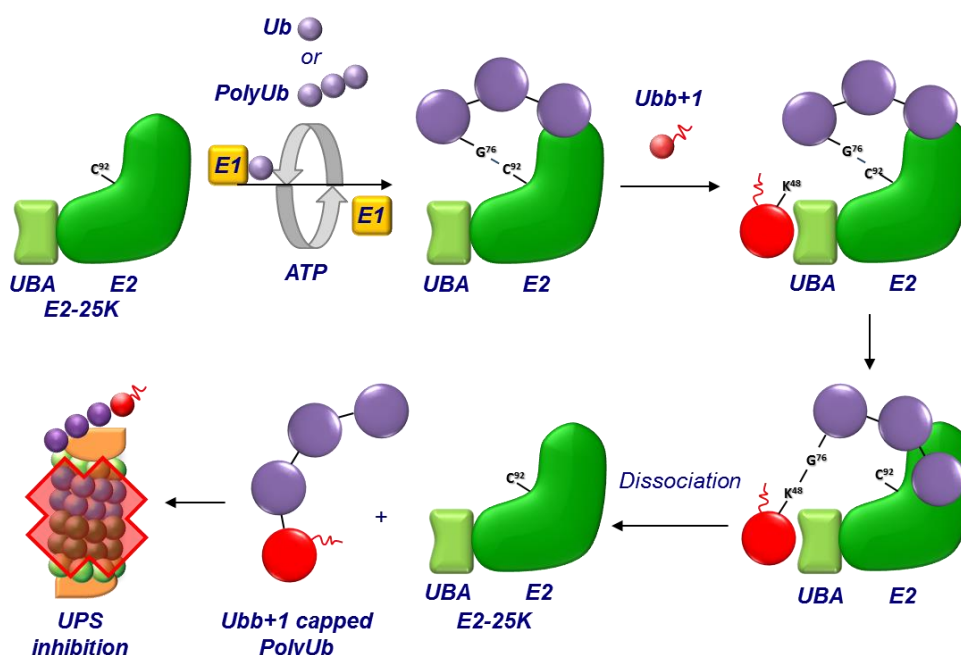
Figure 53 – Proposed mechanism of Ubb+1 capped PolyUb formation

At this point in the process, it is hypothesised that the UBA domain of E2-25K acts as a directing group, binding Ub or Ubb+1 to bring them into proximity with the conjugated ubiquitin. Once bound, an isopeptide bond is formed between Lys^{48} of Ubb+1 with the C–terminal Gly^{76} of the growing PolyUb chain. The Ubb+1 capped unanchored polyubiquitin chain will then dissociate from E2-25K. As these chains are resistant to de-ubiquitinating enzymes, as discussed in Section 1.1.2, they can accumulate in affected cells to potentially toxic levels. It is the longer Ubb+1 capped $PolyUb_n$ chains (where n ≥ 2) which are considered to inhibit the 26S proteasome through blocking the proteasome entrance, disrupting this vital regulatory system.[42]

In principle, the addition of the stapled peptide mimics of E2-25K could decrease, or even stop Ubb+1 incorporation into polyubiquitin chains (Fig. 54). The proposed mechanism of action would be through preventing Ubb+1 association with the UBA domain of E2-25K by selectively blocking the PPI binding site. This could potentially allow regular polyubiquitin processes to be carried out, forming typical PolyUb chains which can be processed by DUBs, whilst halting toxic Ubb+1 capped PolyUb formation.
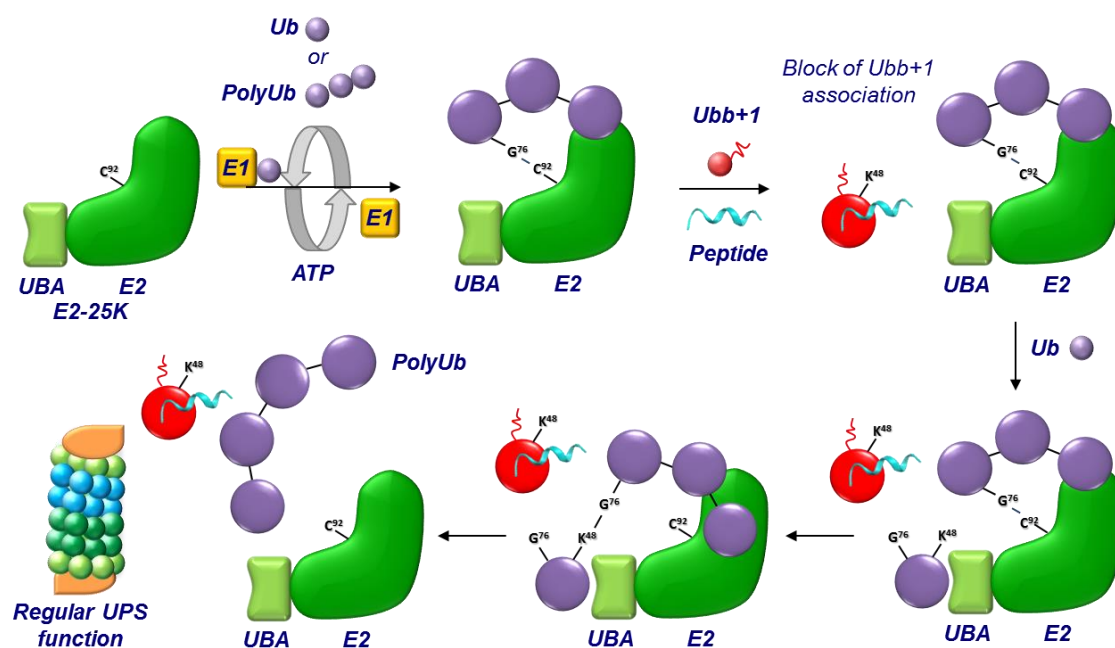
Figure 54 – Proposed mechanism of action of stapled peptides

It was reasoned that the outcome of these asays would be two-fold: determining which peptides are capable of inhibiting Ubb+1 capped PolyUb formation; and, could regular PolyUb chain synthesis carry on as normal, implying any active compounds were selective for Ubb+1 over Ub. If any active compounds were identified, they could be used to develop effective tool compounds to elucidate the wider role Ubb+1 plays in the inhibition of the UPS and, in particular, its relation to Alzheimer's disease.

3.5.2 – Polyubiquitination assays

The first polyubiquitin assays were run *via* a collaboration with the Layfield group at the University of Nottingham,[216] and were composed of Ubb+1 (2 µM), Ub (2 µM), E1 (0.1 µM), E2-25K (1 µM) and the test peptides (30 µM). The reactions were incubated for 4 hours at 37 °C then split into equal aliquots and run on a SDS-PAGE gradient gel to separate the varying lengths of PolyUb chains. One set of samples was probed *versus* anti-ubiquitin and the other *versus* anti-Ubb+1 (Fig. 55). This would allow for a direct comparison of regular PolyUb chain content against Ubb+1 capped PolyUb chains in the reaction. From this initial data, neither the **Wild type**, or any of the eight stapled peptides appeared to have any effect on regular E2-25K mediated polyubiquitination (Fig. 55, A).
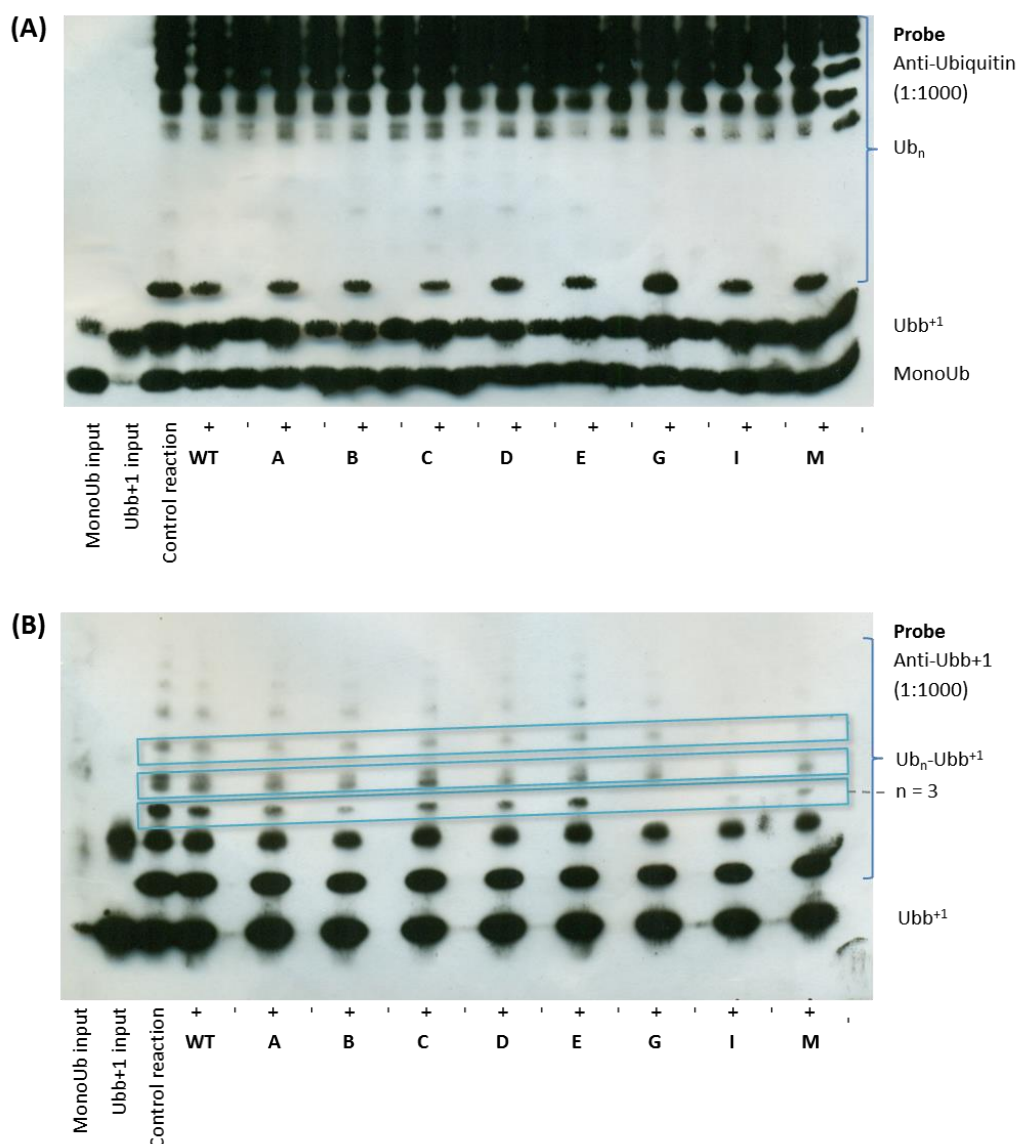
Figure 55 – Four hour polyubiquitination assay of the initial peptide set

A) – Ubiquitin antibody stained results from the polyubiquitination assay. B) – Ubb+1 antibody stained results from the polyubiquitination assay. The higher MW of the PolyUb chain, the higher up the gel plate the spot will run.

There appeared to be little variation between the control reaction lane and the test peptides, which implied that the peptides were not binding to wild type Ubiquitin. The second gel (Fig. 55, B) was more interesting as it showed the extent of Ubb+1 capped polyubiquitin chains. It was very pleasing to observe that some of the test peptides appeared to have an effect on Ubb+1 containing PolyUb chain formation. The most prominent results appeared to be for PolyUb chains with three Ub moieties capped by Ubb+1, as shown by the lowest boxed region (Fig. 55, B). Both **Staples G** and **I** appeared to completely inhibit PolyUb chains of this length, whilst **Staples B** and **M** appeared to have an effect to a lesser extent. **Staple I** appeared to have the most significant effect action as there was little evidence of any longer

Ub$_n$-Ubb+1 chains than n = 2. Despite no quantitative data being available for this assay at present, these functional results were very exciting as it represents the first evidence that stapled peptides were capable of inhibiting the formation of longer Ubb+1 capped PolyUb chains. A qualitative analysis of the lanes implied that the order of the tested peptides, from most effective in binding with Ubb+1 to least was: **I** > **G** > **B**, **M** > **D**, **A**, **C** > **E**, **WT** (Table 25).

Table 25 – Active peptides from the polyubiquitination assay

	Peptide	Staple	Sequence	% Helicity	Charge
Active	Staple I	i, i+4	Ac-L-T-E-**S$_5$**-N-T-L-**S$_5$**-S-V-E-NH$_2$	24	-2
	Staple G	i, i+4	Ac-**S$_5$**-E-T-A-**S$_5$**-E-L-L-L-S-N-NH$_2$	42	-2
	Staple B	i, i+4	Ac-V-E-T-A-**S$_5$**-E-L-L-**S$_5$**-S-N-NH$_2$	41	-2
	Staple M	i, i+4	Ac-V-**E***-T-**S$_5$**-T-E-L-**S$_5$**-L-S-N-NH$_2$	39	-1
Inactive	Staple D *trans*	i, i+7	Ac-**R$_8$**-E-T-A-T-E-L-**S$_5$**-L-S-N-NH$_2$	80	-2
	Staple A	i, i+4	Ac-V-E-T-**S$_5$**-T-E-L-**S$_5$**-L-S-N-NH$_2$	91	-2
	Staple C	i, i+4	Ac-V-E-**S$_5$**-A-T-E-**S$_5$**-L-L-S-N-NH$_2$	42	-2
	Staple E	i, i+4	Ac-V-E-T-**R$_5$**-T-E-L-**R$_5$**-L-S-N-NH$_2$	16	-2
	Wild type	-	Ac-V-E-T-A-T-E-L-L-L-S-N-NH$_2$	16	-2

As the wild type peptide appeared to have little activity in comparison with the stapled analogues, it can be assumed that any activity exhibited by the rest of the series is enhanced by the level of helical structure observed in solution. However, it was noteworthy that the most active peptides (Table 25) only had moderate helicity values, ranging from 24 to 42%. When considering the reported data on helical peptide antagonists of PPIs, this was not surprising as there is no direct correlation between helicity and target affinity. Stapled helical peptides can range from 20% to 100% helicity and remain active against a specified target, with the driving force for affinity being site-specific interactions over extent of secondary structure.[205]

These preliminary results suggested that any activity against Ubb+1 was not directly proportional to peptide helicity, as the stapled peptides with the most rigid secondary structure (**Staples A** and **D**) were inactive in the assay (Fig. 55). This range of results was interesting when considered with the anti-ubiquitin blot as it would appear that the active stapled peptides, in particular **Staples I**, **G**, **B** and **M**, were preferentially binding with Ubb+1 over ubiquitin. This would suggest that some degree of selectivity for Ubb+1 was gained together with target affinity.

3.5.3 – Comparison of polyubiquitination assay results to reported literature

Of particular interest were the parallels between these assay results and that of Ko *et al*, where polyubiquitin assays were used to investigate the role of the UBA binding domain of E2-25K.[59] When the full UBA domain was deleted from E2-25K, there was almost no Ubb+1 capped PolyUb chains synthesised, with only a small amount of Ub_1-Ubb+1 present (Fig. 56).
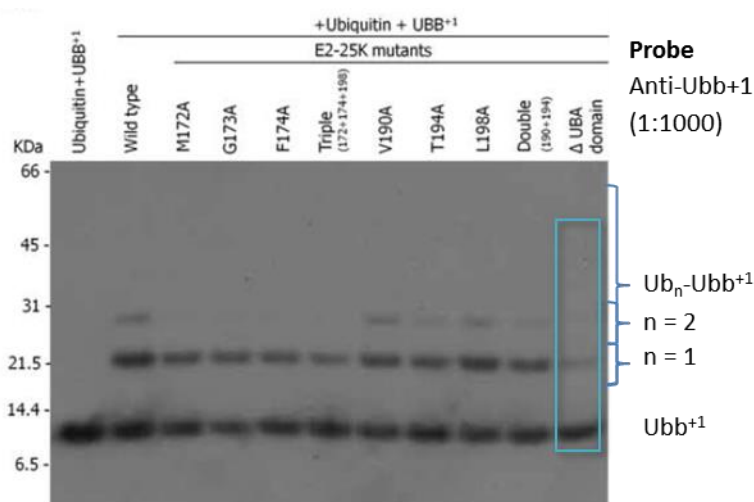
Figure 56 – E2-25K deletions and their effect on polyubiquitination[59]

UBB+1 (50 μM), Ub (50 μM), E1 (0.1 μM), E2-25K and E2-25K mutants (1 μM) incubated for 4 hours at 37 °C

Single residue deletions in the UBA domain had varying effects on levels of Ubb+1 capped polyUb chains compared to the wild type E2-25K. Single point mutations of the key hydrophobic residues of α-9 of E2-25K (Val^{190}, Thr^{194} and Leu^{198}) still resulted in the synthesis of Ub_n-Ubb+1 chains where n = 1 and 2, with the double mutant (Val^{190} and Thr^{194}) only having a small amount of the longer Ub_2-Ubb+1 chains (Fig. 56).

These results were very interesting in relation to this work, as short Ubb+1 capped PolyUb chains were present in the E2-25K mutant assays when key binding residues of the UBA domain had been altered. These short Ub_1-Ubb+1 chains were also still observed to a certain extent when the whole UBA domain was deleted. Therefore, the presence of Ub_n-Ubb+1 chains where n = 1 and 2 against the active peptides in the assay (Fig. 55) is not completely unexpected, as E2-25K can still catalyse the formation of shorter PolyUb chains without the UBA directing domain.

From consideration of the most active peptide **Staple I**, this initial data appears to achieve a similar action to UBA deficient E2-25K by preventing the formation of long chain Ubb+1 capped polyUb chains. These results provide further evidence that the

UBA domain of E2-25K is a directing motif to bring Ub or Ubb+1 into proximity with growing PolyUb chains, but is not essential for the enzyme, as short PolyUb chains can still be formed in the absence of this domain. In respect to the development of inhibitors of the E2-25K/Ubb+1 PPI, this initial evidence that stapled peptides are capable of inhibiting the formation of longer Ubb+1 capped PolyUb chains to varying effect was encouraging, as it is these longer chains which are believed to be the most toxic to the proteasome.[42]

3.5.4 – Investigation into stapled peptide structure activity relationship

With the polyubiquitination results in hand, attention was then turned to the potential relationship between the most active stapled peptides and their structure. As no further information regarding the binding mode and affinity of the peptides could be obtained at this point *via* biological analysis, a simple computational model analogous to that discussed in Section 3.2.8 was designed by the author using MOE software in order to create a putative structure activity relationship (SAR).[206] As before, the X-ray crystal structure of the E2-25K/Ubb+1 PPI was modified to create models of the stapled peptides from the first assay run (Table 25). These structures were energy minimised so that the overall conformation would be more like the peptide in solution (Fig. 41), then minimised against Ubb+1 in order to gain an understanding of how the peptide may bind to Ubb+1. These models were then analysed to find any potential links between the conformation of the peptides against the Ubb+1 binding site and their activity in polyubiquitination assays.

The models created from the most active peptides from the polyubiquitination assays, **Staples I**, **G**, **B** and **M**, provided valuable insight into a potential relationship between these peptides and their activity with Ubb+1. The most active peptide from the polyubiquitination assays, isomeric **Staple I,** appeared to form the key hydrogen bond with Arg[42] of Ubb+1 despite the change from a Glu to Thr residue (Fig. 57). One of the most interesting aspects of the **Staple I** model was an apparent novel hydrogen bond with the surface of Ubb+1 in comparison with **Staples B**, **G** and **M**. The *C*-terminal glutamic acid appeared to form this bond with the backbone carbonyl of Lys[48]. When compared to the model of analogous **Staple A** (not shown) the occurrence of this novel interaction may be due to the absence of hydrophobic interactions with the main PPI binding surface of Ubb+1, allowing for **Staple I** to shift towards the basic lysine residue.

Peptide	Staple	Sequence	% Helicity
Staple I	i, i+4	Ac-L-T-E-S_5-N-T-L-S_5-S-V-E-NH$_2$	24

Peptide	Staple	Sequence	% Helicity
Staple G	i, i+4	Ac-S_5-E-T-A-S_5-E-L-L-L-S-N-NH$_2$	42
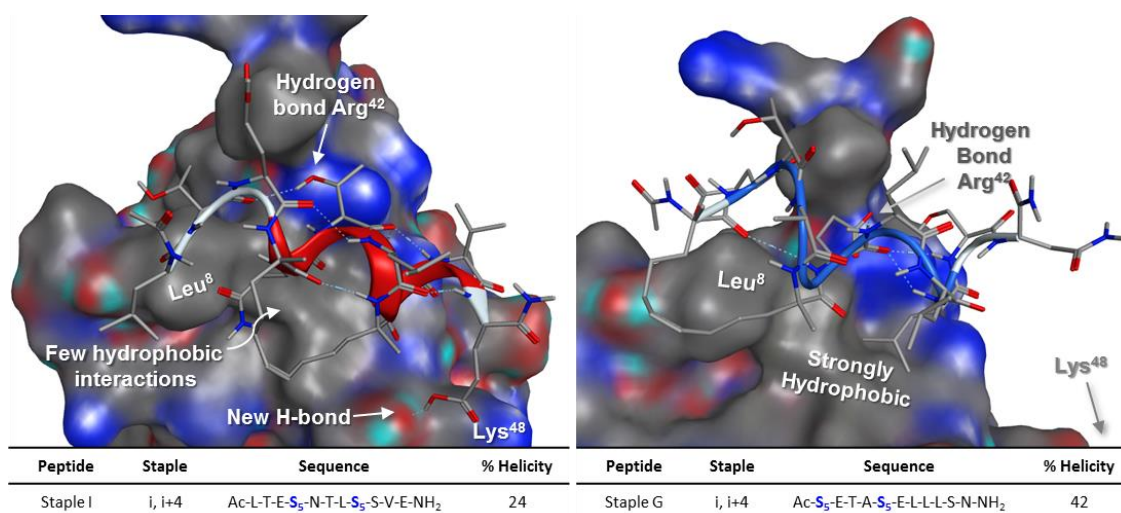
Figure 57 – Models of Staples I and G bound with Ubb+1

At this point it was postulated that this potential H-bond may be key to the apparent activity of **Staple I**. As Lys[48] forms the key isopeptide link with a subsequent ubiquitin moiety during polyubiquitination (Fig. 53), blocking of this residue would in principle decrease the probability of this key bond forming.

The model created for **Staple G** was comparatively different from that of **Staple I** (Fig. 57), with the all-hydrocarbon linker of **Staple G** appearing to lie closely against the hydrophobic surface of Leu[8] of Ubb+1. This potential binding mode was interesting as it would suggest the staple affords novel hydrophobic interactions with the target Ubb+1, as well as providing a helical constraint. The key hydrogen bond with Arg[42] of Ubb+1 also appeared to be formed, despite the peptide having a less helical structure than α-9 of E2-25K.

As with **Staple G**, the all-hydrocarbon link of **Staple B** seemed to lie closely against the surface of Ubb+1 (Fig. 58). However, instead of positioning against Leu[8], the cross-link of **Staple B** appeared to lie towards the main hydrophobic site containing Ile[44] and Val[70] of Ubb+1. As expected, this peptide also made the key hydrogen bond with Arg[42], with the *N*-terminal Val shifting towards Leu[8] of Ubb+1. This was very interesting because **Staples G** and **B** were the only active *i*, *i*+4 peptides in which the linker was proposed to lie against the target protein.

Peptide	Staple	Sequence	% Helicity	Peptide	Staple	Sequence	% Helicity
Staple B	i, i+4	Ac-V-E-T-A-S_5-E-L-L-S_5-S-N-NH$_2$	41	Staple M	i, i+4	Ac-V-E*-T-S_5-T-E-L-S_5-L-S-N-NH$_2$	39
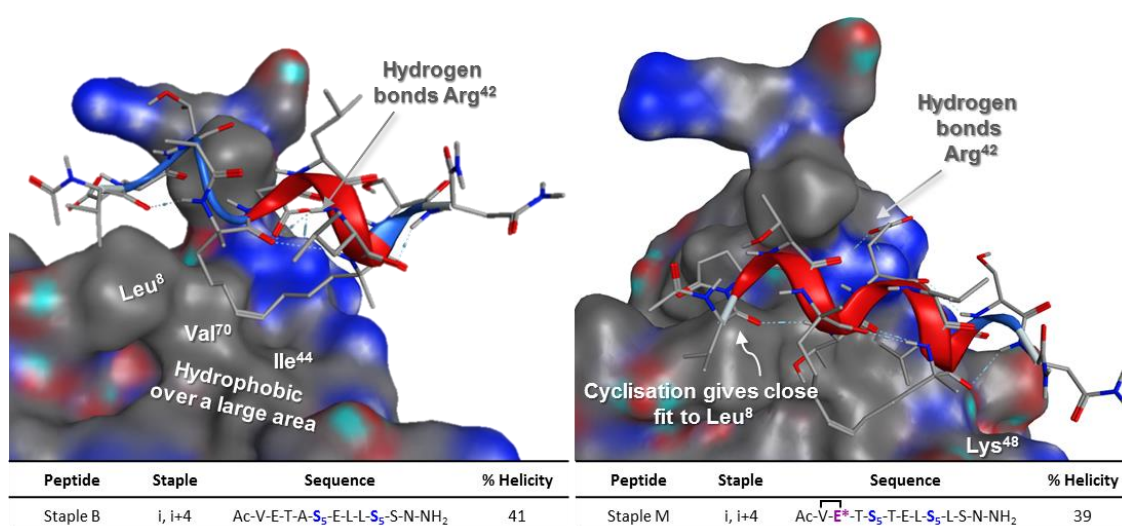
Figure 58 – Models of Staples B and M bound with Ubb+1

Finally, the model of **Staple M** was interesting as unlike **Staples G** and **B**, the all-hydrocarbon linker was proposed to project into the solvent, gaining no extra interactions with the surface of Ubb+1 (Fig. 58). Alternatively, when compared to **Staple A** (not shown) which has an identical primary sequence, the *N*-terminal pyroglutamate moiety would appear to twist **Staple M** closer to Leu[8]. This extra hydrophobic contact in conjunction with the key interactions demonstrated with α-9 of E2-25K would imply that the increased activity of **Staple M** (compared to **Staple A**) is due to the change in conformation induced by the pyroglutamic acid residue.

Overall, the results of these preliminary models would suggest that the activity of **Staple I** is potentially driven by the blocking of Lys[48] of Ubb+1. When Ubb+1 is bound to E2-25K, Lys[48] is unhindered from consideration of the X-ray data and projects into the solvent to allow for PolyUb chain formation (Fig. 5). Therefore, blocking this key site would allow for effective inhibition of Ubb+1 capped PolyUb chain formation. Alternatively, the interactions between **Staples B**, **G** and **M** and Ubb+1 are potentially dominated by putative hydrophobic interactions outwith those made by E2-25K. Of particular interest are the prospective interactions between the all-hydrocarbon staple and the hydrophobic surface of Ubb+1, as suggested by the models of **Staples G** and **B**. Due to their preliminary effect against Ubb+1, **Staples I** and **G**, and to a lesser extent **B** and **M**, were believed to be candidates for further optimisation. Therefore, with the *in silico* modelling in hand, a new generation of stapled peptides could be designed around these favourable sequences in order to potentially gain activity against Ubb+1.

3.6 – Design and synthesis of the hybrid series

Examination of the four most active peptides from the polyubiquitination experiment (Fig. 55) by using a simple *in silico* model revealed three parameters which may have facilitated effective binding with Ubb+1. A hydrogen bond donor at the *C*-terminus could potentially block Lys[48] when in an optimal position, implied by the modelling of **Staple I**. Staple position could also have a profound effect, with linkers potentially lying closely against the hydrophobic surface appearing to be beneficial, such as those utilised in **Staples B** and **G**. Finally, an *N*-terminal pyroglutamate cyclisation could potentially give a favourable change in conformation of the peptide structure which brings the hydrophobic termini towards Leu[8]. With this in mind, six new hybrid stapled peptides were designed to incorporate the most favourable aspects of the active peptides **Staples B**, **G**, **I** and **M** previously identified (Table 26).

Table 26 – Hybrid peptides designed from the 4 most active stapled peptides

Peptide	Staple	Sequence	% Helicity	Hybrid
Staple B	i, i+4	Ac-V-E-T-A-S_5-E-L-L-S_5-S-N-NH$_2$	41	-
Staple G	i, i+4	Ac-S_5-E-T-A-S_5-E-L-L-L-S-N-NH$_2$	42	-
Staple I	i, i+4	Ac-L-T-E-S_5-N-T-L-S_5-S-V-E-NH$_2$	24	-
Staple M	i, i+4	Ac-V-E*-T-S_5-T-E-L-S_5-L-S-N-NH$_2$	39	-
Staple N	i, i+4 stitch	Ac-S_5-E-T-A-B_5-E-L-L-R_5-S-N-NH$_2$	-	Staples B & G
Staple O	i, i+4 stitch	Ac-R_5-E-T-A-B_5-E-L-L-S_5-S-N-NH$_2$	-	Staples B & G
Staple P	i, i+4	Ac-V-E*-T-A-S_5-E-L-L-S_5-S-N-NH$_2$	-	Staples B & M
Staple Q	i, i+4	Ac-V-E-T-A-S_5-E-L-L-S_5-S-N-N-NH$_2$	-	Staples B & I
Staple R	i, i+4	Ac-S_5-E*-T-A-S_5-E-L-L-L-S-N-NH$_2$	-	Staples G & M
Staple S	i, i+4	Ac-S_5-T-E-L-S_5-T-L-N-S-V-E-NH$_2$	-	Staples G & I

The first two hybrid peptides were derived from **Staples B** and **G**, in which the all-hydrocarbon linker lies closely against the hydrophobic surface of Ubb+1. Through use of the emerging technique of peptide stitching,[203] discussed in greater detail in Section 3.6.1, the short 11-mer sequence derived from α-9 of E2-25K could be contiguously stapled.[203] This would enable the synthesis of peptides with staples at the *i*, *i*+4 position from **Staple G** and *i*+4, *i*+8 position from **Staple B**. The *i*+4 residue, B_5 (**164**), is comprised of a bis-pentenyl moiety which has been proven to form two distinct staples with neighbouring *i* and *i*+8 alkenes. Two isomeric peptides, **Staples N** and **O**, were designed in this way, with identical primary sequence aside from the *i*, *i*+8 residues which were opposite diastereomers. When

these sequences were modelled in an analogous fashion to previous peptides (Section 3.5.4), **Staples N** and **O** appeared to bind to Ubb+1 in slightly different conformations (Fig. 59).

Peptide	Staple	Sequence	Hybrid
Staple N	i, i+4 stitch	Ac-**S₅**-E-T-A-**B₅**-E-L-L-**R₅**-S-N-NH₂	Staples B & G

Peptide	Staple	Sequence	Hybrid
Staple O	i, i+4 stitch	Ac-**R₅**-E-T-A-**B₅**-E-L-L-**S₅**-S-N-NH₂	Staples B & G
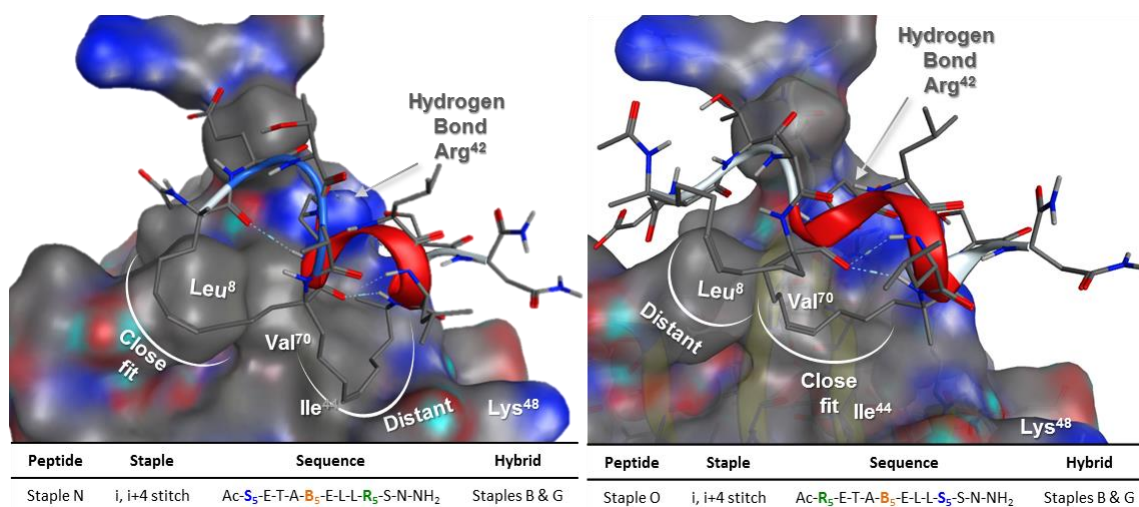
Figure 59 – Models of stitched peptides Staples N and O

In silico modelling of these two stitched sequences suggested that stitch stereochemistry may have an effect on binding conformation. **Staple N**, with the S_5, B_5, R_5 sequence, appeared to have a close fit with Leu[8] towards the *N*-terminal region. This was potentially due to the *N*-terminal staple containing the favourable S_i, S_{i+4} stereochemistry, bringing the hydrocarbon link towards the Ubb+1 surface. By contrast, the central R_{i+4}, R_{i+8} staple appeared to be more distant from the target surface due to the less-favourable stereochemistry. **Staple O** appeared to have the opposite conformation due to the R_5, B_5, S_5 sequence. In particular the *N*-terminal R_i, R_{i+4} staple appeared to be more distant from Leu[8], whilst the S_{i+4}, S_{i+8} linker seeming to lie more closely to the important Val[70] / Ile[44] hydrophobic site.

The next set of hybrid peptides were designed around the sequence of **Staple B**, with a single S_i, S_{i+4} linker. **Staple P** was intended to combine the apparent favourable staple position of **Staple B** with the *N*-terminal pyroglutamate cyclisation of **Staple M** (Table 26). The *in silico* model of **Staple P** against Ubb+1 implied that a similar *N*-terminal twist to that of **Staple M** could occur, bringing the peptide closer to Leu[8] (Fig. 60). The all-hydrocarbon linker of **Staple P** would also appear lie favourably against the Val[70] / Ile[44] hydrophobic surface of Ubb+1 in a similar fashion to the model of **Staple B**. It was also noteworthy that the model suggested that both

of the designed interactions were taking place whilst maintaining the key hydrogen bond with Arg[42] (Fig. 60).

Peptide	Staple	Sequence	Hybrid
Staple P	i, i+4	Ac-V-E*-T-A-S_5-E-L-L-S_5-S-N-NH$_2$	Staples B & M

Peptide	Staple	Sequence	Hybrid
Staple Q	i, i+4	Ac-V-E-T-A-S_5-E-L-L-S_5-S-N-N-NH$_2$	Staples B & I
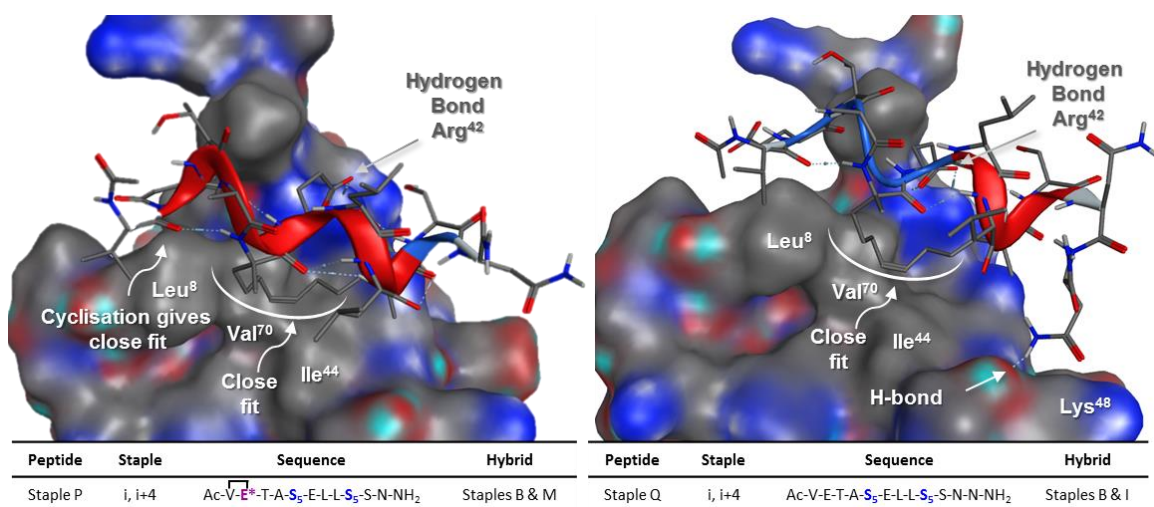
Figure 60 – Models of Staple B sequence hybrids

Despite the fact that these *in silico* models may not necessarily represent an accurate binding mode of the stapled peptides with Ubb+1, it was of interest to determine whether peptides designed soley from these models would prove to be active in the polyubiquitination assay. With this in mind, *in silico* screening of **Staple B** was carried out in order to see if any alterations or extensions in residues at the *C*-terminus of the peptide could be made in order to gain the same hydrogen bond seen in the model of **Staple I** (Fig. 59).

Through extension of the *C*-terminus of **Staple B** with an additional Asn residue, it was proposed that a similar hydrogen bond could be obtained with the backbone carbonyl of Lys[48] as proposed with **Staple I** (Fig. 60). This interaction could only be accomplished through additional residues, creating a twelve-residue peptide compared to **Staple I**. Modelling results suggested that this was due to the close hydrophobic interactions between the staple and the Ubb+1 surface constraining the *C*-terminus away from Lys[48], with this effect only being overcome by the addition of a subsequent residue. The results of **Staple Q** in polyubiquitination assays would be interesting, depending on whether it maintains similar activity to **Staple I**. If this is the case, then it would imply that the encouraging activity of **Staple I** is due to the hydrogen bond demonstrated in these model systems (Fig. 60). Alternatively, if **Staple Q** shows analogous or decreased activity to **Staple B**, then it can be

assumed that the *in silico* models are not an accurate representation of every peptides binding mode with Ubb+1.

The final two hybrid peptides designed were based on the *N*-terminal staple position analogous to that of **Staple G**. It was hypothesised that combining the primary sequence of **Staple G** with the *N*-terminal cyclisation of **Staple M** may give a more favourable fit with the surface of Ubb+1. **Staple R** has the potential to gain strong hydrophobic interactions between the *N*-terminal of the peptide and Leu[8] of Ubb+1 (Fig. 61). The activity of **Staple R** in polyubiquitnation assays would be interesting in relation to the activity of **Staple G**, as this could clarify whether this twist in conformation is favourable in relation to proximity with Leu[8].

Peptide	Staple	Sequence	Hybrid
Staple R	i, i+4	Ac-**S$_5$**-E*-T-A-**S$_5$**-E-L-L-L-S-N-NH$_2$	Staples G & M
Staple S	i, i+4	Ac-**S$_5$**-T-E-L-**S$_5$**-T-L-N-S-V-E-NH$_2$	Staples G & I
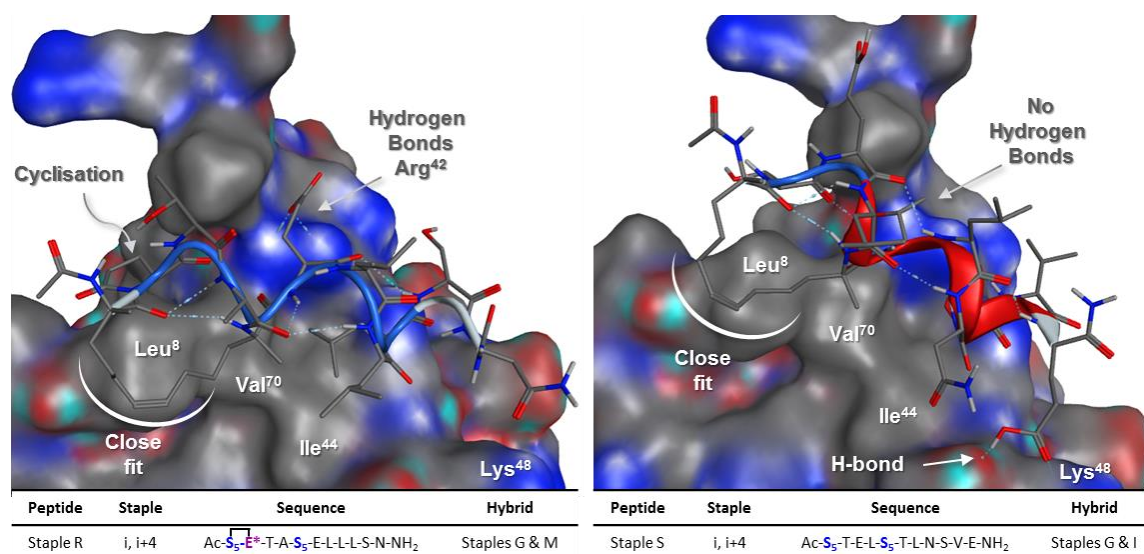
Figure 61 – Hybrid peptides with Staple G hydrocarbon linker position

Finally, the isomeric sequence of **Staple I** was combined with the staple position of **Staple G** to create **Staple S**. The *in silico* model of this analogous peptide to **Staple I** was interesting as it appeared to suggest that the *N*-terminal staple anchored the peptide against the hydrophobic surface of Leu[8] of Ubb+1 whilst the *C*-terminus maintained the putative hydrogen bond with the backbone carbonyl of Lys[48] (Fig. 61). However, it was noted that unlike the model of **Staple I**, **Staple S** appeared to not form the key hydrogen bond with Arg[42]. This is potentially due to **Staple S** adopting a different angle across the surface of Ubb+1, compared to other peptides, due to this anchored isomeric sequence. Therefore, the shorter Thr residue at the key position in the sequence is too distant from Arg[42] to form this key hydrogen bond. Again, the results of **Staple S** in polyubiquitination assays could provide

valuable insight into how accurate these *in silico* models are, and whether the putative hydrogen bond at Lys[48] is more important to Ubb+1 affinity than the native hydrogen bond to Arg[42].

3.6.1 – Stitched peptide synthesis

Stapled peptide stitching was reported by Verdine *et al* in 2014 as an extension of the previously established methodology.[203] These spirocyclic-like peptides were claimed to obtain enhanced structural rigidity compared to their single stapled counterparts, whilst maintaining thermal and proteolytic stability (Scheme 38, **166**). Incorporation of the bis-alkene amino acid B_5 (**164**) into a peptide chain containing two further α-methyl, α-alkenyl amino acids gives a peptide system in which multiple ring-closed products could be obtained (**165**). Comprehensive investigation into the ring-closing metathesis of stitched systems of various length and stereochemistry confirmed that contiguous staples could be obtained (**166**).[203]
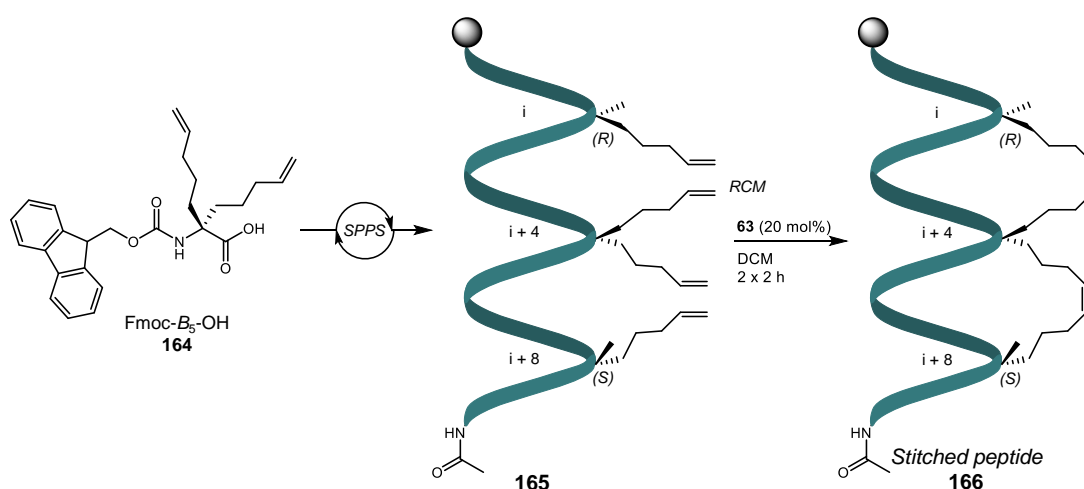
Scheme 38 - General stitched peptide synthesis

For this investigation, the most simple *i*, *i*+4, *i*+8 stitch system was used due to the short length of the α-9 sequence (eleven amino acids). This was hypothesised as obtaining a single product from the ring-closing step containing two *cis* alkene staples (Scheme 38).

The synthesis of the key building block Fmoc-B_5 (**164**) was reported as a significantly more simple process than the chiral α-methyl, α-alkenyl amino acids discussed previously (Section 3.1).[203] Starting from the benzophenone derived glycine ethyl ester Schiff base **167**, dialkylation with iodopentene (**110**) is accomplished using the strong base KHMDS (Scheme 39). Acid hydrolysis and

subsequent Fmoc protection furnish the doubly protected B_5 amino acid **170**. A final ester deprotection using a hard Lewis acid / soft nucleophillic approach gives the required building block **164** in an overall reported yield of 53%.
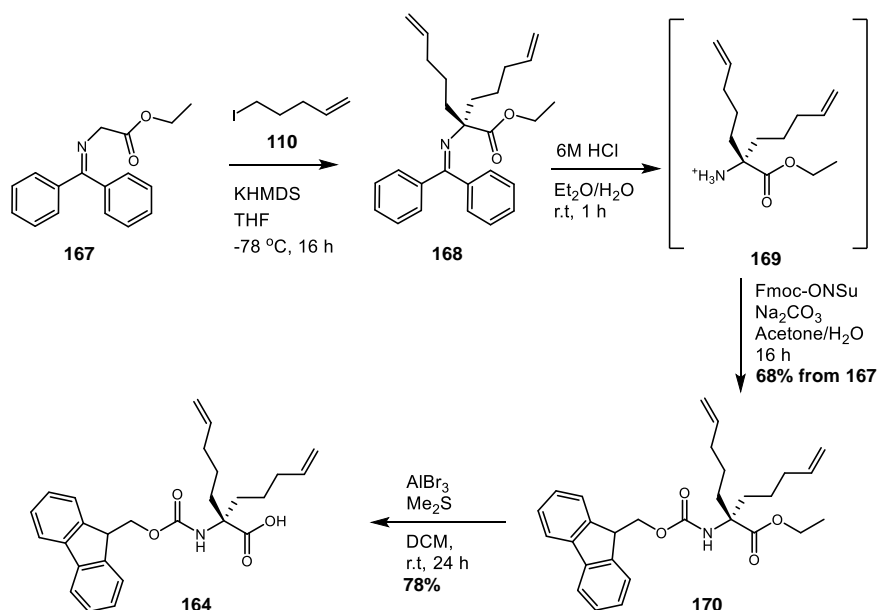
Scheme 39 – Published synthesis towards stitched peptide building block B_5

Initial attempts into synthesising the precursor imine **167** from benzophenone and glycine ethyl ester were low yielding due to the reversible nature of the reaction and the need for Dean-Stark conditions. Upon examination of the literature for alternative Schiff base systems, a 4-chlorobenzaldehyde (**171**) based precursor was chosen due to the more robust reaction conditions (Scheme 40).
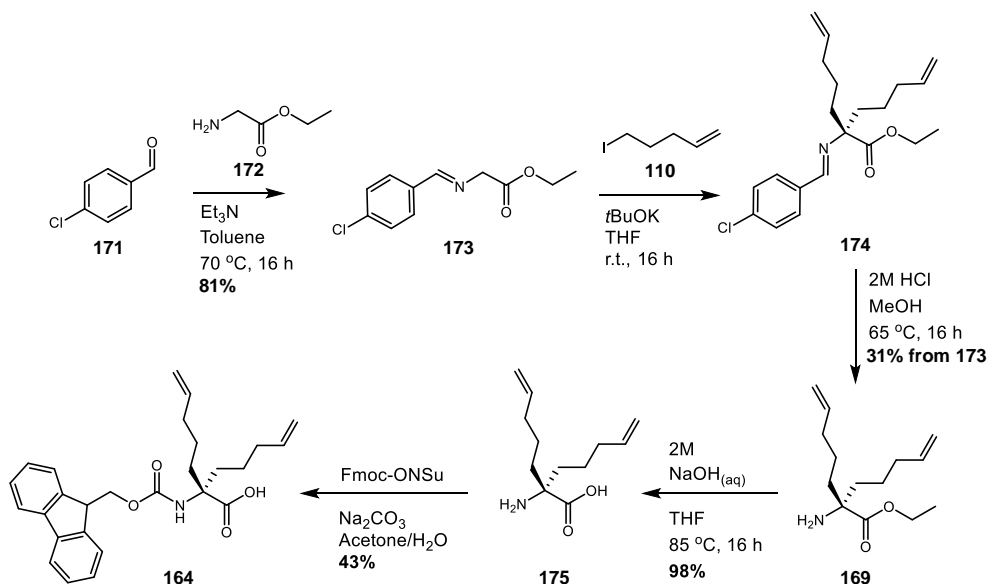
Scheme 40 – Alternative route towards Fmoc-B_5-OH

A simple overnight reaction between **171** and glycine ethyl ester (**172**) furnished the required imine **173** in toluene (Scheme 40). The di-alkylation reaction was carried out according to the procedure developed by the author for the BPB-Ni(II)-Ala complexes (Table 3) due to their relative simplicity in comparison to the literature route (Scheme 39). The intermediate **174** (Scheme 40) was then hydrolysed using 2M HCl to furnish the B_5-OEt protected product **169** which could be isolated cleanly after chromatographic purification. At this point in the synthesis, an attempt was made to follow the Verdine route to **164** (Scheme 39) through Fmoc protection and subsequent ester hydrolysis. However, despite the Fmoc protection step proceeding well, the unconventional ester deprotection conditions were not successful in producing the required product **164**. Therefore, a change in the order of synthesis was implemented (Scheme 40). Ester hydrolysis of **169** and DOWEX purification were effective in isolating the free B_5 amino acid **175**. Subsequent Fmoc protection finally provided the required Fmoc-B_5 **164** in a 43% yield (Scheme 40). Overall, the route towards **164** was found to be relatively inefficient, however without further optimisation, sufficient quantities of the target building block were obtained to support the synthesis of a stitched peptide sequence.

As the synthesis of the stitched peptide building B_5 (**164**) had proven to be low yielding in this instance, it was decided that only a single isomer of the stitched peptide sequence (Table 26) would be synthesised. Prioritisation between synthesis of **Staple N** or **Staple O** was accomplished through consideration of the earlier polyubiquitination assay results (Fig. 55) and *in silico* models (Fig. 59). Both peptides were designed to be hybrids of **Staples B** and **G**, however **Staple N** had a conformation similar to that of **Staple G,** whilst **Staple O** is more similar to **Staple B**. This is due to the positioning of the more favourable S_i, S_{i+4} staple in the stitched peptide sequence. It was hypothesised that **Staple N** (Fig. 59) will have a close fit with Leu[8] of Ubb+1 like that of **Staple G** (Fig. 57), whilst **Staple O** will lie closer to the Val[70]/Ile[44] hydrophobic surface of Ubb+1 like **Staple B** (Fig. 58). Therefore, as **Staple G** was more active on a qualitative basis than **Staple B** in polyubiquitination assays, the stitched peptide that was more analogous to **Staple G** would be expected to be more active against Ubb+1 in theory. Consequently, **Staple N** was deemed more favourable than **Staple O** and was chosen for subsequent synthesis.

SPPS of the primary sequence was accomplished (Table 27) with the coupling method details outlined previously (Table 10). Due to the amount of **164** synthesised

(Scheme 40) only 1.7 equivalents of amino acid were available for coupling with the resin, however a trial cleavage reaction after two hours demonstrated the reaction had gone to completion.

Table 27 – Coupling methodology towards stitched peptide

Peptide	Staple	*N*	Sequence										*C*
Staple N	i, i+4, i+8	Ac	S$_5$	E	T	A	B$_5$	E	L	L	R$_5$	S	N	NH$_2$

Method	Manual / Automated	Amino acid equiv.	Coupling Agent (Equiv.)	Base (Equiv.)	Coupling time
Viii)	Manual	1.7	HATU (1.7)	DIPEA (3.4)	2 h

☐ = Method (i) ☐ = Method (ii) ☐ = Method (iii) ☐ = Method (iv) ☐ = Method (v) ☐ = Method (vi)

Upon synthesis of the full sequence, a trial cleavage reaction demonstrated two main products: the required linear peptide and a by-product with a molecular weight of 811. The identity of this peptide could not be elucidated, however there was deemed to be a sufficient quantity of the target product present in the mixture to carry on to the ring-closing step.

Metathesis was carried out using less concentrated conditions to those used previously in this work (Scheme 34) in order to correspond with the peptide stitching literature (Scheme 41).[203] This was thought to improve the formation of the desired spirocyclic system and decrease other ring-closed by-products.
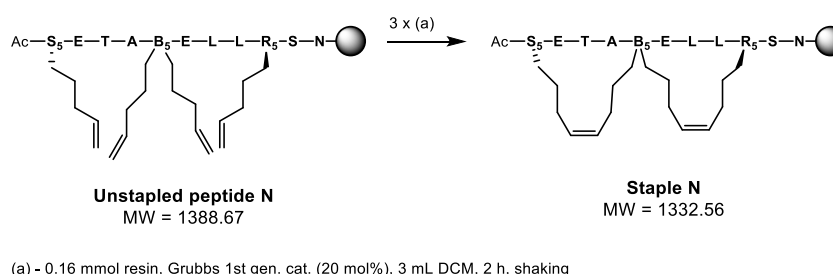
Scheme 41 – Metathesis of the stitched peptide Staple N

Upon three consecutive two hour treatments of Grubbs 1st generation catalyst, a trial cleave of **Staple N** was carried out to analyse the extent of ring-closed products formed. Only a single ring-closed product appeared to be formed (Fig. 62) which had the correct mass of the expected *i*, *i*+4, *i*+8 stitched system.

Satisfied that a single stitched product had been obtained, a full cleavage and purification was carried out to give the product **Staple N**. This peptide was assumed to be the *cis/cis* spirocyclic *i*, *i*+4, *i*+8 (Scheme 41) due to the clean metathesis

reaction and reported precedent.[203] Despite the earlier difficulties in synthesising the Fmoc B_5 building block **164**, the stitched peptide **Staple N** was successfully synthesised to create the doubly stapled hybrid of **Staples B** and **G**.
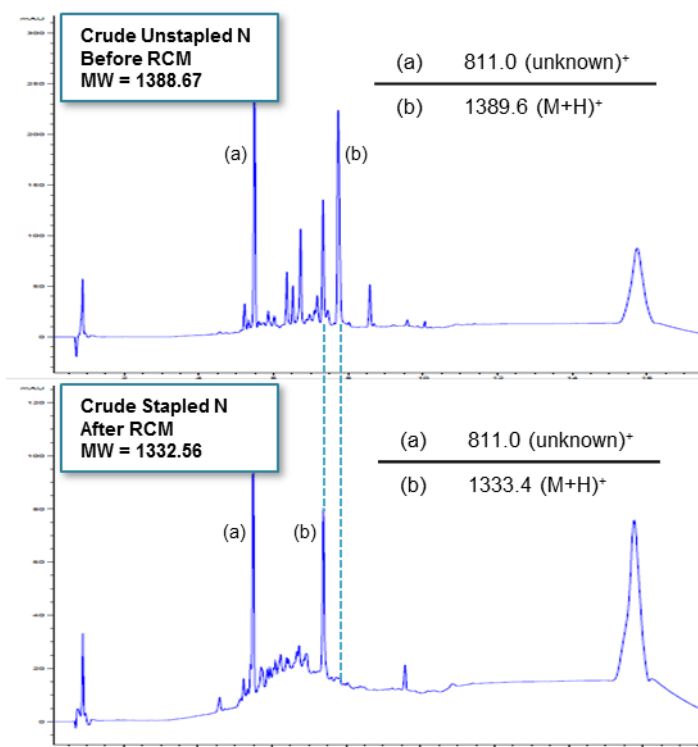
Figure 62 – Trial cleave analysis of Staple N synthesis

3.6.2 – Hybrid peptide synthesis

Synthesis of the four remaining peptides designed in the hybrid series was accomplished using the methods developed for previous sequences (Table 28). Glu(OAllyl) coupling was carried out manually as with the extended series (Table 14) to give the cyclisation precursor peptides to **Staples P** and **R**.

Table 28 – Coupling methodology towards hybrid peptides

Peptide	Staple	N	Sequence													C
Staple P	i, i+4	Ac	V	E*	T	A	S_5	E	L	L	S_5	S	N	-		NH$_2$
Staple Q	i, i+4	Ac	V	E	T	A	S_5	E	L	L	S_5	S	N	N		NH$_2$
Staple R	i, i+4	Ac	S_5	E*	T	A	S_5	E	L	L	L	S	N	-		NH$_2$
Staple S	i, i+4	Ac	S_5	T	E	L	S_5	T	L	N	S	V	E	-		NH$_2$

▪ = *Method (i)*		▫ = *Method (ii)*		▪ = *Method (iii)*		▪ = *Method (iv)*
▪ = *Method (v)*		▪ = *Method (vi)*		▫ = *Method (vii)*		

The synthesis of **Staple Q** was analogous to that of **Staple B**, with the exception of an added *C*-terminal Asn residue. Finally **Staple S** was synthesised in a similar fashion to the previous isomeric peptide **Staple I**, with extended coupling times for both Thr residues in order to overcome any coupling barriers from steric hindrance. In order to afford the pyroglutamic acid containing peptides, **Staple P** and **Staple R**, selective allyl deprotections were carried out on the solid phase to furnish the free glutamic acid for cyclisation (Scheme 42).

(a) - Pd(PPh₃)₄ (10 mol%), N-methylmorpholine (3 equiv.), DCM, 4 x 15 min
(b) HATU (5 equiv.), DIPEA (10 equiv), DMF, 4 h
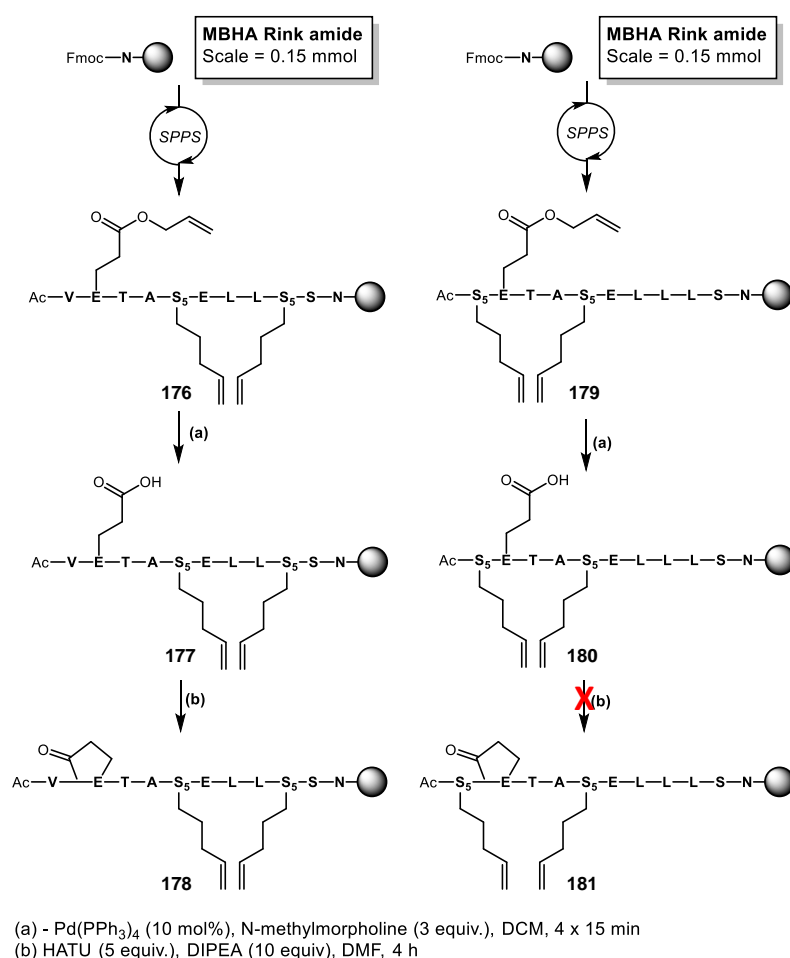
Scheme 42 – Cyclisation to afford pyroglutamate peptides

A slight alteration in deprotection conditions were used, replacing the previous reducing agent, phenylsilane, with *N*-methylmorpholine. This proved to give a more effective deprotection for this sequence, with trial cleavage reaction showing a cleaner HPLC profile with higher conversion to the deprotected products **176** and **179** after four treatments compared to the previous sequences (Schemes 36 & 37). With the allyl deprotection completed, attention then turned to cyclising the glutamic acid onto the peptide backbone to form the pyroglutamic acid sequences **178** and

181. The precursor to **Staple P**, **178**, was successfully cyclised using HATU after 4 hours (Scheme 42). However, a trial cleavage reaction of the **Staple R** precursor, **181**, showed a failed synthesis with a poor HPLC profile displaying multiple components of unknown identity and no product ion present by MS. This was disappointing as the synthesis towards **180** had been successful, yet upon treatment with HATU and DIPEA the peptide degraded. Despite several attempts at synthesising the resin bound species **181**, no product could be observed by LCMS. It was reasoned that the cyclisation was failing due to the presence of the sterically hindered α-methyl, α-alkenyl residue at the *N*-terminus, effectively blocking the coupling reaction from taking place. Consequently, the synthesis of **Staple R** was abandoned as pyroglutamate formation was demonstrated to be unfavourable for this particular sequence.

Metathesis of the final hybrid peptides, **Staples P**, **Q** and **S** was carried out using the conditions used for previous sequences (Scheme 34) to successfully give single ring-closed products in all cases. Full resin cleavage and subsequent purification furnished each of the target hybrid peptides (Table 29).

Table 29 – Isolated hybrid peptides

Peptide	Staple	Sequence	Hybrid	Yield
Staple N	i, i+4 stitch	Ac-**S₅**-E-T-A-**B₅**-E-L-L-**R₅**-S-N-NH₂	Staples B & G	5%
Staple P	i, i+4	Ac-V-**E***-T-A-**S₅**-E-L-L-**S₅**-S-N-NH₂	Staples B & M	17%
Staple Q	i, i+4	Ac-V-E-T-A-**S₅**-E-L-L-**S₅**-S-N-N-NH₂	Staples B & I	2%
Staple S	i, i+4	Ac-**S₅**-T-E-L-**S₅**-T-L-N-S-V-E-NH₂	Staples G & I	6%

As discussed in Section 3.6.1, a substantial by-product of unknown origin was present during the synthesis of **Staple N**, therefore the final yield of the stitched peptide was relatively low. It was, however, pleasing to note that the yield of the pyroglutamate peptide, **Staple P**, was higher than the other hybrid peptides. This was likely due to a combination of improved allyl deprotection conditions and the favourable cyclisation reaction. Low yields were obtained for the elongated sequence, **Staple Q** despite this sequence being relatively simple in comparison to the other hybrids (Table 29). Finally, **Staple S** was isolated in a low yield, however this is due to the isomeric sequence being more challenging to synthesise as discussed in Section 3.2.7 during the synthesis of **Staple I**.

Overall, four hybrid stapled peptides (**Staples N**, **P**, **Q** & **S**) were successfully synthesised out of the six sequences originally designed (Table 26). These peptides are hypothesised as combining the most favourable features of the active peptides screened in polyubiquitination assays from the initial palette of stapled peptides (Table 25).

3.6.3 – Structural analysis of hybrid peptide series

As with the previous stapled peptides, circular dichroism analysis of the new hybrid peptides was carried out in order to determine their helical content (Fig. 63).

Peptide	Hybrid	Staple	Sequence	% Helicity
Staple B	-	i, i+4	Ac-V-E-T-A-S_5-E-L-L-S_5-S-N-NH$_2$	— 41 —
Staple G	-	i, i+4	Ac-S_5-E-T-A-S_5-E-L-L-L-S-N-NH$_2$	— 42 —
Staple I	-	i, i+4	Ac-L-T-E-S_5-N-T-L-S_5-S-V-E-NH$_2$	— 24 —
Staple M	-	i, i+4	Ac-V-**E***-T-S_5-T-E-L-S_5-L-S-N-NH$_2$	— 39 —
Staple N	B & G	stitch	Ac-S_5-E-T-A-B_5-E-L-L-R_5-S-N-NH$_2$	— 42 —
Staple P	B & M	i, i+4	Ac-V-**E***-T-A-S_5-E-L-L-S_5-S-N-NH$_2$	— 22 —
Staple Q	B & I	i, i+4	Ac-V-E-T-A-S_5-E-L-L-S_5-S-N-N-NH$_2$	— 31 —
Staple S	G & I	i, i+4	Ac-S_5-T-E-L-S_5-T-L-N-S-V-E-NH$_2$	— 26 —
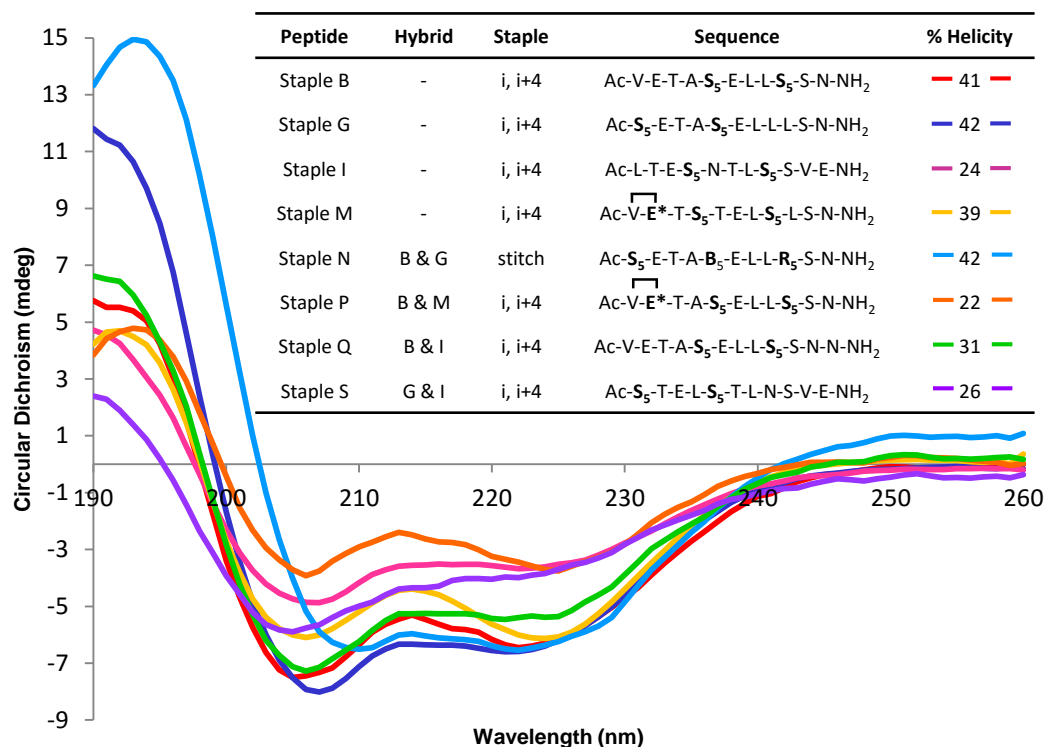
Figure 63 – CD spectra of active peptides with their hybrid analogues

The results of the hybrid peptides in the CD experiment were interesting when compared to the peptides they were derived from. Stitched peptide **Staple N** had a helicity of 42% which was in the same range as **Staples B** and **G**, with the incorporation of the bicyclic system not enhancing the helicity in comparison to the mono-stapled systems. This was surprising in comparison to the reported literature in which *i*, *i*+4, *i*+7 stapled peptides were up to 36% more helical than their mono *i*, *i*+7 stapled analogues.[203] The lack of helicity gained for **Staple N** through stitching compared to the single-stapled analogues is likely due to the length of the sequence, as previous stitched peptides were on longer fifteen-residue peptides

which will be more prone to unravelling. The pyroglutamate peptide, **Staple P**, had a low helicity of 22% compared to the parent sequences **Staples B** and **M**, which are 41% and 39% helical, respectively. However, this result is not surprising when considering that the *N*-terminal cyclisation of **Staple A** produced **Staple M**, which decreased the helicity of the sequence from 91% to 39%. It was pleasing to note that the addition of an additional *C*-terminal Asn residue in **Staple Q** gave a reasonable helicity level of 31% compared to **Staple B**. Finally, **Staple S** was found to be only 26% helical in phosphate buffer, however this was to be expected as the isomeric peptide **Staple I**, on which this sequence was derived, was also relatively unstructured at 24% helicity.

It was pleasing to note that overall, the helicity values of the hybrid series of peptides were comparable to the most active peptides they were derived from. Therefore, it is perhaps likely that their overall conformation would be similar to that of the active peptides. This conformational similarity in conjunction with the optimal sequences and staple position derived from the *in silico* models of **Staples B**, **G**, **I** and **M** potentially indicates that the peptides may exhibit similar activity in polyubiqutination assays.

A thermal stability CD experiment was carried out on **Staple N**, similar to those discussed in Section 3.3.5. Due to the more constrained nature of this peptide, it was of interest how this peptide would unfold under high temperature in comparison to the single stapled *i*, *i*+4 peptides. During the experiment, the overall helicity of **Staple N** decreased by 13% when heated to 80 $^{\circ}$C, to 32% helicity in phosphate buffer (Fig. 64). This was a similar result to the less helical peptides **Staples B** and **M**. However it was interesting to note that compared to single stapled *i*, *i*+4 peptides, the stitched peptide maintained a more constant ratio of $\theta_{222}/\theta_{208}$. This data would imply that **Staple N** maintains an α-helical conformation and is less prone to forming a mixed α/3^{10}-helical conformation observed with **Staples A**, **B** and **M**.

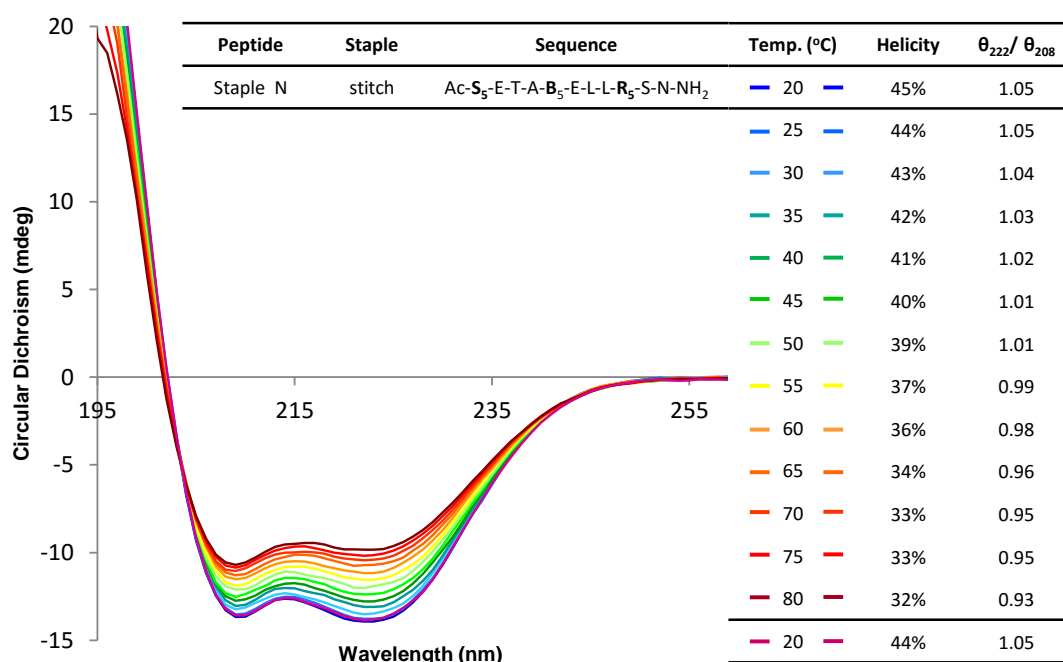| Peptide	Staple	Sequence	Temp. (°C)	Helicity	$\theta_{222}/\theta_{208}$
Staple N	stitch	Ac-**S₅**-E-T-A-**B₅**-E-L-L-**R₅**-S-N-NH₂	20	45%	1.05
			25	44%	1.05
			30	43%	1.04
			35	42%	1.03
			40	41%	1.02
			45	40%	1.01
			50	39%	1.01
			55	37%	0.99
			60	36%	0.98
			65	34%	0.96
			70	33%	0.95
			75	33%	0.95
			80	32%	0.93
			20	44%	1.05

Figure 64 – Temperature ramped CD spectra of Staple N
Sample run at 50 µM in a 2 mm cell

Therefore, for this short sequence, peptide stitching potentially provides a more rigid scaffold preventing helix/coil transitions which have an effect on overall helix conformation. Consequently, the activity of **Staple N** in polyubiquitination assays would determine whether this decreased conformation freedom is beneficial compared to single stapled species.

3.6.4 – Peptides designed to probe putative SAR with Ubb+1

Following the successful synthesis of the hybrid series, attention then turned to determination of their activity againt Ubb+1 in polyubiquitination assays. A total of six new peptides were prepared for the assay, incorporating both the hybrid and the extended series, as well as the *cis* isomer of **Staple D** (Table 30).

Table 30 – Second generation of peptides for testing in polyubiquitination assay

Peptide	Staple	Sequence	Helicity	Charge	Extension
Staple D *cis*	i, i+7	Ac-**R₈**-E-T-A-T-E-L-**S₅**-L-S-N-NH₂	80%	-2	
Staple J	i, i+4	Ac-V-**E***-T-**S₅**-T-E-L-**S₅**-L-S-N-NH₂	10%	-1	**J**
Staple K	i, i+4	Ac-V-**E***-T-**S₅**-T-E-L-**S₅**-L-S-N-NH₂	14%	-1	
Staple N	stitch	Ac-**S₅**-E-T-A-**B₅**-E-L-L-**R₅**-S-N-NH₂	42%	-2	**K**
Staple P	i, i+4	Ac-V-**E***-T-A-**S₅**-E-L-L-**S₅**-S-N-NH₂	22%	-1	
Staple Q	i, i+4	Ac-V-E-T-A-**S₅**-E-L-L-**S₅**-S-N-N-NH₂	35%	-2	**P**
Staple S	i, i+4	Ac-**S₅**-T-E-L-**S₅**-T-L-N-S-V-E-NH₂	26%	-2	

The results of these peptides in the polyubiquitination assay could provide information towards a potential structure-activity relationship between stapled peptide mimics of E2-25K and Ubb+1. As discussed previously in Section 3.2.8, the extended series could provide insight into the conformation of Ubb+1 in solution. If **Staples J** and **K** are more active than the parent sequence, **Staple A**, then it could be assumed that the aromatic side chains bind in the putative hydrophobic pocket designed from consideration of the Ubb+1 X-ray crystal structure (Fig. 40). Alternatively, if these peptides are inactive, in a similar fashion to **Staple A**, then it could be ascertained that the side chain extensions gain no additional interactions with the target, potentially due to the putative binding site being blocked as observed in the NMR structure of Ubb+1 (Fig. 40).

The results obtained for the hybrid series, **Staples N**, **P, Q** and **S**, will also be interesting in relation to how accurate the *in silico* models of the peptide interactions with Ubb+1 are. As discussed in Section 3.6, these peptides were designed from the most active sequences against Ubb+1, so should hypothetically be equally effective in inhibiting Ubb+1 capped polyubiquitin chains. Any variation in activity compared to **Staples B**, **G**, **I** and **M** will provide valuable information towards the putative binding mode of the peptides with Ubb+1. **Staples N** and **P** could afford evidence that the all-hydrocarbon staple plays a key role in forming hydrophobic interactions with Ubb+1, as implied by the *in silico* models (Figs. 59 and 60). Alternatively, the activity of **Staples Q** and **S** could confirm the putative additional hydrogen bond with the backbone of Lys[48] of Ubb+1 implied by the model of **Staple I** (Fig. 57). Finally, it would be of interest to determine if the *cis* isomer of **Staple D** exhibited any difference in activity compared to the trans isomer (Table 24) which had been shown to be inactive against the formation of Ubb+1 capped PolyUb chains tested previously (Fig. 55).

3.6.5 – Final polyubiquitination assay results

As described previously in Sections 3.5.1 and 3.5.2, the polyubiquitin assays were designed to show the extent of both regular and Ubb+1 unanchored polyubiquitin chain formation. Previous results from the initial stapled peptide screen (Fig. 55) had shown that **Staples I** and **G** completely inhibited the formation of Ub_3-Ubb+1 capped PolyUb chains, with **Staples B** and **M** showing a more pronounced effect compared to the inactive peptides. **Staple I** was also shown to inhibit longer Ubb+1 capped PolyUb chains, compared to the control which showed Ub_n-Ubb+1 chains where n =

1 – 7 (Fig. 55). Therefore, in order to ascertain whether the hybrid compounds were as effective as their parent sequences, they would require to show inhibition of Ub_n-Ubb+1 chains, where n = 3 as a minimum.

Western blot analysis of the polyubiquitination products of the second generation peptides (Table 30), again performed through a collaboration,[216] gave some unexpected results (Fig. 65). Initially, it was pleasing to note that none of the tested peptides appeared to have any effect on the formation of standard unanchored PolyUb chains, as shown by the high MW bands in the gel (Fig. 65, A).
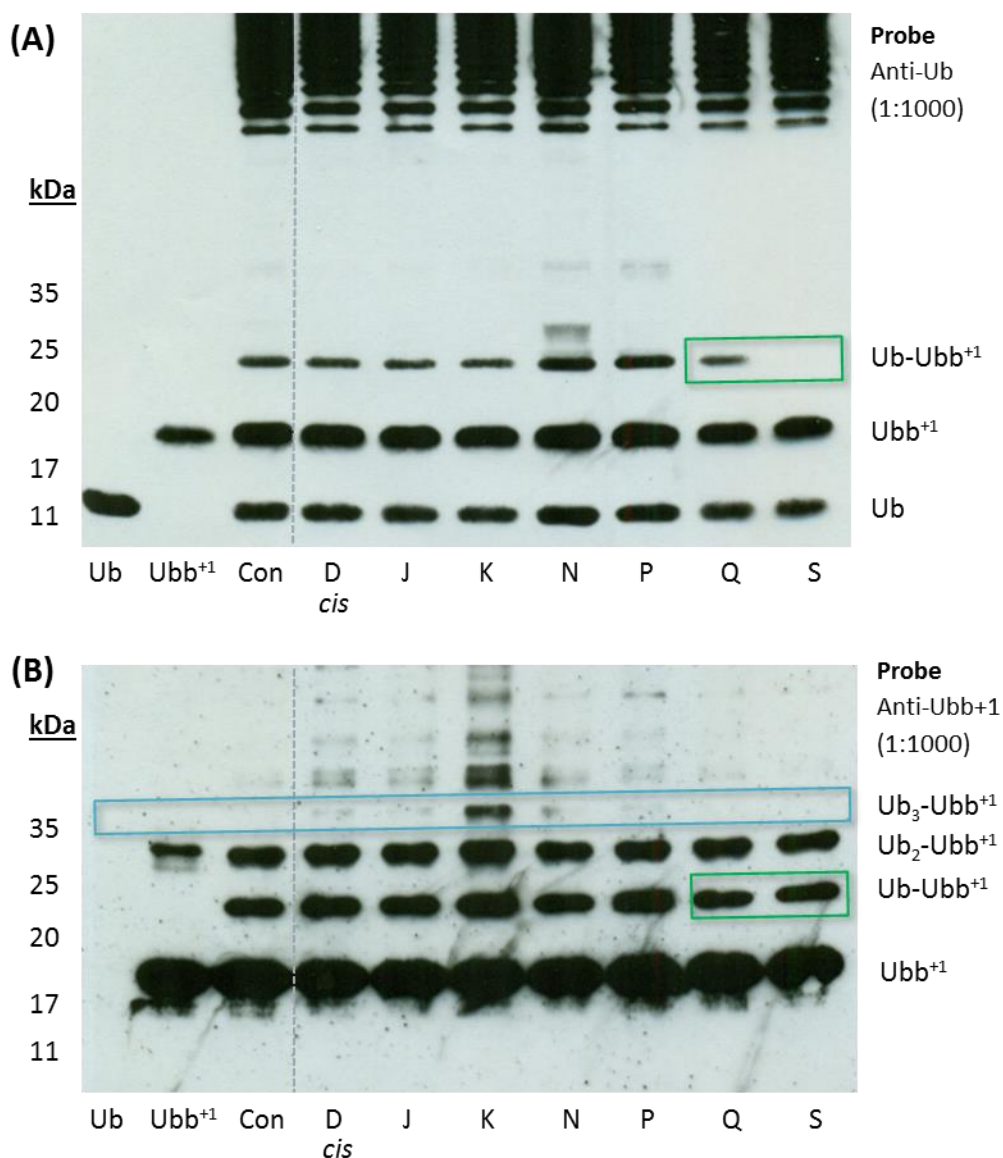

Figure 65 – Four hour polyubiquitination assay of second generation peptides
A) – Ubiquitin antibody stained results from the polyubiquitination assay. B) – Ubb+1 antibody stained results from the polyubiquitination assay.

It was curious that **Staple S** appeared to have an effect on Ub-Ubb+1 capped chains in the anti-Ubiquitin stained blot as shown by the green box (Fig. 65, A). However, when this was compared to the Anti-Ubb+1 stained blot (Fig. 65, B), there were clear spots present for Ub-Ubb+1 chains, implying the absence of a signal in blot A was likely to be an artefact of the assay technique. Unfortunately, the key diagnostic band of Ub_3-Ubb+1 capped PolyUb chains was not visible in the blot, shown by the blue band (Fig. 65, B). This lack of resolution of Ub_n-Ubb+1 chains where n = 1 – 7 in the control (Con) was likely due to differences in blot staining and development compared to previous blots (Fig. 55), as the assays had been run under identical conditions. Therefore, no firm conclusions could be drawn as to whether **Staple D** and the hybrid series (**Staples N**, **P**, **Q** and **S**) were capable of inhibiting the formation of Ub_3-Ubb+1 capped PolyUb chains seen with previously active peptides.

The most interesting results from this round of assays (Fig. 65) was from the extended peptide series, **Staples J** and **K**. Structurally, the only difference between these two peptides is the nature of the heterocycle attached at the extension point: **Staple J** is functionalised with a *meta*-pyridine whilst **Staple K** contains an *ortho*-pyridine side chain (Fig. 66, B).
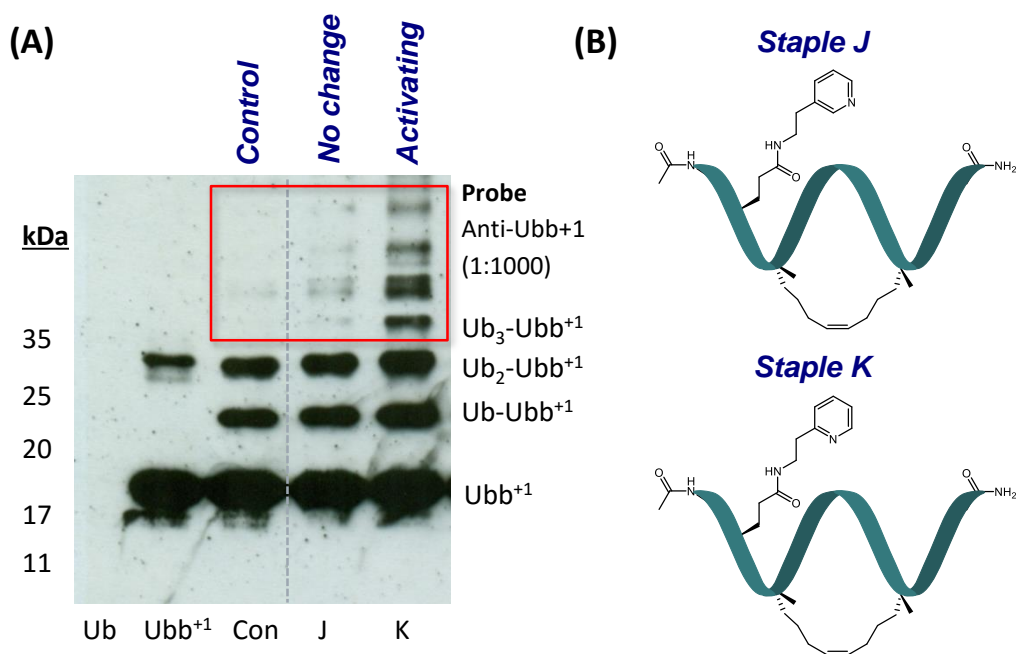

Figure 66 – Difference in activity of the extended series of stapled peptides
A) – Expansion of the Ubb+1 antibody stained results from the polyubiquitination assay. Staple K appears to activate the formation of Ubb+1 capped PolyUb chains B) – Main structural difference between the extended peptides

However, the results of these peptides in the polyubiquitination assay were significantly different as shown in detail below (Fig. 66, A). **Staple K** appeared to promote the formation of Ub_n-Ubb+1 chains where n = 3 – 6 due to the presence of strong bands in the blot compared to the control (Fig. 66, A). This was the opposite effect than was anticipated, as these peptides had been designed to inhibit the formation of Ubb+1 caped PolyUb chains, with the modified side chains proposed to bind with an additional hydrophobic pocket in Ubb+1 (Section 3.2.8). The clear difference in activity of **Staples J** and **K** in this assay, despite their similar structure, implied that the activating effect of **Staple K** was attributable to a chemically specific interaction based on the *ortho*-pyridine group. Overall, these results were very interesting, as they suggested that stapled peptide analogues of α-9 of E2-25K were capable of both inhibiting (**Staple I**) and activating (**Staple K**) Ubb+1 capped PolyUb chain formation. However, whether any SAR around the series of hybrid peptides could be established is still unclear due to the lack of resolution and reproducibility in these particular gel systems.

3.6.6 – Potential insight into Ubb+1 polyubiquitin chain activation

The results of **Staple J** compared to **Staple K** in the polyubiquitination assay (Section 3.6.5, Fig. 66) were suprising as they implied that that Ubb+1 capped polyubiquitin chain formation could be activated by the *ortho*-pyridine extended peptide (**Staple K**). As discussed previously, this was highly unexpected, as these peptides were designed to block the E2-25K binding site of Ubb+1 in order to prevent E2-25K mediated PolyUb chain formation (Fig. 54). Assuming the designed stapled peptides interact with the α-9 binding site of Ubb+1 indicated earlier, further consideration of the conformation of Ubb+1 was required in order to understand the potential activating effect of **Staple K**.

Analysis of the NMR solution structure of E2-25K could provide insight into the formation of Ubb+1 capped PolyUb chains.[59] Apart from NMR K_D data calculated between Ubb+1 or Ub with E2-25K, little is known about E2-25K mediated PolyUb chain formation, and the binding kinetics of each step in the synthesis of these systems. When the twenty lowest energy NMR conformations of Ubb+1 were superimposed, the unstructured tail region of Ubb+1 could adopt various conformations in solution (Fig. 67, A). There is the potential that some of these conformations could block the E2-25K binding site through interaction with the

hydrophobic surface of Ubb+1, potentially slowing the rate of association with E2-25K compared to wild type ubiquitin (Fig. 67).
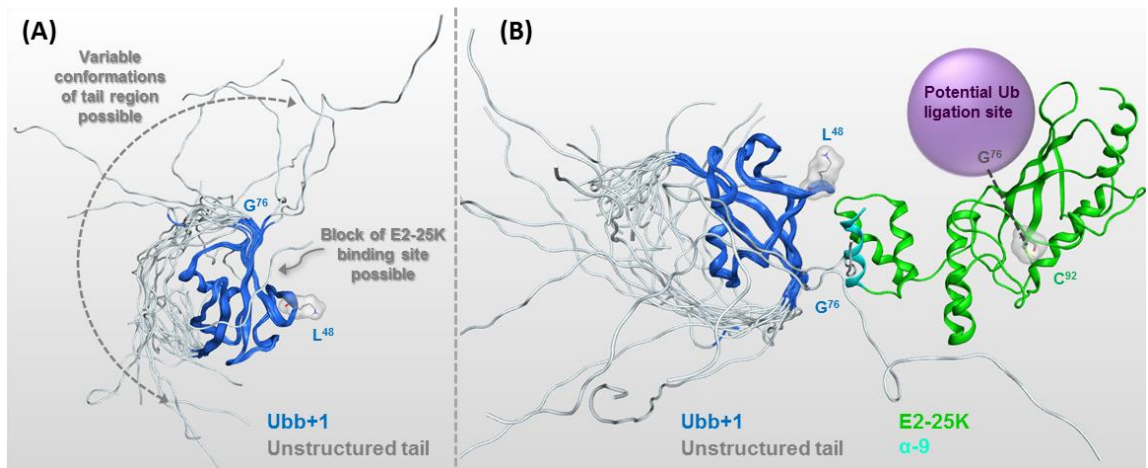

Figure 67 - Lowest energy structures of the Ubb+1 tail and their effect on E2-25K
A) – Superimposed structures of the 20 lowest energy NMR solution structures of E2-25K (PDB ID:2KX0) B) – Tail region of Ubb+1 could block E2-25K binding or disrupt Ub-E2-25K complex isopeptide bond formation

Alternatively, when bound to E2-25K, the tail region of E2-25K could potentially decrease the rate of PolyUb chain formation through disrupting the isopeptide ligation step: the unstructured nature of the tail could disrupt the Ub Gly^{76} – E2-25K Cys^{92} bond formation step, or, the final Ub Gly^{76} – Ubb+1 Lys^{48} isopeptide bond, as illustrated in the above model (Fig. 67, B).

Based on this, it can perhaps be reasoned that constraining the tail region of Ubb+1 through the action of a stapled peptide, could increase the rate of Ubb+1 capped PolyUb chain formation through inducing a more ordered structure in Ubb+1. Modelling would imply that the extended series of stapled peptides have the potential to interact with the tail region of Ubb+1 (Fig. 68, A).
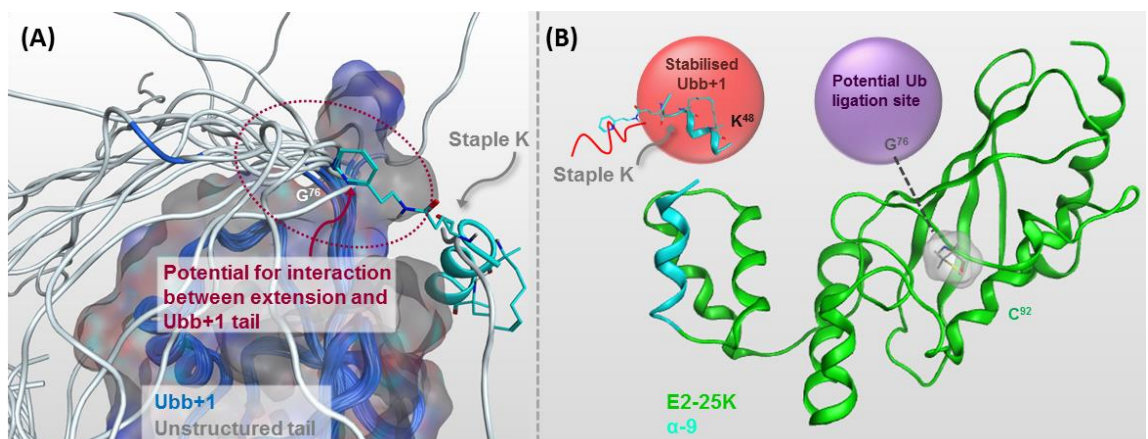

Figure 68 – Potential rational of Staple K activation of Ubb+1 chain formation
A) – Potential interaction between extended series and Ubb+1 tail region B) – Conformationally locked Ubb+1 could form Ubb+1 capped PolyUb chains via the E2-25K mediated mechanism

The sequence of the first five residues of the tail region have multiple residues which are likely to be in proximity to the pyridyl extension of **Staple K**: Tyr[77], Ala[78], Asp[79], Leu[80] and Arg[81]. The data discussed in Section 3.6.5 (Fig. 66), suggests that the *ortho*-pyridyl substituted **Staple K** could make a selective interaction with the tail region of Ubb+1, giving an additional level of constraint to the overall structure of Ubb+1. Accordingly, once the tail region of Ubb+1 has been constrained, the key Lys[48] could become more accessible for PolyUb chain formation, without the participation of E2-2K as a directing group (Fig. 68, B). However, the exact nature of this interaction remains unknown and would require more detailed structural analysis to fully understand the nature of the complex formed between the two species.

Despite this hypothesis, no direct conclusions concerning the activating mechanism of action of **Staple K** can be confirmed. Due to the multi-component nature of the assay there is the underlying possibility that **Staple K** is interacting with other enzymes in the system, such as E1 or E2-25K, with an unknown binding mode. Therefore, until further investigation into activity of **Staple K** is carried out, the only firm conclusion that can be drawn is that this peptide is capable of activating Ubb+1 capped PolyUb chain formation through an as yet unknown mechanism.

3.6.7 – Second generation stapled peptide conclusions

The second generation of stapled peptides tested in polyubiquitination assays were designed using *in silico* modelling to potentially enhance the nascent activity observed in the first generation compounds with Ubb+1. The first compound of interest, the cis-isomer of **Staple D**, was submitted to the assay in order to determine whether the conformation of the alkene has any effect on binding affinity. In general, only the major *trans*-isomer of *i*, *i*+7 stapled peptides are reportedly tested in biological systems. However as *trans*-**Staple D** was inactive it was of interest whether *cis*-**Staple D** showed any variation in activity in polyubiquitination assays. Unfortunately, and as previously discussed in Section 3.6.5, the resolution of the Western blot analysis of the polyubiquitination assay was not sufficiently sensitive to observe the key diagnostic blots of Ub_n-Ubb+1 chains where n ≥ 3 compared to the control lane. Therefore it is still uncertain whether alkene isomerism has any effect on the activity of **Staple D**.

Similarly, the activity of the hybrid series, **Staples N**, **P**, **Q** and **S**, remains unclear based on the resolution of the Western blot analysis. This series were designed from the most active stapled peptides from the previous assay runs, **Staples I**, **G**, **B** and **M**, which had shown varying degrees of inhibition of Ub_3-Ubb+1 capped PolyUb chains. Therefore, as this diagnostic lane is not strongly observed in the analysis (Fig. 65), no conclusion can be drawn as to whether these peptides are equally as active as their parent sequences. Consequently, it remains unclear as to whether the hypothesised SAR derived from the *in silico* models of these peptides against Ubb+1 is valid (Sections 3.5.4 & 3.6). An analogous polyubiquitination assay, with clear higher MW Ub_n-Ubb+1 chains, is required in order to confirm whether the hybrid series of peptides have retained or improved activity than the parent sequences. If **Staples N**, **P**, **Q** and **S** are shown to be active against Ub_n-Ubb+1 chains where $n \geq 3$, then it can be assumed that the predictive models created to investigate the peptides binding with Ubb+1 are relatively accurate. Alternatively, if the hybrid series are less active than their parent stapled peptides (**Staples I**, **G**, **B** and **M**) then further investigation into the SAR of these stapled peptides with Ubb+1 would be required.

Finally, the extended series, **Staples J** and **K**, gave the most interesting results in the polyubiquitination assay (Fig. 66). **Staple K** gives an apparent activation in the formation of unanchored Ubb+1 capped PolyUb chains compared to the isomeric peptide, **Staple J**. These results imply that there is a chemically distinct interaction between *ortho*-pyridyl extended **Staple K** and a component of the assay (Ubb+1, E1 or E2-25K) as the *meta*-pyridyl analogue, **Staple J**, did not exhibit this effect based on the Western blot analysis. Despite the mechanism of this activation being unclear (Section 3.6.6), this peptide remains the first example of a compound capable of selectively increasing the rate of E2-25K mediated Ubb+1 capped PolyUb chain formation, potentially through interaction with the tail region of Ubb+1. Therefore, through the studies carried out in this thesis, both inhibitors and activators of this pathway have been discovered. Once a mode of action has been confirmed, these peptide could be valuable tools in the further understanding of Ubb+1 mediated proteasomal inhibition.

4. Conclusions

The overall aim of this project was to create molecular tools to investigate the potential role of Ubb+1 mediated proteasomal inhibition in Alzheimer's disease. To accomplish this goal, a series of short stapled peptide mimics of the α-9 helix of E2-25K were created with the purpose of antagonising the E2-25K/Ubb+1 PPI. Peptides were designed to inhibit the formation of Ubb+1 capped polyubiquitin chains, whilst allowing regular polyubiquitin chain forming processes to proceed. Any hit compounds found would provide the first step in investigating the hypothesis that inhibition of the 26S proteasome by long, unanchored Ubb+1 capped PolyUb chains is a key process during neuronal degradation, and not the presence of Ubb+1 itself. Successful tool compounds could also provide a basis for creating more drug-like peptides which have the potential to reverse proteasomal inhibition, allowing the proteasome to process excess Ubb+1 before it is incorporated into toxic Ubb+ capped PolyUb chains.[42] Therefore, providing evidence of the chemical tractability of the target.

4.1 – Synthesis of α-methyl, α-alkenyl amino acid building blocks

Utilising the all-hydrocarbon stapling technique to create short stabilised analogues of the α-9 helix of E2-25K proved to be technically challenging due to the requiremement of chiral α-methyl, α-alkenyl building blocks (Scheme 43).
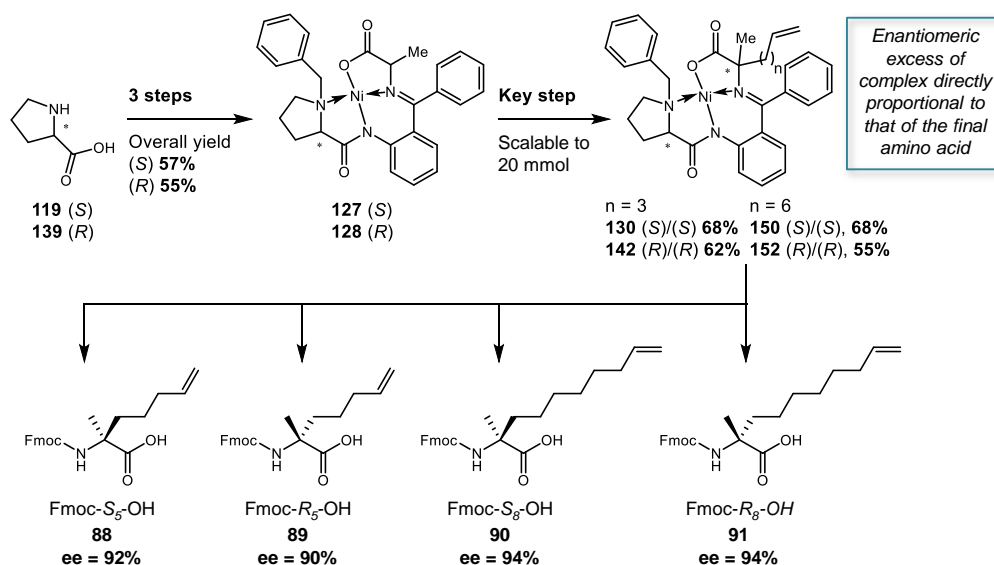
Scheme 43 - Summarised route towards α-methyl, α-alkenyl building blocks

Significant optimisation of the published BPB-Ni(II)-Ala auxiliary approach was required to furnish the required building blocks in optical purity of a high enough

standard for SPPS. As discussed in detail in Section 3.1, a correlation was found between the extent of proline epimerisation during the complexation step, and the final enantiomeric excess of the isolated amino acids. This required extensive investigation into developing a procedure which gave consistently optically pure auxiliaries **127** and **128**, with scale and reaction time being limiting factors. A chiral HPLC assay was enabled for these complexes as a diagnostic indicator of the optical purity of the final amino acid products. The results of this assay were found to be directly proportional to the enantiomeric excess of the final Fmoc amino acids **88** – **91**. Overall, the target building blocks (**88** – **91**) could be isolated in reasonable yields on a scale of 20 mmol with enantiomeric excesses of greater than 90%.

4.2 – Stapled peptide synthesis and analysis

These building blocks were then successfully utilised in the synthesis of stapled peptide analogues of the α-helix of E2-25K. Initial difficulties in synthesising the **Wild type** sequence (Table 2) required an investigation into coupling conditions of the *N*-terminal threonine residue (Section 3.2.3). With optimum conditions in hand, seven out of the nine initial peptides designed around the sequence of α-9 (Table 2) could be prepared and isolated, including the **Wild type** and six stapled analogues: five *i*, *i*+4 peptides (**Staples A**, **B**, **C**, **E** & **G**) and the two separable *cis* and *trans* isomers of the *i*, *i*+7 peptide **Staple D**. (Table 11). When analysed by circular dischroism spectroscopy, a range of helicities were present from 16% to 91% (Table 31), with staple position and stereochemistry having a significant effect on the peptides secondary structure in solution (Section 3.2.6). Due to the high degrees of helicity measured for **Staple A** (91%), various analogues of this sequence were designed to probe the potential binding mode of these stapled peptide with Ubb+1.

An isomeric analogue of **Staple A**, was designed to investigate the important of sequence specific interactions with Ubb+1 (**Staple I**, Table 12). The extended series were also designed around the sequence of **Staple A** to probe whether a hydrophobic cleft noted in the crystal structure of Ubb+1 (Fig. 40) could be used as an additional binding site for stapled peptides. As discussed in Section 3.2.8, two extended peptides were successfully synthesised (**Staples J** and **K**) with an additional cyclised pyroglutamate peptide, **Staple M**, formed as a by-product during the side chain coupling process (Scheme 36). In summary, four analogues of **Staple A** were synthesised with variations in sequence and side-chain extension. The resultant helicities of these peptides ranged from 10% to 39% (Table 31),

demonstrating the important of sequence in helix propagation and that relatively small changes can greatly affect conformation in solution.

For selected peptide sequences, **Staples A**, **G** and **I**, an additional NMR study was carried out to investigate if any further conformational information could be obtained outwith the helicity calculated from CD (91%, 42%, and 24%, respectively). Overall, these NMR studies showed that the precise helical nature of these peptides can be more complex than the simple helicity data derived from CD spectroscopy. Peptides with apparently rigid helical secondary structures, such as **Staple A** at 91% helicity, can exhibit a degree of conformational flexibility between α-helical and 3^{10}-helical populations in solution. Similarly, **Staple G** adopted a much more complex folded-helical structure than the simple 42% helicity calculated from CD. The least helical peptide studied, **Staple I**, was confirmed to be relatively unstructured, with the main proportion of helical character preserved around the *i, i*+4 stapled region.

4.3 – Polyubiquitination assay results and the second generation of peptides

The first generation of stapled peptides tested in polyubiquitination assays, **Staples A**, **B**, **C**, *trans*-**D**, **E**, **G**, **I** & **M** had varying efficacy in inhibiting the formation of Ubb+1 capped polyubiquitin chains (Table 31).

Table 31 – Final stapled peptides and their activity against Ubb+1

	Peptide	Staple	Sequence	Helicity	Charge	Active against Ubb+1	Extension
1	Wild type	-	Ac-V-E-T-A-T-E-L-L-L-S-N-NH$_2$	16%	-2	✗	
2	Staple A	i, i+4	Ac-V-E-T-**S$_5$**-T-E-L-**S$_5$**-L-S-N-NH$_2$	91%	-2	✗	
3	Staple B	i, i+4	Ac-V-E-T-A-**S$_5$**-E-L-L-**S$_5$**-S-N-NH$_2$	41%	-2	✓	
4	Staple C	i, i+4	Ac-V-E-**S$_5$**-A-T-E-**S$_5$**-L-L-S-N-NH$_2$	42%	-2	✗	
5	Staple D *trans*	i, i+7	Ac-**R$_8$**-E-T-A-T-E-L-**S$_5$**-L-S-N-NH$_2$	80%	-2	✗	
6	Staple D *cis*	i, i+7	Ac-**R$_8$**-E-T-A-T-E-L-**S$_5$**-L-S-N-NH$_2$	21%	-2	▬	
7	Staple E	i, i+4	Ac-V-E-T-**R$_5$**-T-E-L-**R$_5$**-L-S-N-NH$_2$	16%	-2	✗	
8	Staple G	i, i+4	Ac-**S$_5$**-E-T-A-**S$_5$**-E-L-L-L-S-N-NH$_2$	42%	-2	✓✓	
9	Staple I	i, i+4	Ac-L-T-E-**S$_5$**-N-T-L-**S$_5$**-S-V-E-NH$_2$	24%	-2	✓✓✓	
10	Staple J	i, i+4	Ac-V-**E***-T-**S$_5$**-T-E-L-**S$_5$**-L-S-N-NH$_2$	10%	-1	▬	**J**
11	Staple K	i, i+4	Ac-V-**E***-T-**S$_5$**-T-E-L-**S$_5$**-L-S-N-NH$_2$	14%	-1	✓	
12	Staple M	i, i+4	Ac-V-**E***-T-**S$_5$**-T-E-L-**S$_5$**-L-S-N-NH$_2$	39%	-1	✓	**K**
13	Staple N	stitch	Ac-**S$_5$**-E-T-A-**B$_5$**-E-L-L-**R$_5$**-S-N-NH$_2$	42%	-2	▬	
14	Staple P	i, i+4	Ac-V-**E***-T-A-**S$_5$**-E-L-L-**S$_5$**-S-N-NH$_2$	22%	-1	▬	**M & P**
15	Staple Q	i, i+4	Ac-V-E-T-A-**S$_5$**-E-L-L-**S$_5$**-S-N-N-NH$_2$	35%	-2	▬	
16	Staple S	i, i+4	Ac-**S$_5$**-T-E-L-**S$_5$**-T-L-N-S-V-E-NH$_2$	26%	-2	▬	

✓ = *Modest activity against Ubb+1 capped PolyUb$_n$ chains where n = 3*   ✗ = *Inactive against Ubb+1*

✓✓ = *Inhibition of Ubb+1 capped PolyUb$_n$ chains where n = 3*   ✓ (orange) = *Activation of Ubb+1 capped PolyUb chains*

✓✓✓ = *Inhibition of Ubb+1 capped PolyUb$_n$ chains where n ≥ 3*   ▬ = *Activity unconfirmed*

Analysis of the Western blot data (Fig. 55) implied that **Staple I** was capable of inhibiting the formation of Ub_n-Ubb+1 PolyUb chains where n ≥ 3, whilst **Staples G**, **B** and **M** had varying activity against Ub_3-Ubb+1 PolyUb chains. *In silico* modelling was used to investigate the putative SAR of these stapled peptides with Ubb+1. From this modelling effort, the hybrid series (**Staples N**, **P**, **Q** and **S**) were designed and synthesised to combine the structural aspects reasoned to be the most beneficial to binding with Ubb+1 which had been highlighted from the *in silico* studies.

4.4 – Design, synthesis and activity of second generation stapled peptides

With the extended and hybrid series of stapled peptides in hand, a further polyubiquitination assay was carried out. The results of this assay were anticipated to provide insight into key binding interactions between the active stapled peptides and Ubb+1, and whether a correlation between *in silico* data and *in vitro* data could be obtained. However, as discussed in detail in Section 3.6.5, the Western blot analysis of the assay lacked the sensitivity in the key Ub_3-Ubb+1 PolyUb chain region. Therefore, the inhibitory potential of **Staples** *cis*-**D**, **J**, **N**, **Q**, **P** and **S** against formation of Ubb+1 capped PolyUb chains could not be confirmed (Table 31). The final assay did, however, provide a very interesting result in that **Staple K** had apparent activating potential in the formation of Ubb+1 capped PolyUb chains. This was potentially attributable to the extended side chain forming an additional interaction with the tail region of Ubb+1, giving a degree of conformational constraint to the overall structure of Ubb+1. This could potentially facilitate the formation of Ubb+1 capped PolyUb chains through enabling the approach of Ubb+1 to the catalytic site of E2-25K. However, the above proposal cannot be confirmed until further structural studies have been carried out.

4.5 – Stapled peptides can exhibit both inhibitory and activating action

During this programme of research, the overall aim was to create a series of short peptides capable of antagonising the E2-25K/Ubb+1 PPI in order to investigate the incorporation of Ubb+1 into polyubiquitin chains, and whether this action was related to the proteasomal inhibition exhibited AD. Consequently, useful molecular tools which could be used to further understand key regulatory pathway have been designed through utilising the all-hydrocarbon stapling technique. These active helical peptides have been shown to be selective for Ubb+1 containing chains against wild type ubiquitin systems. However, whether they exhibit an inhibitory, or

activating effect on the formation of Ubb+1 capped PolyUb chain formation is highly dependent on sequence and structure (Fig. 69). Both **Staples I** and **K** have identical *i*, *i*+4 staple positions and both exhibit low helicity in phosphate buffer, however subtle differences in sequence and side chain functionality have allowed for contrasting effects in polyubiquitination assays.
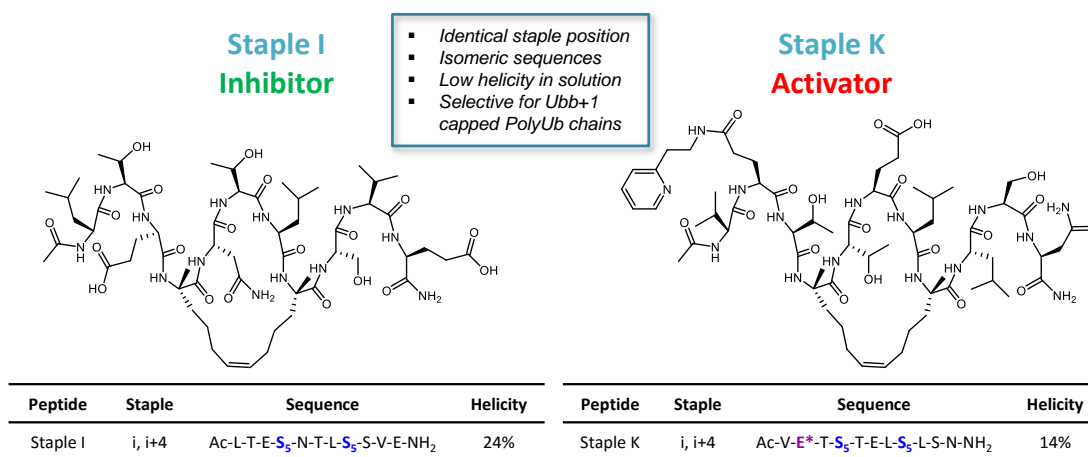

Peptide	Staple	Sequence	Helicity
Staple I	i, i+4	Ac-L-T-E-**S₅**-N-T-L-**S₅**-S-V-E-NH₂	24%

Peptide	Staple	Sequence	Helicity
Staple K	i, i+4	Ac-V-**E***-T-**S₅**-T-E-L-**S₅**-L-S-N-NH₂	14%

Figure 69 – Stapled peptide toos for Ubb+1 capped PolyUb chain formation

These compounds could be used in further studies into the potentially toxic action of Ubb+1 capped polyubiquitin chains. The inhibitory action of **Staple I** could be used in further biological testing to provide early evidence that blocking Ubb+1 capped PolyUb chain formation is beneficial to overall proteasomal function. Activation of this pathway through the action of **Staple K** could not only aid investigation into E2-25K mediated PolyUb chain formation, but also provide further evidence that these unanchored Ubb+1 PolyUb chains are toxic to the cell due to proteasomal inhibition. Whether **Staples I** and **K** would be active in a cellular context is currently unknown as further binding and permeability data would be required. As discussed previously in Section 1.7.3, if cellular assays were of interest, a further screen may be required for both **Staples I** and **K** to tune cell permeability. In order to make these stapled peptides more drug-like, a careful balance would need to be established between activity, cell permeability and protealytic stability for both compounds. However, as tool compounds, this development would likely be less intensive, assuming their mechanism of action could be defined. Despite this, **Staple I** is the most promising candidate from the first generation of stapled peptides capable of blocking Ubb+1 incorporation into PolyUb chains. In addition to this, **Staple K** is the first stapled peptide example of a compound which can potentially activate a complex ligation

system such as the E2-25K mediated synthesis of unanchored Ubb+1 capped PolyUb chains.

5. Future Work

As discussed previously in Section 3.6.5, limitations in the analysis of the polyubiquitination assay resulted in the inhibitory action of **Staples** *cis*-**D**, **J**, **N**, **Q**, **P** and **S** remaining unclear with respect to the formation of Ubb+1 capped polyubiquitin chains. These results are valuable in confirming the putative SAR developed in Section 3.5.4 through *in silico* modelling. Therefore, further assay development would be required to allow for consistent sensitivity in the results. This improved assay could potentially confirm the key interactions between the stapled peptides and Ubb+1, as predicted in Section 3.6. In particular, does the all-hydrocarbon staple play a key role in forming hydrophobic interactions with Ubb+1, and can an additional hydrogen bond with the backbone of Lys^{48} of Ubb+1 improve the affinity of these peptides.

5.1 – Conformation of Ubb+1/stapled peptide binding sites

Throughout the course of this work, both inhibitors and a potential activator of E2-25K mediated Ubb+1 capped PolyUb chain formation have been discovered, as inferred from Western blot analysis of polyubiquitination assays. These assays were initially chosen due to the reltively small amounts of peptide and enzyme required, and their well documented analysis using Western blot techniques. However, a question still remains in relation to the mode of action of these stapled peptides within this system. The *in silico* modelling and biological action of these peptides has been assumed to be through binding selectively with the E2-25K UBA domain binding site of Ubb+1. In order to confirm this proposed mode of action, a series of experiments would be required to quantify binding affinity with Ubb+1.

Isothermal calorimetry (ITC) is a usefull technique to study various biological systems, such as protein-protein and enzyme-inhibitor interactions.[217,218] Assuming titration conditions can be optimised to give clear enthalpy differentials, a single ITC experiment can provide two valuable parameters: affinity data in the form of a dissociation constant, K_D, for the interaction studied, and information regarding the number of binding sites between the two species from molar ratio analysis (Fig. 70). Consequently, stapled peptides which been shown to have interesting activity in the polyubiquitination assays, such as **Staples I** and **K**, could be tested by ITC to gain K_D values of their affinity with Ubb+1. This technique could also be used to investigate whether there is a direct correlation between the binding affinity of a

stapled peptide towards Ubb+1 and the length of Ubb+1 capped PolyUb chains inhibited in the polyubiquitination assay. **Staple G** was shown to inhibit Ub_3-Ubb+1 PolyUb chain formation whilst **Staple I** could inhibit Ub_n-Ubb+1 PolyUb chains where n = 3 – 6. Therefore, it would be interesting to observe if **Staple I** had a lower K_D value than **Staple G**.
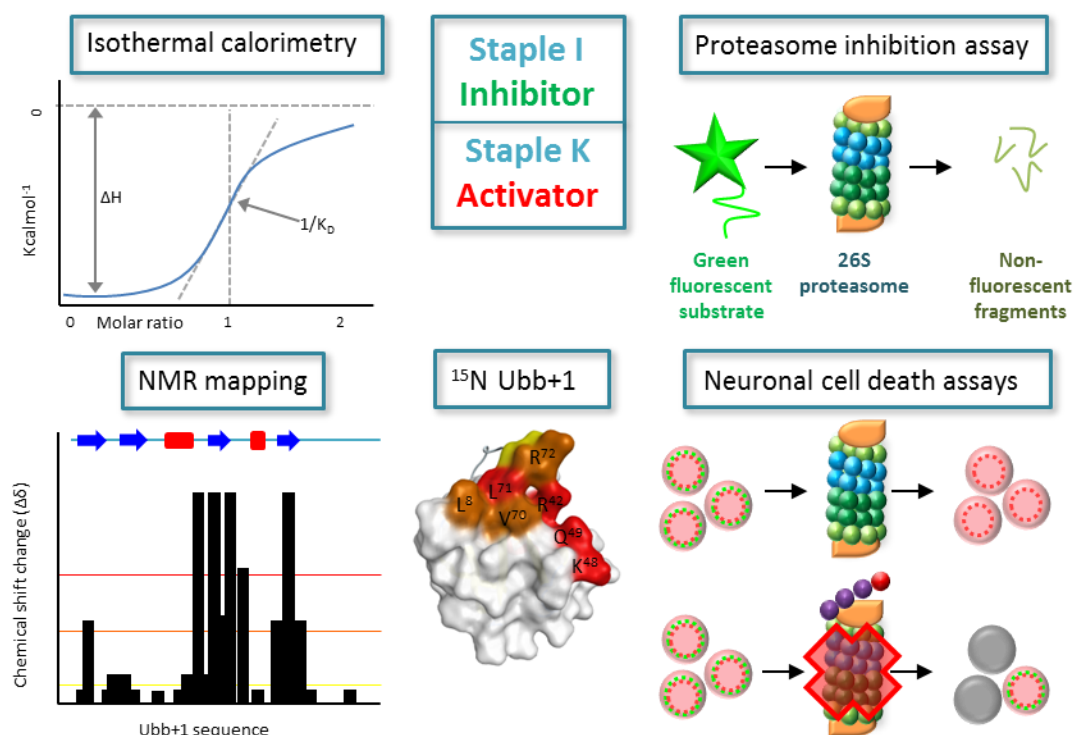

Figure 70 – Structural and biological assays to analyse active stapled peptides

A range of NMR experiments would also provide valuable information regarding the binding mode of Ubb+1 with stapled peptide analogues of α-9 of E2-25K. The first challenge associated with this work would be the cloning and purification of ^{15}N labelled Ubb+1, however this could be accomplished by following published procedures.[59] With this labelled Ubb+1 in hand, the binding mode of the peptides could be examined through analysis of chemical shift changes of Ubb+1 in the presence of the test peptides (Fig. 70). NMR mapping of the Ubb+1/**Staple I** interaction would indicate which residues in Ubb+1 experience the largest shift in chemical environement from the ligand binding. This experiment could confirm if **Staple I** binds to the same residues of Ubb+1 as the UBA domain of E2-25K, as predicted. Similarly, NMR mapping of the Ubb+1/**Staple K** interaction could potentially confirm the proposal that the pyridyl extension of **Staple K** binds to the tail region of Ubb+1 (Section 3.6.6). In principle, if this interaction was present, the

Ubb+1/**Staple K** interaction would have chemical shift changes in the tail region of Ubb+1 which would not be present in the Ubb+1/**Staple I** interaction. In addition to chemical shift analysis, similar titration experiments could be carried out to determine K_D for the binding of **Staples I** and **K** with Ubb+1. This can be calculated from plotting $\Delta\delta^1H$ vs molar ratio for key binding residues, in a similar fashion to the experiment published for the E2-25K/Ubb+1 PPI.[59]

This combination of ITC data with ^{15}N Ubb+1 NMR experiments could confirm the binding mode of these stapled peptides with Ubb+1. Of particular interest would be to determine if the experimental binding modes of these peptides corresponded with those calculated by *in silico* modelling. In addition to this, these experiments would provide valuable information regarding the mechanism of E2-25K mediated Ubb+1 capped PolyUb chain formation, and, in particular, whether **Staple K** can activate this pathway through constraining the unstructured tail of Ubb+1.

5.2 – Further biological evaluation of Ubb+1 in proteasomal inhibition

For inhibitor peptides, such as **Staples G** and **I**, the overall goal for these tool compounds would be to investigate their effectiveness in maintaining proteasomal efficiency through blocking the formation of these toxic Ubb+1 capped PolyUb chains. To accomplish this, several cellular assays could be carried out to investigate proteasomal function, and the subsequent effect on neuronal cell survival (Fig. 70). However, before such assays were carried out, the cell permeability of the stapled peptides of interest would need to be assessed. As discussed in detail in Section 1.7.3, there remains some debate in the published literature regarding the mechanism of cell penetration of such peptides; in particular whether positively charged stapled peptides can destabilise the cell membrane, causing cytotoxicity.[157,158] Despite this, there is strong evidence to suggest that helical peptides are rapidly internalised within the cytosol. Therefore, in order to ascertain whether active peptides, **Staples I** and **K** are cell permeable, fluorescently tagged analogues would need to be synthesised and analysed in cellular systems *via* confocal microscopy (Fig. 71).
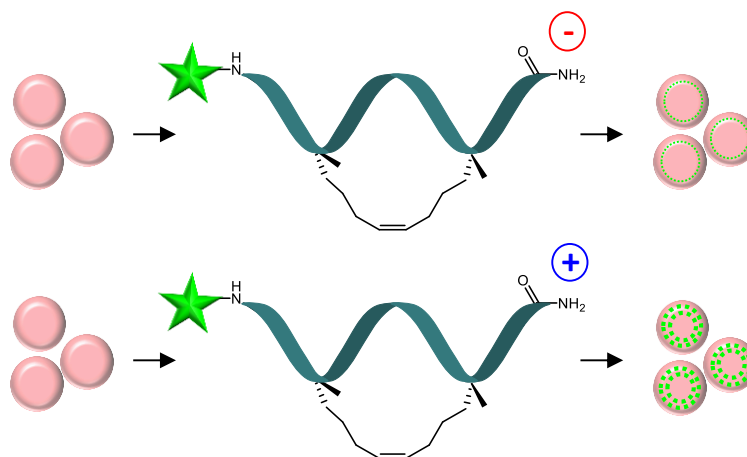
Figure 71 – Establishing stapled peptide cell permeability

There is the possibility that the electronic properties of these peptides which bear an overall negative charge would need to be tuned, as positively charged stapled peptides are more permeable on average.[205,219] However, once the cell permeable of these peptides has been established, further biological analysis of their activity in cellular systems can be investigated.

Proteasomal inhibition and neuronal cell death assays could be accomplished in an analogous fashion to the published data which analysed the effect of the E2-25K/Ubb+1 PPI on proteasomal function (Fig. 70).[59] Rat neuroblastoma cells transfected with E2-25K, GFPu (an artificial proteasome substrate of green fluorescent protein), DsRed (red fluorescent protein) and incubated with the test peptide for twenty four hours can be analysed by fluorescent microscopy to establish proteasomal function. Cells with healthy proteasomal function will clear the green fluorescent proteasome substrate (GFPu) and only exhibit DsRed using fluorescent microscopy. Therefore the relative accumulation of GFPu in the cytosol represents proteasomal inhibition due to lack of clearance, with proteasomally impaired cells exhibiting green/yellow fluorescence. In addition to this experiment, these transfected cells, when left for forty eight hours can be assessed for cell viability through analysing the overall cell morphology under a fluorescent microscope. This can give a percentage of cell death in a proteasomally inhibited cell in comparison to a healthy culture. For both of these cellular assays, the action of the inhibitor peptides, such as **Staple I**, have the potential to decrease proteasomal inhibition through blocking the formation of toxic Ubb+1 capped PolyUb chains. This could, in turn, increase cell survival, allowing the proteasome to retain

regular function and clear mono-Ubb+1 from the cell before it is transformed into toxic Ubb+1 PolyUb chains. A positive result such as this would further confirm the hypothesis that unanchored Ubb+1 capped PolyUb are the toxic component which lead to proteasomal inhibition and eventual cell death in neuronal cells expressing Ubb+1 and E2-25K. Similarly, if **Staple K** was shown to increase the rate of proteasomal inhibition and cell death compared to a negative control, then this adds further evidence that increased levels of Ubb+1 capped PolyUb chains are toxic in neuronal cells. These compounds could then be used to further test the propsed link between proteasomal inhibition and Alzheimer's disease in various model systems.

Overall, the work presented in this research programme provides compelling evidence that the E2-25K/Ubb+1 PPI is a valid target to investigate the effect of unanchored Ubb+1 capped PolyUb chains, and that the current active peptides, **Staple I** and **K**, could be developed further into valuable tool compounds. The further experiments proposed would lead to greater understanding of the mechanism of E2-25K mediated Ubb+1 capped PolyUb chain formation. Consequently, this could lead to further understanding of Ubb+1 mediated proteasomal inhibition and its overall effect on cell survival. As Ubb+1 and E2-25K are both highly expressed in the brains of patients with Alzheimer's disease (Section 1.1.2), it is anticipated that this work could eventually be developed to investigate the link between proteasomal inhibition and neuronal cell death. If proteasomal function could be retained through inhibition of the formation of Ubb+1 capped PolyUb chains, then it is proposed that cell clearance could be improved. This could subsequently decrease the rate of neuronal degradation associated with proteasomal inhibition, and would offer an alternative intervention strategy to the pathology of Alzheimer's disease.

6. Experimental

6.1 - General

All reagents, resins and solvents were obtained from commercial suppliers and were used without further purification unless otherwise stated. Purified solvents were stored in a septum-sealed oven dried flask over previously activated 4 Å molecular sieves, and purged and stored under N_2.

6.2 - Experimental details

I. Purging refers to a vacuum/N_2-refilling procedure
II. Room temperature was generally *ca*. 20 ^{o}C
III. Reactions carried out at elevated temperatures using a temperature regulated hotplate/stirrer
IV. Phase separation was carried out using IST Isolute Phase Separator Cartridges

6.3 – Purification of solvents and reagents

I. Anhydrous THF and DCM were obtained from a PureSolv SPS-400-5 solvent purification system.[220]
II. Benzyl chloride was purified through an alumina column.[221]
III. *t*BuOK was purified via sublimation.[221]

6.4 - Purification of products

I. Thin layer chromatography was carried out using Merck silica plates coated with fluorescent indicator UV254. These were analysed under 254 nm UV light, or developed using potassium permanganate, vanillin or ninhydrin solution.
II. Flash chromatography was carried out using IST Isolute Flash Silica SPE cartridges
III. Strong cation exchange chromatography was carried out using sulfonic acid functionalised DOWEX resin, 50WX8 H-form
IV. Small scale centrifugation carried out using an Eppendorf MiniSpin at 11 rpm for 3 minutes at room temperature.
V. Large scale centrifugation carried out using an Eppindorf 5804 centrifuge at 4000 rpm for 5 minutes at room temperature
VI. Reverse-phase HPLC purification of peptides was carried out using a Gilson preparative HPLC system of 322 pumps coupled to a 151 UV/Vis

spectrometer, 234 Autoinjector and a GX-271 liquid handler using a Agilent Zorbax SB-C18, 21.2 x 150 mm, 5 µm column at room temperature. Purifications were performed using gradient methods ranging from 5-90% MeCN in H_2O over 30 minutes at a flow rate of 10 mL/min, with UV monitoring at 214 nm. Analysis was carried out using Gilson Trilution software.

VII.   Freeze drying carried out on a Christ Alpha 1-2 LD plus freeze drier

6.5 - Analysis of products

I. ^1H and $^{13}C\{^1H\}$ NMR spectra were obtained on a Bruker DRX 500 spectrometer or AV3 500 HD spectrometer at 500 and 126 MHz, respectively; or on a Bruker AV3 400 spectrometer at 400 and 101 MHz, respectively. Chemical shifts are reported in ppm and coupling constants are reported in Hz with $CDCl_3$ referenced at 7.27 (^1H) and 77.23 (^{13}C) ppm and DMSO-d_6 referenced 2.50 (^1H) and 39.51 (^{13}C) ppm.[224]

II.   Fourier transformed infra-red (FTIR) spectra were obtained on a Shimadzu IRAffinity-1 machine.

III.   Low-resolution mass spectra were obtained on a ThermoQuest Finnigan LC duo coupled to a Razel syringe pump

IV.   Optical rotation performed on a Perkin Elmer 341 polarimeter.

V.   UV analysis was carried out on a Varian Cary 50 probe UV-visible spectrometer with spectral analysis carried out using the Varian Cary software

VI.   High-resolution mass spectra were obtained on a Thermofisher LTQ Orbitrap XL instrument at the ESPRC National Mass Spectrometry Service centre in Swansea

VII.   Reverse-phase analytical HPLC analysis of peptides was carried out on an Agilent 1260 Infinity system using a Macherey Nagel, EC 4.6 x 250 mm, Nucleodur C18 Gravity, 5 µm Column. Analysis was performed using a gradient method ranging from 5-90% MeCN in H_2O over 40 minutes at a flow rate of 1 mL/min, with UV monitoring at 214 nm. For spectra in figures 34 and 35 in which the UPLC analysis was conducted on an Acquity UPLC CSH C18 column (50 mm x 2.1 mm i.d. 1.7 µm packing diameter) at 40 degrees centigrade.

VIII.   Circular Dichroism was carried out on an Applied Photophysics Chirascan plus CD spectrometer with temperature control. All samples were prepared

using phosphate buffer solution (50 mM, pH 7). For 0.1 mm and 1 mm cells, peptides were made to a concentration of 200 µM and 50 µM, respectively. Machine parameters for each sample were as follows: Wavelength = 190 – 260 nm, Step resolution = 0.5 nm, accumulations = 10, Bandwidth = 1 nm, Temperature = 20 $^{\circ}$C. All spectra were measured in ellipticity (mdeg) after background substraction. All curves shown are smoothed using standard parameters. All temperature ramp experiments were run in a 2mm with concentrations ranging from 15 to 50 µM, specified per peptide. Temperature was raised by 5 $^{\circ}$C per spectra between 20 $^{\circ}$C and 80 $^{\circ}$C, then a final spectra run once sample was returned to 20 $^{\circ}$C. A baseline temperature ramp experiment was run for the phosphate buffer solution (50 mM, pH 7) to allow for background subtraction.

IX. Helicity calculated from mean residue ellipticity (See Fig. 37) divided by maximum mean residue ellipticity (Table 32) at 222 nm where T = Temp ($^{\circ}$C) = 20 $^{\circ}$C, n = no. of amino acids in peptide = 11, K = Correction factor = 3, C = Sample concentration (M), l = Cell path length (mm)

Table 32 – Calculated maximum mean residue ellipticity at 222 nm

Temp. ($^{\circ}$C)	n	$[\theta_{max}]$
20	11	-28364
20	12	-29250

X. Normal-phase chiral HPLC was carried out on an Agilent 1260 Infinity system using a Chiralpak IA (Amylose tris(3,5-dimethylphenylcarbamate)) column at room temperature. Analysis of nickel complexes was achieved using 40% IPA in hexane over 40 minutes. Separation of Fmoc amino acids was achieved using a gradient of 5 – 20% IPA in hexane over 20 minutes.

6.6 - Peptide experimental details

I. All Fmoc-protected amino acids were purchased from Novabiochem unless stated in the text.

II. 1-[Bis(dimethylamino)methylene]-1*H*-1,2,3-triazolo[4,5-*b*]pyridinium 3-oxide hexafluorophosphate (HATU) and 1-Hydroxy-7-azabenzotriazole (HOAt) were purchased from Fluorochem.

III. Triisopropyl silane (TIS), Piperidine, N-methylmorpholine (NMM) and Trifluoroacetic acid (TFA) were purchased from Alfa Aesar.

IV.   Acetic anhydride, Diisopropylethylamine (DIPEA) and Bis(tricyclohexylphosphine)benzylidine ruthenium(IV) dichloride (Grubbs 1st generation catalyst) were purchased from Sigma-Aldrich.

V.   All final peptides were synthesised using Rink amide MBHA resin (0.78 mmol/g loading) which was purchased from Novabiochem unless otherwise stated in the text.

VI.   All solvents were purchased from Sigma-Aldrich with the exception of dimethylformamide (DMF) which was purchased from Rathburn Chemicals Ltd.

VII. All manual couplings were performed in a Merrifield bubbler attached to a vacuum line, a nitrogen line and large round bottomed flask for waste.

VIII. All automated couplings were carried out on a Protein Technologies, Tribute automated synthesiser. The solvents attached to the synthesiser were: DMF, DCM, 20% (v/v) piperidine in DMF, 0.5 M DIPEA in DMF and 15% (v/v) acetic anhydride in DMF.

IX.   All peptides were cleaved from the resin using a mixture of TFA/TIS/H$_2$O (95:2.5:2.5). For 10 mL of stock solution, TFA (9.5 mL), TIS (250 µL) and H$_2$O (250 µL) were mixed in a clean sample vial which was capped until needed. Solution was discarded after 3 days.

6.7 - Peptide synthesis general procedures

I.   Resin was swollen in DCM (10 mL) for 10 minutes prior to any synthesis.

II.   A washing procedure using DMF (5 x 5 mL x 30 seconds) was carried out between all steps (eg III, IV and V).

III. Deprotections were carried out before all couplings using a solution of 20% (v/v) piperidine in DMF (3 x 5 mL x 5 minutes).

IV.   N-terminal capping was achieved using 15% (v/v) acetic anhydride in DMF (3 x 5 mL x 5 minutes).

V.   Couplings were carried out according to the methods in Table 33 below.

Table 33 – Peptide coupling methods

Method	Manual / Automated	Amino acid Equiv.	Coupling Agent (Equiv.)	Base (Equiv.)	Solvent	Coupling time
i)	Manual	5	HATU (5)	DIPEA (10)	DMF (5 mL)	4 h
ii)	Automated	5	HATU (5)	DIPEA (10)	DMF (5 mL)	20 min
iii)	Manual	2.5	HATU (2.5)	DIPEA (5)	DMF (5 mL)	2 h
iv)	Automated	5	HATU (5)	DIPEA (10)	DMF (5 mL)	2 x 2 h
v)	Automated	5	HATU (5), HOAt (4)	DIPEA (10)	DMF (5 mL)	2 x 2h
vi)	Automated	5	HATU (5)	DIPEA (10)	DMF (5 mL)	2 x 30 min
vii)	Automated	5	HATU (5)	DIPEA (10)	DMF (5 mL)	2 h
viii)	Manual	1.7	HATU (1.7)	DIPEA (3.4)	DMF (5 mL)	2 h

VI.   Ring-closing metathesis was achieved using 40 mol% Grubbs 1st generation catalyst in DCM (10 mM). Methathesis was complete after 3 x 2 h reactions. Stitched peptide **Staple N** was achieved using 20 mol% Grubbs 1st generation catalyst in DCM (10 mM). Washing with DCM (5 x 5 mL x 30 seconds), DMF (5 x 5 mL x 30 seconds) and DCM (5 x 5 mL x 30 seconds) was carried out before resin drying.

VII.   Allyl deprotection of **Staples J**, **K** and **M** were carried out using 4 x Pd(PPh$_3$)$_4$ (10 mol%) and PhSiH$_3$ (10 equiv.) in DCM (5 mL). Allyl deprotection of **Staples P** and **R** were carried out using 4 x Pd(PPh$_3$)$_4$ (10 mol%) and N-methyl morpholine (3 equiv.) in DCM (5 mL). Both reactions were followed by washing with DCM (5 x 5 mL x 30 seconds) and DMF (5 x 5 mL x 30 seconds). Resin was then treated with sodium diethyldithiocarbamate trihydrate (0.8 equiv) in DMF (4 x 5 mL).

VIII.   All peptides were dried when switching between manual and automated methods, or upon completion of the synthesis. Procedure was washing of the resin with DCM (5 x 5 mL x 30 seconds) and drying under vacuum (manual) or a stream of N$_2$ (automated) for 10 minutes.

IX.   Fmoc loading test: two 10 mL volumetric flasks were charged with a known mass of resin (~ 5 mg). The flasks were then filled to the 10 mL mark with 20% piperidine in DMF solution, stoppered and sealed with parafilm. The flasks were simultaneously sonicated for 15 minutes. After this time the UV absorption of each solution at 302 nm was measured. This absorption was then used in the calculation shown in Fig. 72, which is derived from the Beer-Lambert law, to give the loading of the resin. The average value of the two tests was taken as the overall loading of the sample resin.

$$\text{Loading} = \frac{A \times 10}{m \times 7.8}$$

where $A = absorption\ at\ 302\ nm$, $m = mass\ of\ resin\ tested$ (mg)

Figure 72 – Fmoc loading test equation

X. Trial cleavage reactions were carried out using 10 mg of resin with 250 µL of cleavage solution. The resin was left to stir at r.t for 1 h under nitrogen. The resin was then filtered into a 1.5 mL microcentrifuge tube filled with cold Et_2O (1 mL). The sample was then centrifuged for 3 minutes and the supernatant discarded. Two further cycles of cold Et_2O washes and centrifugation were carried out to give the crude peptide as an off white solid. The peptide was then dissolved in H_2O (0.5 mL) and MeCN (0.5 mL). If required, a few drops of TFA or NH_3 were added to allow complete dissolution. The resulting solution was then used for HPLC and MS analysis.

XI. Full cleavage reactions were charged with 10 mL of cleavage solution. The resin was left to stir at r.t for 4 h. The resin was then filtered into a 50 mL falcon tube filled with cold Et_2O (25 mL). The sample was then centrifuged for 3 minutes and the supernatant discarded. Two further cycles of cold Et_2O washes and centrifugation were carried out to give the crude peptide as an off white solid. The peptide was then dissolved in minimal H_2O and MeCN. If required, a few drops of TFA or NH_3 were added to allow complete dissolution. The resulting solution was then purified by preparative HPLC and the product fractions freeze dried. The product peptides were obtained as white solids.

6.8 - Screening of Thr coupling procedures

I. Couplings in Section 3.2.3 were carried out according to methods in Table 34

Table 34 – Screening coupling conditions

Method	Manual / Automated	Amino acid equiv.	Coupling Agent (Equiv.)	Base (Equiv.)	Solvent	Coupling time
i)	Automated	5	HCTU (5)	DIPEA (10)	NMP (5 mL)	2 x 20 min
ii)	Automated	5	HCTU (5)	DIPEA (10)	NMP (5 mL)	2 x 2 h
iii)	Automated	5	HCTU (5)	DIPEA (10)	NMP (5 mL)	20 min
iv)	Automated	5	HCTU (5)	DIPEA (10)	NMP (5 mL)	1 h

II. Synthesis of **Staple A1** (Section 3.2.3) with methods shown in Table 34

Table 35 – Synthesis of Staple A1

Sequence	Ac	V	E	T	S$_5$	T	E	L	S$_5$	L	S	N	NH$_2$
Method		ii)	ii)	ii)	ii)	i)	i)	ii)	ii)	i)	i)	i)	

III.   Synthesis of **Staple A2** (Section 3.2.3) with methods shown in Table 34

Table 36 – Synthesis of Staple A2

Sequence	H$_2$N	S$_5$	T	E	L	S$_5$	L	S	N	NH$_2$
Method		ii)	i)	i)	ii)	ii)	i)	i)	i)	

IV.   Synthesis of **Staple A3** (Section 3.2.3) with methods shown in Table 34

Table 37 – Synthesis of Staple A3

Sequence	Ac	V	E	T	S$_5$	T	E	L	S$_5$	L	S	N	NH$_2$
Method		i)	i)	ii)	iv)	iii)	iii)	iii)	iv)	iii)	iii)	iii)	

V.   Synthesis of **Wild type** screen (Section 3.2.3) with methods shown in Table 34

Table 38 – Synthesis of Wild type peptide screen

Sequence	Ac	V	E	T	S$_5$	T	E	L	S$_5$	L	S	N	NH$_2$
Method		i)	i)	i)	i)	i)	i)	i)	i)	i)	i)	i)	

VI.   Threonine coupling screenof **Staple A2** (Section 3.2.3) was carried out according to the methods in Table 35

Table 39 – Screening of threonine coupling

Method	Manual / Automated	Amino acid equiv.	Coupling Agent (Equiv.)	Base (Equiv.)	Solvent	MW temp. (ºC)	Coupling time
a)	Automated	5	HATU (5), HOAt (4)	DIPEA (10)	NMP (2 mL)		1 h
b)	Automated	5	DIC (5), HOAt (5)		NMP (2 mL)		1 h
c)	Automated	5	HATU (5)	DIPEA (10)	NMP (3 mL)	70	2 x 20 min

6.9 - Peptide NMR

I.   **Staple A** [1]H, NOESY and TOCSY data were obtained at 2 mM in phosphate buffer (50 mM, pH7, 10% D$_2$O, 90% H$_2$O). COSY data was obtained with **Staple A** diluted to 2 mM in D$_2$O. **Staple G** and **I** [1]H, NOESY and TOCSY

data were obtained at 2 mM in phosphate buffer (50 mM, pH7, 10% D_2O, 90% H_2O).

II. All spectra were obtained on a Bruker Advance II$^+$ NMR spectrometer operating at 600.13 MHz for ^1H resonances.

III. Spectra were acquired at a probe temperature of 298 K unless otherwise stated.

IV. A TBI-Z [^1H, ^{13}C, D-BB] 5mm probehead equipped with an actively shielded z-gradient coil was used for data acquisition, carried out at a magnetic field strength of 14.1 T.

V. One-dimensional ^1H NMR data were acquired using a Bruker excitation sculpting sequence (zgesgp) to eliminate the solvent resonance. Data was acquired at 128 scans over a frequency of 7.2 kHz (12 ppm), centered at 4.703 ppm into 32.8K data points (acquisition time of 2.27 s) with a total spectra time of 9 minutes.

VI. For **Staple A**, two dimensional [^1H, ^1H] NMR data sets were acquired as follows: Phase-sensitive 2D NOESY with excitation sculpting using a 180 water selective pulse (noesyesgpph) sequence was applied. Data was acquired using 32 transients for each of 2 x 512 States t_1 increments over a frequency width of 7 kHz (12 ppm) in both ω_2 and ω_1 dimensions, into 4K (acquisition time 284 ms) data points, with a recycle time of 3 s and a mixing time of 150 ms for a total accumulation time of *ca.* 16 h. Phase-sensitive 2D TOCSY with excitation sculpting using a 180 water selective pulse (dipsi2esgpph) sequence was applied. Data was acquired using 32 transients for each of 2 x 512 States t_1 increments over a frequency width of 7 kHz (12 ppm) in both ω_2 and ω_1 dimensions, into 4K (acquisition time 284 ms) data points, with a recycle time of 2 s and a mixing time of 70 ms for a total accumulation time of *ca.* 11 h. Phase-sensitive 2D COSY-DQF (cosydfphps) sequence was applied. Data was acquired using 48 transients for each of 2 x 256 States t_1 increments over a frequency width of 3.6 kHz (6 ppm) in both ω_2 and ω_1 dimensions, into 2K (acquisition time 284 ms) data points, with a recycle time of 2 s for a total accumulation time of *ca.* 8 h.

VII. For **Staples G** and **I**, two dimensional [^1H, ^1H] NMR data sets were acquired as follows: Phase-sensitive 2D NOESY with excitation sculpting using a 180 water selective pulse (noesyesgpph) sequence was applied. Data was acquired using 32 transients for each of 2 x 512 States t_1 increments over a

frequency width of 7 kHz (12 ppm) in both ω_2 and ω_1 dimensions, into 4K (acquisition time 284 ms) data points, with a recycle time of 3 s and a mixing time of 250 ms for a total accumulation time of *ca.* 16 h. Phase-sensitive 2D TOCSY with excitation sculpting using a 180 water selective pulse (dipsi2esgpph) sequence was applied. Data was acquired using 32 transients for each of 2 x 512 States t_1 increments over a frequency width of 7 kHz (12 ppm) in both ω_2 and ω_1 dimensions, into 4K (acquisition time 284 ms) data points, with a recycle time of 2 s. Two spectra with mixing times of 70 ms and 15 ms were acquired separately with total accumulation times of *ca.* 11 h each to give both long and short range signals.

VIII.   SPARKY NMR visualisation software was used to interpret, assign and integrate all 2D spectra.[207]

6.10 - Models

I.   Chemical Computing Group's Molecular Operating Environment (MOE) software was used to visualise, edit and compute all structures.[206]

II.   An AMBER12:EHT force field was used for all energy calculations.[222]

III.   Peptide models were created through modifications of the crystal structure of E2-25K in complex with Ubb+1 (PDB ID 3K9O).[59] The structure of E2-25K was edited to only the α9 segment (Val[190] – Asn[200]) and modified to each peptide structure using the builder function of the software.

IV.   All *i*, *i*+4 staples were assumed to be *cis* configuration and all *i*, *i*+7 staples were assumed to be *trans* based on the work by Verdine et al.[223]

V.   Free peptides were energy minimised, then minimised again against the full Ubb+1 structure.

VI.   Structural comparisons of Ubb+1 with ubiquitin, the X-ray crystal structures of Ubb+1 (PDB ID:3K9O) and ubiquitin (PDB ID:3K9P) in complex with E2-25K were overlayed using the align tool in MOE.

VII.   Structural comparisons between the X-ray crystal structure of Ubb+1 with the calculated NMR solution structure (PDB ID:2KX0) was accomplished using the MOE align tool.

6.11 - Polyubiquitination assays[216]

I.   Reaction buffer stock solution contained 500 mM Tris buffer, 100 mM MgCl$_2$, 10 mM ATP, 10 mM DTT (pH 7.5). Peptides were prepared as a 300 µM stock solution in reaction buffer.

II. All reactions were carried out containing Ubb+1 (2 µM), Ub (2 µM), E1 (0.1 µM), E2-25K (1 µM) and test peptide (30 µM) and made up to 50 µL with distilled water.

III. The reactions were incubated for 4 hours at 37 $^{\circ}$C on a shaking incubator then quenched with 20 µL of SDS-PAGE gel application buffer. The reaction solution was then split into equal 35 µL aliquots and run on a 5-20% SDS-PAGE gradient gel. One set of samples was probed *vs* anti-VU1 (anti-ubiquitin, 1:1000) and the other *vs* anti-Ubb+1 (1:1000)

6.12 - Small molecule data

125 – Benzyl-L-proline hydrochloride
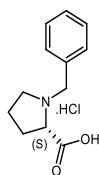
To a round bottomed flask containing 2-propanol (60 mL) at 40 ^{o}C was added L-proline (**119**) (10 g, 86.6 mmol, 1 equiv.) and the reaction mixture stirred at this temperature until fully in solution. The reaction mixture was then cooled to 0 ^{o}C and KOH (19.5 g, 347.2 mmol, 4 equiv.) was added and stirred for 5 minutes. Benzyl chloride (**124**) (15 mL, 130.2 mmol, 1.5 equiv.) was added dropwise over 15 minutes, maintaining the temperature between 0 ^{o}C and 5 ^{o}C. Once addition was complete, the reaction mixture was heated to 40 ^{o}C and stirred for 17 hr. Once complete, the reaction mixture was cooled to room temperature and acidified to pH 4 with conc. HCl. DCM (150 mL) was added and the flask placed in the fridge overnight. The precipitate was then filtered off and the filtrate concentrated *in vacuo*. The residue was suspended in acetone to give a white solid. Filtration and washing with cold acetone afforded the title compound as a white solid (17.242 g, 82%).

v_{max} (neat): 3005, 2993, 2953, 1713, 1672, 1498 cm^{-1}

^{1}H NMR (400 MHz, DMSO-d_6): δ 7.45 – 7.42 (m, 2H, 2 x Aro CH), 7.40 – 7.32 (m, 3H, 3 x Aro CH), 5.12 (br s, 1H, COOH), 4.19 (d, 1H, Benzyl CH, *J* = 13.2 Hz), 3.91 (d, 1H, Benzyl CH, *J* = 13.2 Hz), 3.57 (dd, 1H, Pro CH, *J* = 6, 3.2 Hz), 3.20 – 3.15 (m, 1H, Pro CH), 2.81 – 2.74 (m, 1H, Pro CH), 2.24 – 2.14 (m, 1H, Pro CH), 1.96 – 1.81 (m, 2H, 2 x Pro CH), 1.78 – 1.71 (m, 1H, Pro CH).

^{13}C NMR (101 MHz, DMSO-d_6): δ 171.6, 134.8, 129.6, 128.4, 128.1, 65.8, 57.2, 53.1, 28.4, 22.6

HRMS: (C$_{12}$H$_{16}$O$_2$N$_1$) [M+H]$^+$ requires 206.1176, found [M+H]$^+$ 206.1175

$[α]^{20}_D$ = -28.8 (c = 1, MeOH)

Literature value $[α]^{25}_D$ = -25.8 (c = 1, EtOH)[194]

140 – Benzyl-D-proline hydrochloride
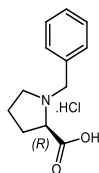
To a round bottomed flask containing 2-propanol (30 mL) at 40 ^{o}C was added D-proline (**139**) (3 g, 26 mmol, 1 equiv.) and the reaction mixture stirred at this temperature utill fully in solution. The reaction mixture was then cooled to 0 ^{o}C and KOH (5.85 g, 104 mmol, 4 equiv.) was added and stirred for 5 minutes. Benzyl chloride (**124**) (4.5 mL, 39 mmol, 1.5 equiv.) was added dropwise over 10 minutes, maintaining the temperature between 0 ^{o}C and 5 ^{o}C. Once addition was complete, the reaction mixture was heated to 40 ^{o}C and stirred for 17 hr. After this time, the reaction mixture was cooled to r.t and acidified to pH 4 with conc. HCl. DCM (100 mL) was added and the flask placed in the fridge overnight. The precipitate was then filtered off and the filtrate concentrated in vacuo. The residue was suspended in acetone to give a white solid. Filtration and washing with cold acetone afforded the title compound as a white solid (5.121 g, 81%).

v_{max} (neat): 2953, 1715, 1672, 1456 cm^{-1}

^{1}H NMR (400 MHz, DMSO-d_6): δ 7.47 – 7.46 (m, 2H, 2 x Aro CH), 7.40 – 7.34 (m, 3H, 3 x Aro CH), 4.26 (d, 1H, Benzyl CH, J = 13.2 Hz), 4.02 (d, 1H, Benzyl CH, J = 12.8 Hz), 3.76 – 3.72 (m, 1H, Pro CH), 3.26 – 3.21 (m, 1H, Pro CH), 2.91 – 2.87 (m, 1H, Pro CH), 2.27 – 2.22 (m, 1H, Pro CH), 1.94 – 1.89 (m, 2H, 2 x Pro CH), 1.88 – 1.78 (m, 1H, Pro CH).

^{13}C NMR (101 MHz, DMSO-d_6): δ 170.7, 132.9, 130.2, 128.7, 128.5, 65.6, 57.1, 53.5, 28.2, 22.2

HRMS: ($C_{12}H_{16}O_2N_1$) [M+H]$^+$ requires 206.1176, found [M+H]$^+$ 206.1174

[α]$^{20}_D$ = +28.2 (c = 1, MeOH)

126 – (*S*)-N-(2-benzoylphenyl)-1-benzylpyrrolidine-2-carboxamide
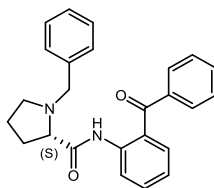
To a round bottomed flask containing dry DCM (475 mL) under N_2 was added **125** (34.5 g, 142.8 mmol, 1 equiv.) to form a cloudy suspension. The reaction mixture was cooled to -20 °C using a mixture of ice and NaCl (1:3), giving (on average) an internal temperature of -5 °C. *N*-Methyl imidazole (31.8 mL, 399.2 mmol, 2.8 equiv.) was then added and stirred for 5 minutes. Methanesulfonyl chloride (12.2 mL, 156.8 mmol, 1.1 equiv.) was then added slowly over 5 minutes, maintaining the internal temperature at between -5 °C and 0 °C. The reaction mixture was then left to stir at -5 °C to 0 °C for 30 minutes. 2-Aminobenzophenone (**138**) (25.3 g, 128.3 mmol, 0.9 equiv.) was then added and the reaction mixture left to stir at room temperature for 17 hr. The reaction mixture was quenched with sat. NH_4Cl and extracted with DCM (3 x 400 mL). The organic layers were combined, dried and concentrated in vacuo to give the crude as a dark brown oil. The crude was then purified by silica chromatography (0-100% EtOAc in Pet. Eth.) to give the title compound as a yellow solid (42.3 g, 86%).

v_{max} (neat): 3248, 2968, 2839, 2810, 1687, 1643, 1576, 1510, 1442 cm^{-1}

^{1}H NMR (400 MHz, CDCl$_3$): δ 11.54 (s, 1H, NH), 8.59 (dd, 1H, Aro CH, *J* = 7.6, 1.2 Hz), 7.82 – 7.80 (m, 2H, 2 x Aro CH), 7.67 – 7.61 (m, 1H, Aro CH), 7.57 – 7.45 (m, 4H, 4 x Aro CH), 7.41 – 7.39 (m, 2H, 2 x Aro CH), 7.18 – 7.15 (m, 3H, 3 x Aro CH), 7.13 – 7.09 (m, 1H, Aro CH), 3.95 (d, 1H, Benzyl CH, *J* = 13.2 Hz), 3.62 (d, 1H, Benzyl CH, *J* = 13.2 Hz), 3.35 (dd, 1H, Pro CH, *J* = 5.2, 4.8 Hz), 3.27 – 3.22 (m, 1H, Pro CH), 2.47 – 2.40 (m, 1H, Pro CH), 2.33 – 2.23 (m, 1H, Pro CH), 2.03 – 1.96 (m, 1H, Pro CH), 1.90 – 1.76 (m, 2H, 2 x Pro CH).

^{13}C NMR (101 MHz, CDCl$_3$): δ 197.5, 174.1, 138.7, 138.1, 137.7, 132.9, 132.1, 132.0, 129.6, 128.7, 127.8, 127.7, 126.6, 124.9, 121.7, 121.1, 67.8, 59.4, 53.4, 30.5, 23.7

HRMS: (C$_{25}$H$_{25}$O$_2$N$_2$) [M+H]$^+$ requires 385.1911, found [M+H]$^+$ 385.1908

$[α]^{20}_D$ = -106.7 (c = 1, MeOH)

Literature value $[α]^{20}_D$ = -134 (c = 1, MeOH)[194]

ee = >98 % by chiral HPLC

141 – (R)-N-(2-benzoylphenyl)-1-benzylpyrrolidine-2-carboxamide
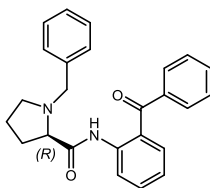
To a round bottomed flask containing dry DCM (50 mL) under N_2 was added **140** (7.395 g, 30.6 mmol, 1 equiv.) to form a cloudy suspension. The reaction mixture was cooled to -20 °C using a mixture of ice and NaCl (1:3), giving (on average) an internal temperature of -5 °C. *N*-Methyl imidazole (9.756 mL, 85.7 mmol, 2.8 equiv.) was then added and stirred for 5 minutes. Methanesulfonyl chloride (2.373 mL, 33.6 mmol, 1.1 equiv.) was then added slowly over 5 minutes, maintaining the internal temperature at between -5 °C to 0 °C. The reaction mixture was then left to stir at -5 °C to 0 °C for 30 minutes. 2-Aminobenzophenone (**138**) (5.432 g, 27.5 mmol, 0.9 equiv.) was then added and the reaction mixture left to stir at room temperature for 17 hr. The reaction mixture was quenched with sat. NH_4Cl and separated with DCM (3 x 100 mL). The organic layers were combined, dried and concentrated in vacuo to give the crude as a dark brown oil. The crude was then purified by silica chromatography (0-100% EtOAc in Pet. Eth.) to give the title compound as a yellow solid (9.0 g, 85%).

v_{max} (neat): 3250, 2963, 2822, 1688, 1640, 1515, 1442 cm^{-1}

^{1}H NMR (400 MHz, CDCl$_3$): δ 11.52 (s, 1H, NH), 8.58 (dd, 1H, Aro CH, J = 7.6, 0.8 Hz), 7.80 – 7.78 (m, 2H, Aro CH), 7.64 – 7.60 (m, 1H, Aro CH), 7.56 – 7.49 (m, 4H, 4 x Aro CH), 7.40 – 7.37 (m, 2H, 2 x Aro CH), 7.17 – 7.14 (m, 3H, 3 x Aro CH), 7.12 – 7.08 (m, 1H, Aro CH), 3.93 (d, 1H, Benzyl CH, J = 12.8 Hz), 3.61 (d, 1H, Benzyl CH, J = 12.8 Hz), 3.33 (dd, 1H, Pro CH, J = 5.2, 4.8 Hz), 3.23 – 3.21 (m, 1H, Pro CH), 2.45 – 2.40 (m, 1H, Pro CH), 2.30 – 2.22 (m, 1H, Pro CH), 2.00 – 1.96 (m, 1H, Pro CH), 1.83 – 1.77 (m, 2H, 2 x Pro CH).

^{13}C NMR (101 MHz, CDCl$_3$): δ 197.5, 174.2, 138.7, 138.1, 137.7, 132.9, 132.1, 132.0, 129.6, 128.7, 127.8, 127.7, 126.6, 124.9, 121.7, 121.1, 67.8, 59.4, 53.4, 30.5, 23.7

HRMS: (C$_{25}$H$_{25}$O$_2$N$_2$) [M+H]$^+$ requires 385.1911, found [M+H]$^+$ 385.1910

[α]$^{20}_D$ = +106.63 (c = 1, MeOH)

ee = >98 % by chiral HPLC

127 - (*S*)-Ni(II)-Ala-BPB
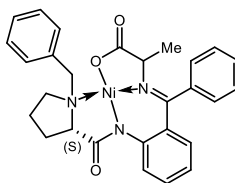
Procedures described in Scheme 23

To a round bottomed flask containing MeOH (50 mL) under N_2 was added **126** (11.521 g, 30.0 mmol, 1 equiv.), DL-Alanine (13.35 g, 149.8 mmol, 5 equiv) and $Ni(NO_3)_2.6H_2O$ (17.438 g, 59.9 mmol, 2 equiv.) and the contents heated to 50 ^{o}C. KOH (13.450 g, 239.7 mmol, 8 equiv) was then added to the reaction vessel. Once addition was complete, the reaction mixture was heated to 50 ^{o}C and left to react overnight. The reaction was cooled to room temperature and neutralised with conc. acetic acid. Water (400 mL) and DCM (250 mL) were added to the reaction vessel and left to stir overnight. The mixture was then separated with DCM (3 x 400 mL) and the organic layers combined, dried and concentrated *in vacuo* to give the crude product as a red oil. The crude material was then purified by silica chromatography (0-100% EtOAc in Pet. Eth., 0-5% MeOH in EtOAc) to give the title compound as a bright red solid (12.667 g, 83%).

$[\alpha]^{20}_D$ = +2091 (c = 0.03, MeOH)
Literature value $[\alpha]^{25}_D$ = +2643 (c = 0.036, MeOH)[194]
de = 98% by ^{1}H NMR

Procedures described in Scheme 28

127a and 127b

To a round bottomed flask containing MeOH (70 mL) under N_2 was added **126** (7.680 g, 20 mmol, 1 equiv.), DL-Alanine (3.60 g, 40 mmol, 2 equiv) and $Ni(NO_3)_2.6H_2O$ (11.630 g, 40 mmol, 2 equiv.) and the contents heated to 40 ^{o}C. A solution of KOH (7.840 g, 140 mmol, 7 equiv.) in MeOH (30 mL) was added dropwise to the reaction vessel over 10 minutes. Once addition was complete, the reaction mixture was heated to 50 ^{o}C and left to react for 2 hours. The reaction was cooled to room temperature and neutralised with conc. acetic acid. Water (400 mL) and DCM (200 mL) were added to the reaction vessel and left to stir overnight. The mixture was then separated with DCM (3 x 300 mL) and the organic layers

combined, dried and concentrated *in vacuo* to give the crude product as a red oil. The crude material was then purified by silica chromatography (0-100% EtOAc in Pet. Eth., 0-5% MeOH in EtOAc) to give the title compound as a bright red solid.

127a (7.928 g, 77%)

127b (7.546 g, 74%).

$[\alpha]^{20}_D$ = +2669 (c = 0.03, MeOH)
Literature value $[\alpha]^{25}_D$ = +2643 (c = 0.036, MeOH)[194]
de = 98% by ^{1}H NMR

Data

ν_{max} (neat): 2976, 2872, 1678, 1622, 1591, 1548, 1440 cm^{-1}
^{1}H NMR (400 MHz, CDCl$_3$): δ 8.12 – 8.06 (m, 3H, 3 x Aro CH), 7.54 – 7.44 (m, 3H, 3 x Aro CH), 7.39 (t, 2H, 2 x Aro CH, *J* = 8.4 Hz), 7.27 – 7. 12 (m, 3H, 3 x Aro CH), 6.96 (d, 1H, Aro CH, *J* = 7.6 Hz), 6.68 – 6.61 (m, 2H, 2 x Aro CH), 4.41 (d, 1H, Benzyl CH, *J* = 12.8 Hz), 3.91 (q, 1H, α-CH, *J* = 7.2 Hz), 3.75 – 3.69 (m, 1H, Pro CH), 3.56 (d, 1H, Benzy CH, *J* = 12.8 Hz), 3.53 – 3.47 (m, 1H, Pro CH), 2.77 – 2.72 (m, 1H, Pro CH), 2.59 – 2.51 (m, 1H, Pro CH), 2.25 – 2.18 (m, 1H, Pro CH), 2.11 – 2.04 (m, 1H, Pro CH), 1.60 (d, 2.9H, Ala CH$_3$, *J* = 7.2 Hz), 1.40 (d, 0.05H, Ala CH$_3$, *J* = 8.8 Hz, peak used to calculate dr)
^{13}C NMR (101 MHz, CDCl$_3$): 180.3, 180.3, 170.1, 142.0, 133.4, 133.3, 133.0, 131.9, 131.4, 129.6, 128.8, 128.7, 127.4, 127.1, 126.3, 123.8, 120.7, 70.1, 66.4, 63.0, 57.2, 30.7, 24.0, 21.7
HRMS: (C$_{28}$H$_{28}$O$_3$N$_3$Ni) [M+H]$^+$ requires 512.1479, found [M+H]$^+$ 512.1467

128 - (*R*)-Ni(II)-Ala-BPB
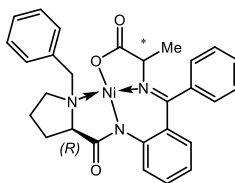
Procedures described in Scheme 23

To a round bottomed flask containing MeOH (30 mL) under N_2 was added **141** (5.885 g, 15.3 mmol, 1 equiv.), DL-Alanine (6.818 g, 76.5 mmol, 5 equiv) and $Ni(NO_3)_2.6H_2O$ (7.982 g, 30.6 mmol, 2 equiv.) and the contents heated to 50 °C. KOH (6.870 g, 122.4 mmol, 8 equiv) was then added to the reaction vessel. Once addition was complete, the reaction mixture was heated to 50 °C and left to react overnight. The reaction was cooled to room temperature and neutralised with conc. acetic acid. Water (200 mL) and DCM (100 mL) were added to the reaction vessel and left to stir overnight. The mixture was then separated with DCM (3 x 200 mL) and the organic layers combined, dried and concentrated *in vacuo* to give the crude product as a red oil. The crude material was then purified by silica chromatography (0-100% EtOAc in Pet. Eth., 0-5% MeOH in EtOAc) to give the title compound as a bright red solid (6.305 g, 80%).

Procedures described in Scheme 28

To a round bottomed flask containing MeOH (20 mL) under N_2 was added **141** (2.0 g, 5,2 mmol, 1 equiv.), DL-Alanine (0.927 g, 10.4 mmol, 2 equiv) and $Ni(NO_3)_2.6H_2O$ (3.025 g, 10.4 mmol, 2 equiv.) and the contents heated to 40 °C. A solution of KOH (2.043 g, 36.41 mmol, 7 equiv) in MeOH (10 mL)) was added dropwise to the reaction vessel over 10 minutes. Once addition was complete, the reaction mixture was heated to 50 °C and left to react for 2 hours. The reaction was cooled to room temperature and neutralised with conc. acetic acid. Water (100 mL) and DCM (50 mL) were added to the reaction vessel and left to stir for 3 hours. The mixture was then separated with DCM (3 x 100 mL) and the organic layers combined, dried and concentrated *in vacuo* to give the crude product as a red oil. The crude material was then purified by silica chromatography (0-100% EtOAc in Pet. Eth., 0-5% MeOH in EtOAc) to give the title compound as a bright red solid (2.358 g, 88%).

$[α]^{20}_D$ = -2043 (c = 0.03, MeOH)

de = 80% by ^{1}H NMR

Data

v_{max} (neat): 3024, 2978, 2872, 1678, 1624, 1591, 1438 cm^{-1}

^{1}H NMR (400 MHz, CDCl$_3$): δ 8.12 – 8.07 (m, 3H, 3 x Aro CH), 7.55 – 7.44 (m, 3H, 3 x Aro CH), 7.38 (t, 2H, 2 x Aro CH, J = 8.4 Hz), 7.31 – 7. 15 (m, 3H, 2 x Aro CH, CDCl$_3$), 7.14 – 7.11 (m, 1H, Aro CH), 6.95 (d, 1H, Aro CH, J = 7.6 Hz), 6.69 – 6.61 (m, 2H, 2 x Aro CH), 4.40 (d, 1H, Benzyl CH, J = 12.8 Hz), 3.91 (q, 1H, α-CH, J = 7.2 Hz), 3.76 – 3.68 (m, 1H, Pro CH), 3.55 (d, 1H, Benzy CH, J = 12.8 Hz), 3.51 – 3.43 (m, 1H, Pro CH), 2.77 – 2.71 (m, 1H, Pro CH), 2.59 – 2.48 (m, 1H, Pro CH), 2.26 – 2.18 (m, 1H, Pro CH), 2.11 – 2.04 (m, 1H, Pro CH), 1.59 (d, 3H, Ala CH$_3$, J = 7.2 Hz), 1.39 (d, 0.3H, Ala CH$_3$, J = 6.8 Hz, peak used to calculate dr)

^{13}C NMR (101 MHz, CDCl$_3$): 180.4, 180.3, 170.2, 142.0, 133.4, 133.3, 133.0, 132.0, 131.4, 129.6, 128.9, 128.4, 127.4, 127.1, 126.4, 123.8, 120.7, 70.0, 66.5, 63.0, 57.2, 30.7, 24.0, 21.8

HRMS: (C$_{28}$H$_{28}$O$_3$N$_3$Ni) [M+H]$^+$ requires 512.1479, found [M+H]$^+$ 512.1470

110 - 5-Iodopent-1-ene
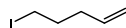
To a round bottomed flask was added 5-bromopent-1-ene (**129**) (5 g, 33.6 mmol, 1 equiv.), KI (11.155 g, 67.2 mmol, 2 equiv.) and acetone (45 mL). The reaction mixture was heated to reflux for 4 hours. The mixture was allowed to cool to room temperature and dilted with water (100 mL) and Et$_2$O (100 mL). The mixture was separated and washed with water (2 x 100 mL) and the aqueous washings back extracted with Et$_2$O (100 mL). The organic layers were combined, dried and concentrated *in vacuo* to give a clear oil, however due to the volatile nature of the product care was taken to minimise product loss upon evaporation. The remaining Et$_2$O was distilled using Kugelrohr distillation (atmospheric pressure, 100 ^{o}C) to give the target compound as a clear oil (6.578 g, 88%).

v$_{max}$ (neat): 3076, 2910, 2839, 1639, 1441, 1427, 1414 cm^{-1}
^{1}H NMR (400 MHz, CDCl$_3$): δ 5.79 - 5.74 (m, 1H, Alkenyl CH), 5.11 – 5.02 (m, 2H, alkenyl CH$_2$), 3.20 (t, 2H, CH$_2$-I, J = 6.4 Hz), 2.20 – 2.15 (m, 2H, CH$_2$), 1.94 – 1.91 (m, 2H, CH$_2$)
^{13}C NMR (101 MHz, CDCl$_3$): δ 136.5, 115.9, 34.2, 32.4, 6.3
HRMS: (C$_5$H$_8$I) [M-H]$^-$ requires 194.9665, found [M-H]$^-$ 194.9663

149 - 8-Iodooct-1-ene
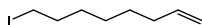
To a round bottomed flask was added 5-bromo-oct-1-ene (**148**) (5 g, 26.2 mmol, 1 equiv.), KI (8.687 g, 52.3 mmol, 2 equiv.) and acetone (30 mL). The reaction mixture was heated to reflux for 4 hours. The mixture was allowed to cool to r.t and dilted with water (100 mL) and hexane (100 mL). The mixture was separated and washed with water (2 x 100 mL) and the aqueous washings back extracted with hexane (100 mL). The organic layers were combined, dried and concentrated *in vacuo* to give a clear oil, however due to the volatile nature of the product care was taken to minimise loss upon evapouration. The remaining hexane was distilled off using kugelrohr distillation (atmospheric pressure, 115 ^{o}C) to give the target compound as a clear oil (5.621 g, 90%).

v_{max} (neat): 3075, 2926, 2853, 1640, 1460, 1427 cm^{-1}

^{1}H NMR (400 MHz, CDCl$_3$): δ 5.85 – 5.75 (m, 1H, alkenyl CH), 5.03 – 4.93 (m, 2H, alkenyl CH$_2$), 3.19 (t, 2H, CH$_2$-I, J = 6.8), 2.08 – 2.02 (m, 2H, CH$_2$), 1.86 - 1.79 (m, 2H, CH$_2$), 1.44 – 1.28 (m, 6H, 3 x CH$_2$)

^{13}C NMR (101 MHz, CDCl$_3$): δ 138.8, 114.4, 33.6, 33.5, 30.3, 28.6, 27.9, 7.1

HRMS: (C$_8$H$_{14}$I) [M-H]$^{-}$ requires 237.0135, found [M-H]$^{-}$ 237.0132

130 - (*S*)-Ni(II)-S$_5$-BPB
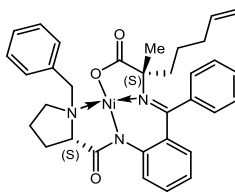
Procedure described in Table 3

To a dry round bottomed flask containing dry THF (30 mL) was added **127** (4.391 g, 8.6 mmol, 1 equiv.) and cooled to 0 °C under N$_2$. TBAI (317 mg, 0.8 mmol, 0.1 equiv.) and sublimed *t*BuOK (2.405 g, 21.4 mmol, 2.5 equiv.) were added and the mixture left to stir for 5 minutes. **110** (4.201 g, 21.4 mmol, 2.5 equiv.) was added dropwise over 5 minutes and the reaction mixture left to stir at room temperature for 17 hr. The reaction mixture was quenched with 0.1 M HCl and separated with DCM (3 x 100 mL). The organic layers combined, dried and concentrated *in vacuo* to give the crude product as a red oil. The crude material was then purified by silica chromatography (0-2% MeOH in EtOAc) to give the title compound as a bright red solid (3.474 g, 70%).

dr = >98% by ^{1}H NMR

Procedure described in Scheme 25

To a dry round bottomed flask containing dry THF (295 mL) was added **127** (12.47 g, 25.3 mmol, 1 equiv.) and cooled to 0 °C under N$_2$. TBAI (899 mg, 2.4 mmol, 0.1 equiv.) and sublimed *t*BuOK (6.828 g, 60.9 mmol, 2.5 equiv.) were added and the mixture left to stir for 5 minutes. **110** (11.930 g, 60.9 mmol, 2.5 equiv.) was added dropwise over 5 minutes and the reaction mixture left to stir at room temperature for 17 hr. The reaction mixture was quenched with 0.1 M HCl and separated with DCM (3 x 400 mL). The organic layers combined, dried and concentrated *in vacuo* to give the crude product as a red oil. The crude material was then purified by silica chromatography (0-2% MeOH in EtOAc) to give the title compound as a bright red solid (7.31 g, 52%).

dr = >98% by ^{1}H NMR,
ee = 84% by chiral HPLC

Procedures described in Scheme 28

130a and 130b

To a dry round bottomed flask containing dry THF (25 mL) was added **127a** (1 g, 1.9 mmol, 1 equiv.) and cooled to 0 ^{o}C under N_2. TBAI (72 mg, 0.2 mmol, 0.1 equiv.) and sublimed tBuOK (547 mg, 4.9 mmol, 2.5 equiv.) were added and the mixture left to stir for 5 minutes. **110** (957 mg, 4.9 mmol, 2.5 equiv.) was added dropwise over 5 minutes and the reaction mixture left to stir at room temperature for 17 hr. The reaction mixture was quenched with 0.1 M HCl and separated with DCM (3 x 40 mL). The organic layers combined, dried and concentrated *in vacuo* to give the crude product as a red oil. The crude material was then purified by silica chromatography (0-2% MeOH in EtOAc) to give the title compound as a bright red solid.

130a (776 mg, 68%)

dr = >98% by ^{1}H NMR

ee = 92% by chiral HPLC

130b (629 mg, 56%).

$[\alpha]^{20}_D$ = +1273 (c = 0.03, MeOH)

dr = >98% by ^{1}H NMR

ee = 94% by chiral HPLC

Data

v_{max} (neat): 2924, 2854, 1670, 1630, 1577, 1533, 1437, 1352 cm^{-1}

^{1}H NMR (400 MHz, CDCl$_3$): δ 8.08 (dd, 2H, 2 x Aro CH, *J* = 7.2, 0.8 Hz), 8.02 (dd, 1H, Aro CH, J = 8.4, 1.2 Hz), 7.51 – 7.44 (m, 2H, 2 x Aro CH), 7.42 – 7.36 (m, 3H, 3 x Aro CH), 7.33 – 7.26 (m, 3H, 2 x Aro CH, CDCl$_3$), 7.15 – 7.11 (m, 1H, Aro CH), 6.98 (d, 1H, Aro CH, *J* = 6.8 Hz), 6.67 – 6.60 (m, 2H, 2 x Aro CH), 5.92 – 5.82 (m, 1H, Alkene CH), 5.11 – 5.01 (m, 2H, Alkene CH$_2$), 4.51 (d, 1H, Benzyl CH, *J* = 13.2 Hz), 3.71 (d, 1H, Benzyl CH, *J* = 12.4 Hz), 3.67 – 3.63 (m, 1H, Pro CH), 3.44 (dd, 1H, Pro CH, *J* = 6, 4.4 Hz), 3.30 – 3.22 (m, 1H, Pro CH), 2.74 – 2.66 (m, 1H, Pro CH), 2.51 – 2.37 (m, 2H, 2 x Pro CH), 2.15 – 2.01 (m, 5H, 2 x CH$_2$ Alkane, 1 x Pro CH), 1.77 – 1.65 (m, 2H, CH$_2$ Alkane), 1.24 (s, 3H, CH$_3$ Ala)

^{13}C NMR (101 MHz, CDCl$_3$): 180.5, 172.3, 141.5, 137.8, 136.5, 133.3, 131.7, 131.4, 130.2, 129.3, 129.0, 127.9, 127.9, 127.3, 126.9, 123.9, 120.7, 115.4, 78.0, 70.0, 63.4, 57.0, 39.9, 33.7, 30.6, 29.5, 25.3, 23.2, 1C not observed (overlapping peaks)

HRMS: (C$_{33}$H$_{36}$O$_3$N$_3$Ni) [M+H]$^+$ requires 580.2105, found [M+H]$^+$ 580.2095

142 - (*R*)-Ni(II)-R₅-BPB
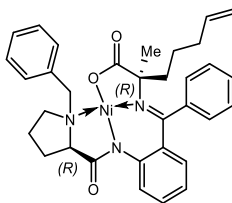
To a dry round bottomed flask containing dry THF (150 mL) was added **128** (6 g, 11.7 mmol, 1 equiv.) and cooled to 0 °C under N_2. TBAI (433 mg, 1.2 mmol, 0.1 equiv.) and sublimed *t*BuOK (2.628 g, 23.4 mmol, 2 equiv.) were added and the mixture left to stir for 5 minutes. **110** (4.590 g, 23.4 mmol, 2 equiv.) was added dropwise over 5 minutes and the reaction mixture left to stir at room temperature for 17 hr. The reaction mixture was quenched with 0.1 M HCl and separated with DCM (3 x 250 mL). The organic layers combined, dried and concentrated *in vacuo* to give the crude product as a red oil. The crude material was then purified by silica chromatography (0-2% MeOH in EtOAc) to give the title compound as a bright red solid (4.242 g, 62%).

v_{max} (neat): 2968, 2942, 2858, 1664, 1635, 1571, 1533, 1435, 1355 cm^{-1}

^{1}H NMR (400 MHz, CDCl$_3$): δ 8.09 (d, 2H, 2 x Aro CH, *J* = 6.8 Hz), 8.03 (d, 1H, Aro CH, J = 9.2 Hz), 7.51 – 7.48 (m, 2H, 2 x Aro CH), 7.44 – 7.40 (m, 3H, 3 x Aro CH), 7.35 – 7.27 (m, 3H, 2 x Aro CH, CDCl$_3$), 7.17 – 7.12 (m, 1H, Aro CH), 7.00 (dd, 1H, Aro CH, *J* = 6.4, 1.2 Hz), 6.68 – 6.62 (m, 2H, 2 x Aro CH), 5.93 – 5.83 (m, 1H, Alkene CH), 5.13 – 5.03 (m, 2H, Alkene CH$_2$), 4.51 (d, 1H, Benzyl CH, *J* = 12.4 Hz), 3.72 (d, 1H, Benzyl CH, *J* = 12.4 Hz), 3.69 – 3.64 (m, 1H, Pro CH), 3.45 (dd, 1H, Pro CH, *J* = 6, 4.8 Hz), 3.31 – 3.24 (m, 1H, Pro CH), 2.76 – 2.68 (m, 1H, Pro CH), 2.53 – 2.39 (m, 2H, 2 x Pro CH), 2.19 – 2.03 (m, 5H, 2 x CH$_2$ Alkane, 1 x Pro CH), 1.79 – 1.69 (m, 2H, CH$_2$ Alkane), 1.25 (s, 3H, CH$_3$ Ala)

^{13}C NMR (101 MHz, CDCl$_3$): 182.2, 180.4, 172.3, 141.4, 136.5, 133.3, 131.7, 131.5, 130.2, 129.4, 129.0, 128.8,128.6, 127.8, 127.3, 126.9, 123.9, 120.7, 115.4, 78.0, 69.9, 63.3, 56.9, 39.8, 33.7, 30.6, 29.5, 25.3, 23.2

HRMS: (C$_{33}$H$_{36}$O$_3$N$_3$Ni) [M+H]$^+$ requires 580.2105, found [M+H]$^+$ 580.2099

$[\alpha]^{20}_D$ = -1262 (c = 0.03, MeOH)

dr = >98% by ^{1}H NMR

ee = 90% by chiral HPLC

113 - (*S*)-2-amino-2-methylhept-6-enoic acid
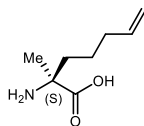
Procedure described in Scheme 25

To a round bottomed flask containing MeOH (209 mL, 0.08 M) was added **130** (7.25 g, 12.5 mmol, 1 equiv.) and 2M HCl (147 mL, 0.06 M). The reaction mixture was heated to reflux for 3 hours turning from a dark red to a yellow solution. The mixture was cooled to r.t and basified to pH 9 with conc. NH_3. Water (250 mL) was added and the mixture separated with DCM (3 x 400 mL). The aqueous layer was concentrated *in vacuo* to give a crude turquoise solid. Dowex resin (80 g) (50WX8 hydrogen form) was swollen in water and packed into a column and washed with water. The crude solid was then dissolved in MeOH:water (1:1) and added to the resin. The column was then washed with MeOH (250 mL) and water (250 mL) to elute impurities. The product was then eluted using 25% NH_3 in water (500 mL) and concentrated *in vacuo*. The white solid was then dissolved in water and freeze dried to give the title compound as a fluffy white solid (1.624 g, 75%).

Procedure described in Scheme 28

To a round bottomed flask containing MeOH (13 mL, 0.08 M) was added **130** (583.2 mg, 1.1 mmol, 1 equiv.) and 2M HCl (18 mL, 0.06 M). The reaction mixture was heated to reflux for 3 hours turning from a dark red to a yellow solution. The mixture was cooled to r.t and basified to pH 9 with conc. NH_3. Water (50 mL) was added and the mixture separated with DCM (3 x 100 mL). The aqueous layer was concentrated *in vacuo* to give a crude turquoise solid. Dowex resin (40 g) (50WX8 hydrogen form) was swollen in water and packed into a column and washed with water. The crude solid was then dissolved in MeOH:water (1:1) and added to the resin. The column was then washed with MeOH (120 mL) and water (120 mL) to elute impurities. The product was then eluted using 25% NH_3 in water (200 mL) and concentrated *in vacuo*. The white solid was then dissolved in water and freeze dried to give the title compound as a fluffy white solid (101 mg, 80%).

$[\alpha]^{20}_D$ = +2 (c = 0.15, MeOH)
Literature value $[\alpha]^{20}_D$ = +3.59 (c = 0.05, MeOH)[169]

Data

v_{max} (neat): 3053, 2947, 1585, 1539, 1458, 1404 cm^{-1}

^{1}H NMR (400 MHz, DMSO-d_6): δ 7.61 (br s, 3H, NH$_2$, COOH), 5.81 - 5.72 (m, 1H, Alkene CH), 5.04 – 4.94 (m, 2H, Alkene CH$_2$), 2.00 – 1.95 (m, 2H, Alkane CH$_2$), 1.68 – 1.60 (m, 1H, Alkane CH), 1.55 – 1.43 (m, 2H, Alkane CH$_2$), 1.30 – 1.23 (m, 4H, Alkane CH, Me CH$_3$).

^{13}C NMR (101 MHz, DMSO-d_6): δ 138.4, 114.8, 59.7, 37.4, 33.3, 23.2, 22.7 1C not observed (overlapping peaks)

HRMS: (C$_8$H$_{16}$O$_2$N) [M+H]$^+$ requires 158.1176, found [M+H]$^+$ 158.1176

143 - (*R*)-2-amino-2-methylhept-6-enoic acid
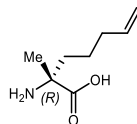
To a round bottomed flask containing MeOH (90 mL, 0.08 M) was added **142** (4.2 g, 7.2 mmol, 1 equiv.) and 2M HCl (121 mL, 0.06 M). The reaction mixture was heated to reflux for 3 hours turning from a dark red to a yellow solution. The mixture was cooled to r.t and basified to pH 9 with conc. NH_3. Water (150 mL) was added and the mixture separated with DCM (3 x 200 mL). The aqueous layer was concentrated *in vacuo* to give a crude turquoise solid. Dowex resin (40 g) (50WX8 hydrogen form) was swollen in water and packed into a column and washed with water. The crude solid was then dissolved in MeOH:water (1:1) and added to the resin. The column was then washed with MeOH (150 mL) and water (150 mL) to elute impurities. The product was then eluted using 25% NH_3 in water (250 mL) and concentrated *in vacuo*. The white solid was then dissolved in water and freeze dried to give the title compound as a fluffy white solid (675 mg, 78%)

v_{max} (neat): 3049, 2980, 2947, 1585, 1458, 1402 cm^{-1}

^{1}H NMR (400 MHz, DMSO-d_6): δ 7.49 (br s, 3H, NH_2, COOH), 5.82 - 5.72 (m, 1H, Alkene CH), 5.04 – 4.94 (m, 2H, Alkene CH_2), 1.20 – 1.94 (m, 2H, Alkane CH_2), 1.68 – 1.60 (m, 1H, Alkane CH), 1.54 – 1.43 (m, 2H, Alkane CH_2), 1.30 – 1.23 (m, 4H, Alkane CH, Me CH_3).

^{13}C NMR (101 MHz, DMSO-d_6): δ 138.4, 114.8, 59.7, 37.4, 33.3, 23.1, 22.7 1C not observed (overlapping peaks)

HRMS: ($C_8H_{14}O_2N$) [M-H]$^-$ requires 156.1030, found [M-H]$^-$ 156.1032

$[α]^{20}_D$ = -12 (c = 0.15, MeOH)

88 - (*S*)-2-((((9*H*-Fluoren-9-yl)methoxy)carbonyl)amino)-2-methylhept-6-enoic acid
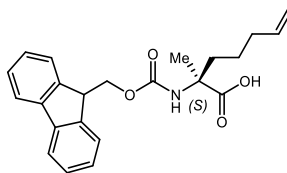
Procedure described in Scheme 26

To a round bottomed flask containing H_2O (75 mL) and dioxane (75 mL) was added **113** (9.167 g, 52.6 mmol, 1 equiv.) and Na_2CO_3 (1.944 g, 18.3 mmol, 2 equiv.) to form a cloudy solution. The reaction mixture was cooled to 0 ^{o}C and 9-Fluorenylmethyl *N*-succinimidyl carbonate (6.185 mg, 18.3 mmol, 2 equiv.) was added in small portions over 2 hours, with the reaction temperature being maintained between 0 ^{o}C to 5 ^{o}C. Once addition was complete the reaction was left to stir at r.t for 17 hr. The reaction mixture was then concentrated *in vacuo* and the residue separated with water (3 x 400 mL) and Et_2O 400 mL). The aqueous washings were back extracted with Et_2O (400 mL), combined and acidified to pH 4 using 1 M HCl. The aqueous solution was then extracted with EtOAc (2 x 400 mL) and the organic layers washed with 1M HCl (2 x 400 mL). The organic layers combined, dried and concentrated *in vacuo* to give the crude product as a yellow oil. The crude material was then purified by silica chromatography (0 - 3% MeOH in DCM) to give the title compound as a yellow gummy solid (1.711 g, 49%).

ee = 82% by chiral HPLC

Procedure described in Scheme 28

To a round bottomed flask containing H_2O (9 mL) and dioxane (9 mL) was added **113** (170 mg, 1.1 mmol, 1 equiv.) and Na_2CO_3 (229 mg, 2.2 mmol, 2 equiv.) to form a cloudy solution. The reaction mixture was cooled to 0 ^{o}C and 9-Fluorenylmethyl *N*-succinimidyl carbonate (730 mg, 2.2 mmol, 2 equiv.) was added in small portions over 2 hours, with the reaction temperature being maintained between 0 ^{o}C to 5 ^{o}C. Once addition was complete the reaction was left to stir at r.t for 17 hr. The reaction mixture was then concentrated *in vacuo* and the residue separated with water (3 x 100 mL) and Et_2O 100 mL). The aqueous washings were back extracted with Et_2O (100 mL), combined and acidified to pH 4 using 1 M HCl. The aqueous solution was

then extracted with EtOAc (2 x 100 mL) and the organic layers washed with 1M HCl (2 x 100 mL). The organic layers combined, dried and concentrated *in vacuo* to give the crude product as a yellow oil. The crude material was then purified by silica chromatography (0 - 3% MeOH in DCM) to give the title compound as a yellow gummy solid (344 mg, 84%).

$[\alpha]^{20}_D$ = +18.1 (c = 0.15, MeOH)
Literature value $[\alpha]^{20}_D$ = +3.5 (c = 1, MeOH)[169]
ee = 92% by chiral HPLC

Data

v_{max} (neat): 2939, 1705, 1641, 1506, 1450 cm^{-1}
^{1}H NMR (400 MHz, DMSO-d_6): δ 7.90 (d, 2H, 2 x Aro CH, *J* = 7.6 Hz), 7.73 (d, 2H, 2 x Aro CH, *J* = 7.6 Hz), 7.46 – 7.40 (m, 3H, 2 x Aro CH, NH), 7.34 (td, 2H, 2 x Aro CH, *J* = 6.8, 0.8 Hz), 5.83 – 5.73 (m, 1H, Alkene CH), 5.03 – 4.95 (m, 2H, Alkene CH$_2$), 4.28 – 4.19 (m, 3H, Fmoc CH. Fmoc CH$_2$), 2.01 – 1.97 (m, 2H, Alkane CH$_2$), 1.78 – 1.68 (m, 2H, Alkane CH$_2$), 1.36 – 1.26 (m, 5H, Me CH$_3$, Alkane CH$_2$)
^{13}C NMR (101 MHz, DMSO-d_6): 175.3, 154.8, 143.8, 140.7, 138.5, 127.6, 127.0, 125.2, 120.0, 114.9, 65.2, 58.2, 46.7, 36.2, 33.2, 22.5, 1C not observed (overlapping peaks)
HRMS: (C$_{23}$H$_{26}$O$_4$N) [M+H]$^+$ requires 380.1856, found [M+H]$^+$ 380.1858

89 - (*R*)-2-((((9*H*-Fluoren-9-yl)methoxy)carbonyl)amino)-2-methylhept-6-enoic acid
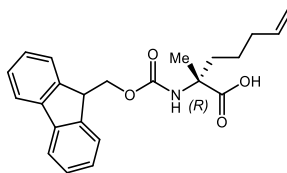
To a round bottomed flask containing H_2O (27.5 mL) and dioxane (27.5 mL) was added **143** (517 mg, 3.3 mmol, 1 equiv.) and Na_2CO_3 (697 mg, 6.6 mmol, 2 equiv.) to form a cloudy solution. The reaction mixture was cooled to 0 °C and 9-Fluorenylmethyl *N*-succinimidyl carbonate (2.219 g, 6.6 mmol, 2 equiv.) was added in small portions over 2 hours, with the reaction temperature being maintained between 0 °C to 5 °C. Once addition was complete the reaction was left to stir at r.t for 17 hr. The reaction mixture was then concentrated *in vacuo* and the residue separated with water (3 x 200 mL) and Et_2O (200 mL). The aqueous washings were back extracted with Et_2O (200 mL), combined and acidified to pH 4 using 1 M HCl. The aqueous solution was then extracted with EtOAc (2 x 200 mL) and the organic layers washed with 1M HCl (2 x 200 mL). The organic layers combined, dried and concentrated in vacuo to give the crude product as a yellow oil. The crude material was then purified by silica chromatography (0 - 3% MeOH in DCM) to give the title compound as a yellow gummy solid (690 mg, 55%).

v_{max} (neat): 2939, 1705, 1641, 1504, 1448 cm^{-1}

^{1}H NMR (400 MHz, DMSO-d_6): δ 7.90 (d, 2H, 2 x Aro CH, *J* = 7.6 Hz), 7.73 (d, 2H, 2 x Aro CH, *J* = 7.6 Hz), 7.42 (dd, 3H, 2 x Aro CH, NH, *J* = 7.6, 7.2), 7.34 (dd, 2H, 2 x Aro CH, *J* = 7.6, 7.2), 5.82 – 5.75 (m, 1H, Alkene CH), 5.03 – 4.94 (m, 2H, Alkene CH_2), 4.28 – 4.19 (m, 3H, Fmoc CH. Fmoc CH_2), 2.01 – 1.99 (m, 2H, Alkane CH_2), 1.78 – 1.69 (m, 2H, Alkane CH_2), 1.36 – 1.26 (m, 5H, Me CH_3, Alkane CH_2)

^{13}C NMR (101 MHz, DMSO-d_6): 175.4, 154.8, 143.9, 140.7, 138.4, 127.6, 127.1, 125.3, 120.0, 114.9, 65.2, 58.3, 46.8, 36.2, 33.3, 22.5, 22.4

HRMS: ($C_{23}H_{26}O_4N$) [M+H]$^+$ requires 380.1856, found [M+H]$^+$ 380.1859

$[\alpha]^{20}_D$ = -13.5 (c = 0.15, MeOH)

ee = 90% by chiral HPLC

150 – (*S*)-Ni(II)-S$_8$-BPB
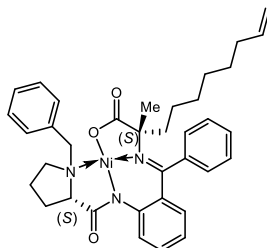
To a dry round bottomed flask containing dry THF (150 mL) was added **127** (5.378 g, 10.5 mmol, 1 equiv.) and cooled to 0 °C under N$_2$. TBAI (388 mg, 1.0 mmol, 0.1 equiv.) and sublimed *t*BuOK (2.356 g, 21.0 mmol, 2 equiv.) were added and left to stir for 5 minutes. **149** (5 g, 21.0 mmol, 2 equiv.) was added dropwise over 5 minutes and the reaction mixture left to stir at r.t for 17 hours. The reaction mixture was quenched with 0.1 M HCl and separated with DCM (3 x 250 mL). The organic layers combined, dried and concentrated *in vacuo* to give the crude product as a red oil. The crude material was then purified by silica chromatography (0-2% MeOH in EtOAc) to give the title compound as a bright red solid (4.432 g, 68%).

v_{max} (neat): 2926, 2854, 1670, 1638, 1574, 1533, 1468, 1437 cm^{-1}

^{1}H NMR (400 MHz, CDCl$_3$): δ 8.08 (dd, 2H, 2 x Aro CH, *J* = 7.2, 1.6 Hz), 8.02 (dd, 1H, Aro CH, *J* = 8, 0.8 Hz), 7.51 – 7.45 (m, 2H, 2 x Aro CH), 7.43 – 7.38 (m, 3H, 3 x Aro CH), 7.34 – 7.26 (m, 2H, 2 x Aro CH), 7.15 – 7.11 (m, 1H, Aro CH), 6.98 – 6.96 (m, 1H, Aro CH), 6.67 – 6.61 (m, 2H, 2 x Aro CH), 5.88 – 5.77 (m, 1H, Alkene CH), 5.04 – 4.94 (m, 2H, Alkene CH$_2$), 4.51 (d, 1H, Benzyl CH, *J* = 12.8 Hz), 3.71 (d, 1H, Benzyl CH, *J* = 12.4 Hz), 3.67 – 3.63 (m, 1H, Pro CH), 3.46 – 3.42 (m, 1H, Pro CH), 3.32 – 3.25 (m, 1H, Pro CH), 2.74 – 2.66 (m , 1H, Pro CH), 2.52 – 2.46 (m, 1H, Pro CH), 2.38 – 2.33 (m, 1H, Pro CH), 2.11 – 1.98 (m, 5H, Pro CH, 2 x Alkane CH$_2$), 1.75 – 1.57 (m, 2H, Alkane CH$_2$), 1.47 – 1.38 (m, 4H, 2 x Alkane CH$_2$), 1.34 – 1.29 (m, 2H, Alkane CH$_2$), 1.25 (s, 3H, Me CH$_3$).

^{13}C NMR (101 MHz, CDCl$_3$): δ 172.3, 141.5, 136.6, 133.3, 131.7, 131.5, 130.3, 129.3, 129.0, 128.9, 128.7, 127.9 , 127.2, 126.7, 120.7, 114.4, 77.2, 70.0, 63.4, 57.0, 40.3, 33.7, 30.6, 29.6, 29.5, 29.1, 28.9, 26.0, 23.2, 3C not observed (overlapping peaks)

HRMS: (C$_{36}$H$_{42}$O$_3$N$_3$Ni) [M+H]$^+$ requires 622.2574, found [M+H]$^+$ 622.2565

[α]^{20}$_D$ = +1803 (c = 0.03, MeOH)

dr = >98% by ^{1}H NMR

ee = 96% by chiral HPLC

152 – (R)-Ni(II)-R$_8$-BPB
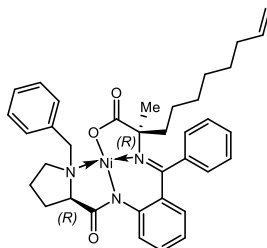
To a dry round bottomed flask containing dry THF (75 mL) was added **128** (4.767 g, 9.3 mmol, 1 equiv.) and cooled to 0 °C under N$_2$. TBAI (344 mg, 0.93 mmol, 0.1 equiv.) and sublimed *t*BuOK (2.089 g, 18.6 mmol, 2.5 equiv.) were added and left to stir for 5 minutes. **149** (4.432 g, 18.6 mmol, 2.5 equiv.) was added dropwise over 5 minutes and the reaction mixture left to stir at r.t for 17 hours. The reaction mixture was quenched with 0.1 M HCl and separated with DCM (3 x 200 mL). The organic layers combined, dried and concentrated *in vacuo* to give the crude product as a red oil. The crude material was then purified by silica chromatography (0-2% MeOH in EtOAc) to give the title compound as a bright red solid (1.781 g, 55%).

v_{max} (neat): 2924, 2854, 1668, 1633, 1574, 1537, 1470, 1437 cm^{-1}

^{1}H NMR (400 MHz, CDCl$_3$): δ 8.09 (dd, 2H, 2 x Aro CH, *J* = 7.2, 0.8 Hz), 8.00 (dd, 1H, Aro CH, *J* = 8.8, 0.8 Hz), 7.50 – 7.46 (m, 2H, 2 x Aro CH), 7.43 – 7.37 (m, 3H, 3 x Aro CH), 7.35 – 7.27 (m, 2H, 2 x Aro CH), 7.14 (qd, 1H, Aro CH, *J* = 4, 2.4, 2 Hz), 6.99 – 6.97 (m, 1H, Aro CH), 6.68 – 6.62 (m, 2H, 2 x Aro CH), 5.88 – 5.78 (m, 1H, Alkene CH), 5.05 – 4.94 (m, 2H, Alkene CH$_2$), 4.51 (d, 1H, Benzyl CH, *J* = 12.4 Hz), 3.72 (d, 1H, Benzyl CH, *J* = 13.2 Hz), 3.67 – 3.63 (m, 1H, Pro CH), 3.47 – 3.43 (m, 1H, Pro CH), 3.36 – 3.23 (m, 1H, Pro CH), 2.74 – 2.67 (m , 1H, Pro CH), 2.55 – 2.45 (m, 1H, Pro CH), 2.40 – 2.35 (m, 1H, Pro CH), 2.11 – 2.00 (m, 5H, Pro CH, 2 x Alkane CH$_2$), 1.76 – 1.59 (m, 2H, Alkane CH$_2$), 1.47 – 1.42 (m, 4H, 2 x Alkane CH$_2$), 1.27 – 1.29 (m, 2H, Alkane CH$_2$), 1.26 (s, 3H, Me CH$_3$).

^{13}C NMR (101 MHz, CDCl$_3$): δ 182.4, 180.4, 172.2, 138.9, 136.6, 133.6, 131.7, 131.4, 130.3, 129.3, 128.9, 128.8, 128.7, 128.3, 127.8, 127.2, 126.9, 123.9, 120.7, 114.3, 78.1, 69.9, 63.3, 56.9, 40.2, 33.7, 30.6, 29.6, 29.5, 29.1, 28.8, 26.0, 23.2

HRMS: (C$_{36}$H$_{42}$O$_3$N$_3$Ni) [M+H]$^+$ requires 622.2574, found [M+H]$^+$ 622.2571

$[α]^{20}_D$ = -1840 (c = 0.03, MeOH)

dr = >98% by ^{1}H NMR

ee = 96% by chiral HPLC

151 – (S)-2-Amino-2-methyldec-9-enoic acid
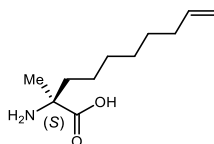
To a round bottomed flask containing MeOH (40 mL, 0.08 M) was added **150** (2.050 g, 3.3 mmol, 1 equiv.) and 2 M HCl (55 mL, 0.06 M). The reaction mixture was heated to reflux for 3 hr turning from a dark red to a yellow solution. The mixture was cooled to r.t and basified to pH 9 with conc. NH_3. Water (150 mL) was added and the mixture separated with DCM (3 x 300 mL). The aqueous layer was concentrated *in vacuo* to give a crude turquoise solid. Dowex resin (40 g) (50WX8 hydrogen form) was swollen in water and packed into a column and washed with water. The crude solid was then dissolved in MeOH:water (1:1) and added to the resin. The column was then washed with MeOH (150 mL) and water (150 mL) to elute impurities. The product was then eluted using 25% NH_3 in water (250 mL) and concentrated *in vacuo*. The white solid was then dissolved in water and freeze dried to give the title compound as a fluffy white solid (260 mg, 36%).

v_{max} (neat): 3064, 2924, 2854, 1595, 1556, 1531, 1458, 1402, cm^{-1}

^{1}H NMR (400 MHz, DMSO-d_6): δ 7.3 (br s, 3H, COOH, NH_2), 5.85 – 5.75 (m, 1H, Alkene CH), 5.03 – 4.92 (m, 2H, Alkene CH_2), 2.04 – 1.99 (m, 2H, Alkane CH_2), 1.61 – 1.58 (m, 1H, Alkane CH), 1.53 – 1.47 (m, 1H, Alkane CH_2), 1.36 – 1.20 (m, 11H, 4 x Alkane CH_2, Me CH_3)

^{13}C NMR (101 MHz, CDCl$_3$): δ 138.8, 59.8, 37.9, 33.1, 29.1, 28.4, 28.1, 23.2 3C not observed (overlapping peaks)

HRMS: (C$_{11}$H$_{22}$O$_2$N) [M+H]$^+$ requires 200.1645, found [M+H]$^+$ 200.1643

[α]$^{20}_D$ = +16 (c = 0.15, MeOH)

Literature value [α]$^{20}_D$ = +3.59 (c = 0.05, MeOH)[169]

153 – (*R*)-2-Amino-2-methyldec-9-enoic acid
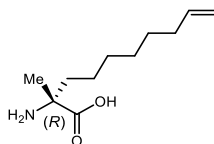
To a round bottomed flask containing MeOH (35 mL, 0.08 M) was added **152** (1.740 g, 2.8 mmol, 1 equiv.) and 2M HCl (47 mL, 0.06 M). The reaction mixture was heated to reflux for 3 hr turning from a dark red to a yellow solution. The mixture was cooled to r.t and basified to pH 9 with conc. NH_3. Water (100 mL) was added and the mixture separated with DCM (3 x 200 mL). The aqueous layer was concentrated in vacuo to give a crude turquoise solid. Dowex resin (30 g) (50WX8 hydrogen form) was swollen in water and packed into a column and washed with water. The crude solid was then dissolved in MeOH:water (1:1) and added to the resin. The column was then washed with MeOH (150 mL) and water (150 mL) to elute impurities. The product was then eluted using 25% NH_3 in water (200 mL) and concentrated *in vacuo*. The white solid was then dissolved in water and freeze dried to give the title compound as a fluffy white solid (297 mg, 89%).

v_{max} (neat): 3049, 2924, 2853, 1595, 1572, 1528, 1458, 1400, cm^{-1}

^{1}H NMR (400 MHz, DMSO-d_6): δ 7.044 (br s, 2H, NH_2), 5.85 – 5.75 (m, 1H, Alkene CH), 5.03 – 4.92 (m, 2H, Alkene CH_2), 2.04 – 1.98 (m, 2H, Alkane CH_2), 1.61 – 1.56 (m, 1H, Alkane CH), 1.47 – 1.44 (m, 1H, Alkane CH_2), 1.36 – 1.19 (m, 11H, 4 x Alkane CH_2, Me CH_3), 1H not observed (exchangeable proton)

^{13}C NMR (101 MHz, CDCl$_3$): δ 138.8, 59.8, 37.9, 33.1, 29.1, 28.4, 28.1, 23.2 (3C not observed, overlapping peaks)

HRMS: (C$_{11}$H$_{22}$O$_2$N) [M+H]$^+$ requires 200.1645, found [M+H]$^+$ 200.1644

[α]$^{20}_D$ = -16 (c = 0.15, MeOH)

90 – (*S*)-2-((((9*H*-fluoren-9-yl)methoxy)carbonyl)amino)-2-methyldec-9-enoic acid
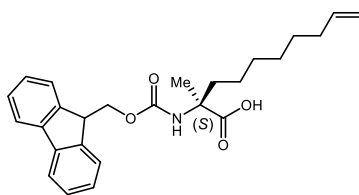
To a round bottomed flask containing H_2O (16 mL) and dioxane (16 mL) was added **151** (130 mg, 1.1 mmol, 1 equiv.) and Na_2CO_3 (231 mg, 1.2 mmol, 2 equiv.) to form a cloudy solution. The reaction mixture was cooled to 0 °C and 9-Fluorenylmethyl *N*-succinimidyl carbonate (737 mg, 2.2 mmol, 2 equiv.) was added in small portions over 2 hours, with the reaction temperature being maintained between 0 °C to 5 °C. Once addition was complete the reaction was left to stir at room temperature for 17 hours. The reaction mixture was then concentrated *in vacuo* and the residue separated with water (3 x 50 mL) and Et_2O (100 mL). The aqueous washings were back extracted with Et_2O (100 mL), combined and acidified to pH 4 using 1M HCl. The aqueous solution was then extracted with EtOAc (2 x 100 mL) and the organic layers washed with 1 M HCl (2 x 100 mL). The organic layers combined, dried and concentrated *in vacuo* to give the crude product as a yellow oil. The crude material was then purified by preparative HPLC (5-95% MeCN in H_2O over 30 minutes) to give the title compound as a yellow gummy solid (217 mg, 47%).

v_{max} (neat): 2926, 2855, 1708, 1639, 1504, 1450 cm^{-1}

^{1}H NMR (400 MHz, DMSO-d_6): δ 12.36 (br s, 1H, COOH), 7.90 (d, 2H, 2 x Aro CH, *J* = 7.6 Hz), 7.72 (d, 2H, 2 x Aro CH, *J* = 7.6 Hz), 7.42 (t, 2H, 2 x Aro CH, J = 7.2 Hz), 7.37 – 7.31 (m, 3H, 2 x Aro CH, NH), 5.84 – 5.73 (m, 1H, Alkene CH), 5.01 – 4.92 (m, 2H, Alkene CH$_2$), 4.27 – 4.19 (m, 3H, Fmoc CH, Fmoc CH$_2$), 2.03 – 1.98 (m, 2H, Alkane CH$_2$), 1.76 – 1.69 (m, 2H, Alkane CH$_2$), 1.33 – 1.24 (m, 11H, 4 x Alkane CH$_2$, Me CH$_3$).

^{13}C NMR (101 MHz, CDCl$_3$): 175.3, 143.8, 140.7, 138.8, 127.6, 127.0, 125.2, 120.0, 114.6, 65.2, 58.3, 46.7, 36.6, 29.0, 28.4, 28.1, 23.1, 22.3, 2C not observed (overlapping peaks)

HRMS: ($C_{26}H_{32}O_4N$) [M+H]$^+$ requires 422.2326, found [M+H]$^+$ 422.2326

[α]$^{20}_D$ = +8.67 (c = 0.15, MeOH)

Literature value [α]$^{20}_D$ = +5.89 (c = 1, CHCl$_3$)[169]

ee = 94% by chiral HPLC

91 – (*R*)-2-((((9*H*-fluoren-9-yl)methoxy)carbonyl)amino)-2-methyldec-9-enoic acid
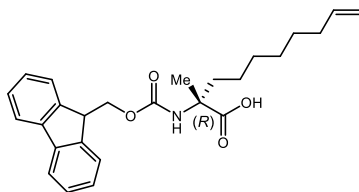
To a round bottomed flask containing H_2O (9 mL) and dioxane (9 mL) was added **153** (219 mg, 1.1 mmol, 1 equiv.) and Na_2CO_3 (233 mg, 2.2 mmol, 2 equiv.) to form a cloudy solution. The reaction mixture was cooled to 0 °C and 9-Fluorenylmethyl *N*-succinimidyl carbonate (741 mg, 2.2 mmol, 2 equiv.) was added in small portions over 2 hours, with the reaction temperature being maintained between 0 °C to 5 °C. Once addition was complete the reaction was left to stir at room temperature for 17 hours. The reaction mixture was then concentrated *in vacuo* and the residue separated with water (3 x 50 mL) and Et_2O (100 mL). The aqueous washings were back extracted with Et_2O (100 mL), combined and acidified to pH 4 using 1M HCl. The aqueous solution was then extracted with EtOAc (2 x 100 mL) and the organic layers washed with 1 M HCl (2 x 100 mL). The organic layers combined, dried and concentrated *in vacuo* to give the crude product as a yellow oil. The crude material was then purified by preparative HPLC (5-95% MeCN in H_2O over 30 minutes) to give the title compound as a yellow gummy solid (125 mg, 30%).

v_{max} (neat): 3067, 2926, 2854, 1705, 1642, 1504, 1450 cm^{-1}

^{1}H NMR (400 MHz, DMSO-d_6): δ 7.90 (d, 2H, 2 x Aro CH, *J* = 7.6 Hz), 7.73 (d, 2H, 2 x Aro CH, *J* = 7.6 Hz), 7.42 (dt, 2H, 2 x Aro CH, J = 6.4, 0.8 Hz), 7.37 – 7.31 (m, 3H, 2 x Aro CH, NH), 5.84 – 5.74 (m, 1H, Alkene CH), 5.02 – 4.92 (m, 2H, Alkene CH_2), 4.27 – 4.19 (m, 3H, Fmoc CH, Fmoc CH_2), 2.03 – 1.98 (m, 2H, Alkane CH_2), 1.76 – 1.68 (m, 2H, Alkane CH_2), 1.33 – 1.24 (m, 11H, 4 x Alkane CH_2, Me CH_3)

^{13}C NMR (101 MHz, $CDCl_3$): 175.4, 154.7, 143.9, 140.7, 138.8, 127.6, 127.0, 125.3, 120.1, 114.6, 65.2, 58.3, 46.7, 36.6, 33.1, 29.0, 28.4, 28.2, 23.1, 22.4

HRMS: ($C_{26}H_{32}O_4N_1$) [M+H]$^+$ requires 422.2326, found [M+H]$^+$ 422.2325

$[\alpha]^{20}_D$ = -8.9 (c = 0.15, MeOH)

ee = 94% by chiral HPLC

173 - Ethyl-2-((4-chlorobenzylidene)amino)acetate
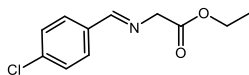
To a round bottomed flask containing Toluene (25 mL) was added 4-Chlorobenzaldehyde (**171**) (5 g, 35.6 mmol, 1 equiv.) and glycine ethyl ester (**172**) (5.213 g, 37.3 mmol, 1.05 equiv.) under N_2. Et_3N (5.7 mL, 40.9 mmol, 1.15 equiv.) was then added dropwise to the reaction mixture over 5 minutes. The reaction mixture was heated to 70 ^{o}C and left to stir for 16 hours. Once complete the mixture was separated with water (3 x 100 mL) and brine (100 mL). The organic layer was dried and concentrated *in vacuo* to give the crude product as a clear oil (Total mass 8.277 g, 40% toluene by ^{1}H NMR, 81% yield).

v_{max} (neat): 2980, 1734, 1647, 1595, 1489 cm^{-1}

^{1}H NMR (500 MHz, CDCl$_3$): δ 8.26 (s, 1H, Imine CH), 7.74 (d, 2H, 2 x Aro CH, ^3J = 8.5 Hz), 7.42 (d, 2H, 2 x Aro CH ^3J = 8.5 Hz), 4.43 (d, 2H, 2 x αH, ^3J = 1.2 Hz), 4.26 (quart, 2H, OEt CH$_2$, ^3J = 7.1 Hz), 1.33 (t, 3H, OEt CH$_3$, ^3J = 7.2 Hz).

^{13}C NMR (101 MHz, CDCl$_3$): 169.9, 163.9, 137.2, 129.64, 129.0, 128.9, 61.9, 61.1, 14.2

HRMS: (C$_{11}$H$_{13}$O$_2$N$_1$Cl$_1$) [M+H]$^+$ requires 226.0629, found [M+H]$^+$ 226.0631

169 - Ethyl 2-amino-2-(pent-4-en-1-yl)hept-6-enoate
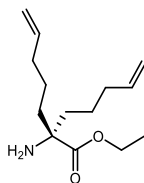
A round bottomed flask containing **173** (6.5 g, 40% toluene, 22.7 mmol, 1 equiv.) in THF (114 mL) under N_2 was cooled to 0°C. Sublimed *t*BuOK (2.547 g, 22.7 mmol, 1 equiv.) was added and the reaction mixture stirred at 0°C for 15 minutes, turning a deep red colour. **110** (5.081 g, 25.9 mmol, 1.1 equiv.) was added dropwise and the reaction mixture allowed to warm to room temperature over 1 hour. The reaction mixture was then cooled to 0°C and sublimed *t*BuOK (2.547 g, 22.7 mmol, 1 equiv.) was added and the reaction mixture stirred at 0 $^{\circ}$C for 15 minutes. **110** (5.081 g, 25.9 mmol, 1.1 equiv.) was added dropwise and the reaction mixture allowed to warm to room temperature over 16 hours, turning to a straw yellow solution. The reaction mixture was then quenched with sat. NH_4Cl (100 mL) and separated with EtOAc (200 mL). The organic layer was extracted with sat. $Na_2S_2O_3$ (100 mL) and brine (100 mL), and the aqueous washings back extracted with EtOAc (200 mL). The organic layers combined, dried and concentrated *in vacuo* to give the crude product **174** as a yellow oil. The oil was then dissolved in 2M HCl (200 mL) and MeOH (100 mL) and refluxed at 65°C for 16 hours. The reaction mixture was then cooled to room temperature and neutralised using conc. NH_3. The solution was then separated with DCM (300 mL) and washed with H_2O (100 mL) and brine (100 mL). The organic layer was then dried and concentrated *in vacuo* to give the crude product as an oil. The crude material was then purified by silica chromatography (0 - 25% Pet. Eth. in EtOAc) to give the title compound as a yellow gummy solid (1.66 g, 31%).

v_{max} (neat): 2924, 1726, 1639, 1456, 1442 cm^{-1}

^{1}H NMR (500 MHz, CDCl$_3$): δ 5.82 – 5.74 (m, 2H, 2 x Alkene CH), 5.03 – 4.95 (m, 4H, 2 x Alkene CH$_2$), 4.18 (quart, 2H, OEt CH$_2$, ^3J = 7.1 Hz), 2.07 – 2.03 (m, 4H, 2 x Alkane CH$_2$) 1.75 (td, 2H, 2 x Alkane CH, ^3J = 8.8, 4.9 Hz.), 1.55 (td, 2H, 2 x Alkane CH, ^3J = 8.5, 4.3 Hz.), 1.50 – 1.45 (m, 2H, 2 x Alkane CH), 1.28 (t, 3H, OEt CH$_3$, ^3J = 7.3 Hz), 1.27 – 1.22 (m, 2H, 2 x Alkane CH).

^{13}C NMR (101 MHz, CDCl$_3$): δ 177.1, 138.2, 114.8, 60.9, 39.5, 33.8, 23.1, 14.3. 1C not observed (overlap with solvent)

HRMS: (C$_{14}$H$_{26}$O$_2$N$_1$) [M+H]$^+$ requires 240.1958, found [M+H]$^+$ 240.1956

175 - 2-Amino-2-(pent-4-en-1-yl)hept-6-enoic acid
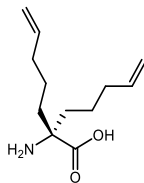
A round bottomed flask containing **169** (965 mg, 4.0 mmol, 1 equiv.) in THF (1 mL) and 2M NaOH (4 mL) was heated to 85 °C and left to reflux for 16 hours. The reaction mixture was the neutralised with conc. HCl and concentrated *in vacuo* to give a crude white solid. 10 g of Dowex resin (50WX8 hydrogen form) was swollen in water and packed into a column and washed with water. The crude solid was then dissolved in MeOH:water (1:1) and added to the resin. The column was then washed with MeOH (50 mL) and water (100 mL) to elute impurities. The product was then eluted using 25% NH_3 in water (200 mL) and concentrated *in vacuo*. The white solid was then dissolved in water and freeze dried to give the title compound as a fluffy white solid (836 mg, 98%).

v_{max} (neat): 2981, 1624, 1597, 1490 cm^{-1}

^{1}H NMR (500 MHz, DMSO-d_6): δ 6.87 (br s, 2H, NH_2), 5.81 – 5.73 (m, 2H, 2 x Alkene CH), 5.02 – 4.94 (m, 4H, 2 x Alkene CH_2), 1.96 (quart., 4H, 2 x Alkane CH_2 , ^3J = 6.6 Hz), 1.63 – 1.57 (m, 2H, 2 x Alkane CH), 1.53 – 1.43 (m, 4H, 2 x Alkane CH_2), 1.27 – 1.23 (m, 2H, 2 x Alkane CH), no peak for COOH observed.

^{13}C NMR (101 MHz, DMSO-d_6): δ 138.6, 114.7, 63.0, 36.4, 33.5, 22.5 1C not observed (overlap with solvent)

HRMS: ($C_{12}H_{22}O_2N_1$) [M+H]$^+$ requires 212.1645, found [M+H]$^+$ 212.1644

164 - 2-((((9H-Fluoren-9-yl)methoxy)carbonyl)amino)-2-(pent-4-en-1-yl)hept-6-enoic acid
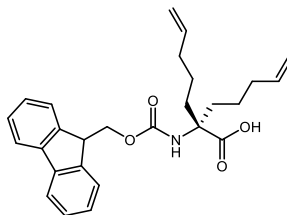
To a round bottomed flask containing H_2O (2.5 mL) and acetone (2.5 mL) was added **175** (90 mg, 0.4 mmol, 1 equiv.) and Na_2CO_3 (90 mg, 0.8 mmol, 2 equiv.) to form a cloudy solution. The reaction mixture was cooled to 0 ^{o}C and 9-fluorenylmethyl *N*-succinimidyl carbonate (127 mg, 0.6 mmol, 1.5 equiv.) was added in small portions over 30 minutes, with the reaction temperature being maintained between 0 ^{o}C to 5 ^{o}C. Once addition was complete the reaction was left to stir at room temperature for 16 hours. The reaction mixture was then concentrated *in vacuo* and the residue separated with water (3 x 10 mL) and Et_2O (20 mL). The aqueous washings were back extracted with Et_2O (20 mL), combined and acidified to pH4 using 1M HCl. The aqueous solution was then extracted with EtOAc (2 x 20 mL) and the organic layers washed with 1 M HCl (2 x 10 mL). The organic layers combined, dried and concentrated *in vacuo* to give the crude product as an oil. The crude material was then purified by silica chromatography (0 - 2% MeOH in DCM) to give the title compound as a white solid (55 mg, 43%).

v_{max} (neat): 3402, 2920, 1699, 1642, 1504, 1448 cm^{-1}

^{1}H NMR (400 MHz, DMSO-d_6): δ 12.68 (br s, 1H, COOH), 7.90 (d, 2H, 2 x Aro CH, ^3J = 7.5 Hz), 7.71 (d, 2H, 2 x Aro CH, ^3J = 7.0 Hz), 7.42 (t, 2 x Aro CH, ^3J = 7.5 Hz), 7.33 (td, 2 x Aro CH, ^3J = 6.5, 1.0 Hz), 7.02 (br s, 1H, NH), 5.79 – 5.72 (m, 2H, 2 x Alkene CH), 5.01 – 4.93 (m, 4H, 2 x Alkene CH$_2$), 4.29 – 4.22 (m, 3H, 3 x Fmoc CH), 1.98 (quart., 4H, 2 x Alkane CH$_2$, ^3J = 6.5 Hz), 1.82 – 1.74 (m, 4H, 2 x Alkane CH$_2$), 1.24 – 1.16 (m, 4H, 2 x Alkane CH$_2$).

^{13}C NMR (101 MHz, DMSO-d_6): δ 174.7, 154.0, 143.8, 140.7, 138.4, 127.6, 127.0, 125.2, 120.1, 114.9, 65.0, 61.6, 46.7, 33.1, 22.5. 1C not observed (overlap with solvent)

HRMS: ($C_{27}H_{31}O_4N_1$) [M-H]$^-$ requires 432.2180, found [M-H]$^-$ 432.2172

6.13 - Peptide synthesis data

Wild type
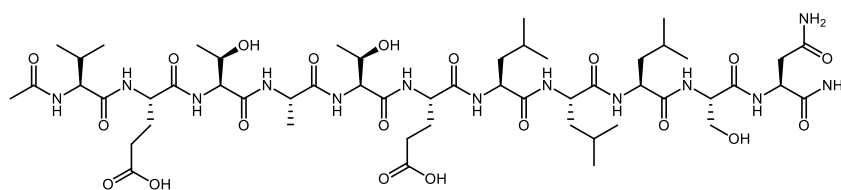
Peptide scale based on resin loading value = 0.18 mmol (507 mg)

Order of synthesis according to general procedures (Section 6,7):

Resin swelling (I), Loading (V, IX), Peptide synthesis (V), *N*-terminal capping (IV), Full cleave (IX)

Peptide synthesis (Refer to Table 33 for method details):

Sequence	Ac	V	E	T	A	T	E	L	L	L	S	N	NH$_2$
Method		vi)	vi)	v)	ii)	ii)	ii)	ii)	ii)	ii)	ii)	i)	

Yield = 3% (8 mg)

HRMS: (C$_{53}$H$_{92}$O$_{20}$N$_{13}$) [M+H]$^+$ requires 1230.6576, found [M+H]$^+$ 1230.6566

Analytical HPLC:
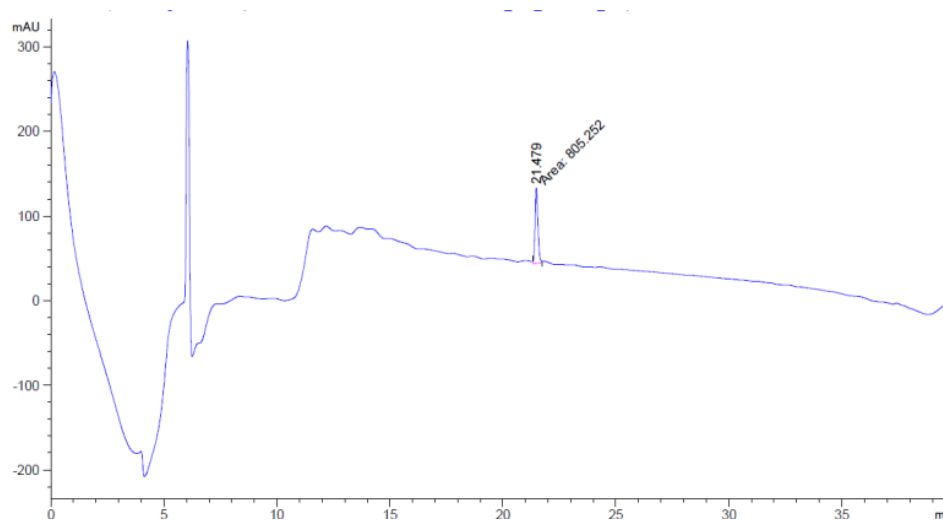
Retention time = 21.479 minutes

Purity = >95%

203

CD spectra:
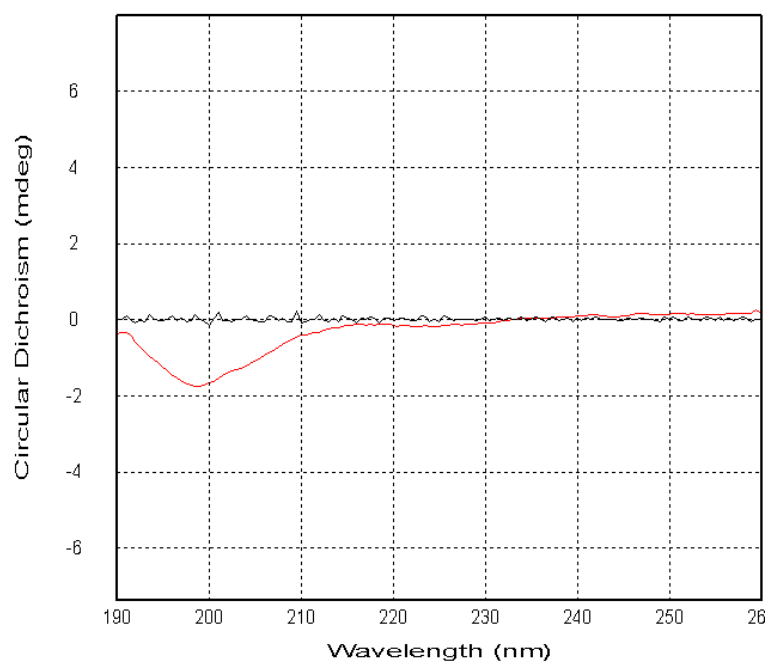
θ_{obs} = -0.972824, C = 200 µM, l = 0.1 mm, n = 11

Calculated helicity = 16%

Staple A
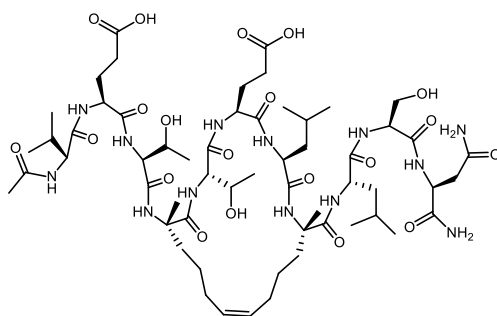
Peptide scale based on resin loading value = 0.15 mmol (218 mg)

Order of synthesis according to general procedures (Section 6,7):

Resin swelling (I), Peptide synthesis (V), *N*-terminal capping (IV), RCM (VI), Full cleave (X)

Peptide synthesis (Refer to Table 33 for method details):

Sequence	Ac	V	E	T	S_5	T	E	L	S_5	L	S	N	NH$_2$
Method		vi)	vi)	v)	iii)	ii)	ii)	iv)	iii)	ii)	ii)	ii)	

Yield = 16% (32 mg)

HRMS: ($C_{58}H_{98}O_{20}N_{13}$) [M+H]$^+$ requires 1296.7046, found [M+H]$^+$ 1296.7038

Analytical HPLC:
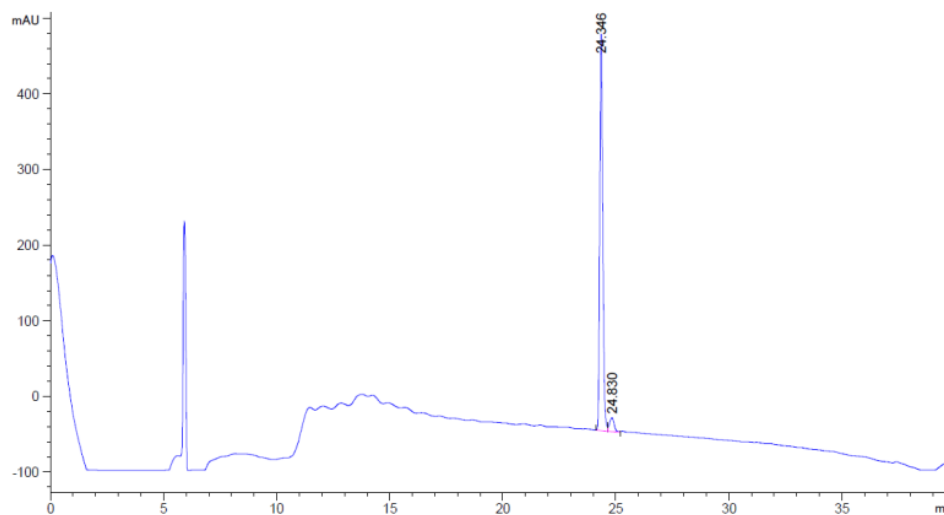
Retention time = 24.346 minutes

Purity = 95%
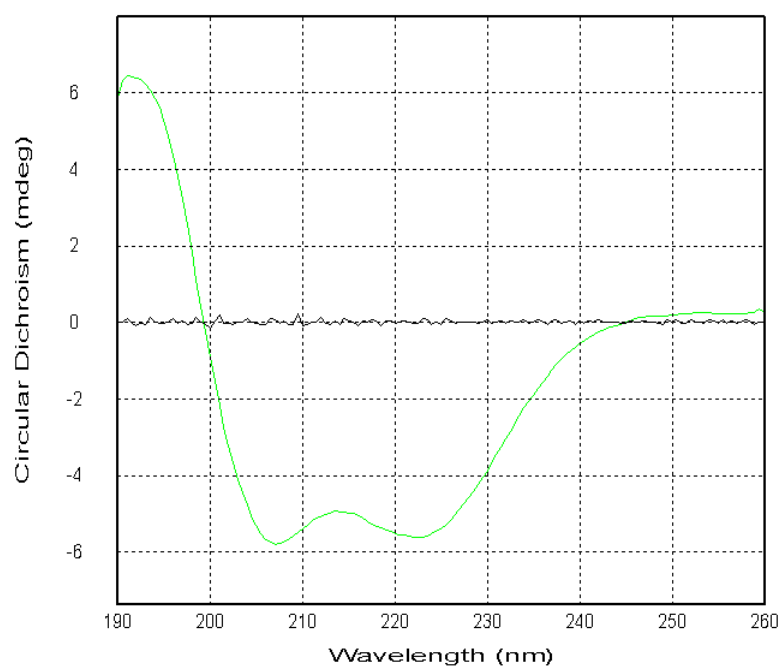
CD spectra:

θ_{obs} = -5.653790, C = 200 μM, l = 0.1 mm, n = 11

Calculated helicity = 91%

Temperature ramp CD spectra:

Temp. (°C)	20	25	30	35	40	45	50	55	60	65	70	75	80	20
θ_{222}	-8.37	-8.24	-8.06	-7.83	-7.58	-7.39	-7.18	-7.02	-6.83	-6.73	-6.53	-6.44	-6.37	-8.34

C = 15 μM, l = 2 mm, n = 11

Staple B
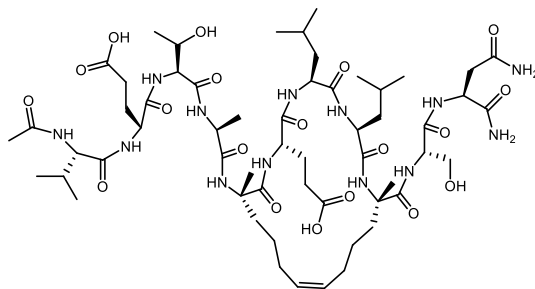
Peptide scale based on resin loading value = 0.29 mmol (876 mg)

Order of synthesis according to general procedures (Section 6,7):
Resin swelling (I), Loading (V, IX), Peptide synthesis (V), *N*-terminal capping (IV),
RCM (VI), Full cleave (X)

Peptide synthesis (Refer to Table 33 for method details):

Sequence	Ac	V	E	T	A	S_5	E	L	L	S_5	S	N	NH_2
Method		vi)	vi)	v)	iv)	iii)	ii)	ii)	iv)	iii)	ii)	i)	

Yield = 5% (32 mg)

HRMS: ($C_{57}H_{96}O_{19}N_{13}$) $[M+H]^+$ requires 1266.6940, found $[M+H]^+$ 1266.6929

Analytical HPLC:
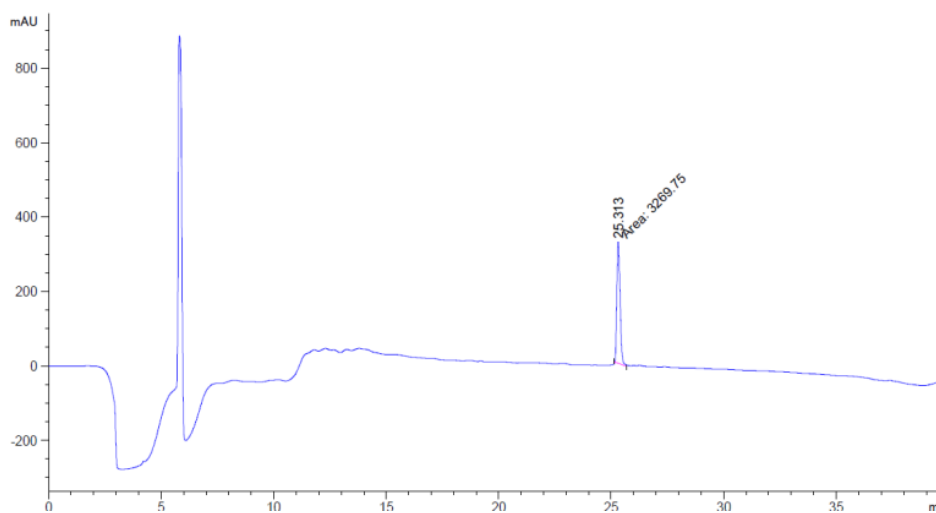
Retention time = 25.313 minutes

Purity = > 95%
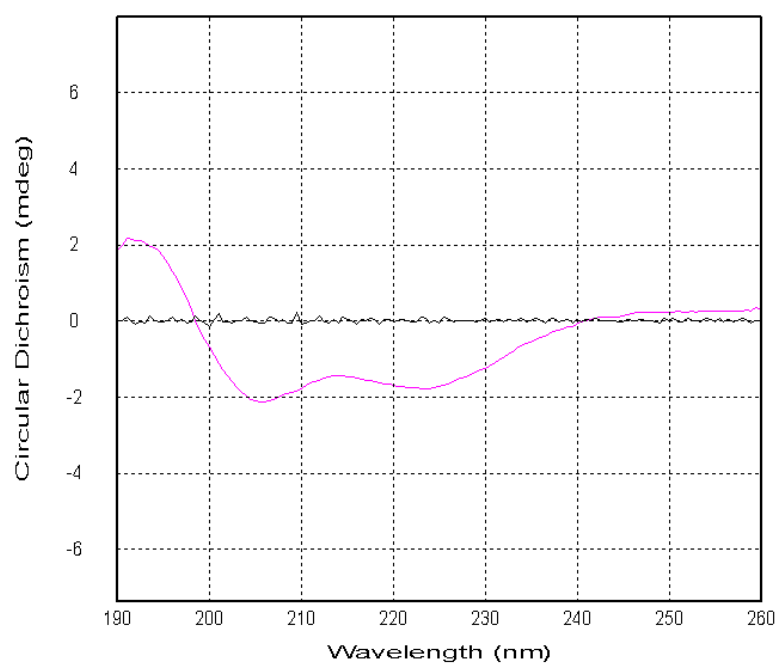
CD spectra:

θ_{obs} = -2.560140, C = 200 μM, l = 0.1 mm, n = 11

Calculated helicity = 41%

Temperature ramp CD spectra:

Temp. (°C)	20	25	30	35	40	45	50	55	60	65	70	75	80	20
θ_{222}	-8.21	-8.00	-7.81	-7.60	-7.37	-7.20	-7.04	-6.92	-6.71	-6.63	-6.59	-6.57	-6.42	-8.03

C = 35 μM, l = 2 mm, n = 11

Staple C
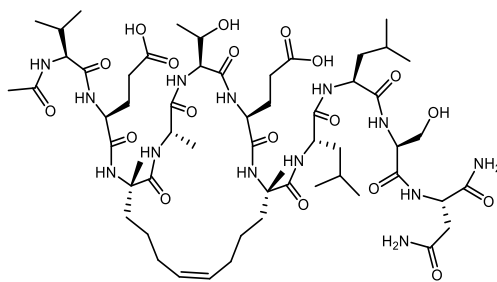
Peptide scale based on resin loading value = 0.23 mmol (786 g)

Order of synthesis according to general procedures (Section 6,7):

Resin swelling (I), Loading (V, IX), Peptide synthesis (V), *N*-terminal capping (IV), RCM (VI), Full cleave (X)

Peptide synthesis (Refer to Table 33 for method details):

Sequence	Ac	V	E	S$_5$	A	T	E	S$_5$	L	L	S	N	NH$_2$
Method		vi)	iv)	iii)	ii)	ii)	iv)	iii)	ii)	ii)	ii)	i)	

Yield = 13% (39 mg)

HRMS: (C$_{57}$H$_{97}$O$_{19}$N$_{13}$) [M+H]$^{2+}$ requires 633.8506, found [M+H]$^{2+}$ 633.8504

Analytical HPLC:
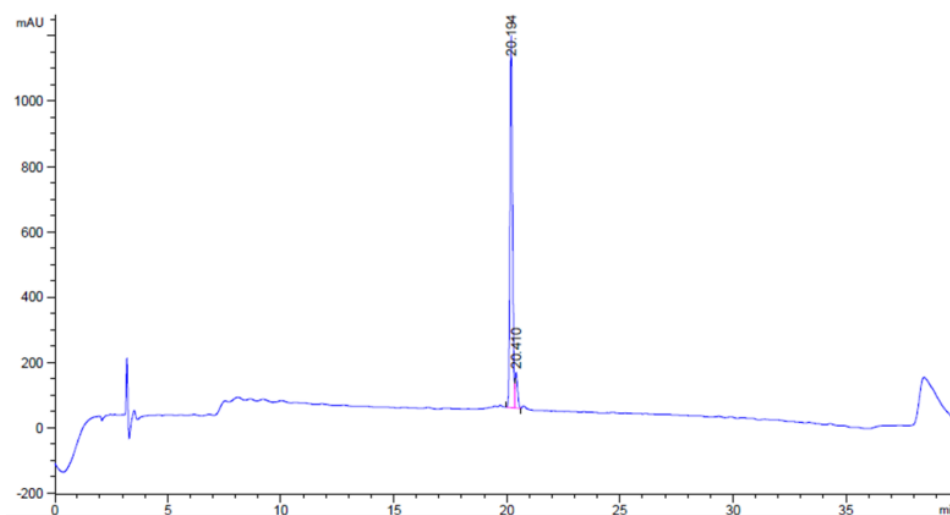
Retention time = 20.194 minutes

Purity = 91%

CD spectra:
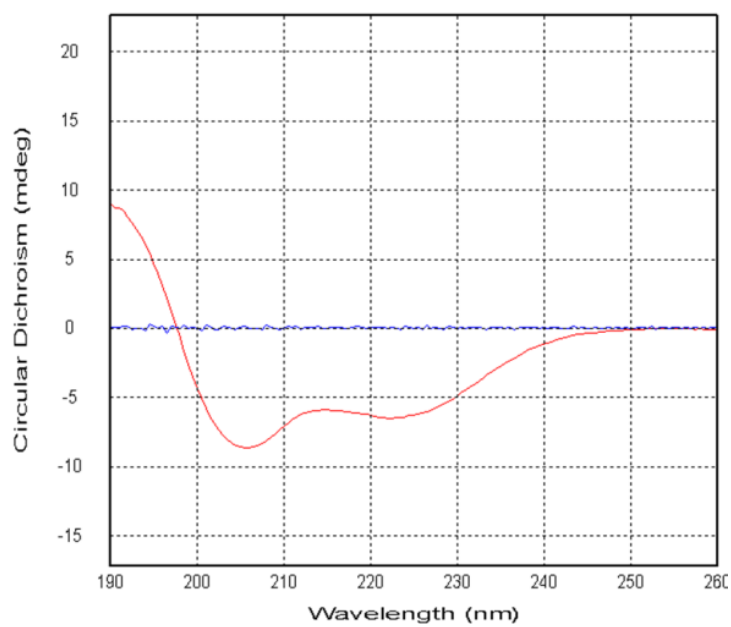
θ_{obs} = -6.529320, C = 50 μM, l = 1 mm, n = 11

Calculated helicity = 42%

Staple D
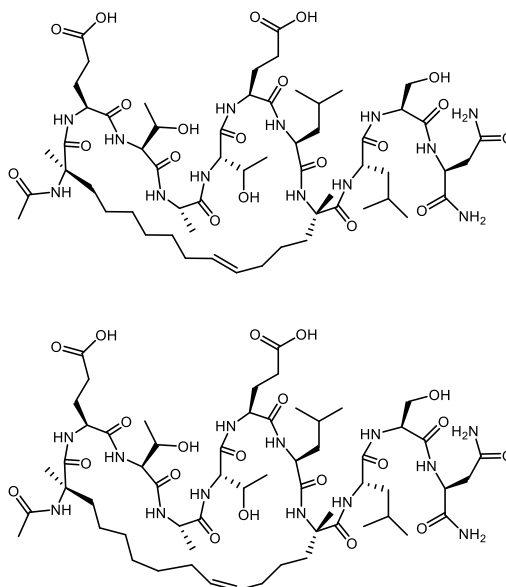
Peptide scale based on resin loading value = 0.1 mmol (145 mg)

Order of synthesis according to general procedures (Section 6,7):
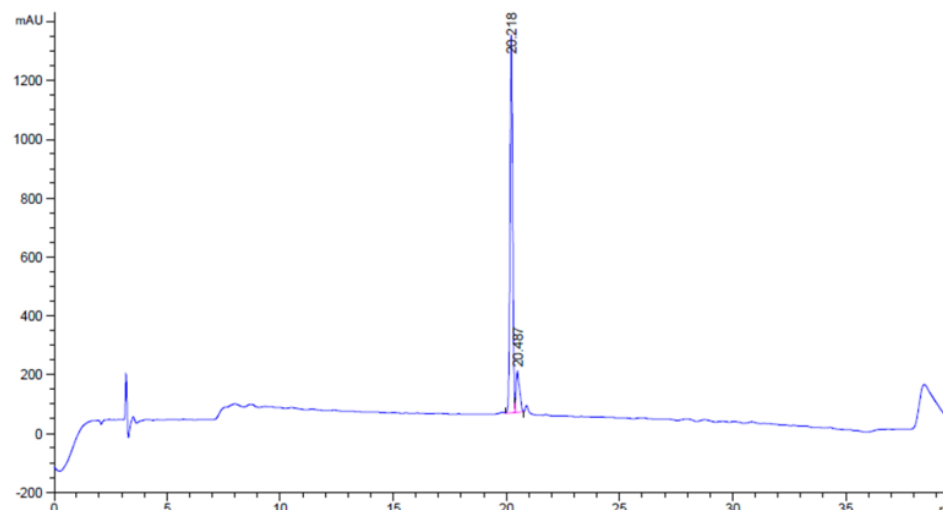Resin swelling (I), Peptide synthesis (V), *N*-terminal capping (IV), RCM (VI), Full cleave (X)

Peptide synthesis (Refer to Table 33 for method details):

Sequence	Ac	R$_8$	E	T	A	T	E	L	S$_5$	L	S	N	NH$_2$
Method		iii)	vi)	v)	ii)	ii)	ii)	iv)	iii)	ii)	ii)	ii)	

Trans Yield = 4% (5 mg)
Cis Yield = 1% (1 mg)

Trans HRMS: (C$_{59}$H$_{101}$O$_{20}$N$_{13}$) [M+H]$^{2+}$ requires 655.8637, found [M+H]$^{2+}$ 655.8637
Cis HRMS: (C$_{59}$H$_{99}$O$_{20}$N$_{13}$) [M-H]$^{2-}$ requires 653.8492, found [M-H]$^{2-}$ 653.8473

Trans Analytical HPLC:
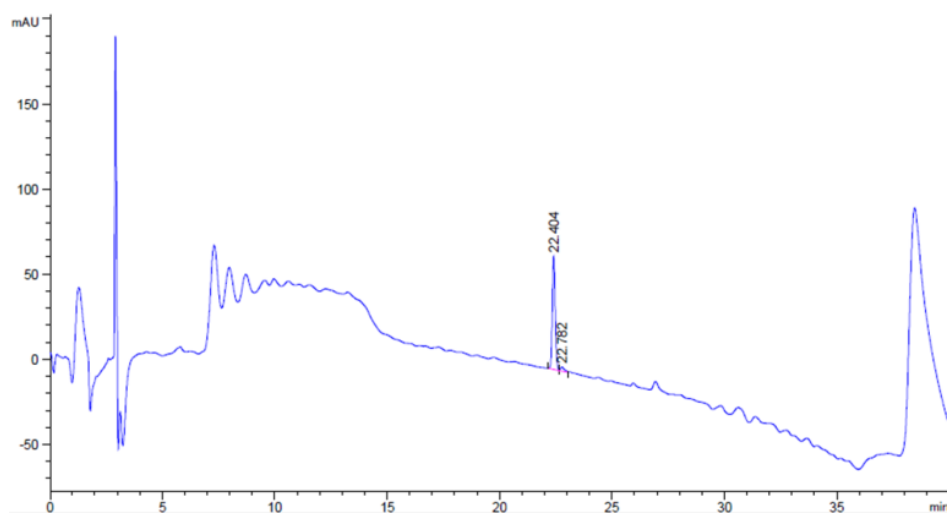
Retention time = 22.404 minutes

Purity = > 95%

Cis Analytical HPLC:
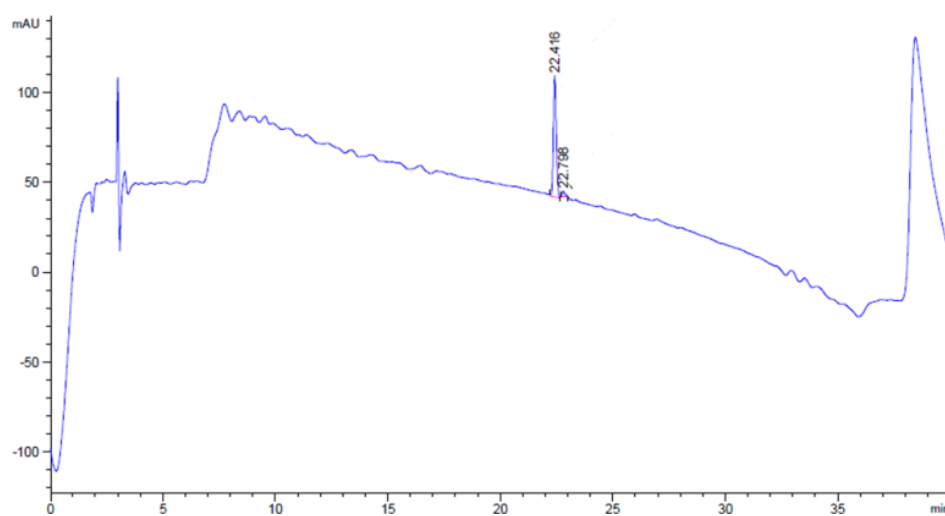
Retention time = 22.416 minutes

Purity = 95%

Trans CD spectra:
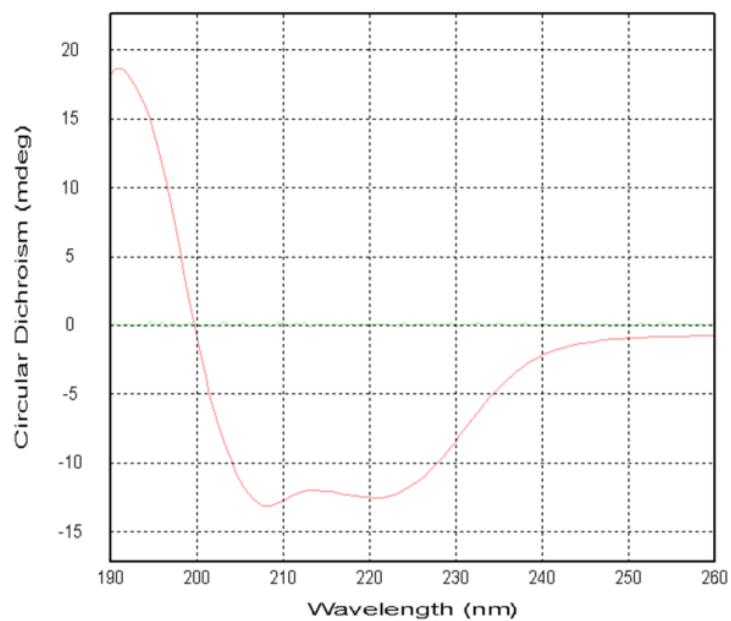
θ_{obs} = -12.421400, C = 50 µM, l = 1 mm, n = 11

Calculated helicity = 80%

Cis CD spectra:
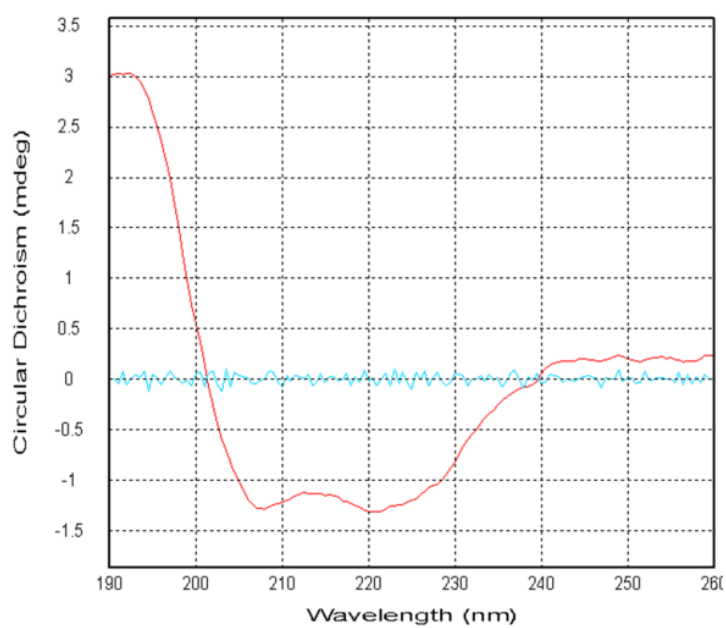
θ_{obs} = -1.294979, C = 200 µM, l = 0.1 mm, n = 11

Calculated helicity = 21%

Staple E
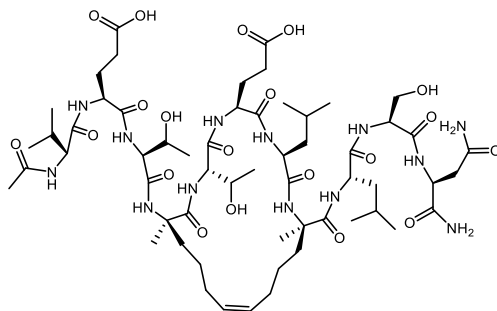
Peptide scale based on resin loading value = 0.25 mmol (767 g)

Order of synthesis according to general procedures (Section 6,7):

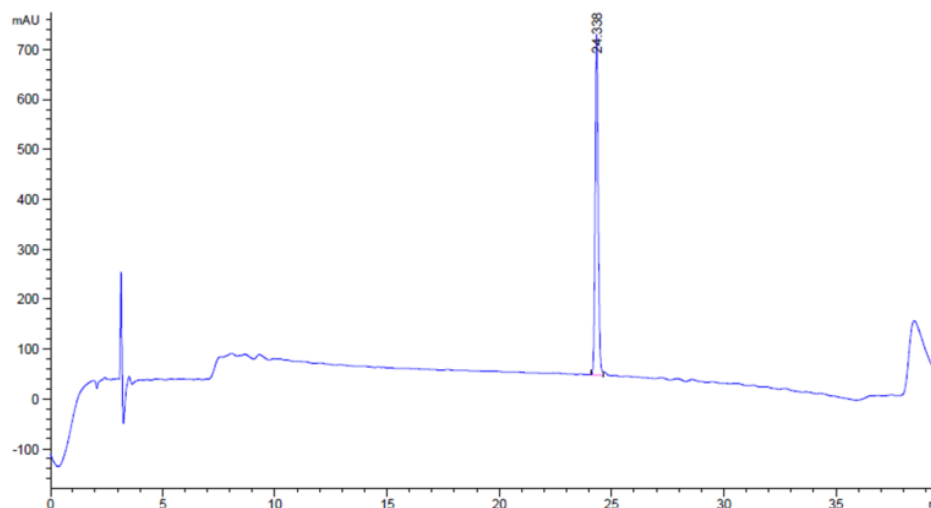Resin swelling (I), Loading (V, IX), Peptide synthesis (V), *N*-terminal capping (IV), RCM (VI), Full cleave (X)

Peptide synthesis (Refer to Table 33 for method details):

Sequence	Ac	V	E	T	R$_5$	T	E	L	R$_5$	L	S	N	NH$_2$
Method		vi)	vi)	v)	iii)	ii)	ii)	iv)	iii)	ii)	ii)	i)	

Yield = 17% (55 mg)

HRMS: (C$_{58}$H$_{99}$O$_{20}$N$_{13}$) [M+H]$^{2+}$ requires 648.8559, found [M+H]$^{2+}$ 648.8560

Analytical HPLC:

Retention time = 20.218 minutes

Purity = 91%

CD spectra:
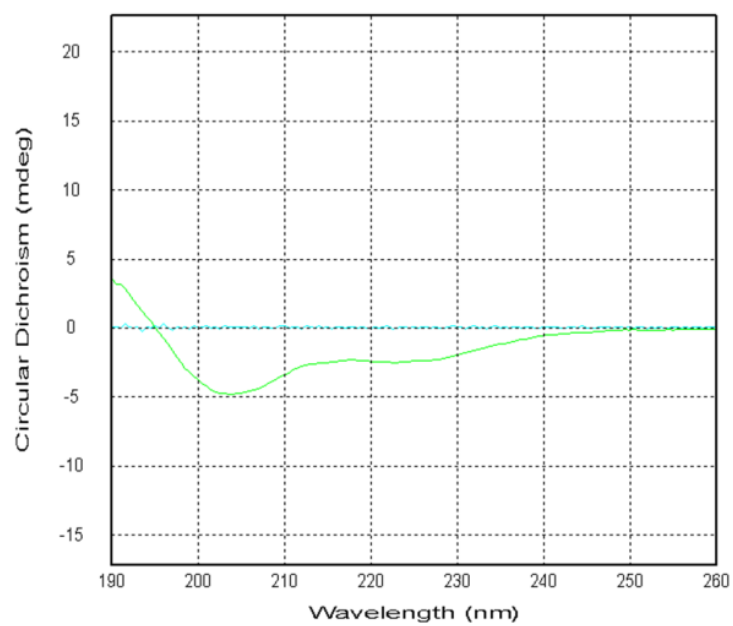
θ_{obs} = -2.527690, C = 50 μM, l = 1 mm, n = 11

Calculated helicity = 16%,

Staple G
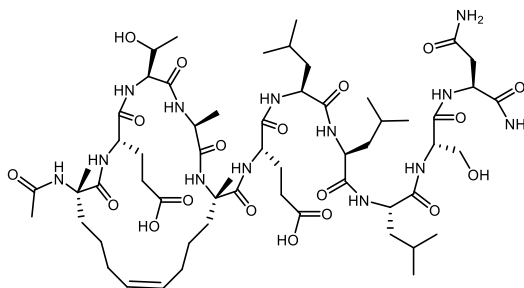
Peptide scale based on resin loading value = 0.1 mmol (145 mg)

Order of synthesis according to general procedures (Section 6,7):

Resin swelling (I), Peptide synthesis (V), *N*-terminal capping (IV), RCM (VI), Full cleave (X)

Peptide synthesis (Refer to Table 33 for method details):

Sequence	Ac	S_5	E	T	A	S_5	E	L	L	L	S	N	NH_2
Method		iii)	vi)	v)	iv)	iii)	ii)	ii)	ii)	ii)	ii)	ii)	

Yield = 7% (9 mg)

HRMS: ($C_{58}H_{99}O_{19}N_{13}$) $[M+H]^{2+}$ requires 640.8585, found $[M+H]^{2+}$ 640.8585

Analytical HPLC:

Retention time = 24.338 minutes

Purity = > 95%

CD spectra:
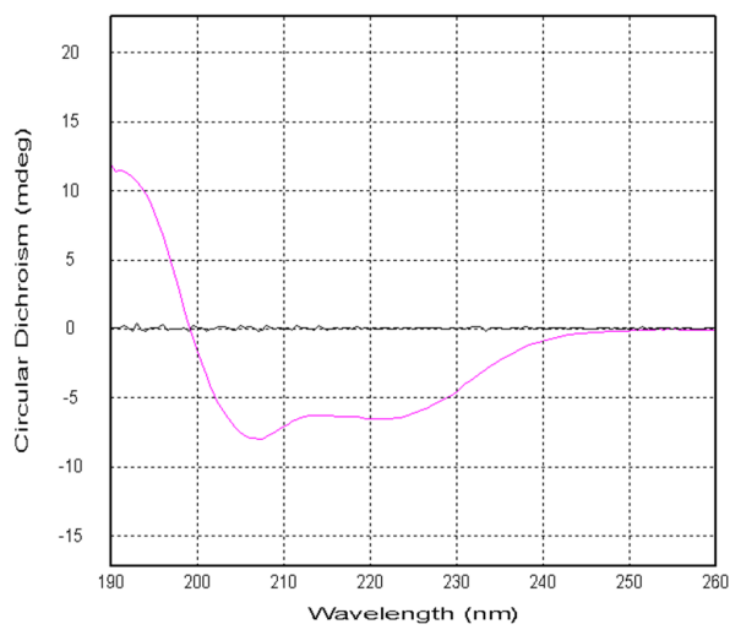
θ_{obs} = -6.590330, C = 50 µM, l = 1 mm, n = 11

Calculated helicity = 42%,

Staple I
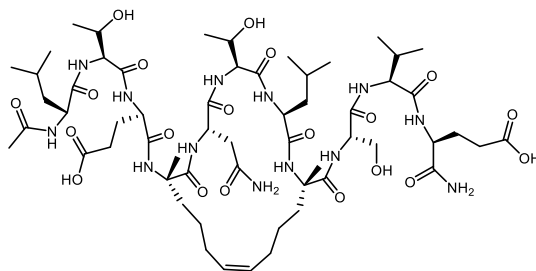
Peptide scale based on resin loading value = 0.1 mmol (145 mg)

Order of synthesis according to general procedures (Section 6,7):
Resin swelling (I), Peptide synthesis (V), *N*-terminal capping (IV), RCM (VI), Full cleave (X)

Peptide synthesis (Refer to Table 33 for method details):

Sequence	Ac	L	T	E	S$_5$	N	T	L	S$_5$	S	V	E	NH$_2$
Method		vi)	v)	iv)	iii)	ii)	v)	iv)	iii)	ii)	ii)	ii)	

Yield = 3% (23 mg)

HRMS: ($C_{58}H_{99}O_{20}N_{13}$) $[M+H]^{2+}$ requires 648.8559, found $[M+H]^{2+}$ 648.8558

Analytical HPLC:
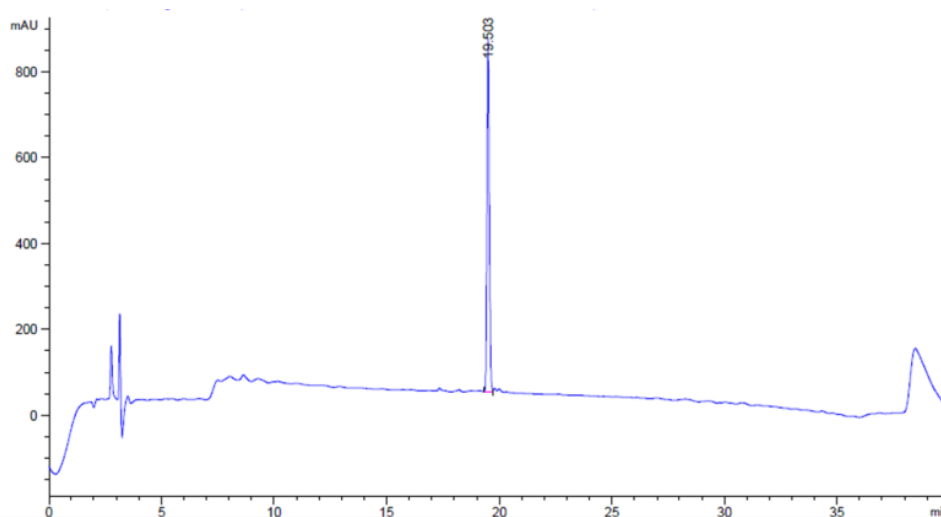
Retention time = 19.503 minutes

Purity = > 95%

CD spectra:
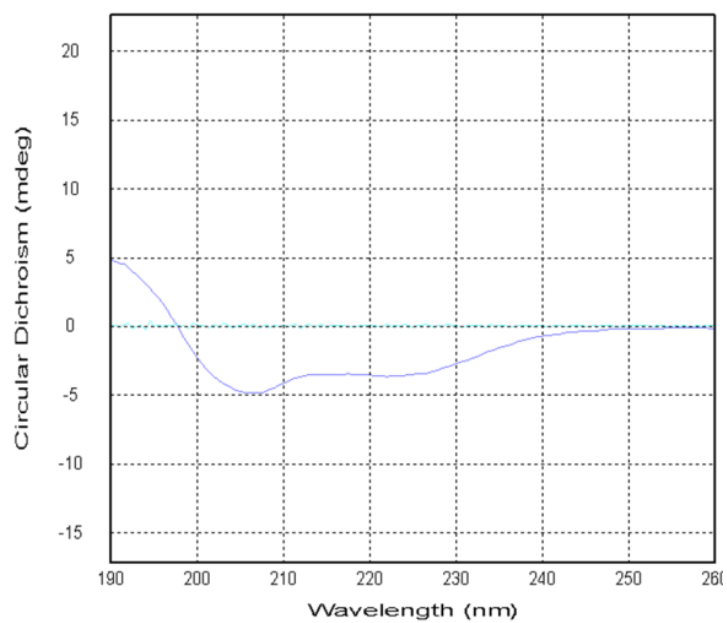
θ_{obs} = -3.677910, C = 50 µM, I = 1 mm, n = 11

Calculated helicity = 24%,

Staple J
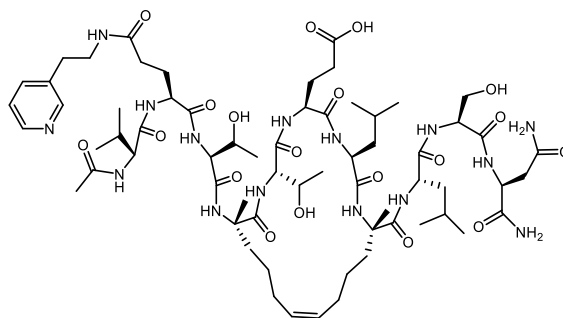
Peptide scale based on resin loading value = 0.1 mmol (145 mg)

Order of synthesis according to general procedures (Section 6,7):
Resin swelling (I), Peptide synthesis (V), *N*-terminal capping (IV), Allyl deprotection (VII), Amine coupling (Below), RCM (VI), Full cleave (X)

Amine coupling: 3-(2-aminoethyl)pyridine (**160**) (61 mg, 0.5 mmol, 5 equiv.), HATU (190 mg, 0.5 mmol, 5 equiv.), DIPEA (175 µL, 1 mmol, 10 equiv.), DMF (5 mL), 2 h
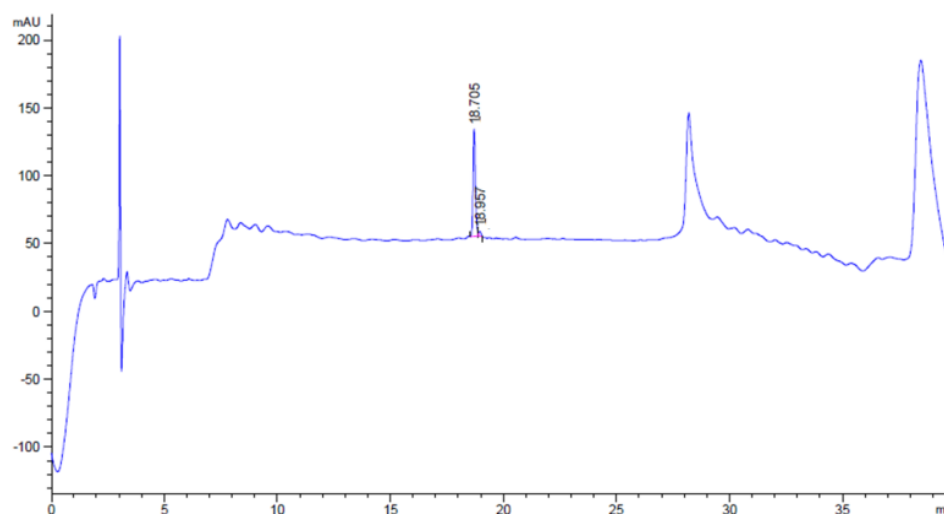
Peptide synthesis (Refer to Table 33 for method details):

Sequence	Ac	V	E*	T	S_5	T	E	L	S_5	L	S	N	NH$_2$
Method		vi)	vii)	v)	iii)	ii)	ii)	iv)	iii)	ii)	ii)	ii)	

E* = Fmoc-Glu(OAll)-OH

Yield = 2% (1 mg)

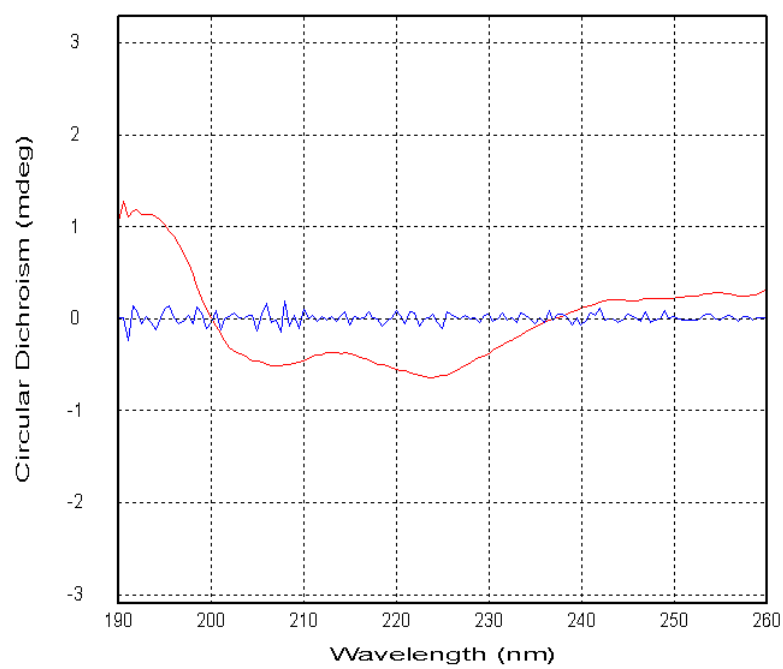HRMS: ($C_{65}H_{106}O_{19}N_{15}$) [M+H]$^+$ requires 1400.7784, found [M+H]$^+$ 1400.7783
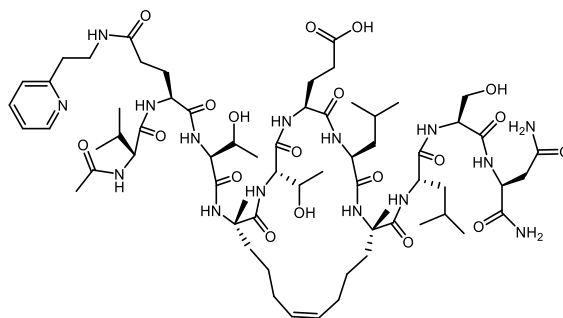
Analytical HPLC:

Retention time = 18.705 minutes

Purity = 95%

CD spectra:

θ_{obs} = -0.608199, C = 200 μM, l = 0.1 mm, n = 11

Calculated helicity = 10%

Staple K

Peptide scale based on resin loading value = 0.13 mmol (500 mg)

Order of synthesis according to general procedures (Section 6,7):

Resin swelling (I), Loading (V, IX), Peptide synthesis (V), *N*-terminal capping (IV), RCM (VI), Allyl deprotection (VII), Amine coupling (Below), Full cleave (X)

Amine coupling: 2-(2-Pyridyl)ethylamine (**162**) (78 mg, 0.6 mmol, 5 equiv.), HATU (243 mg, 0.6 mmol, 5 equiv.), DIPEA (223 µL, 1.3 mmol, 10 equiv.), DMF (5 mL), 2 h
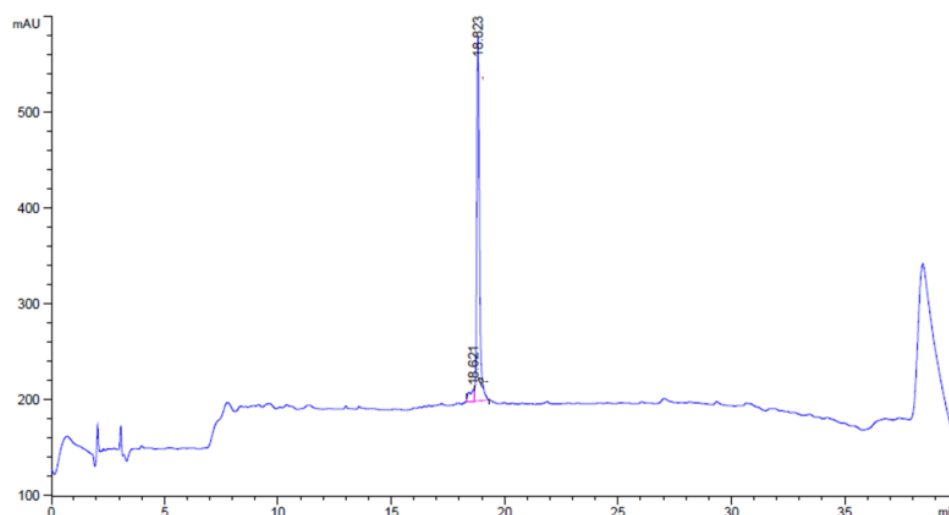
Peptide synthesis (Refer to Table 33 for method details):

Sequence	Ac	V	E*	T	S$_5$	T	E	L	S$_5$	L	S	N	NH$_2$
Method		vi)	vii)	v)	iii)	ii)	ii)	iv)	iii)	ii)	ii)	i)	

E* = Fmoc-Glu(OAll)-OH

Yield = 2% (4 mg)

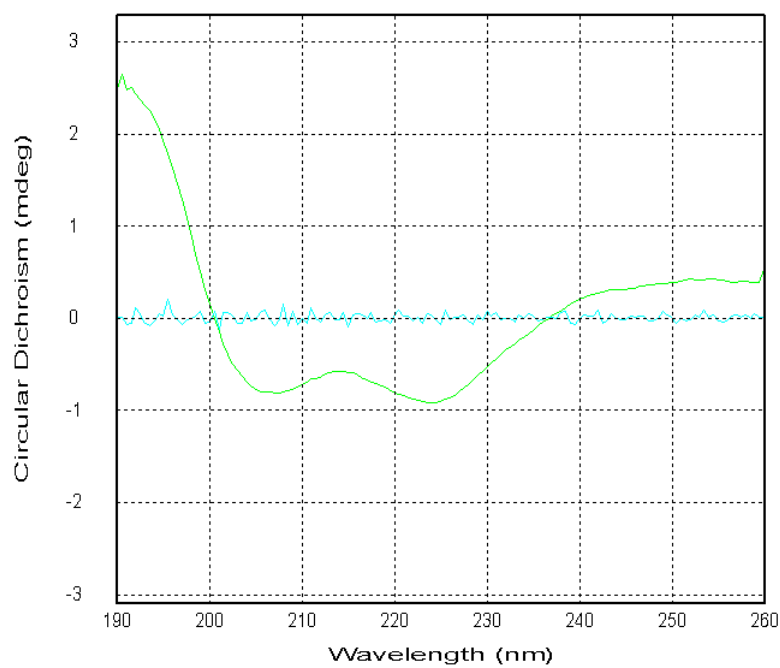HRMS: (C$_{65}$H$_{105}$O$_{19}$N$_{15}$Na$_1$) [M+H]$^+$ requires 1422.7603, found [M+H]$^+$ 1422.7626

Analytical HPLC:

Retention time = 18.823 minutes

Purity = 95%
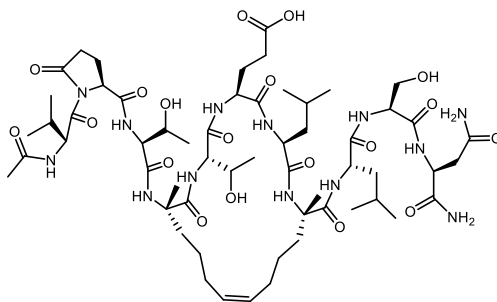
CD spectra:

θ_{obs} = -0.881275, C = 200 μM, l = 0.1 mm, n = 11

Calculated helicity = 14%

Staple M

Peptide scale based on resin loading value = 0.1 mmol (145 mg)

Order of synthesis according to general procedures (Section 6,7):
Resin swelling (I), Peptide synthesis (V), *N*-terminal capping (IV), Allyl deprotection (VII), Amine coupling (Below), RCM (VI), Full cleave (X)

Amine coupling: HATU (190 mg, 0.5 mmol, 5 equiv.), DIPEA (175 µL, 1 mmol, 10 equiv.), DMF (5 mL), 2 h
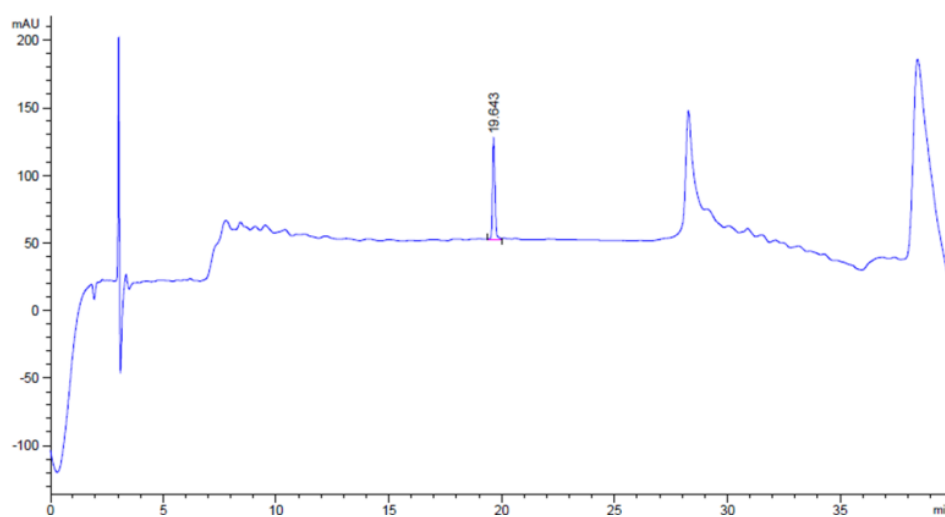
Peptide synthesis (Refer to Table 33 for method details):

Sequence	Ac	V	E*	T	S$_5$	T	E	L	S$_5$	L	S	N	NH$_2$
Method		vi)	vii)	v)	iii)	ii)	ii)	iv)	iii)	ii)	ii)	ii)	

E* = Fmoc-Glu(OAll)-OH

Yield = 10% (5 mg)

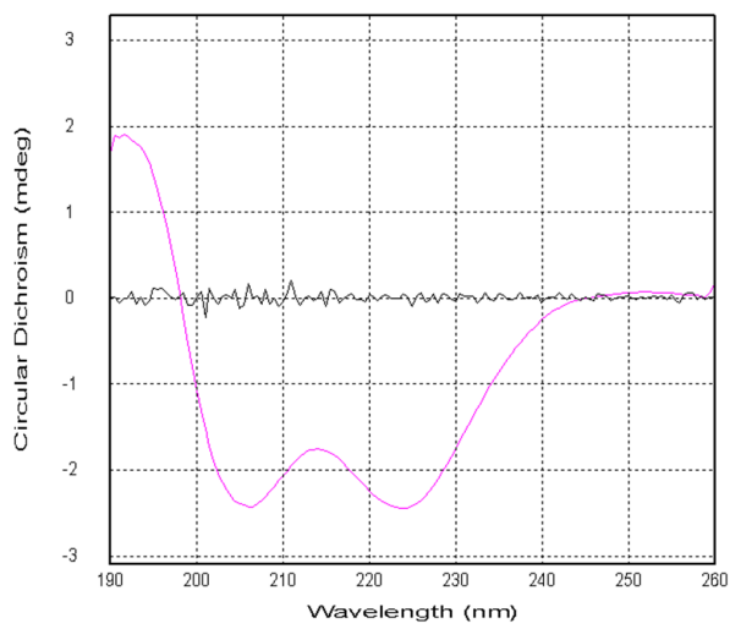HRMS: (C$_{58}$H$_{96}$O$_{19}$N$_{13}$) [M+H]$^+$ requires 1278.6940, found [M+H]$^+$ 1278.6936

Analytical HPLC:

Retention time = 19.643 minutes

Purity = > 95%

CD spectra:

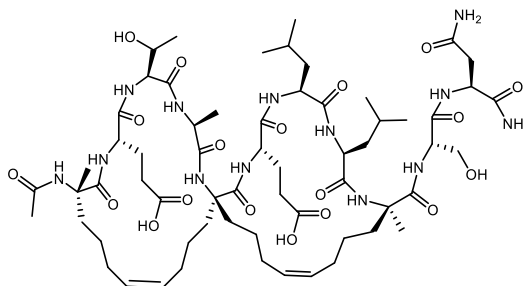
θ_{obs} = -2.402659, C = 200 µM, l = 0.1 mm, n = 11

Calculated helicity = 39%

Temperature ramp CD spectra:

Temp. (°C)	20	25	30	35	40	45	50	55	60	65	70	75	80	20
θ_{222}	-8.65	-8.69	-8.46	-8.23	-7.99	-7.79	-7.58	-7.33	-7.11	-6.90	-6.80	-6.63	-6.45	-8.72

C = 35 µM, l = 2 mm, n = 11

225

Staple N

Peptide scale based on resin loading value = 0.16 mmol (500 mg)

Order of synthesis according to general procedures (Section 6,7):

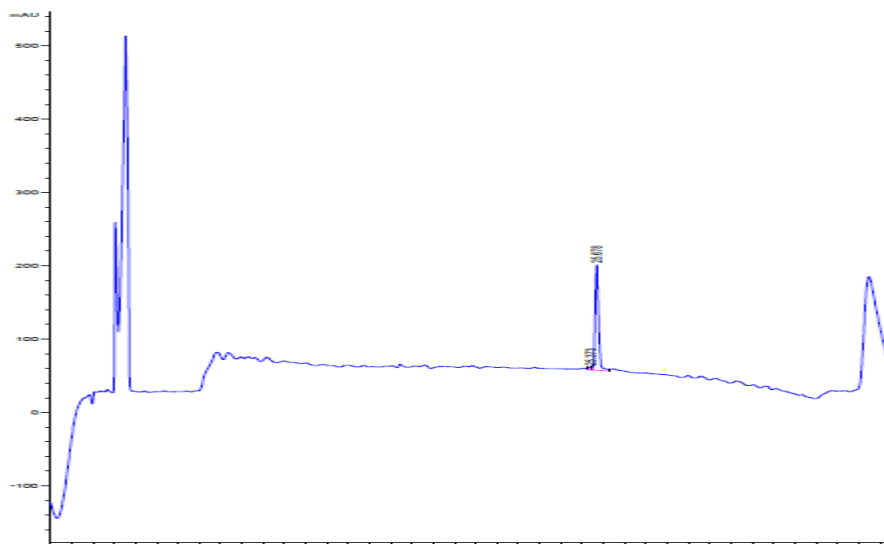Resin swelling (I), Loading (V, IX), Peptide synthesis (V), *N*-terminal capping (IV), RCM (VI), Full cleave (X)

Peptide synthesis (Refer to Table 33 for method details):

Sequence	Ac	S_5	E	T	A	B_5	E	L	L	R_5	S	N	NH_2
Method		iii)	vi)	v)	iv)	viii)	ii)	ii)	iv)	iii)	ii)	i)	

Yield = 5% (11 mg)

HRMS: ($C_{62}H_{99}O_{19}N_{13}$) [M-H]$^{2-}$ requires 664.8596, found [M-H]$^{2-}$ 664.8576
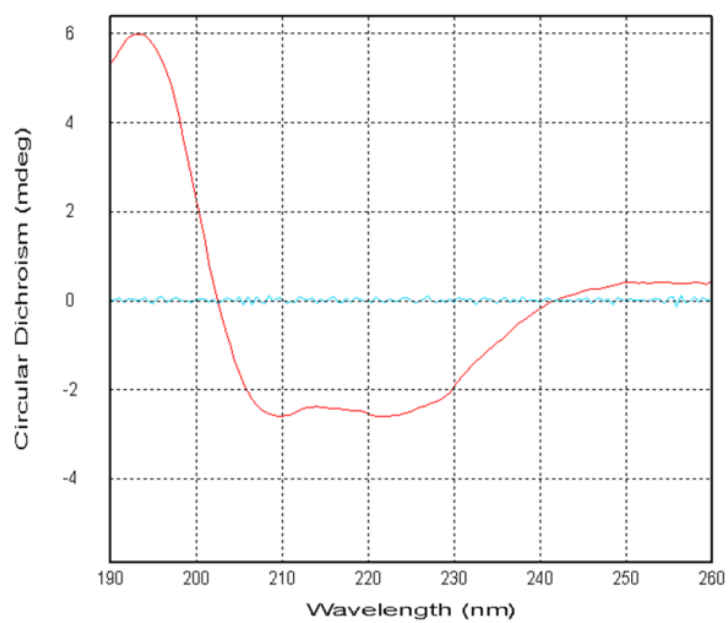
Analytical HPLC:

Retention time = 25.678 minutes

Purity = 97%

CD spectra:

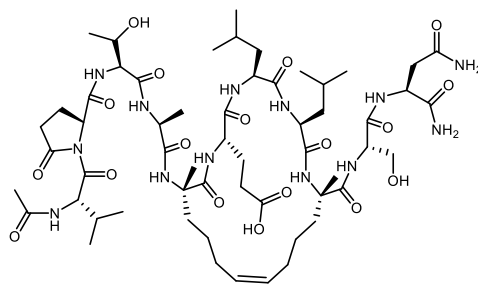
θ_{obs} = -2.617129, C = 200 µM, l = 0.1 mm, n = 11

Calculated helicity = 42%

Temperature ramp CD spectra:

Temp. (°C)	20	25	30	35	40	45	50	55	60	65	70	75	80	20
θ_{222}	-13.9	-13.8	-13.5	-13.1	-12.8	-12.4	-12.0	-11.5	-11.2	-10.7	-10.4	-10.2	-9.8	-13.9

C = 50 µM, l = 2 mm, n = 11

Staple P

Peptide scale based on resin loading value = 0.15 mmol (500 mg)

Order of synthesis according to general procedures (Section 6,7):
Resin swelling (I), Loading (V, IX), Peptide synthesis (V), *N*-terminal capping (IV),
Allyl deprotection (VII), Amine coupling (Below), RCM (VI), Full cleave (X)

Amine coupling: HATU (260 mg, 0.7 mmol, 5 equiv.), DIPEA (244 µL, 1.4 mmol, 10 equiv.), DMF (5 mL), 2 h
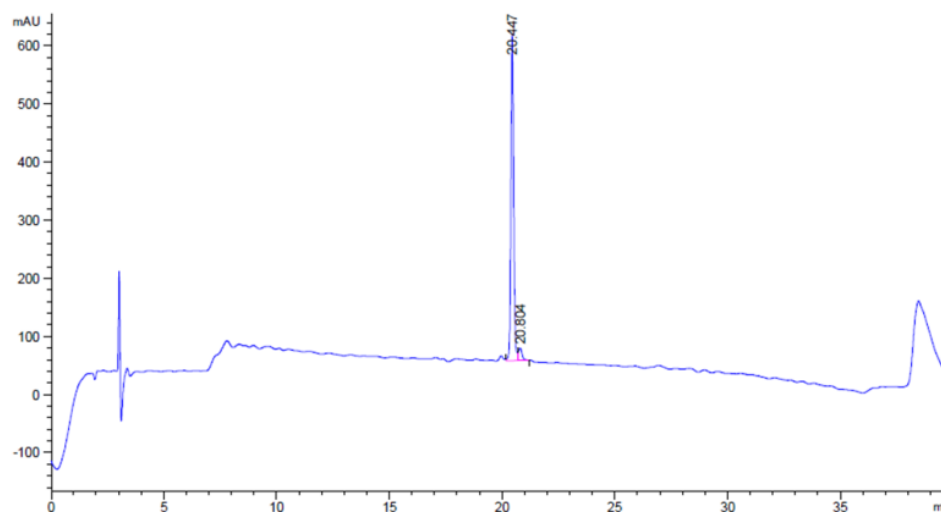
Peptide synthesis (Refer to Table 33 for method details):

Sequence	Ac	V	E*	T	A	S_5	E	L	L	S_5	S	N	NH$_2$
Method		vi)	vii)	v)	iv)	iii)	ii)	ii)	iv)	iii)	ii)	i)	

E* = Fmoc-Glu(OAll)-OH

Yield = 17% (32 mg)

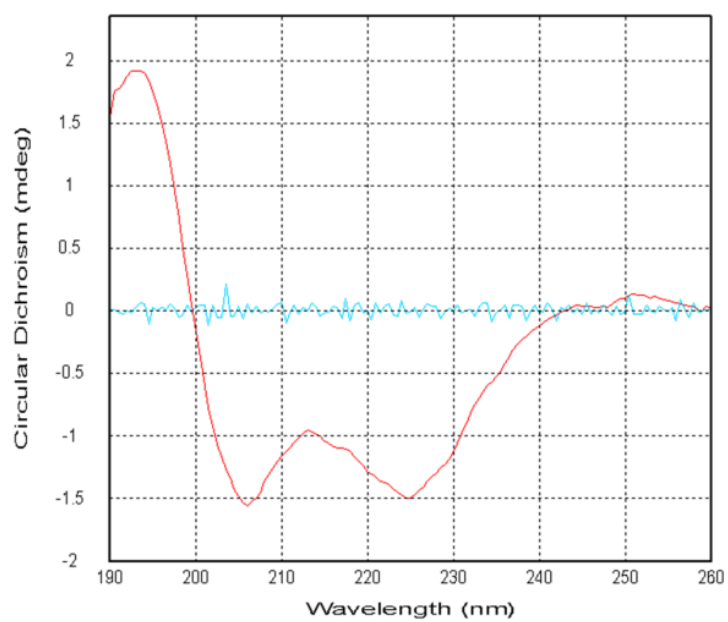HRMS: ($C_{57}H_{93}O_{18}N_{13}Na_1$) [M+H]$^+$ requires 1270.6654, found [M+H]$^+$ 1270.6631

Analytical HPLC:

Retention time = 20.447 minutes

Purity = 95%
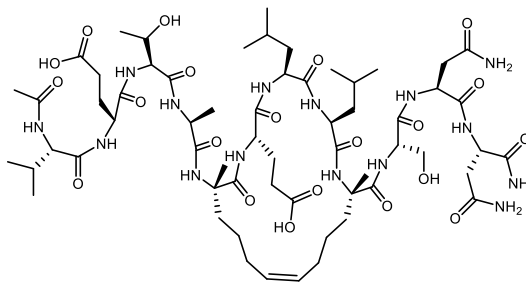
CD spectra:

θ_{obs} = -1.378150, C = 200 μM, l = 0.1 mm, n = 11

Calculated helicity = 22%

Staple Q

Peptide scale based on resin loading value = 0.11 mmol (500 mg)

Order of synthesis according to general procedures (Section 6,7):

Resin swelling (I), Loading (V, IX), Peptide synthesis (V), *N*-terminal capping (IV), RCM (VI), Full cleave (X)

Peptide synthesis (Refer to Table 33 for method details):

Sequence	Ac	V	E	T	A	S_5	E	L	L	S_5	S	N	N	NH_2
Method		vi)	vi)	v)	iv)	iii)	ii)	ii)	iv)	iii)	ii)	ii)	i)	

Yield = 2% (3 mg)

HRMS: ($C_{61}H_{101}O_{21}N_{15}Na_1$) [M+H]$^+$ requires 1402.7189, found [M+H]$^+$ 1402.7162

Analytical HPLC:

Retention time = 19.291 minutes

Purity = > 95%

CD spectra:

θ_{obs} = -2.157359, C = 200 µM, l = 0.1 mm, n = 12

Calculated helicity = 31%

Staple S

Peptide scale based on resin loading value = 0.12 mmol (500 mg)

Order of synthesis according to general procedures (Section 6,7):
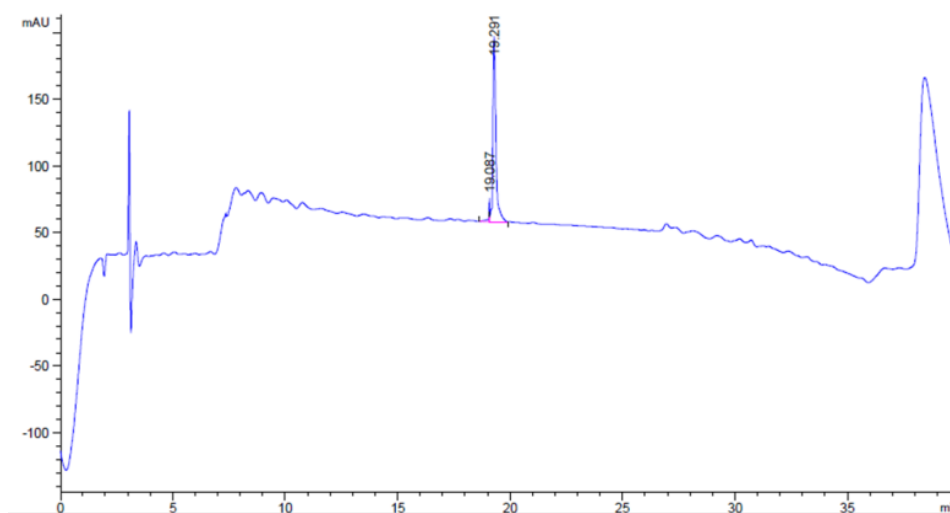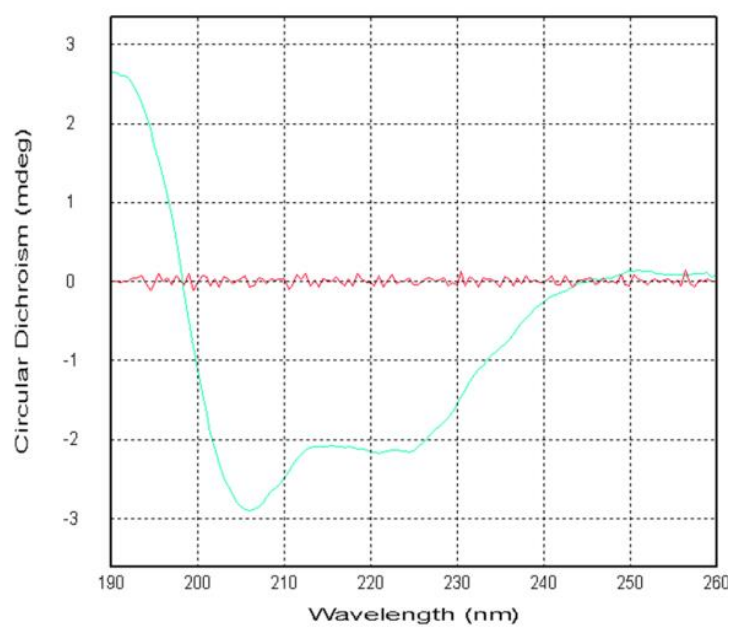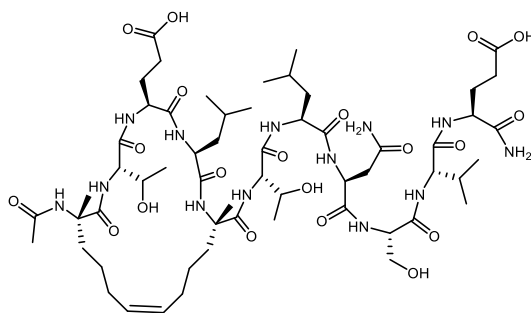Resin swelling (I), Loading (V, IX), Peptide synthesis (V), *N*-terminal capping (IV), RCM (VI), Full cleave (X)

Peptide synthesis (Refer to Table 33 for method details):

Sequence	Ac	S_5	T	E	L	S_5	T	L	N	S	V	E	NH$_2$
Method		iii)	v)	ii)	iv)	iii)	v)	ii)	ii)	ii)	ii)	i)	

Yield = 6% (9 mg)

HRMS: (C$_{58}$H$_{97}$O$_{20}$N$_{13}$) [M-H]$^{2-}$ requires 646.8414, found [M-H]$^{2-}$ 646.8396

Analytical HPLC:
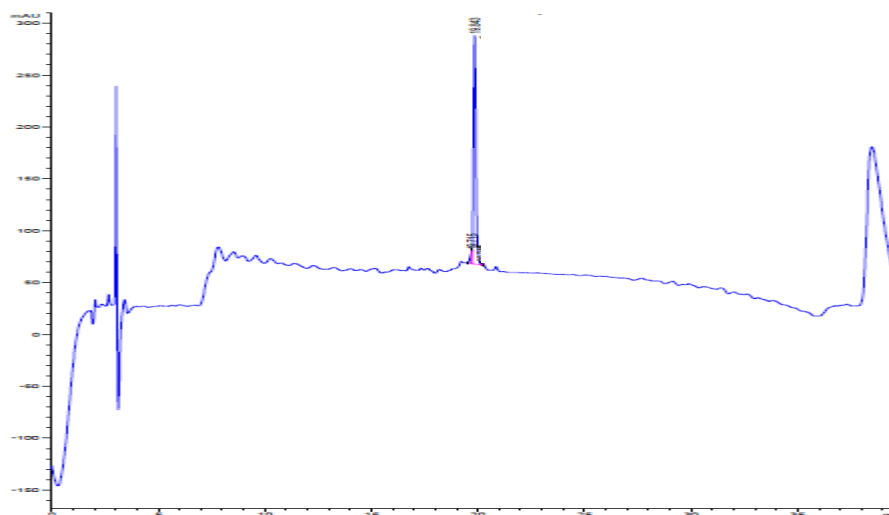
Retention time = 19.843 minutes

Purity = 95%

CD spectra:
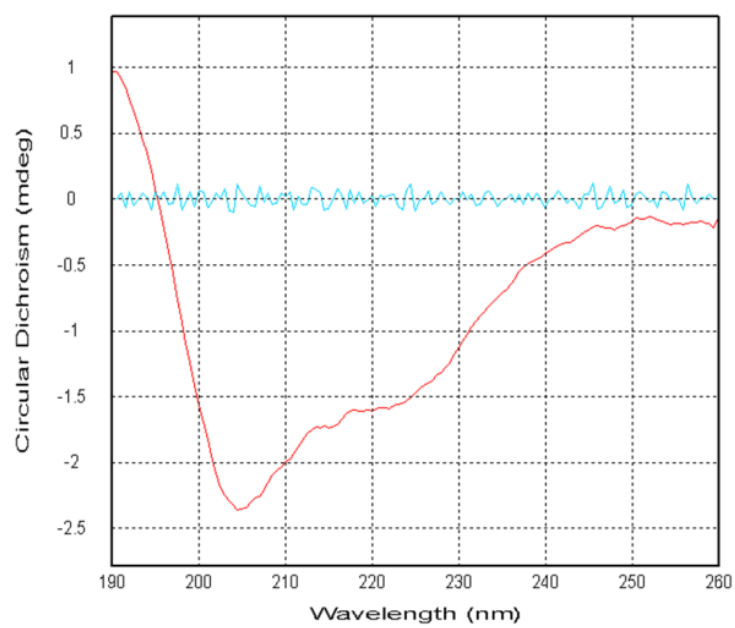
θ_{obs} = -1.596760, C = 200 µM, l = 0.1 mm, n = 11

Calculated helicity = 26%

6.14 – Additional chiral HPLC data

Some slight shifts in retention time are present. These were due to variations in temperature of the column. Racemic mixtures were run after all samples to ensure separation was accurate.
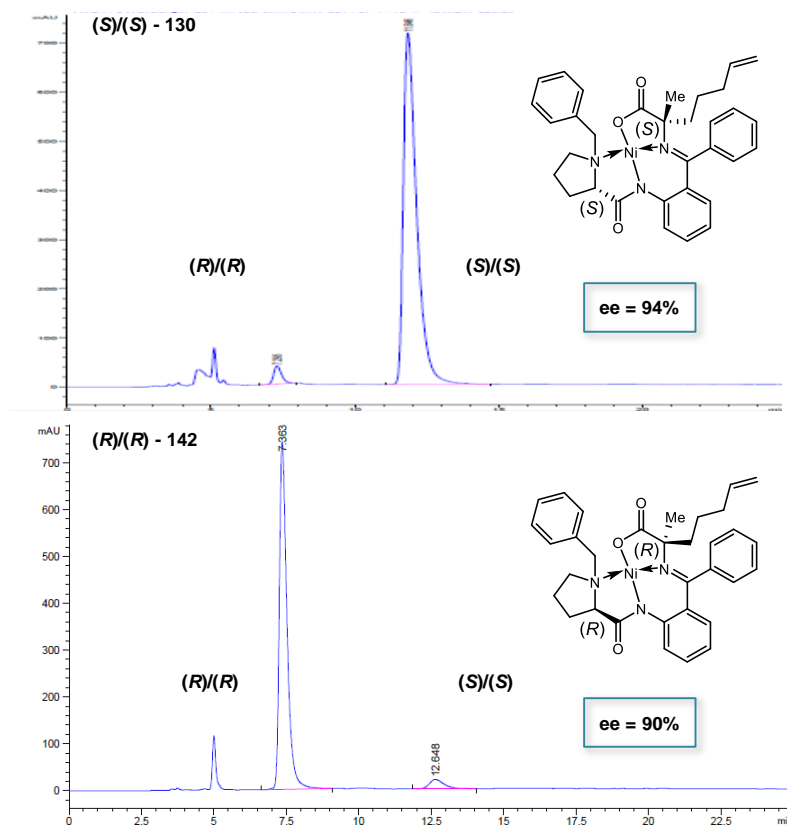
Figure 73 - Chiral HPLC analysis of α-methyl, α-alkenyl complexes **130** & **142**

Figure 74 - Chiral HPLC analysis of Fmoc protected pentenyl amino acis **88** & **89**

Figure 75 – Chiral HPLC analysis of α-methyl, α-alkenyl complexes **150** & **152**

Figure 76 - Chiral HPLC analysis of Fmoc protected octenyl amino acis **90** & **91**

11. References

1   A. Abbott, *Nature*, 2011, **475**, S2–S4.

2   M. Prince, A. Wimo, M. Guerchet, A. Gemma-Claire, Y. T. Wu and M. Prina, *World Alzheimer Report, Alzheimer's Dis. Int.*, 2015, 1–84.
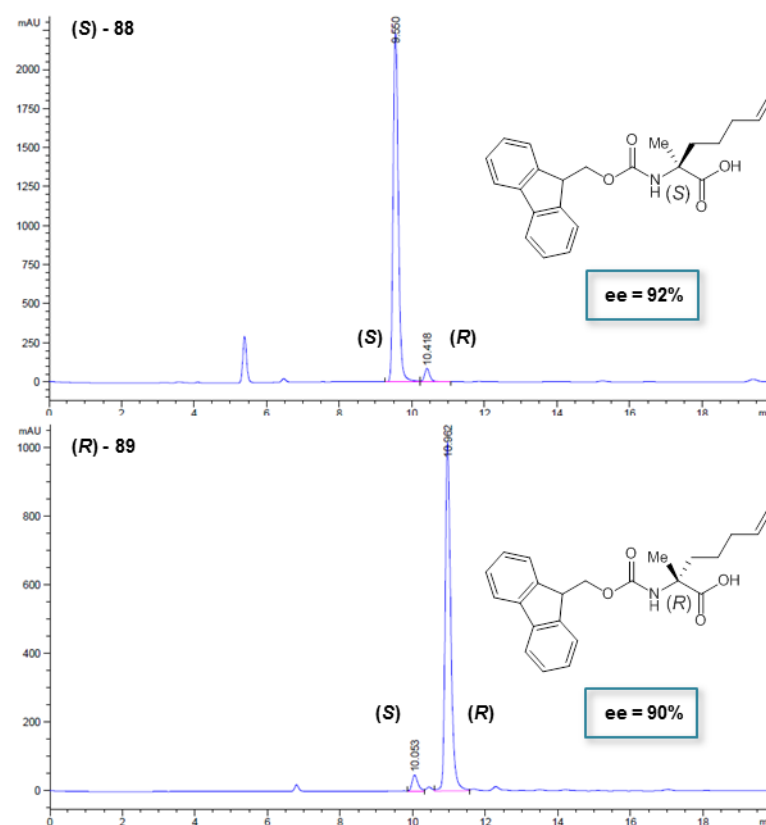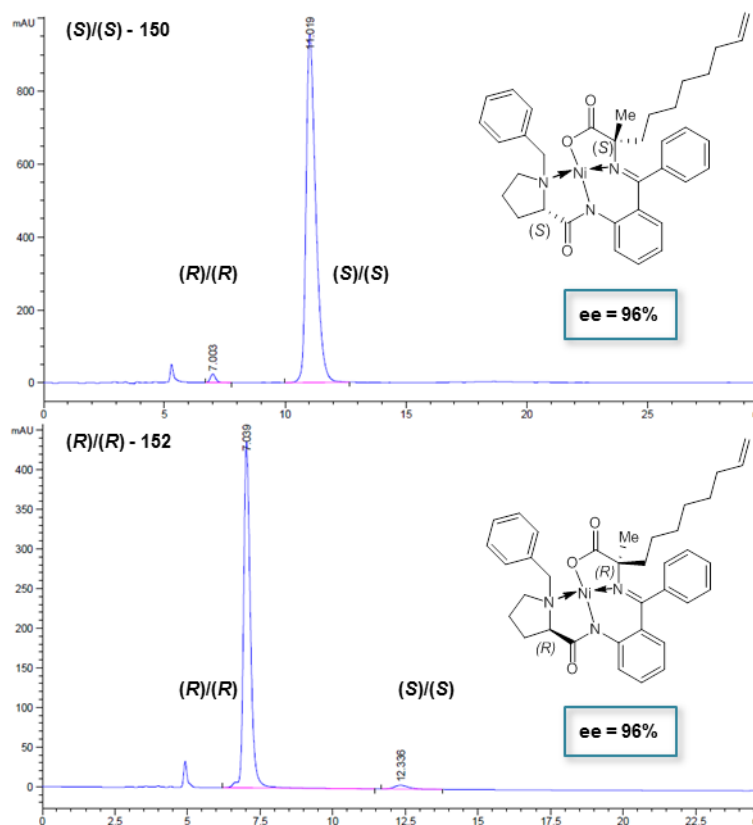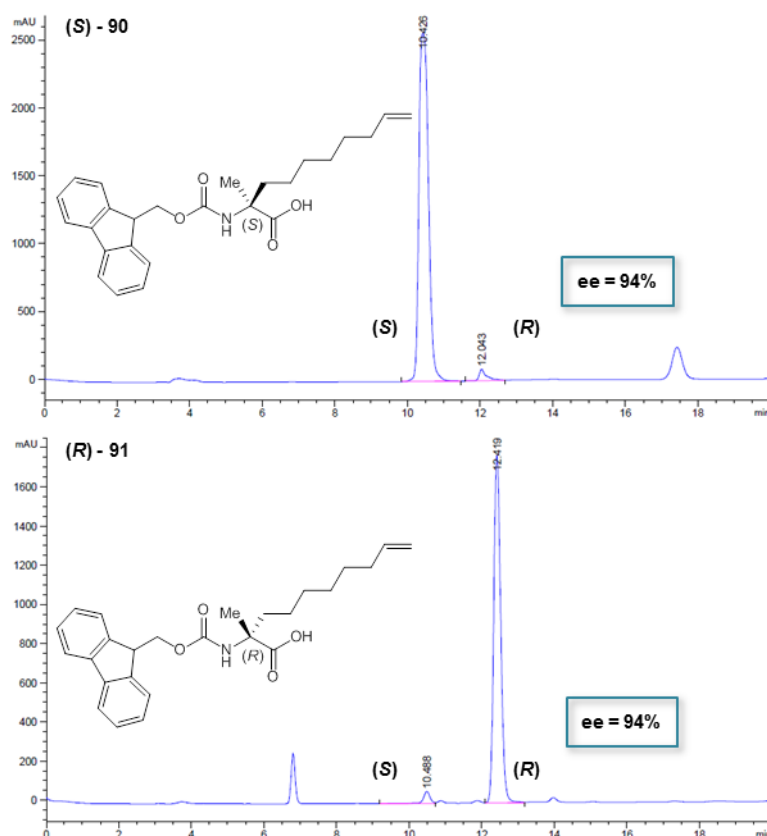
3   M. S. Parihar and T. Hemnani, *J. Clin. Neurosci.*, 2004, **11**, 456–467.

4   W. Y. W. Yau, D. L. Tudorascu, E. M. McDade, S. Ikonomovic, J. James, D. Minhas, W. Mowrey, L. K. Sheu, B. E. Snitz, L. Weissfeld, P. J. Gianaros, H. J. Aizenstein, J. C. Price, C. a Mathis, O. L. Lopez and W. E. Klunk, *Lancet. Neurol.*, 2015, **14**, 804–813.

5   J. Hardy and D. J. Selkoe, *Science*, 2002, **297**, 353–536.

6   J. Augustinack, A. Schneider, E. Mandelkow and B. Hyman, *Acta Neuropathol.*, 2002, **103**, 26–35.

7   P. T. Francis, A. M. Palmer, M. Snape and G. K. Wilcock, *J. Neurol. Neurosurg. Psychiatry*, 1999, **66**, 137–147.

8   E. K. Perry, P. H. Gibson, G. Blessed, R. H. Perry and B. E. Tomlinson, *J. Neurol. Sci.*, 1977, **34**, 247–265.

9   R. J. Rylett, M. J. Ball and E. H. Colhoun, *Brain Res.*, 1983, **289**, 169–175.

10   L. Nilsson, A. Nordberg, J. Hardy, P. Wester and B. Winblad, *J. Neural Transm.*, 1986, **67**, 275–285.

11   G. Kryger, I. Silman and J. L. Sussman, *Structure*, 1999, **7**, 297–307.

12   D. S. Geldmacher, *Expert Rev. Neurother.*, 2004, **4**, 5–16.

13   G. Homor and P. Kasa, *Acta Histochem.*, 1978, **62**, 293–301.

14   B. Reisberg, R. Doody, A. Stoffler, F. Schmitt, S. Ferris and H. J. Mobius, *N. Engl. J. Med.*, 2003, **348**, 1333–1341.

15   B. Winblad and N. Poritis, *Int. J. Geriatr. Psychiatry*, 1999, **14**, 135–146.

16   X. Luo and R. Yan, *Int. J. Clin. Exp. Pathol*, 2010, **3**, 618–628.

17   S. L. Roberds, J. Anderson, G. Basi, M. J. Bienkowski, D. G. Branstetter, K. S. Chen, S. B. Freedman, N. L. Frigon, D. Games, K. Hu, K. Johnson-Wood, K. E. Kappenman, T. T. Kawabe, I. Kola, R. Kuehn, M. Lee, W. Liu, R. Motter, N. F. Nichols, M. Power, D. W. Robertson, D. Schenk, M. Schoor, G. M. Shopp, M. E. Shuck, S. Sinha, K. A. Svensson, G. Tatsuno, H. Tintrup, J.

Wijsman, S. Wright and L. Mcconlogue, *Hum. Mol. Genet.*, 2001, **10**, 1317–1324.

18   Y. Luo, B. Bolon, S. Kahn, B. D. Bennett, S. Babu-Khan, P. Denis, W. Fan, H. Kha, J. Zhang, Y. Gong, L. Martin, J. Louis, Q. Yan, W. G. Richanrds, M. Citron and R. Vassar, *Nat. Neurosci.*, 2001, **4**, 231–233.

19   H. Cai, Y. Wang, D. McCarthy, H. Wen, D. R. Borchelt, D. L. Price and P. Wong, *Nat. Neurosci.*, 2001, **4**, 233–234.

20   S. Sinha, J. P. Anderson, R. Barbour, G. S. Basi, R. Caccavello, D. Davis, M. Doan, H. Dovey, N. Frigon, J. Hong, K. Jacobson-Croak, N. Jewett, P. Keim, J. Knops, I. Lieberburg, M. Power, H. Tan, G. Tatsuno, J. Tung, D. Schenk, P. Seubert, S. M. Suomensaari, S. Wang, D. Walker, J. Zhao, L. McConlogue and V. John, *Nature*, 1999, **402**, 537–540.

21   L. Hong, G. Koelsch, X. Lin, S. Wu, S. Terzyan, A. K. Ghosh, X. C. Zhang and J. Tang, *Science*, 2000, **290**, 150–153.

22   I. Hussain, J. Hawkins, D. Harrison, C. Hille, G. Wayne, L. Cutler, T. Buck, D. Walter, E. Demont, C. Howes, A. Naylor, P. Jeffrey, M. I. Gonzalez, C. Dingwall, A. Michel, S. Redshaw and J. B. Davis, *J. Neurochem.*, 2007, **100**, 802–809.

23   A. V Savonenko, T. Melnikova, F. M. Laird, K. Stewart, D. L. Price and P. C. Wong, *Proc. Natl. Acad. Sci.*, 2008, **105**, 5585–5590.

24   P. H. Kuhn, K. Koroniak, S. Hogl, A. Colombo, U. Zeitschel, M. Willem, C. Volbracht, U. Schepers, A. Imhof, A. Hoffmeister, C. Haass, S. Roßner, S. Bräse and S. F. Lichtenthaler, *EMBO J.*, 2012, **31**, 3157–3168.

25   S. Filser, S. V. Ovsepian, M. Masana, L. Blazquez- Llorca, A. Brandt Elvang, C. Volbracht, M. B. Müller, C. K. E. Jung and J. Herms, *Biol. Psychiatry*, 2015, **77**, 729–739.

26   Lilly Press release, *https://investor.lilly.com/releasedetail.cfm?ReleaseID=771353* , June 13, 2013.

27   Merck Newsroom press release, *http://www.mercknewsroom.com/press-release/alzheimers-disease/merck-presents-findings-phase-1b-study-investigational-bace-inhibit,* July 14, 2013

28   B. M. Riederer, G. Leuba, A. Vernay and I. M. Riederer, *Exp. Biol. Med.*, 2011, **236**, 268–276.

29   A. L. Haas and T. J. Siepmann, *FASEB*, 1997, **11**, 1257–1268.

30   D. Vogues, P. Zwickl and W. Baumeister, *Annu. Rev. Biochem.*, 1999, **68**, 1015–1068.

31   I. Rose, *Angew. Chem. Int. Ed.*, 2005, **44**, 5926–5931.

32   A. Hershko, H. Heller, S. Elias and A. Ciechanover, *J. Biol. Chem*, 1983, **258**, 8206–8214.

33   A. Ciechanover, *Angew. Chem. Int. Ed.*, 2005, **44**, 5944–67.

34   J. N. Keller, K. B. Hanni and W. R. Markesbery, *J. Neurochem.*, 2000, **75**, 436–439.

35   L. Jones, J. C. Lambert, L. S. Wang, S. H. Choi, D. Harold, A. Vedernikov, V. Escott-Price, T. Stone, A. Richards, C. Bellenguez, C. A., Ibrahim-Verbaas, A. C. Naj, R. Sims, A. Gerrish, G. J and P. A. Holmans, *Alzheimer's Dement.*, 2014, **11**, 658–671.

36   H. Mori, J. Kondo and Y. Ihara, *Science*, 1987, **235**, 1641–1644.

37   G. Perry, R. Friedman and G. Shawt, *Proc. Natl. Acad. Sci.*, 1987, **84**, 3033–3036.

38   E. M. H. Tank and H. L. True, *PLoS Genet.*, 2009, **5**, e1000382.

39   F. W. van Leeuwen, D. P. V. De Kleijn, H. H. van der Hurk, A. Neubauer, M. A. F. Sonnemans, J. A. Sluijs, S. Koycu, R. D. J. Ramdjielal, A. Salehi, G. J. M. Martens, F. G. Grosveld, J. P. H. Burbach and E. M. Hol, *Science*, 1998, **279**, 242–247.

40   R. J. G. Gentier, B. M. Verheijen, M. Zamboni, M. M. Stroeken, D. J. H. P. Hermes, B. Küsters, H. W. M. Steinbusch, D. Hopkins and F. W. Van Leeuwen, *Front. Neuroanat.*, 2015, **9**, 1–21.

41   R. B. Emerson, *Annu. Rev. Neurosci.*, 1996, **19**, 27–52.

42   K. Lindsten, F. M. S. de Vrij, L. G. G. C. Verhoef, D. F. Fischer, F. W. van Leeuwen, E. M. Hol, M. G. Masucci and N. P. Dantuma, *J. Cell Biol.*, 2002, **157**, 417–427.

43   F. M. S. DeVrij, J. A. Sluijs, L. Gregori, D. F. Fischer, W. I. M. T. J. M. C.

Hermens, D. Goldgaber and J. Verhaagen, *FASEB*, 2001, **15**, 2680–2688.

44   L. G. G. C. Verhoef, C. Heinen, Selivanova, E. F. Halff, F. Salomons and N. P. Dantuma, *FASEB J.*, 2009, **23**, 123–133.

45   Y. Lam, C. M. Pickart, A. Alban, M. Landon, C. Jamieson, R. Ramage, R. J. Mayer and R. Layfield, *Proc. Natl. Acad. Sci.*, 2000, **97**, 9902–9906.

46   P. van Tijn, F. M. S. de Vrij, K. G. Schuurman, N. P. Dantuma, D. F. Fischer, F. W. van Leeuwen and E. M. Hol, *J. Cell Sci.*, 2007, **120**, 1615–1623.

47   S. Dayal, A. Sparks, J. Jacob, N. Allende-Vega, D. P. Lane and M. K. Saville, *J. Biol. Chem.*, 2009, **284**, 5030–5041.

48   T. W. Kim, W. H. Pettingell, O. G. Hallmark, R. D. Moir, W. Wasco and R. E. Tanzi, *J. Biol. Chem.*, 1997, **272**, 11006–11010.

49   H. Steiner, A. Capell, B. Pesold, M. Citron, P. M. Kloetzel, D. J. Selkoe, H. Romig, K. Mendla and C. Haass, *J. Biol. Chem*, 1998, **273**, 32322–32331.

50   P. Marambaud, K. Ancolio, E. Lopez-Perez and F. Checler, *Mol. Med*, 1998, **4**, 147–157.

51   B. De Strooper, P. Saftig, K. Craessaerts, H. Vanderstichele, G. Guhde, W. Annaert, K. Von Figura and F. Van Leuven, *Nature*, 1998, **391**, 387–390.

52   M. S. Wolfe, W. Xia, B. L. Ostaszewski, T. S. Diehl, W. T. Kimberly and D. J. Selkoe, *Nature*, 1999, **398**, 513–517.

53   R. J. Braun, C. Sommer, C. Leibiger, R. J. G. Gentier, V. I. Dumit, K. Paduch, T. Eisenberg, L. Habernig, G. Trausinger, C. Magnes, T. Pieber, F. Sinner, J. Dengjel, F. W. van Leeuwen, G. Kroemer and F. Madeo, *Cell Rep.*, 2015, **10**, 1557–1571.

54   Z. Chen, C. M. Pickart, J. B. Chem and M. Pickarts, *J. Biol. Chem*, 1990, **265**, 21835–21842.

55   M. T. Haldeman, G. Xia, E. M. Kasperek and C. M. Pickart, *Biochemistry*, 1997, **36**, 10526–10537.

56   S. Song, S. Kim, Y. Hong, D. Jo, J. Lee, S. M. Shim, C. Chung, S. J. Seo, Y. J. Yoo, J. Koh, M. C. Lee, A. J. Yates, H. Ichijo and Y. Jung, *Mol. Cell*, 2003, **12**, 553–63.

57   R. de Pril, D. F. Fischer, R. a C. Roos and F. W. van Leeuwen, *Mol. Cell. Neurosci.*, 2007, **34**, 10–9.

58   S. Song, H. Lee, T. Kam, M. L. Tai, J. Lee, J. Noh, S. M. Shim, S. J. Seo, Y. Kong, T. Nakagawa, C. Chung, D. Choi, H. Oubrahim and Y. Jung, *J. Cell Biol.*, 2008, **182**, 675–84.

59   S. Ko, G. B. Kang, S. M. Song, J. Lee, D. Y. Shin, J. Yun, Y. Sheng, C. Cheong, Y. H. Jeon, Y. Jung, C. H. Arrowsmith, G. V Avvakumov, S. Dhe-Paganon, Y. J. Yoo, S. H. Eom and W. Lee, *J. Biol. Chem.*, 2010, **285**, 36070–36080.

60   J. Drews, *Science*, 2000, **287**, 1960–1964.

61   G. L. Verdine and L. D. Walensky, *Clin. Cancer Res.*, 2007, **13**, 7264–70.

62   M. W. Peczuh and A. D. Hamilton, *Chem. Rev.*, 2000, **100**, 2479–2494.

63   S. Jones and J. M. Thornton, *Proc. Natl. Acad. Sci.*, 1996, **93**, 13–20.

64   D. C. Fry, *Biopolymers*, 2006, **84**, 535–552.

65   M. D. Wendt, *Topics in Medicinal Chemistry*, 2012.

66   L. Lo Conte, C. Chothia and J. Janin, *J. Mol. Biol.*, 1999, **285**, 2177–2198.

67   J. Wells and C. L. McClendon, *Nature*, 2007, **450**, 1001–1009.

68   S. Raasi, R. Varadan, D. Fushman and C. Pickart, *Nat. Struct. Mol. Biol.*, 2005, **12**, 708–714.

69   P. D. Leeson and B. Springthorpe, *Nat. Rev. Drug Discov.*, 2007, **6**, 881–890.

70   N. Kong, E. A. Liu and B. T. Vu, 2004, US:6734302 B2.

71   S. Chavala and T. C. Lee, *US2015/0231136 A1*, **2015**.

72   F. Christ, A. Voet, A. Marchand, S. Nicolet, B. A. Desimmie, D. Marchand, D. Bardiot, N. J. Van der Veken, B. Van Remoortel, S. V. Strelkov, M. de Maeyer, P. Chaltin and Z. Debyser, *Nat. Chem. Biol.*, 2010, **6**, 442–448.

73   A. G. Cochran, *Chem. Biol.*, 2000, **7**, 85–94.

74   P. Vlieghe, V. Lisowski, J. Martinez and M. Khrestchatisky, *Drug Discov. Today*, 2010, **15**, 40–56.

75   A. Kaspar and J. M. Reichert, *Drug Discov. Today*, 2013, **18**, 807–817.

76   N. Lee and A. Wald, *Core Evid.*, 2012, **7**, 39–47.

77   S. K. Sinha, T. Lacaze-Masmonteil, A. Valls i Soler, T. E. Wiswell, J. Gadzinowski, J. Hajdu, G. Bernstein, M. Sanchez-Luna, R. Segal, C. J.

Schaber, J. Massaro and R. D'Agostino, *Pediatrics*, 2005, **115**, 1030–1038.

78   R. A. Feelders, C. Bruin, A. M. Pereira, R. T. Netea-Maier, A. R. Hermus, P. M. Zelissen, R. Heerebeek, F. H. Jong, A. J. Lely, W. W. Herder, L. J. Hofland and S. W. Lamberts, *N. Engl. J. Med.*, 2010, **362**, 1846–1848.

79   D. J. Craik, D. P. Fairlie, S. Liras and D. Price, *Chem. Biol. Drug Des.*, 2013, **81**, 136–147.

80   K. Fosgerau and T. Hoffmann, *Drug Discov. Today*, 2014, **20**, 122–128.

81   L. Andersson, L. Blomberg, M. Flegel, L. Lepsa, B. Nilsson and M. Verlander, *Biopolymers*, 2000, **55**, 227–250.

82   R. B. Merrifield, *J. Am. Chem. Soc.*, 1963, **85**, 2149–2154.

83   R. B. Merrifield, *Science*, 1965, **150**, 178–185.

84   E. Atherton, H. Fox, D. Harkiss, C. J. Logan, R. C. Sheppard and B. J. Williams, *J.C.S. Chem. Comm.*, 1978, **538**, 537–539.

85   L. A. Carpino and G. Y. Han, *J. Am. Chem. Soc.*, 1970, **92**, 5748–5749.

86   W. C. Chan and P. D. White, *Fmoc Solid Phase Peptide Synthesis*, Oxford University Press, Oxford, UK, 1st Edtn., 2000.

87   F. Guillier, D. Orain and M. Bradley, *Chem. Rev.*, 2000, **100**, 2091–2157.

88   L. A. Carpino, S. Ghassemi, D. Ionescu, M. Ismail, D. Sadat-Aalaee, G. A. Truran, E. M. E. Mansour, G. A. Siwruk, J. S. Eynon and B. Morgan, *Org. Process Res. Dev.*, 2003, **7**, 28–37.

89   A. El-Faham and F. Albericio, *Chem. Rev.*, 2011, **111**, 6557–6602.

90   O. Marder and F. Albericio, *Chem. Oggi*, 2003.

91   W. Konig and R. Geiger, *Chem. Ber.*, 1970, **103**, 788–798.

92   L. A. Carpino, *J. Am. Chem. Soc.*, 1993, **115**, 4397–4398.

93   K. D. Wehrstedt, P. Wandrey and D. Heitkamp, *J. Hazard. Mater.*, 2005, **A126**, 1–7.

94   B. Castro and J. R. Dormoy, *Bull. Soc. Chim. Fr.*, 1973, **12**, 3359.

95   E. Frerot, J. Coste, A. Pantaloni, M. N. Dufour and P. Jouin, *Tetrahedron*, 1991, **47**, 259–270.

96   O. Marder, Y. Shvo and F. Albericio, *Chim. Oggi*, 2002, **20**, 37–42.

97   D. Hudson, *J. Org. Chem.*, 1988, **53**, 617–624.

98   A. El-Faham, R. Subirós Funosas, R. Prohens and F. Albericio, *Chem. A Eur. J.*, 2009, **15**, 9404–9416.

99   L. A. Carpino, A. El-faham, C. A. Minor and F. Albericio, *J. Chem. Soc. Chemm. Comm.*, 1994, 201–203.

100 C. A. Chantell, M. A. Onaiyekan and M. Menakuru, *J. Pept. Sci.*, 2012, **18**, 88–91.

101 C. A. Hood, G. Fuentes, H. Patel, K. Page, M. Menakuru and J. H. Park, *J. Pept. Sci.*, 2008, **14**, 97–101.

102 G. Sabatino, B. Mulinacci, M. C. Alcaro, M. Chelli, P. Rovero and A. M. Papini, *Lett. Pept. Sci.*, 2002, **9**, 119–123.

103 L. Gentilucci, R. de Marco and L. Cerisoli, *Curr. Pharm. Des.*, 2010, **16**, 3185–3202.

104 A. L. Jochim and P. S. Arora, *Mol. Biosyst.*, 2009, **5**, 924–926.

105 M. Guharoy and P. Chakrabarti, *Bioinformatics*, 2007, **23**, 1909–1918.

106 B. N. Bullock, A. L. Jochim and P. S. Arora, *J. Am. Chem. Soc.*, 2011, **133**, 14220–14223.

107 B. H. Zimm, P. Doty and K. Iso, *Proc. Natl. Acad. Sci.*, 1959, **45**, 1601–1607.

108 J. M. Scholtz and R. L. Baldwin, *Annu. Rev. Biophys. Biomol. Struct.*, 1992, **21**, 95–118.

109 C. Rohl and R. L. Baldwin, *Methods Enzymol.*, 1998, **295**, 1–26.

110 E. Cabezas and A. C. Satterthwait, *J. Am. Chem. Soc.*, 1999, **121**, 3862–3875.

111 R. N. Chapman, G. Dimartino and P. S. Arora, *J. Am. Chem. Soc.*, 2004, **126**, 12252–12253.

112 A. B. Mahon and P. S. Arora, *Chem. Commun.*, 2012, **48**, 1416–1418.

113 D. Wang, K. Chen, J. L. Kulp Iii and P. S. Arora, *J. Am. Chem. Soc.*, 2006, **128**, 9248–56.

114 M. R. Ghadiri and A. K. Fernholz, *J. Am. Chem. Soc.*, 1990, **112**, 9633–9635.

115 F. Ruan, Y. Chen and P. B. Hopkins, *J. Am. Chem. Soc.*, 1990, **112**, 9403–

9404.

116   S. Marqusee and R. L. Baldwin, *Proc. Natl. Acad. Sci.*, 1987, **84**, 8898–902.

117   M. Chorev, E. Roubini, R. L. Mckee, S. W. Gibbons, M. E. Goldman, M. P. Caulfield and M. Rosenblatt, *Biochemistry*, 1991, **230**, 5968–5974.

118   G. Osapay and J. W. Taylor, *J. Am. Chem. Soc.*, 1992, **114**, 6966–6973.

119   J. C. Phelan, N. J. Skelton, A. C. Braisted and R. S. McDowell, *J. Am. Chem. Soc.,* 1997, **119**, 455–460.

120   N. E. Shepherd, H. N. Hoang, G. Abbenante and D. P. Fairlie, *J. Am. Chem. Soc.*, 2005, **127**, 2974–2983.

121   K. Fujimoto, M. Kajino and M. Inouye, *Chem. A Eur. J.*, 2008, **14**, 857–863.

122   A. Leduc, J. O. Trent, J. L. Wittliff, K. S. Bramlett, S. L. Briggs, N. Y. Chirgadze, Y. Wang, T. P. Burris and A. F. Spatola, *Proc. Natl. Acad. Sci.*, 2003, **100**, 11273–11278.

123   H. Jo, N. Meinhardt, Y. Wu, S. Kulkarni, X. Hu, K. E. Low, P. L. Davies, W. F. DeGrado and D. C. Greenbaum, *J. Am. Chem. Soc.*, 2012, **134**, 17704–17713.

124   A. M. Spokoyny, Y. Zou, J. J. Ling, H. Yu, Y. Lin and B. L. Pentelute, *J. Am. Chem. Soc.*, 2013, **135**, 5946–5949.

125   E. V. Vinogradova, C. Zhang, A. M. Spokoyny, B. L. Pentelute and S. L. Buchwald, *Nature*, 2015, **526**, 687–691.

126   D. Y. Jackson, D. S. King, J. Chmielewski, S. Singh and P. G. Schultz, *J. Am. Chem. Soc.*, 1991, **113**, 9391–9392.

127   M. M. Madden, A. Muppidi, Z. Li, X. Li, J. Chen and Q. Lin, *Bioorg. Med. Chem. Lett.*, 2011, **21**, 1472 – 1475.

128   Y. Wang and D. H. C. Chou, *Angew. Chem. Int. Ed.*, 2015, **54**, 10931–10934.

129   J. R. Kumita, O. S. Smart and G. Woolley, *Proc. Natl. Acad. Sci.*, 2000, **97**, 3803–3808.

130   S. Kneissl, E. J. Loveridge, C. Williams, M. P. Crump and R. K. Allemann, *ChemBioChem*, 2008, **9**, 3046–3054.

131   H. C. Kolb, M. G. Finn and K. B. Sharpless, *Angew. Chem. Int. Ed.*, 2001, **40**, 2004–2021.

132   C. W. Tornøe, C. Christensen and M. Meldal, *J. Org. Chem.*, 2002, **67**, 3057–3064.

133   S. Cantel, A. L. C. Isaad, M. Scrima, J. J. Levy, R. D. DiMarchi, P. Rovero, J. Halperin, A. M. D'Ursi, A. M. Papini and M. Chorev, *J. Org. Chem.*, 2008, **73**, 5663–5674.

134   Y. H. Lau and D. R. Spring, *Synlett*, 2011, **13**, 1917–1919.

135   Y. H. Lau, P. de Andrade, S.-T. Quah, M. Rossmann, L. Laraia, N. Sköld, T. J. Sum, P. J. E. Rowling, T. L. Joseph, C. Verma, M. Hyvönen, L. S. Itzhaki, A. R. Venkitaraman, C. J. Brown, D. P. Lane and D. R. Spring, *Chem. Sci.*, 2014, **5**, 1804.

136   Y. H. Lau, P. Andrade, N. Skold, G. J. McKenzie, A. R. Venkitaraman, C. Verma, D. P. Lane and D. Spring, *Org. Biomol. Chem.*, 2014, **12**, 4074–4077.

137   Y. H. Lau, P. de Andrade, G. J. McKenzie, A. R. Venkitaraman and D. R. Spring, *ChemBioChem*, 2014, **15**, 2680–2683.

138   Y. H. Lau, Y. Wu, M. Rossmann, B. X. Tan, P. de Andrade, Y. S. Tan, C. Verma, G. J. McKenzie, A. R. Venkitaraman, M. Hyvönen and D. R. Spring, *Angew. Chemie Int. Ed.*, 2015, **54**, 15410–15413.

139   R. H. Grubbs and S. Chang, *Tetrahedron*, 1998, **54**, 4413–4450.

140   T. M. Trnka and R. H. Grubbs, *Acc. Chem. Res.*, 2001, **34**, 18–29.

141   N. Calderon, *Acc. Chem. Res.*, 1972, 127–132.

142   S. K. Armstrong, *J. Chem. Soc. Perkin Trans. 1*, 1998, 371–388.

143   S. T. Nguyen, L. K. Johnson, R. H. Grubbs and J. W. Ziller, *J. Am. Chem. Soc.,* 1992, **114**, 3974–3975.

144   P. Schwab, R. H. Grubbs and J. W. Ziller, *J. Am. Chem. Soc.*, 1996, **118**, 100–110.

145   P. Schwab, M. B. France, J. W. Ziller and R. H. Grubbs, *Angew. Chem. Int. Ed.*, 1995, **34**, 2039–2041.

146   M. Scholl, S. Ding, C. W. Lee and R. H. Grubbs, *Org. Lett.*, 1999, **1**, 953–956.

147   E. L. Dias, S. T. Nguyen and R. H. Grubbs, *J. Am. Chem. Soc.*, 1997, **119**, 3887–3897.

148   S. J. Miller, H. E. Blackwell and R. H. Grubbs, *J. Am. Chem. Soc.*, 1996, **118**,

9606–9614.

149   H. E. Blackwell and R. H. Grubbs, *Angew. Chem. Int. Ed.*, 1998, **37**, 3281–
3284.

150   M. E. Karpen, P. L. de Haseth and K. E. Neet, *Protein Sci.*, 1992, **1**, 1333–
1342.

151   C. E. Schafmeister, J. Po and G. L. Verdine, *J. Am. Chem. Soc.*, 2000, **122**,
5891–5892.

152   P. C. Lyu, J. C. Sherman, Chen and N. R. Kallenbach, *Proc. Natl. Acad. Sci.*,
1991, **88**, 5317–20.

153   Y. W. Kim and G. L. Verdine, *Bioorg. Med. Chem. Lett.*, 2009, **19**, 2533–
2536.

154   L. D. Walensky, A. L. Kung, I. Escher, T. J. Malia, S. Barbuto, R. D. Wright,
G. Wagner, G. L. Verdine and S. J. Korsmeyer, *Science*, 2004, **305**, 1466–
1470.

155   F. Bernal, A. F. Tyler, S. J. Korsmeyer, L. D. Walensky and G. L. Verdine, *J.
Am. Chem. Soc.*, 2007, **129**, 2456–2457.

156   F. Milletti, *Drug Discov. Today*, 2012, **17**, 850–860.

157   Y. Li, L. W. Rodewald, K. F. Wertman, G. M. Wahl, Y. Li, L. W. Rodewald, C.
Hoppmann, E. T. Wong, S. Lebreton and P. Safar, *CellReports*, 2014, **9**,
1946–1958.

158   Q. Chu, R. E. Moellering, G. J. Hilinski, Y. Kim, T. N. Grossmann, T. Yeh and
G. L. Verdine, *MedChemComm*, 2015, **6**, 111–119.

159   Y. S. Chang, B. Graves, V. Guerlavais, C. Tovar, K. Packman, K. H. To, K.
Olson, K. Kesavan, P. Gangurde, A. Mukherjee, T. Baker, K. Darlak, C. Elkin,
Z. Filipovic, F. Z. Qureshi, H. Cai, P. Berry, E. Feyfant, X. E. Shi, J. Horstick,
D. A. Annis, A. M. Manning, N. Fotouhi, H. Nash, L. T. Vassilev and T. K.
Sawyer, *Proc. Natl. Acad. Sci.*, 2013, **110**, E3445–3454.

160   Y. Grigoryev, *Nat. Med.*, 2013, **19**, 120.

161   Aileron Therapeutics Press Release,
*http://www.businesswire.com/news/home/20150212005199/en/Aileron-
Therapeutics-Initiates-Phase-1-Cancer-Study*, February 12, 2015.

162   K. Takada, D. Zhu, G. H. Bird, K. Sukhdeo, J. J. Zhao, M. Mani, M. Lemieux,

D. E. Carrasco, J. Ryan, D. Horst, M. Fulciniti, N. C. Munshi, W. Xu, A. L. Kung, R. Shivdasani, L. D. Walensky and D. R. Carrasco, *Sci. Transl. Med.*, 2012, 4, 1–13.

163 W. Nomura, H. Aikawa, N. Ohashi, E. Urano, M. Métifiot, M. Fujino, K. Maddali, T. Ozaki, A. Nozue, T. Narumi, C. Hashimoto, T. Tanaka, Y. Pommier, N. Yamamoto, J. a Komano, T. Murakami and H. Tamamura, *ACS Chem. Biol.*, 2013, **8**, 2235–2244.

164 Y. Q. Long, S. X. Huang, Z. Zawahir, Z. L. Xu, H. Y. Li, T. W. Sanchez, Y. Zhi, S. De Houwer, F. Christ, Z. Debyser and N. Neamati, *J. Med. Chem.*, 2013, **56**, 5601–5612.

165 H. K. Cui, J. Qing, Y. Guo, Y. J. Wang, L. J. Cui, T. H. He, L. Zhang and L. Liu, *Bioorg. Med. Chem.*, 2013, **21**, 3547–3554.

166 C. Phillips, L. R. Roberts, M. Schade, R. Bazin, A. Bent, N. L. Davies, R. Moore, A. D. Pannifer, A. R. Pickford, S. H. Prior, C. M. Read, A. Scott, D. G. Brown, B. Xu and S. L. Irving, *J. Am. Chem. Soc.*, 2011, **133**, 9696–9699.

167 B. R. Green, B. D. Klein, H. K. Lee, M. D. Smith, H. Steve White and G. Bulaj, *Bioorg. Med. Chem.*, 2013, **21**, 303–310.

168 D. J. Yeo, S. L. Warriner and A. Wilson, *Chem. Comm.*, 2013, **49**, 9131–9133.

169 B. Aillard, N. S. Robertson, A. R. Baldwin, S. Robins and A. G. Jamieson, *Org. Biomol. Chem.*, 2014, **12**, 8775–8782.

170 U. Schollkopf, *Tetrahedron*, 1983, **39**, 2085–2091.

171 J. Chen, S. P. Corbin and N. J. Holman, *Org. Process Res. Dev.*, 2005, **9**, 185–187.

172 S. Neelamkavil, B. P. Mowery, E. R. Thornton, A. B. Smith and R. Hirschmann, *J. Pept. Res.*, 2005, **65**, 139–142.

173 C. Ma, X. Liu, S. Yu, S. Zhao and J. M. Cook, *Tetrahedron Lett.*, 1999, **40**, 657–660.

174 F. Cavelier, D. Marchand and J. Martinez, *Chem. Biodivers.*, 2008, **5**, 1279–1287.

175 M. Andrei, C. Römming and K. Undheim, *Tetrahedron: Asymmetry*, 2004, **15**, 1359–1370.

176 M. Andrei, C. Römming and K. Undheim, *Tetrahedron: Asymmetry*, 2004, **15**, 2711–2717.

177 P. J. Sinclair, D. Zhai, J. Reibenspies and R. M. Williams, *J. Am. Chem. Soc.*, 1986, **108**, 1103–1104.

178 R. M. Williams, P. J. Sinclair, D. Zhai and D. Chen, *J. Am. Chem. Soc.*, 1988, **110**, 1547–1557.

179 R. M. Williams and M. N. Im, *J. Am. Chem. Soc.*, 1991, **113**, 9276–9286.

180 D. Seebach and R. Naef, *Helv. Chem. Acta*, 1981, **64**, 2704–2708.

181 D. Seebach, M. Boes, R. Naef and W. B. Schweizer, *J. Am. Chem. Soc.*, 1983, **105**, 5390–5398.

182 A. K. Beck, S. Blank, K. Job, D. Seebach, T. Sommerfeld, F. Narjes and L. E. Overman, *Org. Synth.*, 1998, **9**, 626–634.

183 Y. N. Belokon, A. G. Bulychev, S. V. Vitt, Y. T. Struchkov, A. S. Batsanov, T. V Timofeeva, V. A. Tsyryapkin, M. C. Ryzhov, L. A. Lysova, V. I. Bakhmutov and V. M. Belikov, *J. Am. Chem. Soc.*, 1985, **107**, 4252–4259.

184 V. A. Soloshonok, D. V Avilov and V. P. Kukhar, *Tetrahedron: Asymmetry*, 1996, **7**, 1547–1550.

185 V. A. Soloshonok, D. V Avilov, V. P. Kukhar, L. Van Meervelt and N. Misehenko, *Tetrahedron Lett.*, 1997, **38**, 4671–4674.

186 J. Wang, S. Zhou, D. Lin, X. Ding, H. Jiang and H. Liu, *Chem. Commun.*, 2011, **47**, 8355–8357.

187 V. Soloshonok, C. Cai, T. Yamada, H. Ueki, Y. Ohfune and V. J. Hruby, *J. Am. Chem. Soc.*, 2005, **127**, 15296–15303.

188 V. A. Soloshonok, C. Cai and V. J. Hruby, *Tetrahedron: Asymmetry*, 1999, **10**, 4265–4269.

189 J. Wang, T. Shi, G. Deng, H. Jiang and H. Liu, *J. Org. Chem.*, 2008, **73**, 8563–8570.

190 S. Zhou, J. Wang, D. Lin, F. Zhao and H. Liu, *J. Org. Chem.*, 2013, **78**, 11204–11212.

191 S. Collet, P. Bauchat, R. Danion-Bougot and D. Danion, *Tetrahedron: Asymmetry*, 1998, **9**, 2121–2131.

192   K. Hung, P. W. R. Harris and M. Brimble, *J. Org. Chem.*, 2010, **75**, 8728–8731.

193   J. Wang, D. Lin, S. Zhou, X. Ding, V. A. Soloshonok and H. Liu, *J. Org. Chem.*, 2011, **76**, 684–687.

194   Y. N. Belokon, V. I. Tararov, V. I. Maleev, T. F. Savel'eva and M. G. Ryzhov, *Tetrahedron: Asymmetry*, 1998, **9**, 4249–4252.

195   F. Xu, Y. Liu, P. Zhang and Y. Gao, *Beiking Okeanos Technol. Co*, 2009, CN101565390.

196   H. M. Nash, R. Kapeller-Lieberman, T. K. Sawyer, N. Kawahata, V. Guerlavais and M. Iasanza, *Aelerion Ther. Inc.*, WO 2009/126292 A2, **2009**.

197   H. Ueki, T. K. Ellis, C. H. Martin, T. U. Boettiger, S. B. Bolene and V. A. Soloshonok, *J. Org. Chem.*, 2003, **68**, 7104–7107.

198   Alan Kennedy, *University of Strathclyde*, 2013.

199   SiliCycle, *http://www.silicycle.com/eu/products/functionalized-silica-gels/siliabond-acids-bases-others/siliabond-acids/spe-r51230b*, 2014, 25th July.

200   DowChemicalCompany, *http://msdssearch.dow.com/PublishedLiteratureDOWCOM/dh_006f/0901*, 2013, 17th April.

201   Y. N. Belkon, V. I. Maleev, A. A. Petrosayan, T. F. Savel'eva, N. S. Ikonnikov, A. S. Peregudov, V. N. Khrustalev and A. S. Saighiyan, *Russ. Chem. Bull. Int. Ed.*, 2002, **51**, 1593–1599.

202   D. J. Smith, G. P. Yap, J. Kelley and J. P. Schneider, *J. Org. Chem.*, 2011, **76**, 1513–1520.

203   G. J. Hilinski, Y. W. Kim, J. Hong, P. S. Kutchukian, C. M. Crenshaw, S. S. Berkovitch, A. Chang, S. Ham and G. L. Verdine, *J. Am. Chem. Soc.*, 2014, **136**, 12314–12322.

204   S. Kelly and N. Price, *Curr. Protein Pept. Sci.*, 2000, **1**, 349–384.

205   G. H. Bird, E. Gavathiotis, J. L. LaBelle, S. G. Katz and L. D. Walensky, *ACS Chem. Biol.*, 2014, **9**, 831–837.

206   Chemical computing group Inc, *Molecular Operating Environment*, 2013, 1010 Sherbooke St. West, Suite 910, Montreal, QC, .

207   T. D. Goddard and D. G. Kneller, https://www.cgl.ucsf.edu/home/sparky, 2015, 21st September.

208   Y. Wang and O. Jardetzky, *Protein Sci.*, 2002, **11**, 852–861.

209   D. S. Wishart, B. D. Sykes and F. M. Richards, *Biochemistry*, 1992, **31**, 1647–1651.

210   R. Armen, D. O. V. Alonso and V. Daggett, *Protein Sci.*, 2003, **12**, 1145–1157.

211   P. Rezácová, D. Borek, S. F. Moy, A. Joachimiak and Z. Otwinowski, *Proteins*, 2008, **70**, 311–319.

212   F. B. Sheinerman and C. L. Brooks, *J. Am. Chem. Soc.*, 1995, **117**, 10098–10103.

213   F. Formaggio, M. Crisma, P. Rossi, P. Scrimin, B. Kaptein, Q. B. Broxterman, J. Kamphuis and C. Toniolo, *Chem. Eur. J.*, 2000, **6**, 4498–4504.

214   N. H. Andersen, Z. Liu and K. S. Prickett, *FEBS Lett.*, 1996, **399**, 47–52.

215   L. Ismer, J. Ireta and J. Neugebauer, *J. Phys. Chem. B*, 2008, **112**, 4109–4112.

216   Dr Robert Layfield, *University of Nottingham*, 2015.

217   M. M. Pierce, C. S. Raman and B. T. Nall, *Methods*, 1999, **19**, 213–221.

218   E. Freire and S. Leavitt, *Curr. Opin. Struct. Biol.*, 2001, **11**, 560–566.

219   A. T. Jones and E. J. Sayers, *J. Control. Release*, 2012, **161**, 582–591.

220   PureSolvMD5, *http://www.solventpurification.co.uk/md*, 2014, 25th July.

221   W. L. F. Armarego and C. L. L. Chai, *Purification of Laboratory Chemicals*, Elsevier Inc., Oxford, UK, 6th Edtn., 2009.

222   R. Salomon-Ferrer, D. A. Case and R. C. Walker, *WIREs Comput. Mol. Sci.*, 2013, **3**, 198–210.

223   Y. W. Kim, T. N. Grossmann and G. L. Verdine, *Nat. Protoc.*, 2011, **6**, 761–771.

224. H. E. Gottlieb, V. Kotlyar and A. Nudelman, *J. Org. Chem.*, 1997, **62**(21), 7512-7515

Appendix – Peptide NMR data

## A1 – Key for peptide labels used during NMR assignment

Each amino acid residue was assigned a number relating to sequence position. Some of the numbering shown in this section is different to that discussed in Section 3.3. Peak assignment in this section is according to the labelling system shown in Tables 34, 35 and 36. S_5 residues are denoted as the * symbol.
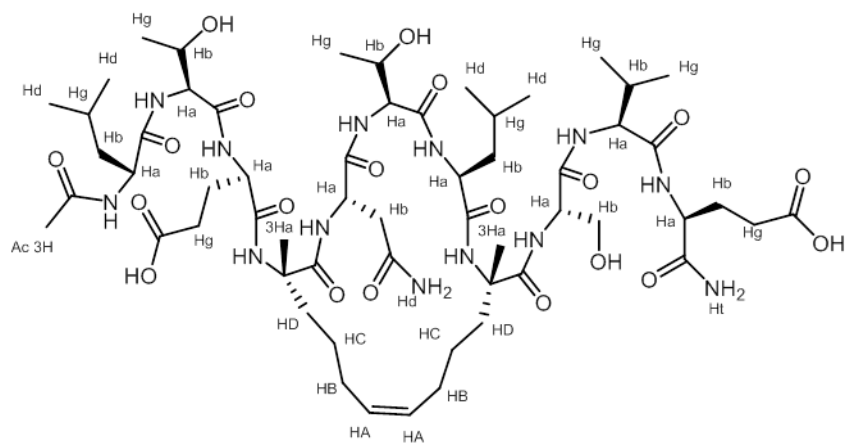
Table 40 – Staple A sequence numbering
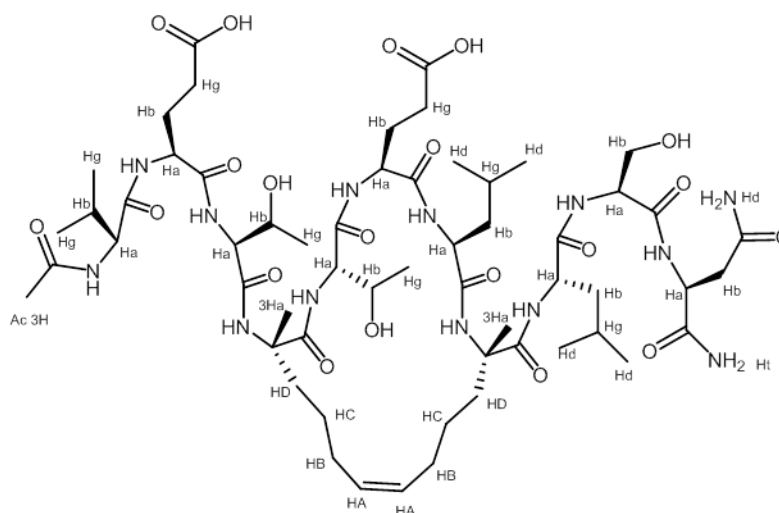
Number	Ac	11	10	9	8	7	6	5	4	3	2	1	NH$_2$
Sequence	Ac	V	E	T	S$_5$	T	E	L	S$_5$	L	S	N	NH$_2$

Table 41 - Staple G sequence numbering
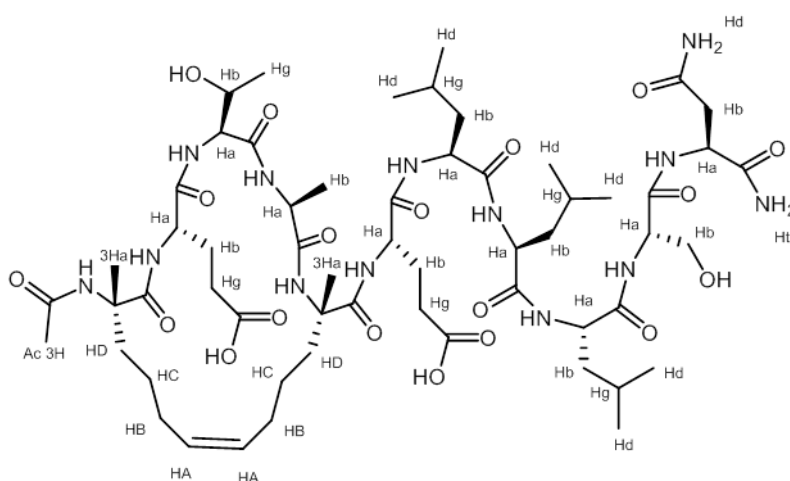
Number	Ac	11	10	9	8	7	6	5	4	3	2	1	NH$_2$
Sequence	Ac	S$_5$	E	T	A	S$_5$	E	L	L	L	S	N	NH$_2$

251

Table 42 - Staple I sequence numbering

Number	Ac	11	10	9	8	7	6	5	4	3	2	1	NH₂
Sequence	Ac	L	T	E	S₅	N	T	L	S₅	S	V	E	NH₂

A2 – NH region of ^{1}H NMR spectra used in peptide backbone investigation
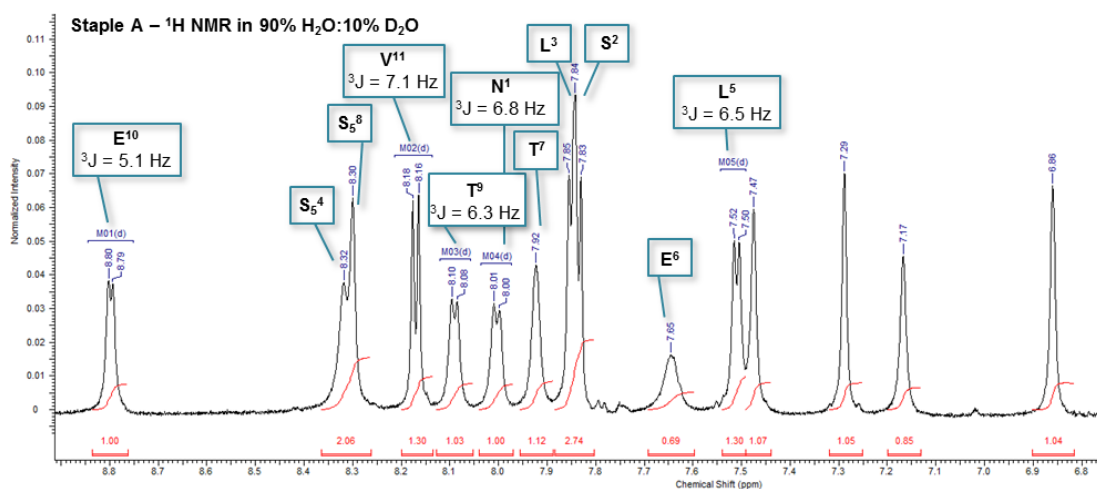

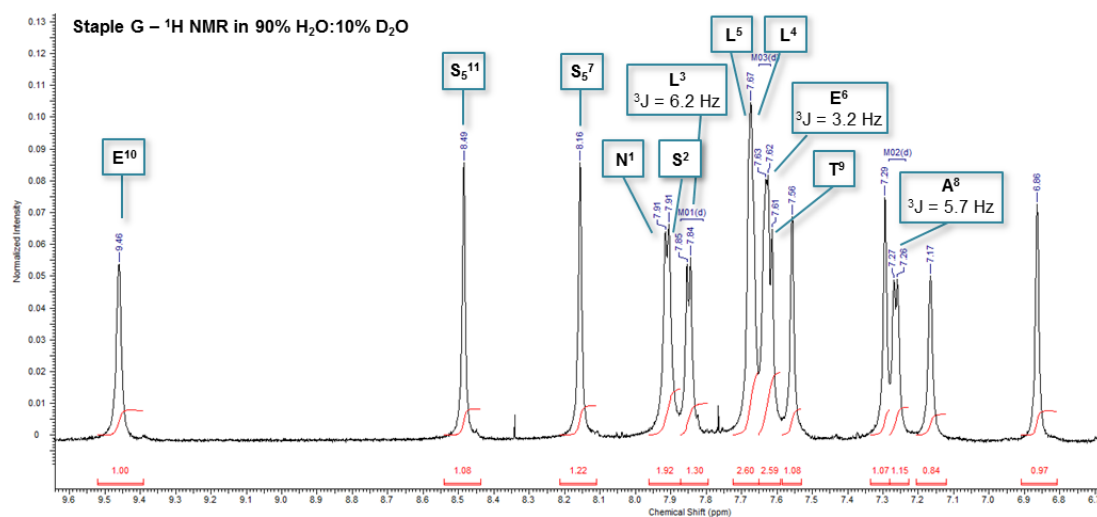**Figure 77 –** Key peaks and coupling constants in the NH region of Staple A

Figure 78 - Key peaks and coupling constants in the NH region of Staple G

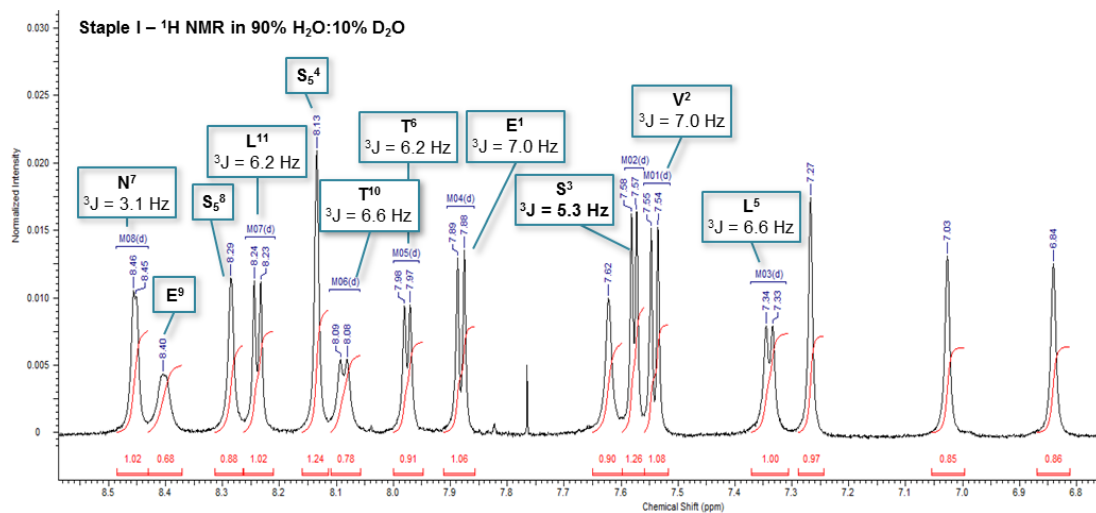**Figure 79 -** Key peaks and coupling constants in the NH region of Staple I
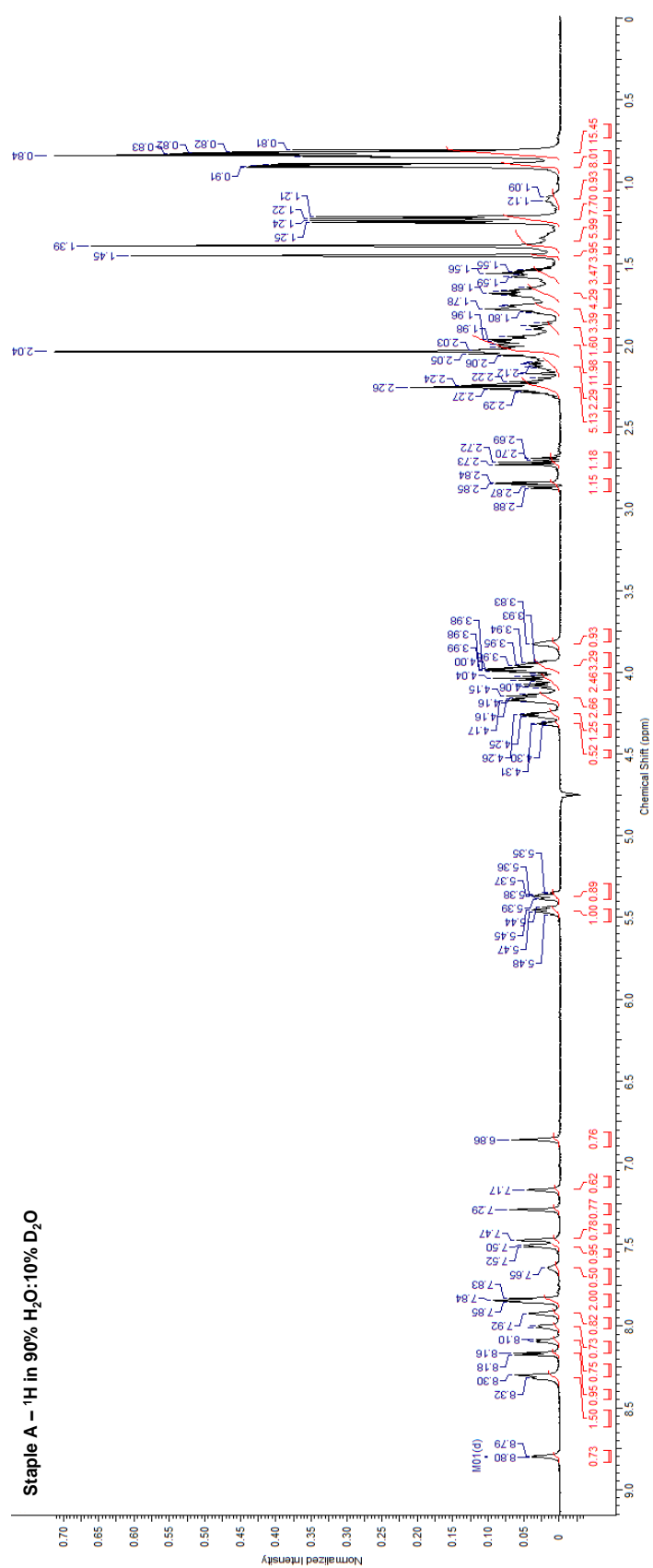
A3 – Full ¹H spectra of peptides

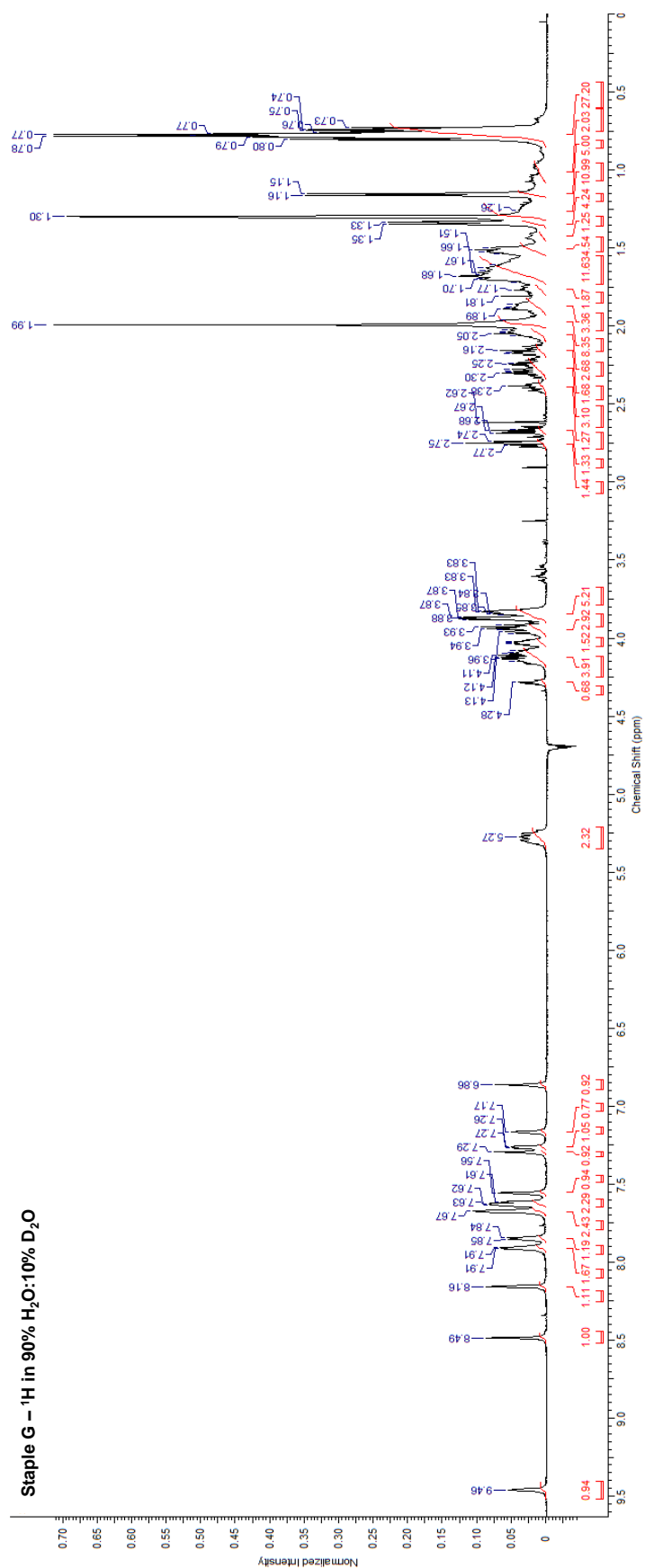**Figure 80 –** ¹H NMR spectra of Staple A
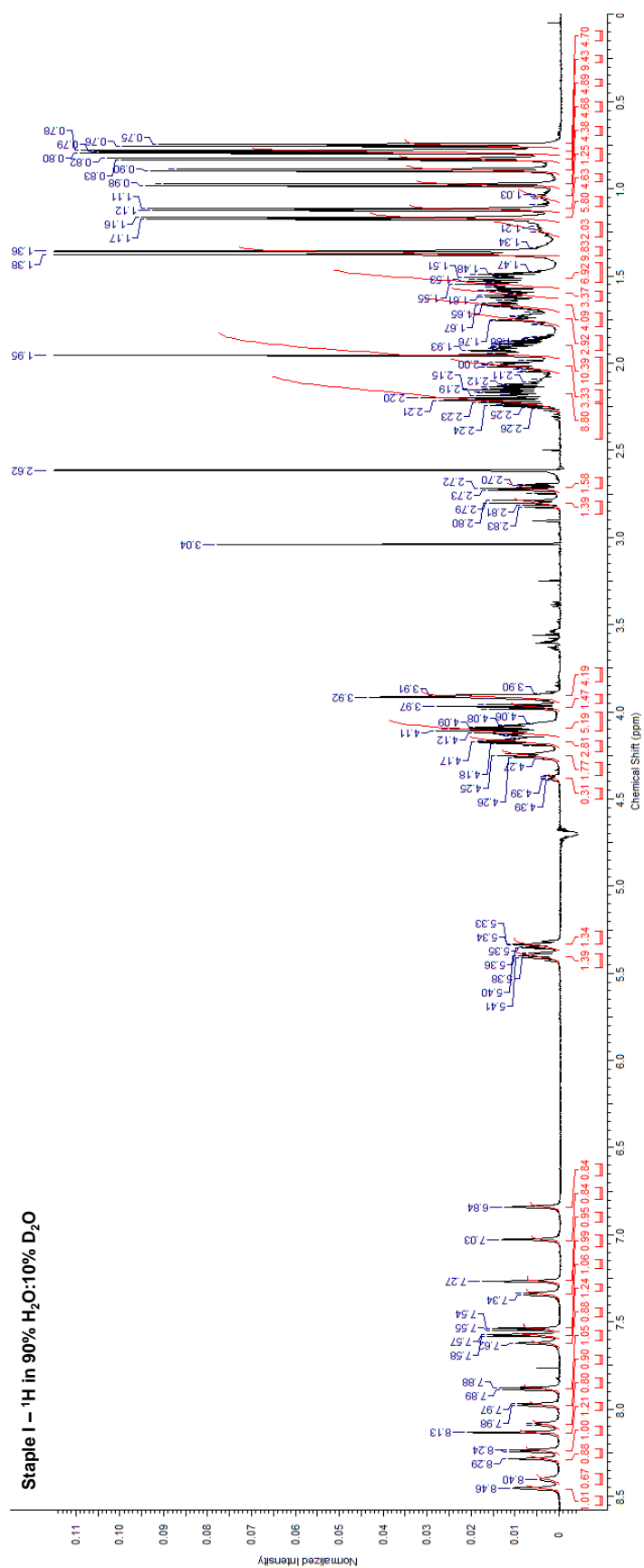
Figure 81 - ^{1}H NMR spectra of Staple G

Figure 82 - ^{1}H NMR spectra of Staple I

A4 – ¹H peak assignment of peptides

Assignment tables were generated from SPARKY upon interpetaion of 2D [¹H, ¹H] NMR spectra discussed in Section x for each peptide. Unassigned resonances were left blank for **Staples G** and **I**.

Table 43 – ¹H NMR chemical shift assignments for Staple A

	HN	Ha	Hb	Hb1	Hb2	Hd	Hd1	Hd2	Hg	Hg1	Hg2	Ht1	Ht2
Ac													
N1	7.955	4.656		2.814	2.679		7.428	6.815				7.241	7.122
S2	7.791	4.271	3.938										
L3	7.804	4.111	1.738			0.792			1.523				
*4	8.271												
L5	7.464	4.035		1.735	1.636	0.784			1.508				
E6	7.599	3.905		2.075	1.994					2.246	2.189		
T7	7.875	3.782	4.101						1.201				
8*	8.251												
T9	8.044	4.214	4.131						1.178				
E10	8.751	4.220	1.926							2.212	1.996		
V11	8.122	3.994	2.005						0.858				

	3H	3Ha	HA	HB1	HB2	HC1	HC2	HD1	HD2
Ac	1.405								
N1									
S2									
L3									
*4		1.357	5.415	2.027	1.930	1.916	1.646	1.542	1.295
L5									
E6									
T7									
8*		1.362	5.330	2.002	1.934	1.837	1.647	1.619	1.068
T9									
E10									
V11									

Table 44 - ¹H NMR chemical shift assignments for Staple G

	3H	3Ha	HA	HD2	HN	Ha	Hb	Hb1	Hb2	Hd	Hd1	Hd2	Hg	Hg1	Hg2	Ht1	Ht2
Ac	-																
N1					7.909	4.607		2.753	2.672	7.557	6.864					7.295	7.167
S2					7.911	4.287	3.876										
L3			*Unassignable*		7.852	4.152		1.703	1.503	0.778			1.634				
L4					7.671	4.092	1.676			0.747			1.513				
L5					7.677	4.031		1.770	1.680	0.787			1.515				
E6					7.634	3.832		2.044	1.980					2.300	2.161		
*7		1.301	5.297	-	8.155												
A8					7.264	3.960	1.346										
T9					7.620	3.930	4.121						1.160				
E10					9.460	3.837	1.990							2.395	2.238		
*11		1.301	5.258	-	8.484												

Table 45 - ^{1}H NMR chemical shift assignments for Staple I

	3H	3Ha	HA	HD2	HN	Ha	Hb	Hb1	Hb2	Hd	Hd1	Hd2	Hg	Hg1	Hg2	Ht1	Ht2
Ac	-																
E1					7.882	4.130		2.017	1.875					2.242	2.158	7.266	7.029
V2					7.542	3.973	2.137							0.980	0.895		
S3					7.577	4.181	3.918										
*4		-	-	-	8.134												
L5					7.341	4.116		1.674	1.617		0.796	0.753	1.499				
T6					7.976	4.250	3.917						1.172				
N7					8.453	4.382		2.808	2.718		7.623	6.842					
*8		-	-	-	8.285												
E9					8.404	4.078		2.013	1.930				2.206				
T10					8.087	4.164	4.101						1.121				
L11					8.238	4.253	1.551				0.831	0.789	1.505				

Unassignable (column between HA and HD2)

A5 - Staple A NOESY spectra

Regions of interest of the 150 ms 2D [^{1}H, ^{1}H] NOESY NMR spectrum of **Staple A**. The characterstic helical "walk" along the peptide backbone is denoted by the lines in Fig. 67 and 68.
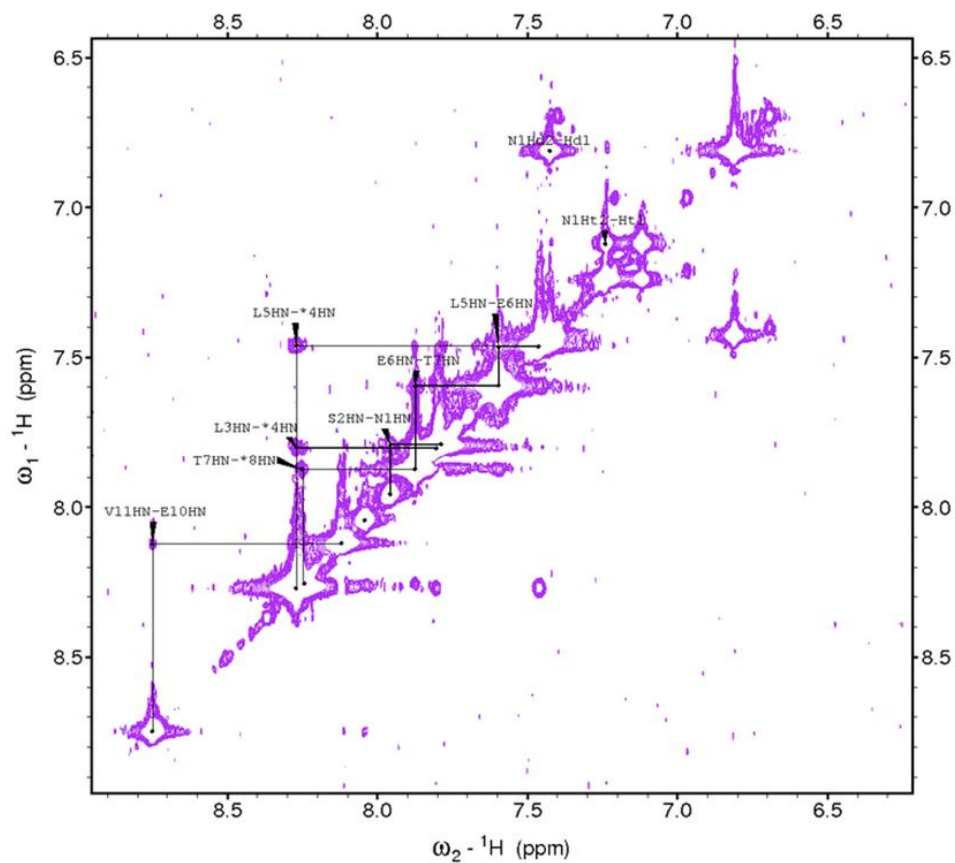

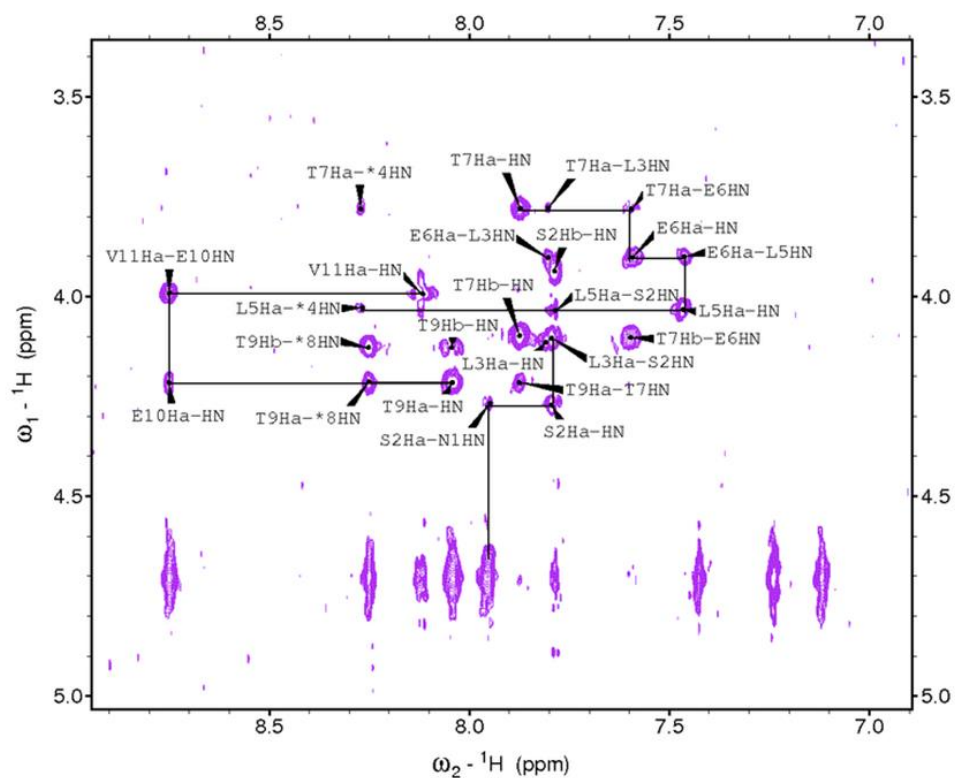**Figure 83 –** NH-NH region from the NOESY spectra of Staple A

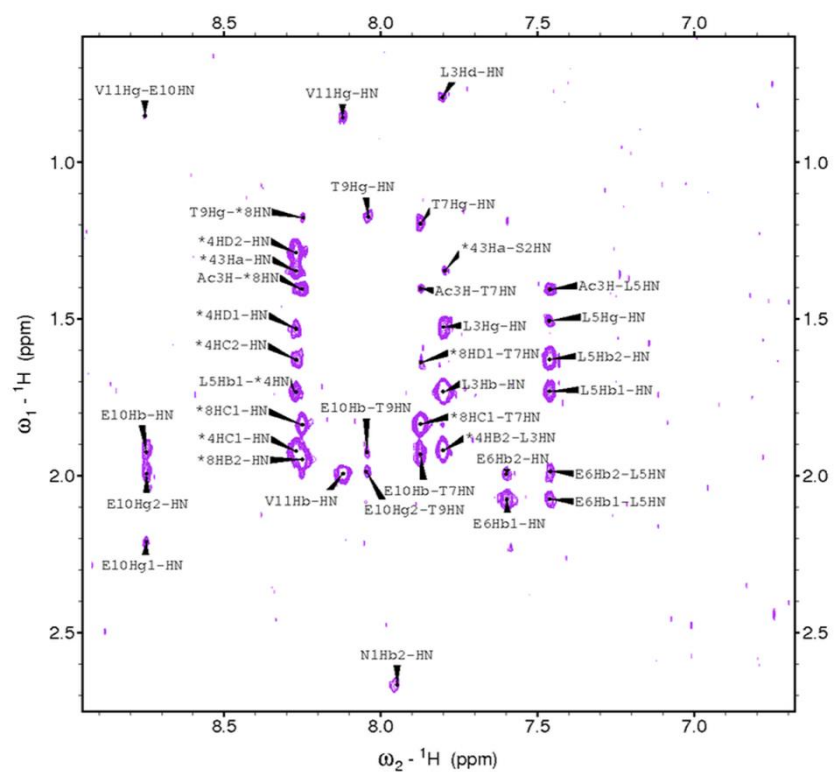**Figure 84 –** NH-αH region from the NOESY spectra of Staple A

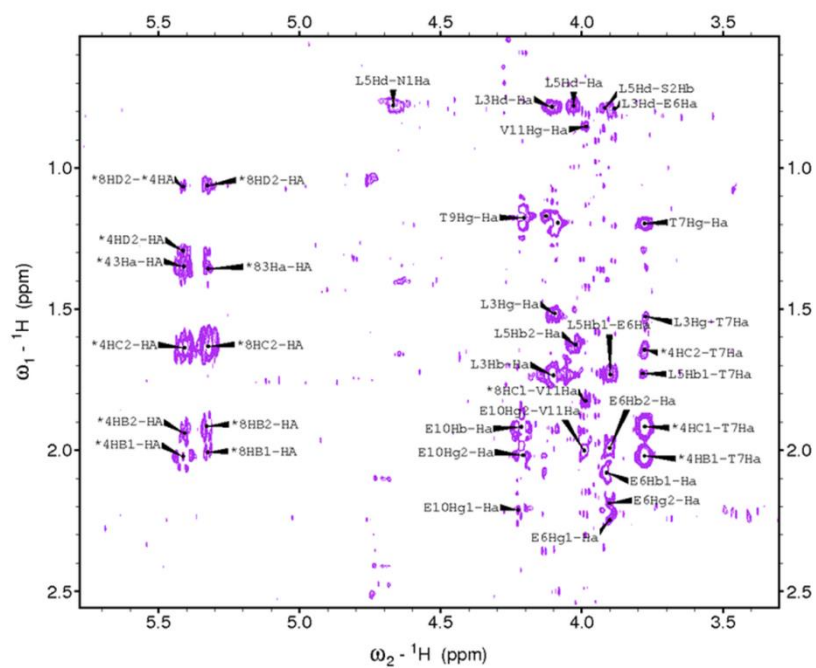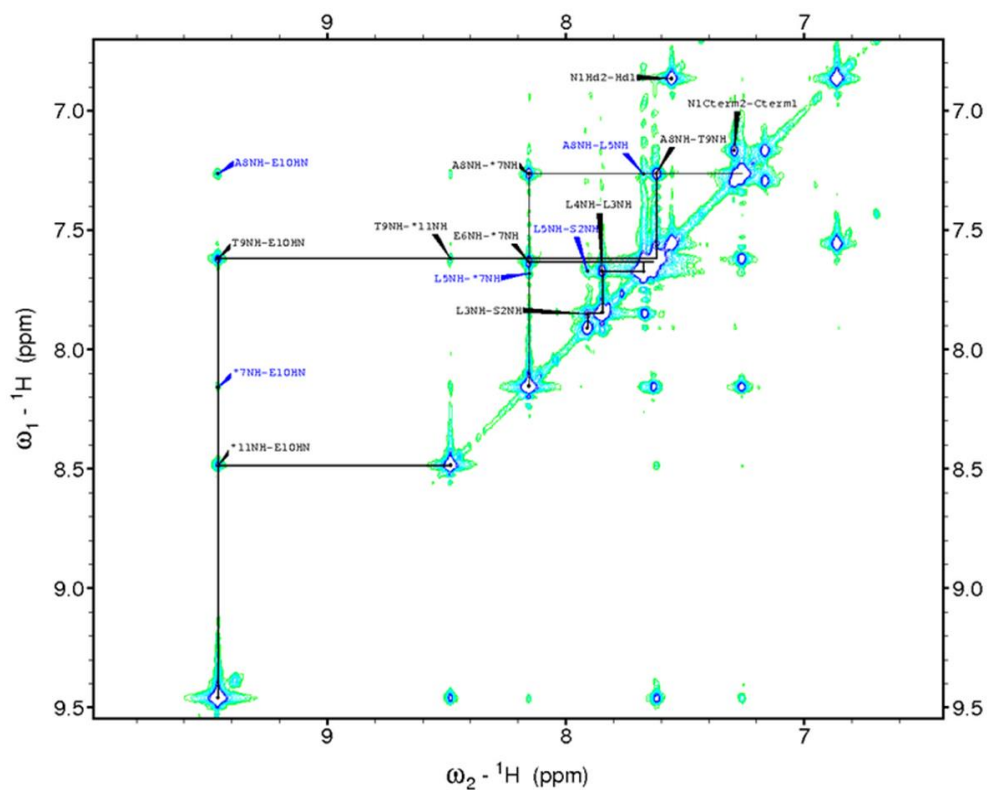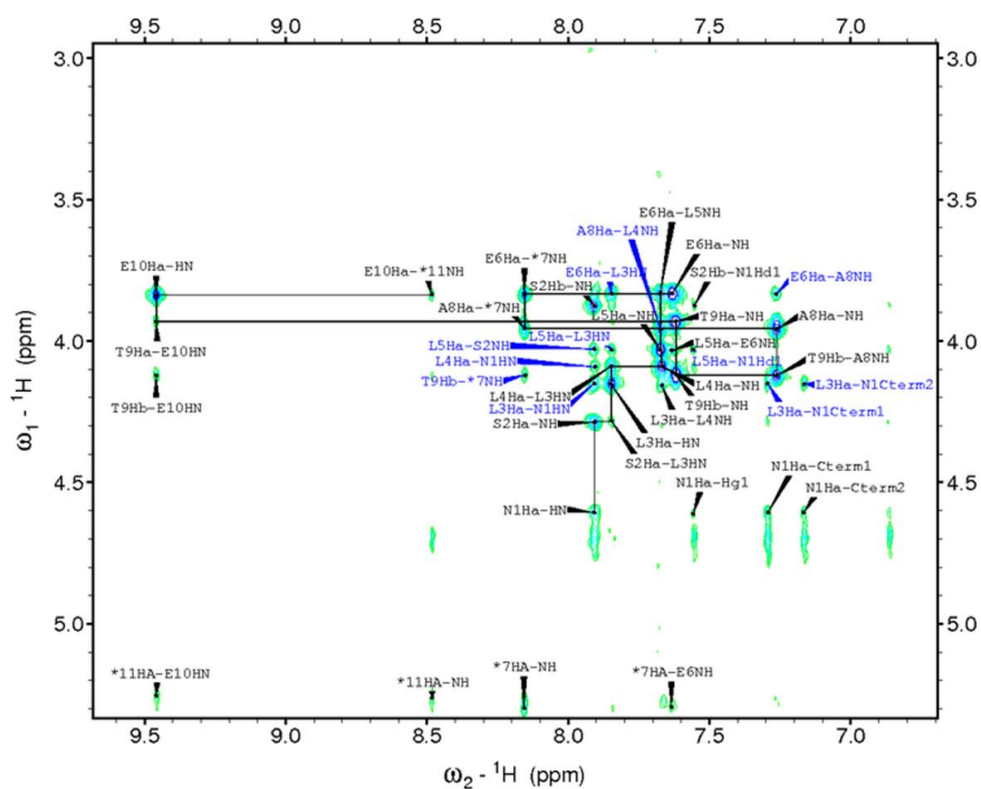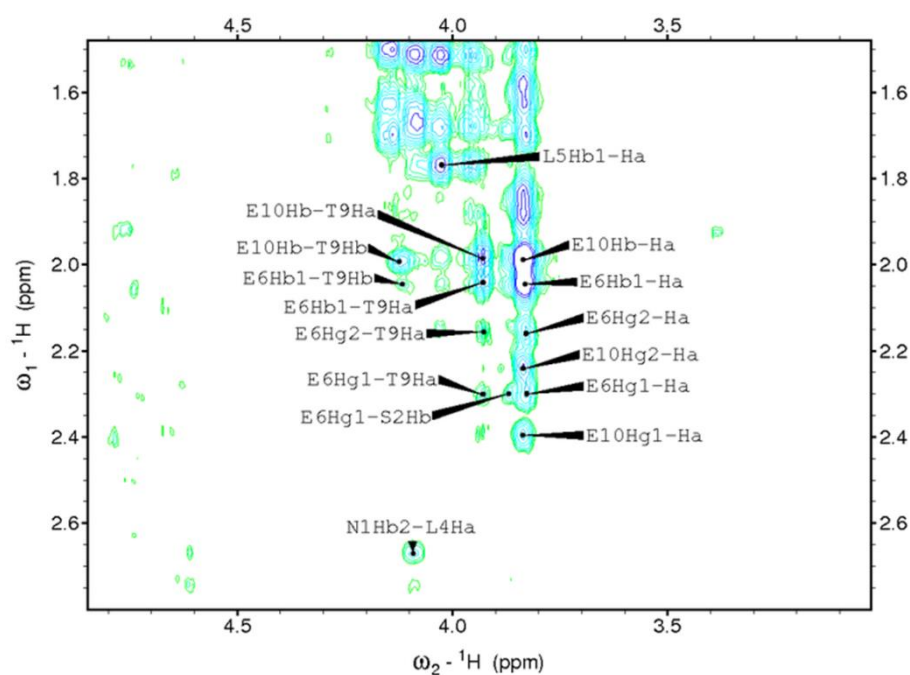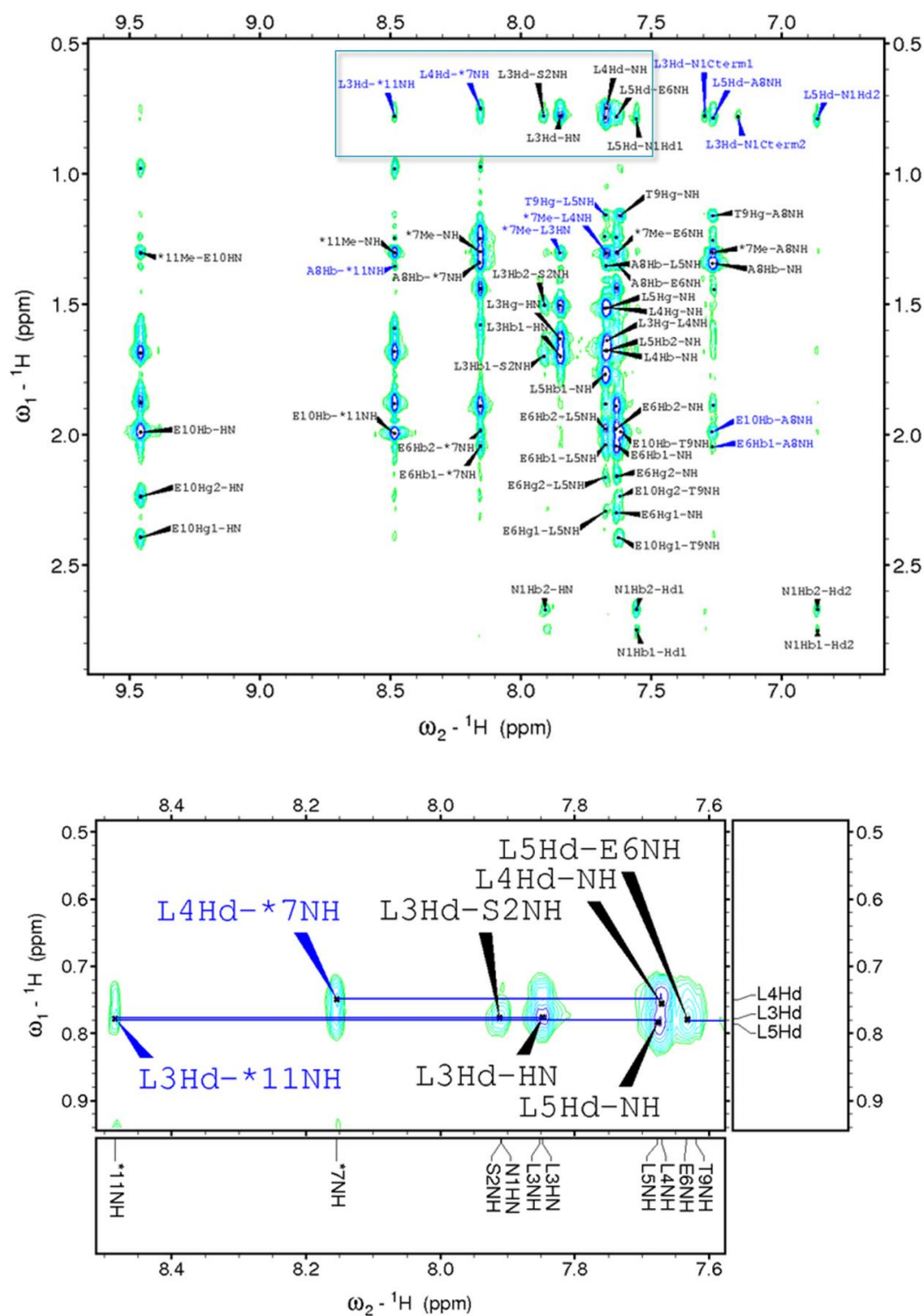**Figure 85 -** NH-Aliphatic region from the NOESY spectra of Staple A

Figure 86 – αH-Aliphatic region from the NOESY spectra of Staple A

A6 - Staple G NOESY spectra

Regions of interest of the 250 ms 2D [^{1}H, ^{1}H] NOESY NMR spectrum of **Staple G**. The characterstic helical "walk" along the peptide backbone is denoted by the lines in Fig. 71 and 72. Unassigned NOEs from the all-hydrocarbon staple have been left blank for clarity. NOEs with blue labels represent long range signals between *i*, *i*+2 residues or longer.

Figure 87 - NH-NH region from the NOESY spectra of Staple G

Figure 88 - NH-αH region from the NOESY spectra of Staple G

Figure 89 - αH-Aliphatic region from the NOESY spectra of Staple G

Figure 90 - NH-Aliphatic region from the NOESY spectra of Staple G

*Boxed region of main spectra is enlarged to show weak NOE between N-terminal S5 NH (*11) and the side chain of either L5 or L3. The peak in question has been labelled L3Hd – *11NH due to the leucine resonane being closer to that of L3, however a definite assignement can not be assumed. This i, i+6 or i+8 NOE is key in elucidating the folded structure of Staple G*

A7 - Staple I NOESY spectra

Regions of interest of the 250 ms 2D [^{1}H, ^{1}H] NOESY NMR spectrum of **Staple I**. The characterstic helical "walk" along the peptide backbone is denoted by the lines in Fig. 75 and 76. Unassigned NOEs from the all-hydrocarbon staple have been left blank for clarity. The NOE with a blue labels represents the only *i*, *i*+3 signal found.
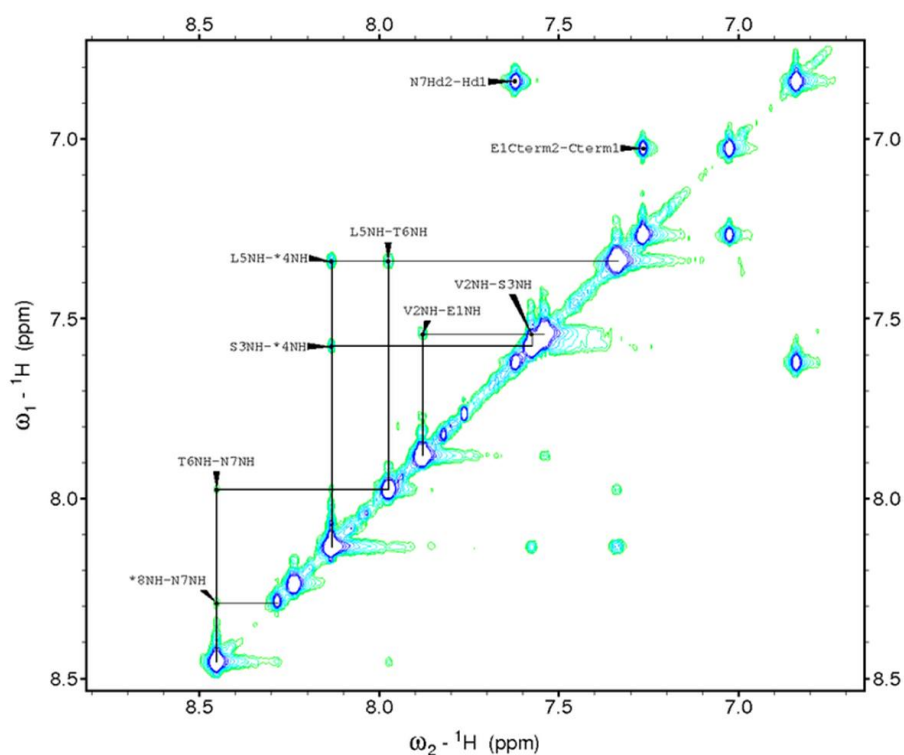

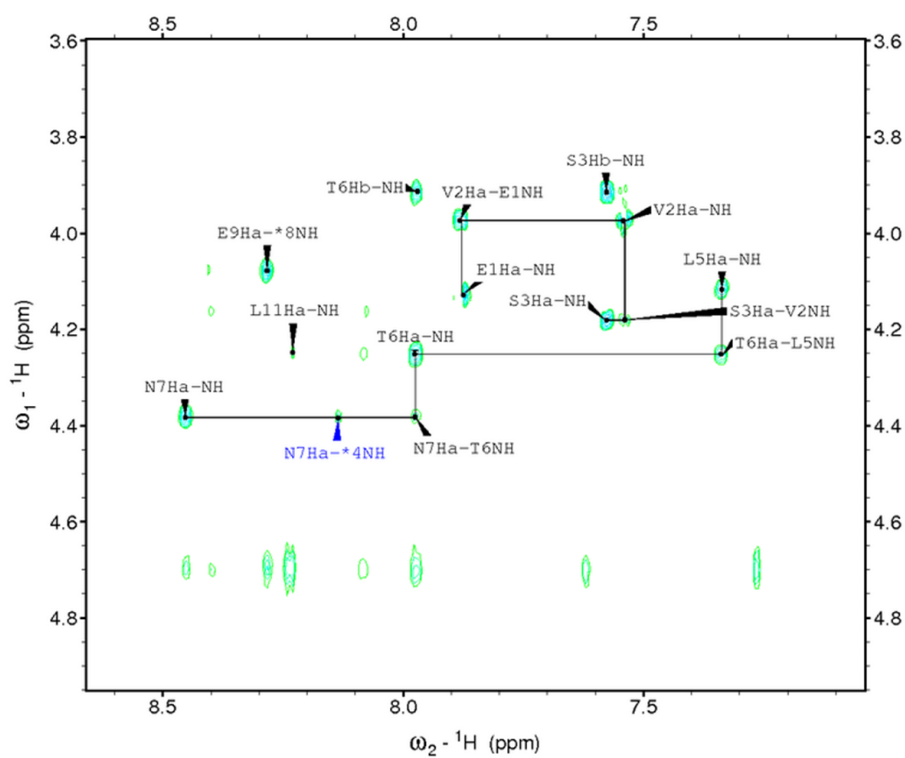**Figure 91 -** NH-NH region from the NOESY spectra of Staple I

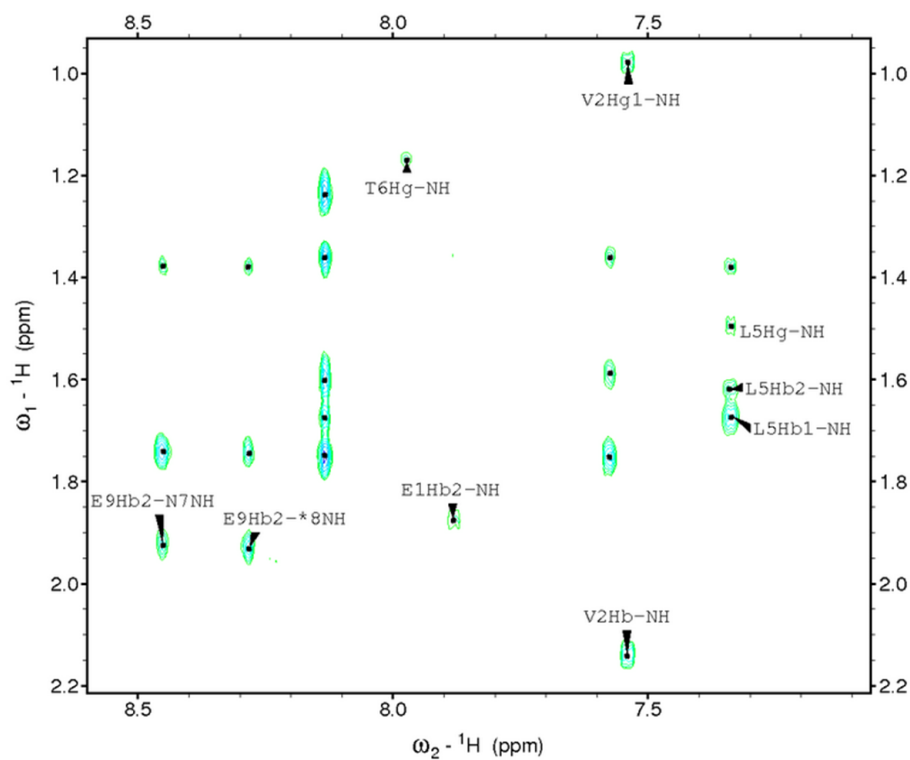**Figure 92 -** NH-αH region from the NOESY spectra of Staple I

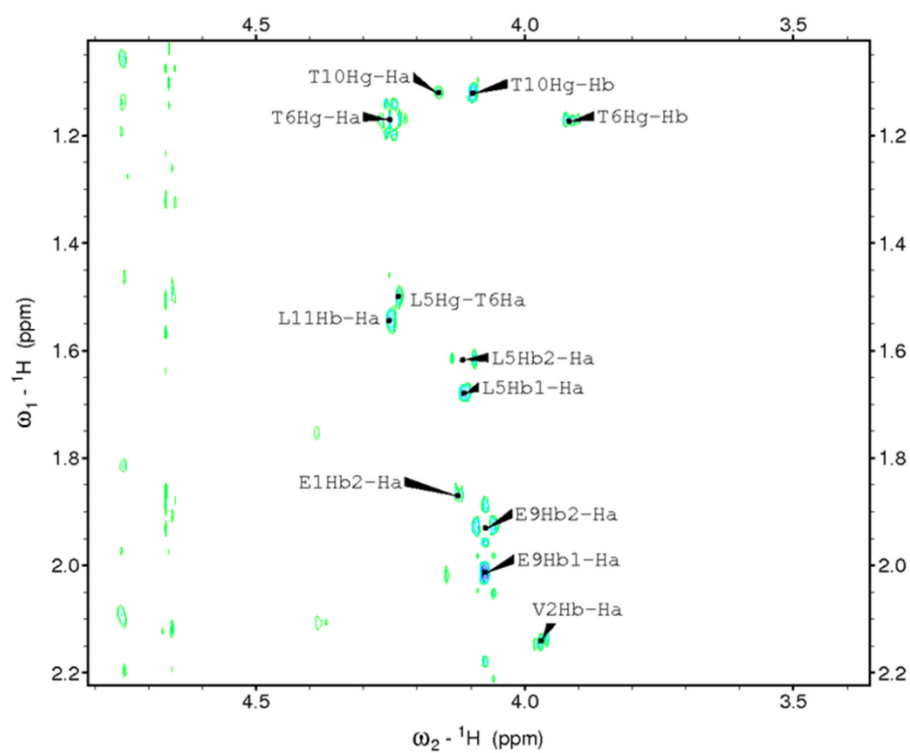**Figure 93 -** NH-Aliphatic region from the NOESY spectra of Staple I

Figure 94 - αH-Aliphatic region from the NOESY spectra of Staple I